2010

Borate based bioactive glass scaffolds for hard and soft tissue engineering

Steven B. Jung

BORATE BASED BIOACTIVE GLASS SCAFFOLDS FOR HARD AND SOFT TISSUE ENGINEERING

by

STEVEN B. JUNG

A DISSERTATION

Presented to the Faculty of the Graduate School of the

MISSOURI UNIVERSITY OF SCIENCE AND TECHNOLOGY

In Partial Fulfillment of the Requirements for the Degree

DOCTOR OF PHILOSOPHY

in

MATERIALS SCIENCE AND ENGINEERING

2010

Approved by

Delbert E. Day, Advisor

Mohamed N. Rahaman

Richard K. Brow

Roger F. Brown

David Henthorn

PUBLICATION DISSERTATION OPTION

The body of the dissertation has been compiled in the format of peer reviewed journals for eventual publication. The main body has been divided into six papers in the following order. The first paper, "Preliminary Evaluation of Bioactive Borate Glass Fiber Scaffolds for Mammalian Tissue Regeneration," was written for publication in the *Journal of Biomedical Materials Research Part B Applied Biomaterials,* and consumes pages 15 to 57. The second paper, "Potential Toxicity of Bioactive Borate Glasses In-Vitro and In-Vivo," was written to *Acta Biomaterialia* and consumes pages 58 to 99. The third paper, "Angiogenic Bioactive Borate Glasses," was written to *Acta Biomaterialia* and consumes pages 100 to 144. The fourth paper, "Bone Growth on Bioactive Borate Glass Scaffolds," was written for submission to the *Acta Biomaterialia* and consumes pages 145 to 185. The fifth paper, "Conversion of Bioactive Borate Glasses In-Vivo," was written for submission in *Acta Biomaterialia* and consumes pages 186 to 247. The sixth paper, "Bioactive Borate Glass Fibers for the Treatment of Wounds" was written for submission to *Journal of Biomedical Materials Research Part B Applied Biomaterials* and consumes pages 248 to 273.

Three papers not included in the main body of the dissertation are given in the appendix. The first paper, "Bioactive Glass Scaffolds for Soft Tissue Engineering," was written to provide supplemental information. The second paper, "Comparison of Self-Bonded Three Dimensional Bioactive Glass Fiber Scaffolds After In-Vivo Implantation in Rats," was accepted for publication in the proceedings of the Pacific Rim 8 Conference (June 2009, Vancouver Canada). The third paper, "Conversion Kinetics of Silicate, Borosilicate, and Borate Bioactive Glasses to Hydroxyapatite," was published in the

European Journal of Glass Science and Technology B - Physics and Chemistry of Glasses (Vol 50, Issue 2, pages 85 to 88).

ABSTRACT

The main objectives of this dissertation were to evaluate bioactive borate glass scaffolds for hard and soft tissue applications and determine the potential toxicity of the borate glasses on the adjacent and systemic tissues. Porous randomly oriented fiber scaffolds composed of bioactive borate glass were implanted in subcutaneous soft tissue sites and in calvaria defects of laboratory rats and no signs of toxicity (necrotic tissue, increase in macrophages or other immune cells) were detected in any of the adjacent tissues (hard or soft). Systemic organs (kidney and liver) of laboratory rats implanted with bioactive borate scaffolds were analyzed for possible systemic toxicity and no adverse effects were found beyond normal incidental changes. Bone was found to grow statistically better ($p<0.05$) in bioactive borate glass scaffolds when compared to similar scaffolds composed of borosilicate and silicate based bioactive glasses. For the first time, elements were added to a bioactive glass for the purposes of promoting angiogenesis. The elements copper and zinc were shown to significantly increase the number of blood vessels ($p<0.05$) present in the soft tissue inside bioactive borate glass scaffolds when compared to the un-doped scaffolds. Bioactive borate glass fibers were also demonstrated as a new material that may be useful in the treatment of chronic wounds. A full thickness cutaneous defect (15mm diameter) on the back of a laboratory rats were healed in similar time (18 days), but with a higher quality scar than the control (un-treated wound). The results from the full thickness cutaneous defect opens the door for new potential uses of bioactive borate glass fibers such as the treatment of chronic wounds and severe burns.

ACKNOWLEDGEMENTS

I would like to thank my advisor, Dr. Delbert E. Day for his guidance and his patience for the past nine years. Beyond the scholarly lessons and the life lessons, I think the most important lessons he has instilled in me is that learning is a continuous process and there is always a shortage of good people.

Without Dr. Roger Brown's assistance and guidance, much of the in-vivo work presented here would not have been possible. I would like to thank the rest of my committee, Dr. Richard Brow, Dr. David Henthorn, and Dr. Mohamed Rahaman for the helpful discussions, comments, and constructive suggestions throughout my education.

I would like to thank Dr. Keith Strassner (MS&T) for his staff, and Paul Fleischut of Senniger Powers LLP that supported the patenting of the disclosed intellectual property.

The following people helped me with completing my experiments or gave guidance on the direction of my research, and I eternally thank you here in no particular order: Dr. Vladimir Dusevich (UMKC), Dr. Lian Bi (UMKC), Dr. Lynda Bonewald (UMKC), Jennifer Rosser (UMKC), Jackie Taylor (UMKC), Dr. Paul Cook (PCRMC), Penny Taylor (PCRMC), Qiang Fu (MS&T), Vernon Modglin (MS&T).

I cannot say enough about the support I have received from my parents. They have done everything from encourage me to go to graduate school to watch my dog while I was off travelling the world. Last but not least, I need to thank my best friend Rachel Kluesner for her support and encouragement over the last four years. I don't think I could have done this without you.

TABLE OF CONTENTS

SECTION

LIST OF ILLUSTRATIONS

PAPER 1

APPENDIX B

APPENDIX C

APPENDIX E

LIST OF TABLES

APPENDIX E

1. PURPOSE OF DISSERTATION

The purpose of this dissertation was to evaluate bioactive borate glass scaffold composed of randomly oriented glass fibers *in-vivo* to determine potential toxicity in adjacent and systemic tissues, compare borate glasses to silicate based bioactive glasses such as 45S5 and 13-93 as a bone repair material, improve the angiogenic properties of bioactive glass, study the reaction of the borate glasses *in-vivo*, and experiment with using bioactive borate glass as a soft tissue wound healing material.

Borate glasses react considerably faster than silicate glasses when in the presence of body fluids or an aqueous solution such as simulated body fluid. The increased reaction rate is thought to be an advantage in that the glass converts to hydroxyapatite faster, and can then be remodeled by the body sooner for complete removal of the implant material. Unfortunately, the scientific community has limited interest in borate glasses because of poor performance by static *in-vitro* cell culture. Borate glasses are thought to be toxic to cells and adjacent tissue due to the fast release of alkali and localized alterations in pH. The present work uses animal models and histological evaluations of adjacent and systemic tissues along with indirect toxicity measurements such as bone growth to evaluate borate glass toxicity.

Angiogenesis (blood vessel formation) is another critical aspect of this research in that scaffolds, particularly larger load bearing scaffolds made from metal and/or ceramics do not stimulate blood vessel formation and therefore do not promote tissue growth. Borate glasses react fast and may be used as a delivery vehicle for ions that can promote endothelial cell migration into the interconnected pores inside the scaffolds to improve tissue growth.

2. BACKGROUND

2.1. TISSUE ENGINEERING WITH BIOACTIVE GLASS

Tissue engineering is the process of using materials (natural or synthetic) to mimic or replace the natural function of damaged or diseased tissue. Devices composed of plastic, metal, glass and ceramics, along with donor tissues are used to treat or replace almost any part of the body. One subset of materials used for tissue engineering are silicate based bioactive glasses such as 45S5 (wt%, 45% SiO_2, 24.5% Na_2O, 24.5% CaO, 6% P_2O_5) as they have been known to bond to bone and soft tissue for almost 40 years [1]. Bioactive glasses are useful materials for tissue engineering due to the high degree of biocompatibility with the body.

Bioactive glasses and glass-ceramics have been used in clinical applications including periodontal repair [2], inner ear replacement [3], and filler for bone cement [4,5] to name a few. Three dimensional scaffolds composed of bioactive glasses in a variety of microstructures have recently been under investigation for bone defects for load bearing and non-load bearing applications [6-10].

Soft tissue from several mammalian species has been known to bond to 45S5 and similar silicate based bioactive glasses for decades [11]. The emphasis in the past has been placed primarily on bioactive glasses bonding to bone, so the soft tissue analysis was usually based on bond interface with the glass, or if the tissue merely grew adjacent to the glass with no bonding [11,12].

Researchers have started to look into the possible angiogenic effects of bioactive glasses such as 45S5 coated with vascular endothelial growth factor (VEGF) for

increasing the vascular network inside of a scaffold [13]. Further study on 45S5 as a proangiogenic material has demonstrated that it is angiogenic in low concentrations and has been hypothesized to up regulate VEGF production from the soluble reaction products when co-cultured with human microvascular endothelial cells *in-vitro* [14]. These angiogenic findings on bioactive glasses such as 45S5 make them interesting materials for soft tissue engineering applications as they are relatively unexplored for soft tissue applications such as wound care.

Silicate based bioactive glasses however have been shown to react relatively slowly *in-vivo* taking months to years to fully react to hydroxyapatite (HA) [15]. The rate at which silicate bioactive glasses convert to HA (stoichiometric composition is $Ca_{10}(PO_4)_6(OH)_2$) and is relatively slow, on the order of months to years depending on the size of the bioactive glass particle and the glass composition [16]. Due to this slow reaction rate, faster reacting bioactive glasses containing boron have been developed with significantly faster reaction rates than silicate glasses [17]. Borate based bioactive glasses submerged in phosphate solutions convert to HA similar to silicate based bioactive glasses, but at a much faster rate [17,18].

2.2. PAST WORK ON BORATE CONTAINING GLASSES FOR *IN-VIVO* USE

Borate based bioactive glasses have been studied for several *in-vivo* applications including, bone replacement, a treatment for osteoarthritis, and drug delivery systems[19]. Richard implanted particles of a 45S5 borate analog (complete exchange of boron for silica) in rat femurs and the glass converted to hydroxyapatite at a significantly accelerated rate and bone grew in and attached to the glass particles [20]. Han [21], Vanderspiegel [22], Huang [19], and Fears [23] investigated the use of hydroxyapatite shells

converted from borate based glasses to act as rate controlled drug delivery systems in the body.

White [24] and Conzone [25,26] demonstrated the application of using irradiated borate based glass microspheres for treatment of osteoarthritis and other *in-vivo* radiotherapies. The borate glasses degraded without radiation leakage as the glasses converted to chemically durable rare earth phosphate materials. Zhao et al implanted similar dysprosium lithium borate glasses in rat livers and reported no toxicity after two weeks *in-vivo* [27].

Jai et al. [28] made pellets composed of borate glass particles (<50μm) mixed with four and eight weight percent teicoplanin for the treatment of osteomyelitis. The pellets released approximately 80% of the teicoplanin within 15 days *in-vitro*, and the compressive strength decreased from 22 MPa to about 12 MPa after six days in PBS solution. The *in-vivo* results from New Zealand White rabbits were comparable to what was seen *in-vitro*, as the teicoplanin released in a controlled manner and the implants had sufficient load bearing strength. No toxic effects were seen in the adjacent bone from the borate glass as the glass converted to HA and supported the growth of new bone into the scaffolds.

Liu et al. [29] treated osteomyelitis in the tibia of New Zealand White rabbits with a scaffold consisting of borate glass particles and a polymer binder loaded with Vancomycin. After eight weeks *in-vivo*, no observable tissue damage or inhibition of bone growth was present at the implant sites. Approximately 80% of the osteomyelitis infected tibia tested negative for the infection after eight weeks. The outer perimeter of

the scaffolds had visible vascular growth that was claimed to have been participating in the bone regeneration.

Bioactive silicate glasses, such as 45S5, have been modified with up to 3wt% B_2O_3 with positive results [11,30]. Particles of 45S5 with 2wt% added B_2O_3 had significantly increased the amount of bone present after 15 days post-implantation in the intramedullary canal of a rat tibia, and the Ca/P ratio surrounding the boron doped particles was significantly higher than 45S5 glass particles[30]. Similar results were reported for a series of silicate glasses with up to 3wt% B_2O_3 added. Direct bone bonding of the surface of the glass particles and rabbit bone was present, and a well defined calcium phosphate layer was reported at the surface of the particles after eight weeks[11].

2.3. BORATE GLASSES SUITABLE FOR MAKING SCAFFOLDS

The borate glass studied by Richard [20] was successful for growing bone and reacting to form hydroxyapatite *in-vivo*. Huang, through *in-vitro* weight loss experiments, showed that this glass could react significantly faster than the well known and widely studied silicate based 45S5 glass[17]. Jung showed that the reaction kinetics of the borate glass was approximately five times greater than that of the silicate glass[18]. The borate glass reacted in a controllable and continuous manner until complete reaction of the glass, while the silicate based 45S5 reaches a point where the mechanism of the hydroxyapatite conversion reaction changes and the reaction kinetics decrease significantly [17,18]. The borate based 45S5 glass crystallizes easily upon heating and cannot be heat treated to form a three dimensional scaffold without crystallizing. The

borate analog of 45S5 was therefore deemed unusable as a scaffold material. Therefore, a new material had to be found that was more suitable for thermal processing.

Another bioactive glass known as 13-93 is a silicate based glass containing 53wt% SiO_2 along with materials such as MgO and K_2O that allows for glass fibers to be pulled and can be heat treated to make three dimensional scaffolds [6,9,31]. The 13-93 glass was modified similarly to the 45S5 glass where all the silica was replaced by boron[17,32], and this glass is now known as 13-93B3 (wt%, 53% B_2O_3, 20% CaO, 12% K_2O, 6% Na_2O, 5% MgO, and 4% P_2O_5). The 13-93B3 glass exhibits reaction kinetics similar to the 45S5 analog glass [33], and, can be easily pulled into glass fibers. It can be heat treated to form a three dimensional porous scaffold [33].

2.4. SOURCES OF BORON, MAMMALIAN INTERACTION, AND INTAKE

Boron is an element that most humans ingest on a daily basis. Fruits, vegetables, and nuts are humans' greatest source for boron [34-36], as boron is a trace element required for cell wall formation in most plants [34]. Ground water has relatively little boron as determined by the World Health Organization, as the range of boron in water is typically between 0.1 and 0.3mg/L, however, this depends on the water source [34]. Ingestion of boron usually takes place as boric acid, either from water or food sources, and meat and dairy products tend to be poor sources of boron [34]. Boron can be inhaled; however, this is not a significant source of intake, except for people that work in borosilicate glass production or other industrial process that involves large amounts of airborne borate materials [34-36]. Absorption of boron through the skin is also limited unless there is an open wound or severely abraded section of skin, then boric acid will enter the body [36,37].

Humans and animals metabolize boron, or boric acid, similarly [34]. Typically, greater than 90% of ingested boric acid is excreted through urine, and this takes place relatively quickly, usually in the first 96 hours after ingestion [34,36]. Boric acid distributes equally throughout most soft tissues, however, boron when administered at a dose of 9000ppm boric acid to male Fischer rats, has been reported to accumulate up to approximately 20 times normal levels in bone [38].

Little is known about the interactions boron has with humans. Few human studies about boron exist, but boron is a known trace element that is present in human cadaver bones [39-41]. Several investigators have suspected boron as an essential trace element to bone functionality and/or metabolism; however, this has not yet been proven [42-46]. No data has been reported linking boron to cancer in humans [36], and no animal experiments have adequately addressed any potential link [36]. An estimated value of 0.2mg/kg-day of boron has been established from data of several animal studies as maximum average lifetime ingestion; however, this number is not based off of human data [36]. Animal models comparing ingested boric acid in rats versus control rats has determined a benchmark dose level (BMDL) of 55mg/kg/day of boric acid. This means that 55mg/kg/day of boric acid correspond to the level of boric acid required to induce an adverse response as compared to the control animals [35].

2.5. THE NEED FOR IMPROVED ANGIOGENESIS IN TISSUE ENGINEERING SCAFFOLDS AND WOUND CARE

Angiogenesis is the process by which blood vessels are formed in the body. Wounds need sustained blood flow to deliver nutrients and growth factors needed for repair of tissues along with a means to remove waste products [47,48]. The maximum distance tissue can survive is approximately 100 to 200μm from a blood vessel, so new

blood vessel formation is necessary for wounds to heal [47]. Specific to placing artificial materials such as bioactive glass scaffolds in the body, tissues cannot grow into and fill the scaffold until a network of blood vessels have first penetrated the scaffold or at least are promoted to penetrate the scaffold as surrounding tissues infiltrate. The importance of vascularization on wound healing is significant and should not be ignored [47]. Vascular endothelial growth factor has been isolated as one of the most important signals for wound healing. Several growth factors natural to the body have been identified as important to wound healing, however, none are as prevalent or have the long-term stimulatory effects for vascular growth as VEGF [48].

Bone is a vascular material and among its obvious structural function, red blood cells are produced inside the marrow cavity of bone. Bone cells require a relatively high oxygen supply for growth and natural function, as all osteocytes are located within 200μm of a blood capillary [49]. Scaffolds are important for growth of damaged bone because bones grow entirely by apposition [49]. Bone needs a preexisting surface in which osteocytes can attach and form a calcified bone matrix [49]. Several methods of improving vascularization of engineered scaffolds are currently under investigation including growth factors, the addition of trace elements, co-culturing of cells on the scaffold, and *in-vivo* prevascularization.

Rouwkema reported that bone growth could be enhanced simply by co-culturing endothelial cells (the cells that line blood vessels) with mesenchymal stem cells to form vessels at the same time as bone[47]. Another method Rouwkema reported was to do a procedure called *in-vivo* prevascularization. A scaffold is placed it in the vicinity of an artery or a vascular tissue such as muscle of the patient long enough for the artery or

vascular tissue to penetrate the scaffold, then the scaffold is surgically removed and placed in the bone defect site[47]. This implies that if a vascular network is in place when bone growth is initiated, then the bone can grow faster due to the increased oxygen and nutrients being supplied.

Previous work completed by multiple researchers has confirmed that certain elements such as copper and tin may be beneficial for the promotion of angiogenesis [48,50-53]. Copper ions released in the vicinity of engineered scaffolds, usually in the form of a copper sulfate salt, have increased vascularization in calcium phosphate [53] and hyaluronan-based hydrogel [54] scaffolds. A major benefit of copper ion release for increasing vascular density is that it is a much more cost effective method as opposed to attachment of expensive growth factors like VEGF [47].

2.6. POTENTIAL BENEFITS OF DOPING BIOACTIVE GLASS WITH BIOLOGICAL TRACE ELEMENTS

Several elements at physiological levels are used to trigger or control reactions in the body that are required for living. Trace elements such as zinc, boron, strontium, copper, and iron have been studied for specific biological responses and are all elements found in human cadaver bone [41]. Endothelial cell migration has been stimulated by copper ions [55] and the presence of copper is required for blood vessel formation (angiogenesis) [56]. Zinc is a cofactor responsible for keratinocyte migration during wound healing which promotes re-epithelialization and improves epithelial cell apoptosis [57]. Zinc oxide is also useful in decreasing blood clotting time [58]. Boron, in the form of boric acid (1 to 10mM concentrations), significantly increased mRNA uptake of human placental cells similar to what would be expected if a growth factor were present [59]. Strontium, >99% located in the skeleton [60], has been shown to have severe implications

on bone mineralization. Finally, iron is part of several enzymes and is present in bone marrow and red blood cells [61]. The release of these ions from bioactive glass is hypothesized to locally promote these biological functions when released at physiological concentrations.

2.7. SOFT TISSUE INTERACTIONS WITH BIOACTIVE BORATE GLASSES

Borate based bioactive glasses have not been investigated for soft tissue use; however they have traits that make them attractive such as fast reaction rates [18], and controllable and continuous reaction to completion when in the presence of body fluids. The previously mentioned *in-vivo* animal data for bioactive borate glasses in bone repair indicated that immune response is likely to be minimal and bone bonded directly to the surface of the reacted borate glass particles [28,29,33]. The release of trace elements from a bioactive borate glass may further promote the formation of blood vessels in soft tissue and the calcium (a potential regulator in wound healing) might be beneficial to the treatment of wounds and stimulate the release of growth factors [62].

2.8 REFERENCES

1. Hench LL, Paschall HA. Direct chemical Bond of Bioactive Glass-Ceramic Materials to Bone and Muscle. Journal of Biomedical Materials Research 1973;4:25-42.
2. Froum SJ, Weinberg MA, Tarnow D. Comparison of bioactive glass synthetic bone graft particles and open debridement in the treatment of human periodontal defects. A clinical study. Journal of Periodontology 1998;69:698-709.
3. Hench LL, Hench JW, Greenspan DC. Bioglass: A short history and bibliography. Journal of Australian Ceramic Society 2004;40:1-42.
4. Sanus GZ, Tanriverdi T, Kafadar AM, Ulu MO, Uzan M. Use of Cortoss for reconstruction of anterior cranial base: a preliminary clinical experience. European Journal of Plastic Surgery 2005;27:371-377.
5. Larsson S. Cement Augmentation in Fracture Treatment. Scandivanian Journal of Surgery 2006;95:111-118.
6. Jung SB, Day DE, Brown RF. Comparison of self-bonded three dimensional bioactive glass fiber scaffolds after in-vivo implantation in rats. Journal of the American Ceramic Society 2009.
7. Fu Q, Rahaman MN, Bal BS, Brown RF, Day DE. Mechanical and InVitro Performance of 13-93 Bioactive Glass Scaffolds Prepared By a Polymer Foam Replication Technique. Acta Biomaterialia 2008;4(6):257-293.
8. Chen QZ, Thompson ID, Boccaccini AR. 45S5 Bioglass-derived glass-ceramic scaffolds for bone tissue engineering. Biomaterials 2006;27(11):2414-2425.
9. Pirhonen E, Moimas L, Haapanen J. Porous Bioactive 3-D Glass Fiber Scaffolds for Tissue Engineering Applications Manufactured by Sintering Technique. Key Engineering Materials 2003;240-242:237-240.
10. Rahaman MN, Day DE, Brown RF, Fu Q, Jung SB. Nanostructured Bioactive Glass Scaffolds for Bone Repair. 32nd International Conference on Advanced Ceramics and Composites 2008.
11. Yamamuro T, Hench LL, Wilson J. Handbook of Bioactive Ceramics Vol. I - Bioactive Glasses and Glass-Ceramics. Boca Raton FL: CRC Press; 1990. 355 p.
12. Merolli A, Tranquiilli P, Guidi PL, Gabbi C. Comparison in In Vivo Response Between a Bioactive Glass and a Non-Bioactive Glass. Journal of Materials Science: Materials in Medicine 2000;11:219-222.
13. Leach JK, Kaigler D, Wang Z, Krebsbach PH, Mooney DJ. Coating of VEGF-releasing scaffolds with bioactive glass for angiogenesis and bone regeneration. Biomaterials 2006;27:3249-3255.
14. Leu A, Leach JK. Proangiogenic Potential of Collagen/Bioactive Glass Substrate. Pharmaceutical Research 2008;25(5):1222-1229.
15. Moimas L, Biasotto M, Lenarda RD, Olivo A, Schmid C. Rabbit pilot study on the resorbability of three-dimensional bioactive glass fibre scaffolds. Acta Biomaterialia 2006;2(2):191-199.

16. Asikainen AJ, Hagstrom J, Sorsa T, Noponen J, Kellomaki M, Juuti H, Lundqvist C, Hietanen J, Suuronen R. Soft Tissue Reactions to Bioactive Glass 13-93 Combined with Chitosen. Journal of Biomedical Materials Research 2007;83A:530-537.
17. Huang W, Day DE, Kittiratanapiboon K, Rahaman MN. Kinetics and Mechanisms of the Conversion of Silicate (45S5), Borate, and Borosilicate Glasses to Hydroxyapatite in Dilute Phosphate Solution Journal of Materials Science: Materials in Medicine 2006;17:583-596.
18. Jung SB, Day DE. Conversion kinetics of silicate, borosilicate, and borate bioactive glasses to hydroxyapatite. Physics and Chemistry of Glasses 2009;50(2):85-88.
19. Huang W. Biological Application of Soluble Borate Glass; 2008. 22 p.
20. Richard M. Bioactive behavior of a borate glass. Rolla: University of Missouri-Rolla; 2000. 140 p.
21. Han X. Reaction of sodium calcium borate glass to form hydroxyapatite and preliminary evaluation of hydroxyapatite microspheres used to adsorb and separate proteins. Rolla, MO: University of Missouri-Rolla; 2003.
22. Vanderspiegal N. Reaction of potassium calcium borate glasses to form apatite and dicalcium phosphate dihydrate. Rolla: University of Missouri-Rolla; 2004.
23. Fears K. Formation of hollow hydroxyapatite microspheres. Rolla, MO: University of Missouri-Rolla; 2001. 74 p.
24. White JE. Rare Earth-Lithium-Borate Glasses for use as degradable radiopharmaceuticals. Rolla, MO: University of Missouri-Rolla; 1995. 228 p.
25. Conzone S. Biodegradable dysprosium lithium borate glasses for radiation synvectomy treatment. Rolla: University of Missouri-Rolla; 1996.
26. Conzone S. Glass microspheres for medical applications. Rolla: University of Missouri-Rolla; 1999. 262 p.
27. Zhao D, Yu J, Huang W, Zhou N, Wang D, Yin W, Chen Y. Dysprosium lithium borate glass microspheres for radiation synvectomy: The in-vitro and in-vivo performance evaluation. Materials Science and Engineering C 2010;30:970-974.
28. Jai W-T, Zhang X, Luo S-H, Liu X, Huang W-H, Rahaman MN, Day DE, Zhang C-Q, Xie Z-P, Wang J-Q. Novel borate glass/chitosen composite as a delivery vehicle for teicoplanin in the treatment of chronic osteomyelitis. Acta Biomaterialia 2009.
29. Liu X, Xie Z, Zhang C, Pan H, Rahaman MN, Zhang X, Fu Q, Huang W. Bioactive borate glass scaffolds: in vitro and in vivo evaluation for use as a drug delivery system in the treatment of bone infection. Journal of Materials Science: Materials in Medicine 2009;online.
30. Gorustovich AA, Lopez JMP, Guglielmotti M, Cabrini ML. Biological performance of boron-modified bioactive glass particles implanted in rat tibia bone marrow. Biomedical Materials 2006;1:100-105.
31. Jung SB. Silicate based bioactive glass fiber scaffolds for bone tissue regeneration. Rolla, MO: University of Missouri-Rolla; 2007.
32. Huang W, Rahaman MN, Day DE, Li Y. Mechanisms for Converting Bioactive Silicate, Borate, and Borosilicate Glasses to Hydroxyapatite in Dilute Phosphate Solution. Physics and Chemistry of Glasses 2006;47B(6):1-12.

33. Fu Q. Freeze casting of bioactive glass and ceramic scaffolds for bone tissue engineering. Rolla: Missouri University of Science and Technology; 2009. 294 p.
34. Smallwood C. Boron in Drinking-water. Volume 2. Geneva: World Health Organization; 2003.
35. Price CJ, Strong PL, Marr MC, Myers CB, Murray FJ. Developmental Toxicity NOAEL and postnatal recovery in rats fed boric acid during gestation. Fundamental and Applied Toxicology 1996;32:179-193.
36. Smallwood CL, Lipscomb J, Swartout J, Teuschler L. Toxicological Report of Boron and Compounds. In: Agency USEP, editor. Washington D.C.: EPA; 2004. p 134.
37. Draize JH, Kelley EA. The urinary excretion of boric acid preparations following oral administration and topical applications to intact and damaged skin of rabbits. Toxicological applications in Pharmacology 1959;1:267-276.
38. Ku WW, Chapin RE, Moseman RF. Tissue disposition of boron in male Fischer rats. Toxicology and Applied Pharmacology 1991;111:145-151.
39. Alexander GV, Nusbaum RE, MacDonald NS. The boron and lithium content of human bones. Journal of Biological chemistry 1951;192:489-496.
40. Forbes RM, Cooper AR, Mitchell HH. On the occurrence of beryllium, boron, cobalt and mercury in human tissues. Journal of Biological Chemistry 1954;209:857-865.
41. Becker RO, Spadaro JA, Berg EW. The Trace Elements of Human Bone. Journal of Bone and Joint Surgery (American) 1968;50:326-334.
42. Nielsen FH. Nutritional Requirements for Boron, Silicon, Vanadium, Nickel, and Arsenic: Current Knowledge and Speculation. FASEB Journal 1991;5:2661-2667.
43. Nielsen FH. Facts and fallacies about boron. Nutrition Today 1992;27:6-12.
44. Mertz W. Essential trace metals: new definition based on new paradigms. Nutritional Review 1993;51(10):287-295.
45. Devirian TA, Volpe SL. The physiological effects of dietary boron. Critical Reviews in Food Science and Nutrition 2003;43(2):219-231.
46. Bilezikian JP, Raisz LG, Rodan GA, editors. Principles of Bone Biology. San Diego CA: Academic Press; 1996.
47. Rouwkema J, Rivron NC, Blitterswijk CAv. Vascularization in Tissue Engineering. Trends in Biotechnology 2008;26(8):434-441.
48. Sen CK, Khanna S, Venojarvi M, Trikha P, Ellison EC, Hunt TK, Roy S. Copper-induced vascular endothelial growth factor expression and wound healing. American Journal of Physiology 2002;282:H1821-H1827.
49. Cormack DH. Ham's Histology. Philadelphia PA: J. B. Lippincott Company; 1987.
50. Hu G-f. Copper Stimulates Proliferation of Human Endothelial Cells Under Culture. Journal of Cellular Biochemistry 1998;69:326-335.
51. Rest JR. The Histological Effects of Copper and Zinc on Chick Embryo Skeletal Tissues in Organ Culture. British Journal of Nutrition 1976;36(2):243-254.
52. Lin MT, Chen Y-l. Effect of copper ion on collagenase release. Investigative Ophthalmology and Visual Science 1992;33:558-563.

53. Barralet J, Gbureck U, Habibovic P, Vorndran E, Gerard C, Doillon CJ. Angiogenesis in calcium phosphate scaffolds by inorganic copper ion release. Tissue Engineering 2009;15:1-9.
54. Giavaresi G, Torricelli P, Fornasari PM, Giardino R, Barbucci R, Leone G. Blood vessel formation after soft tissue implantation of hyaluronan-based hydrogel supplemented with copper ions. Biomaterials 2005;26:3001-3008.
55. McAuslan BR, Reilly W. Endothelial Cell Phagokinesis in Response to Specific Metal Ions. Experimental Cell Research 1980;130:147-157.
56. Harris ED. A Requirement for Copper in Angiogenesis. Nutrition Reviews 2004;62:60-64.
57. Lansdown ABG, Mirastschijski U, Stubbs N, Scanlon E, Agren MS. Zinc in Wound Healing: Theoretical, Experimental, and Clinical Aspects. Wound Repair and Regeneration 2006;15:2-15.
58. Ostomel TA, Shi Q, Stoimenov PK, Stucky GD. Metal Oxide Surface Charge Mediated Hemostasis. Langmuir 2007;23:11233-11238.
59. Dzondo-Gadet M, R M-N, Hess K, Nabet P, Belleville F, Dousset B. Action of Boron at the Molecular Level. Biological Trace Element Research 2002;85:23-33.
60. Cabrera WE, Schrooten I, Broe MED, D'Haese PC. Strontium and Bone. Journal of Bone and Mineral Research 1999;14:661-668.
61. Goldhaber SB. Trace Element Risk Assessment: Esentiality vs. Toxicity. Regulatory Toxicology and Pharmacology 2003;38:232-242.
62. Lansdown ABG. Calcium: a potential central regulator in wound healing in the skin. Wound Repair and Regeneration 2002;10:271-285.

1. PRELIMINARY EVALUATION OF BIOACTIVE BORATE GLASS FIBER SCAFFOLDS FOR MAMMALIAN TISSUE REGENERATION

Steven B. Jung[1], Delbert E. Day[1], and Roger F. Brown[2]

[1]Graduate Center for Materials Research, Materials Science and Engineering Department, Missouri University of Science and Technology, Rolla, MO, 65409-1170

[2]Department of Biological Sciences, Missouri University of Science and Technology, Rolla, MO, 65409-1170

1.1 ABSTRACT

After four weeks in rat subcutaneous tissue, scaffolds composed of randomly oriented, self-bonded bioactive glass fibers with an open and interconnected porosity of 51 ± 2% were completely reacted to nanocrystalline carbonated hydroxyapatite (HA) and the interconnected pores had become significantly infiltrated with soft tissue. The bioactive borate glass fibers reacted to form hollow HA channels that soft tissue and blood vessels infiltrated. Histological staining with both the PAS and VVG stains positively stained vessels from the 93B3 scaffolds. The PAS stain also positively stained macrophages which were sparsely present throughout the adjacent soft tissue; however, there was no negative immune reaction due to the presence of the reacted scaffold (HA). Fibers composed of bioactive borate glass could have future applications as blood vessel, bone, or other tissue guides, as porous scaffolds for hard and soft tissue regeneration, or for wound care of soft tissue.

1.2 INTRODUCTION

Boron is an element that most humans ingest on a daily basis from fruits, vegetables, and nuts [1-3]. Boron is a trace element required for cell wall formation in most

plants [1]. Ground water has a relatively low boron concentration as determined by a study done by the World Health Organization. The boron concentration in water is typically between 0.1 and 0.3mg/L, but, this depends on the water source [1]. Ingestion of boron usually occurs as boric acid (BA), either from water or food sources. Meat and dairy products tend to be poor sources of boron [1]. Boron can be inhaled, but, this is not a significant source of intake, except for persons working in borosilicate glass production or other industrial environments where large amounts of airborne borate materials are produced [1-4]. Absorption of boron through the skin is also limited unless there is an open wound or severely abraded section of skin, then BA will enter the body [3,5].

Humans and animals metabolize boron, or boric acid, similarly [1]. Typically, greater than 90% of the ingested BA is excreted through urine, usually in ~96 hours after ingestion [1,3]. Boric acid distributes equally throughout most soft tissues, but, when boron was administered at a dose of 9000ppm BA to male Fisher rats, it was reported to accumulate up to approximately 20 times normal levels in bone [6].

Little is known about the interaction boron has in humans. Few human studies about boron exist, but it is a known trace element that is present in human cadaver bones [7-9]. Several investigators have suspected boron to be an essential trace element to bone functionality and/or metabolism, but, this has not yet been proven [10-14]. No data has been reported linking boron to cancer in humans [3], and no animal experiments have adequately addressed any potential link [3]. An estimated value of 0.2mg/kg-day of boron has been established from several animal studies as the maximum average lifetime ingestion, but, this number is not based on human data [3]. A study of airborne boron ingestion for humans working with borax (a mixture of three sodium tetraborate materials, $Na_2B_4O_7$,

$Na_2B_4O_7$-$5H_2O$, and $Na_2B_4O_7$-$10H_2O$) found that the average boron consumption 27.90 mg/day or 1.9mg/kg/day of BA, no progressive accumulation of boron was observed in the test subjects [4].

Studies on the developmental toxicity of BA in mice (248 to 1003mg/kg/day), rabbits (62.5 to 250mg/kg/day), and rats (78 to 539mg/kg/day), found that there were measurable increases in the weight of the kidney and liver, and renal lesions were formed in mice [15]. These reported levels of BA were associated with lower fetal weights and higher fetal mortality in all species. The occurrence of wavy ribs in rats was also observed, but this was attributed to significant decreases in fetal weight [15]. Animal models comparing ingested boric acid in rats versus control rats determined the benchmark dose level (BMDL) was 55mg/kg/day of BA. This represents the amount of BA required to induce an adverse response as compared to the control animals [2].

Borate based bioactive glasses have been studied for several *in-vivo* applications including, bone replacement, a treatment for osteoarthritis, and drug delivery systems [16]. Richard implanted particles of a borate glass in rat femurs and the glass converted to hydroxyapatite (HA) at a significantly higher rate than silicate glasses and bone grew and attached to the glass particles [17]. White [18] and Conzone [19,20] demonstrated the application of using radioactive borate glass microspheres for treating osteoarthritis and other *in-vivo* radiotherapies. The radioactive borate glasses degraded without radiation leakage as the glasses converted to a chemically durable rare earth phosphate material that prevented the release of the radioisotope. Han [21], Vanderspiegel [22], Huang [16], and Fears [23] investigated the use of hydroxyapatite shells converted from borate based glass microspheres to act as rate controlled drug delivery systems in the body.

Jai et al. [24] used pellets composed of borate glass particles (<50μm) mixed with four and eight weight percent teicoplanin to treat osteomyelitis. The pellets released approximately 80% of the teicoplanin within 15 days *in-vitro*, and the compressive strength decreased from 22 MPa to ~12 MPa after six days in phosphate buffered saline (PBS) solution. The *in-vivo* results from New Zealand White rabbits were comparable to what was seen *in-vitro*, as the teicoplanin was released in a controlled manner and the implants had sufficient load bearing strength. No toxic effects were seen in the bone adjacent to the borate glass as the glass converted to HA and supported the growth of new bone into the scaffolds.

Liu et al. [25] treated osteomyelitis in the tibia of New Zealand White rabbits with a scaffold consisting of borate glass particles and a polymer binder loaded with Vancomycin. After eight weeks *in-vivo*, no observable tissue damage or inhibition of bone growth was detected at the implant sites. Approximately 80% of the osteomyelitis infected tibia tested negative for the infection after eight weeks. The outer perimeter of the scaffolds had visible vascular growth that was claimed to have participated in bone regeneration.

Bioactive silicate glasses, such as 45S5 (Table 1), have been modified with up to 3wt% B_2O_3 with positive results *in-vivo* [26,27]. Particles of 45S5 with 2wt% added B_2O_3 had increased the amount of bone present after 15 days post-implantation in the intramedullary canal of a rat tibia, and the Ca/P ratio of the bone surrounding the boron doped particles was significantly higher than the Ca/P ratio in the 45S5 glass particles [26]. Direct bone bonding of the surface of the glass particles and rabbit bone was present, and

a well defined calcium phosphate layer was reported at the surface of the boron doped glass particles after eight weeks *in-vivo* [27].

Soft tissue from several mammalian species has been known to bond to 45S5 and similar silicate based bioactive glasses for decades [27]. The emphasis in the past has been primarily on bioactive glasses bonding to bone, so the soft tissue analysis was usually based on whether or not the tissue bonded with the glass, or if the tissue merely grew adjacent to the glass without forming a bond [27,28].

More recently, researchers have looked into the possible angiogenic effects of bioactive glasses such as 45S5 coated with vascular endothelial growth factor (VEGF) for increasing the vascular network inside a scaffold [29]. Further study on 45S5 as a proagiogenic material has demonstrated that it is angiogenic in low concentrations and has been hypothesized to up regulate VEGF production from the soluble reaction products when co-cultured with human microvascular endothelial cells *in-vitro* [30]. These proangiogenic findings for silicate based bioactive glasses, such as 45S5, make them interesting materials for soft tissue engineering applications as they are relatively unexplored for soft tissue applications such as wound care.

Borate based bioactive glasses have not been investigated for soft tissue use; but they have traits that make them attractive, such as higher reaction rates [31], and controllable and continuous reaction to completion when in the presence of body fluids. The previously mentioned *in-vivo* data for borate glasses in bone repair also indicate that immune response is likely to be minimal [24,25,32].

The borate glass studied by Richard known as 45S5B1 (Table 1) [17] successfully bonded to bone and reacted to form HA *in-vivo*. Huang, used *in-vitro* weight loss

experiments to show that a 45S5B1 glass reacted significantly faster than the well known and widely studied silicate based 45S5 glass [33]. Jung et al analyzed the *in-vitro* weight loss data from Huang and found that the reaction kinetics of the 45S5B1 glass was approximately five times greater than that of the 45S5 [31]. The 45S5B1 glass reacted in a controllable and continuous manner until the glass was completely reacted, while the 45S5 silicate glass reached a point where the mechanism for HA conversion reaction changed and the reaction kinetics decreased significantly [31,33].

Through preliminary experiments, the 45S5B1 glass crystallized easily upon heating and could not be heat treated to form a three dimensional porous scaffold without crystallizing. The 45S5B1 glass was therefore deemed unusable as a scaffold material and a new glass was needed that was more suitable for thermal processing.

Another bioactive glass known as 13-93 (Table 1) is a silicate based glass containing 53wt% SiO_2 along with materials such as MgO and K_2O that allow glass fibers to be pulled which can be heat treated to make three dimensional porous scaffolds without crystallization [34-36]. The 13-93 glass was modified similarly to the 45S5 glass by replacing all the SiO_2 with B_2O_3 [33,37]. This glass is hereafter referred to as 93B3 (Table 1). The 93B3 glass has reaction kinetics similar to the 45S5B1 glass [32], and, can be easily pulled into fibers and can be heat treated to form a three dimensional porous scaffold [32].

The purpose of the present work was to investigate 93B3 glass fiber scaffolds in a mammalian *in-vivo* environment to determine if these scaffolds would be useful in treating hard and soft tissue defects.

1.3. MATERIALS AND METHODS

1.3.1 Glass and Fiber Preparation

The bioactive 93B3 glass (Table 1) was melted at 1050^{o}C in a furnace for one hour in a platinum crucible. The glass batch was made using reagent grade chemicals of H_3BO_3, $CaCO_3$, Na_2CO_3, $MgCO_3$, $NH_4(H_2PO_4)$, and K_2CO_3. Fibers in the range of 100 to 300µm were hand pulled from the melt, collected, and broken into ~2 to 3mm lengths which were used to manufacture porous randomly oriented fiber scaffolds.

1.3.2 Scaffold Preparation

Seventy milligrams of 93B3 glass fibers (weighed using a Sartorius model R200D (Sartorius Corporation, Edgewood, NY) balance accurate to ±0.1mg) were placed inside a cylindrical ceramic (mullite) mold. The molds holding the randomly oriented glass fibers were placed into an oven preheated to 575^{o}C, and heated for 45 minutes. After heating, the molds were removed from the oven and cooled to room temperature. The scaffolds, 7 ± 0.1 mm in diameter and 2 ± 0.2mm thick and were stored in a desiccator until used. The scaffold shown in Fig 1 is representative of an as-made three dimensional scaffold composed of self-bonded, randomly oriented 93B3 fibers.

1.3.3 Scaffold Porosity

The open, interconnected porosity of the scaffolds was measured using a liquid displacement technique. The scaffolds were first weighed with a digital scale (Mettler Toledo XS105 ±0.00001g) to obtain a dry weight (M_1), and then submerged in kerosene under vacuum for one hour to fill the open pores with kerosene. The scaffold was weighed while suspended in kerosene (M_2), and again while saturated with kerosene in air (M_3). The open porosity (P_o) of the scaffold was calculated from Eqn.1.

$$P_o = \frac{M_3 - M_1}{M_3 - M_2} \times 100\% \quad (1)$$

The open porosity of the 93B3 scaffolds was measured prior to implantation into the rats, and the average open porosity calculated from 12 scaffolds by Eqn 1. was 51 ± 2%.

1.3.4 Scaffold Sterilization and Implantation

Scaffolds of 93B3 were dry heat sterilized in a fused silica glass vial covered with aluminum foil by heating to 300^{o}C in a small oven (Ney Vulcan 3-130) for four hours. Once cool, the scaffolds were ready for implantation.

Two rats were used for the *in-vivo* subcutaneous experiment were Fisher 344 rats (Fisher Scientific, St. Louis MO) between the age of 10 and 12 weeks. The rats were anaesthetized with a mixture of isoflorine and oxygen and shaved to remove hair from the base of the neck to the base of the tail. Loose hair was removed from the animal by washing first with iodine and then 70% ethanol prior to incisions.

Figure 2 shows the location of the four implant sites, above each shoulder and above each hind leg, on the back of the rat. A pocket ~15mm wide by 15mm long was made under the skin at each site for scaffold placement. The image in Fig 3 shows a scaffold being inserted into subcutaneous tissue. After implantation, the implant site was gently compressed to remove air, and the incision was sealed with super glue. After all four scaffolds were implanted; the rat was marked by labeling the ear, injected with 0.2ml of penicillin, and placed on a heating pad and exposed to fresh air during recovery.

1.3.5 X-Ray Diffraction

A 93B3 scaffold was x-rayed (Scintag XDS 2000 using Cu K_α radiation with a step scan mode with a 0.05^{o} step) after four weeks *in-vivo* over the range of 10 to 70 degrees 2θ to determine what crystalline phase(s), if any, were present.

1.3.6 Micro Raman

Micro Raman (LabRAM ARAMIS, Horiba Jobin Yvon) was used to analyze the reacted 93B3 fibers from scaffolds implanted for four weeks in rat subcutaneous tissue. A 50x objective was used to view the fibers, and the spectra were collected using a diode laser (785nm) with a collection time of five seconds. LABSpec5 software was used to capture the image and analyze the peak positions.

1.3.7 Scanning Electron Microscopy

An environmental scanning electron microscope ESEM (ESEM FEG XL30 from FEI, Hillsboro, OR (Formerly Philips)) was used to image the cross section of a 93B3 scaffold implanted four weeks. The scaffold was sectioned with a razor blade to expose the tissue and fibers located inside the scaffold. The scaffold section was coated with approximately 100nm of Au/Pd to minimize charging effects.

1.3.8 Scaffold Recovery, Fixation, and Dehydration

After four weeks, the scaffolds were excised for histological and SEM analysis. The animals were sacrificed in a sealed container filled with CO_2. The scaffolds were removed from the subcutaneous tissue and fixed in 5mL of 10% formalin solution (10:1 formalin to scaffold volume ratio) for four days. The scaffolds were then dehydrated with a series of ethanol solutions from 70% to 100% in a microwave tissue processor (EBSciences H2850 Microwave Processor). The microwave was set to 70% power, the sample temperature was set to 37^{o}C, and the microwave was operated for 2.5 minutes for each solution. The scaffolds were in each solution for a minimum of 15 minutes (including time in the microwave).

1.3.9 Sample Preparation and Staining (Histology)

Dehydrated scaffolds were placed in a tissue processor (AutoTechnicon Model 2A) filled with fluid paraffin mounting wax (Paraplast Tissue Embedding Medium, McCormick Scientific LLC) at 45^{o}C for four hours to allow the wax to infiltrate the scaffold and tissue. The scaffold was then mounted in a wax block for histological sectioning with a paraffin mounting system (Leica EG 1150H). Sections, 18μm thick, were cut with a microtome (Leica RM 2235 microtome) with TBS Shur/sharp blades, (Triangle Biomedical Sciences, Durham NC) and floated on a water bath (Lipshaw Electric Tissue Float, model number 375, Detroit MI) (40^{o}C) prior to mounting on a glass slide (Fisher Brand Superfrost microscope slides, St. Louis MO). Three to four tissue sections were placed on a single slide, and dried overnight on a slide dryer (Fisher Scientific slide warmer, St. Louis MO). The slides were stained with hematoxylin and eosin (H&E), periodic acid schiff (PAS), and Verhoeff's Van Gieson (VVG) to identify soft tissues and verify the presence of blood vessels. Stained slides were viewed with an optical microscope (Olympus BX50, Olympus Optical Co) at magnifications of 40, 200, and 400X. Imaging software (DP Controller, Olympus Optical Co) was used to capture images.

1.3.9.1 Hematoxylin and Eosin (H&E) Staining Protocol

H&E staining was completed in a Leica CV 5030 Autostainer XL. The slides were immersed in 95% xylene, 5% ethanol for two minutes (two stations) and 100% xylene for two minutes (two stations) to remove the wax. Each slide was dipped 15 times in distilled water, and immersed in hematoxylin stain for three minutes. The slides were washed in a series of four distilled water stations, one minute each, followed by 15 dips

in acid alcohol and immersion in eosin stain for one minute. The slides were then dewatered with a series of ethanol solutions, 80% for 30 seconds, 95% for one minute (two stations), and 100% ethanol for one minute (three stations). The slides were immersed in xylene for one minute (three stations) prior to mounting with a coverslip.

1.3.9.2 Periodic Acid Schiff (PAS) Staining Protocol

Prior to staining, slides were deparaffinized in xylene and hydrated in distilled water. Sections were placed in 0.5% periodic acid solution for five minutes at room temperature and then washed with a series of three washes in distilled water. Sections were then placed in the Schiff reagent for 15 minutes followed by two washes in 0.55% potassium metabisulfite to remove excess stain. Sections were rinsed in tap water for 10 minutes to develop color prior to a 30 second counter stain with 1% light green. Sections were washed with tap water and then dehydrated in a 95% ethanol solution. Xylene was used to remove all the alcohol prior to mounting with a synthetic resin. After staining, blood vessels should be light blue, and red blood cells green.

1.3.9.3 Verhoeff's Van Gieson (VVG) Staining Protocol

Slides were deparaffinized in xylene and hydrated in distilled water. Slides were immersed in Verhoeff's stain for 20 seconds and then washed in a series of distilled water baths for one minute (three stations). Sections were placed in 2% ferric chloride until elastic fibers were distinct and the background was colorless to light gray under microscopic view. The sections were then rinsed in distilled water before immersion in sodium thiosulfate for one minute. Sections were washed in tap water for five minutes prior to counterstaining in Van Gieson stain for one minute. Sections were then

dehydrated in a series of ethanol solutions, cleared with xylene, and mounted with a coverslip.

1.4. RESULTS

1.4.1 93B3 Scaffold Removal

Figure 4 shows a 93B3 scaffold after four weeks *in-vivo* before being removed from the subcutaneous tissue. The area labeled SM is the skeletal muscle and the area labeled ST is the subcutaneous tissue. Soft tissue had grown into the scaffold with vessels (black arrows) visibly penetrating the outer perimeter. The originally transparent (colorless) 93B3 fibers became white and the scaffold was soft to the touch, which indicates that the fibers had reacted with body fluids to form amorphous calcium phosphate (ACP) or possibly a crystalline calcium phosphate such as HA.

1.4.2 Backscattered SEM of a Sectioned 93B3 Scaffold After Four Weeks *In-Vivo*

The SEMBSE image in Fig 5 shows the cross section of a 93B3 scaffold after four weeks *in-vivo*. The soft tissue is black, and the reacted fibers are a light gray. Several of the fibers were broken while cutting; but, many of the fibers that did not break are hollow as shown in Fig 5.

A fiber from the 93B3 scaffold which had fully reacted is shown in Fig 6. The image in Fig 6A shows the end of a reacted fiber, as the fiber is cut perpendicular to its longitudinal fiber axis. The center of the fiber has a relatively rough surface and does not contain any original glass. Figure 6B shows a higher magnification of the hollow core of the fiber where several nodules of calcium phosphate are present. The nodules are magnified in Fig 6C, and are made of a porous network of nanocrystals. Figure 6D is a magnified image of the nanocrystals in Fig 6C, and the needle-like structure is similar to

that of HA. The crystals are approximately 50nm in length, and the overall structure is highly porous.

1.4.3 X-Ray Diffraction of a 93B3 Scaffold after Four Weeks *In-Vivo*

The XRD pattern shown in Fig 7 is from a reacted 93B3 fiber scaffold after four weeks *in-vivo*. The peaks present match those for HA ($Ca_{10}(PO_4)_6(OH)_2$) PDF card #72-1243, a mineral similar to that found in the inorganic component of bone. The broad peaks in the XRD pattern are due to the nano-sized crystals of hydroxyapatite, see Fig 6D.

1.4.4 Micro Raman of a Reacted 93B3 Fiber after Four Weeks *In-vivo*

A reacted 93B3 fiber analyzed by micro raman and the four spots analyzed across the fiber diameter are shown in Fig 8. A white dashed line has been added to show the fiber perimeter more easily. The raman spectra are shown in Fig 9, position one is at the outer edge of the fiber and position four at the center of the reacted fiber. The three peaks associated with HA (431cm^{-1} (PO_4^{3-} v2), 965cm^{-1} (PO_4^{3-} v1), 1065 to 1070cm^{-1} (CO_3^{2-} v1) and 1076cm^{-1} PO_4^{3-} v3) [38] are denoted by dashed lines. The solid lines are due the mounting medium (PMMA) as indicated by the spectra at the top of Fig 9.

Positions three and four located toward the center of the fiber in Fig 8 have the highest intensities for the phosphate and carbonate peaks indicating a difference in the amount of each species distributed throughout the fiber. The presence of a carbonate peak at 1065 to 1070cm^{-1} (CO_3^{2-} v1) indicates that the fibers are carbonated, similar to natural bone. The difference in the amount of phosphate and carbonate measured could be due to differences in the density of the reacted fiber.

1.4.5 Histological and Vascular Assessment of Soft Tissue

A cross sectioned 93B3 glass scaffold prior to implantation into soft tissue would look similar to that shown in Fig 10. The fibers (dark gray) are randomly oriented, so the shape of the fibers (circular to elliptical), is dependant on the fiber orientation. Several fibers are indicated with arrows, and the open space (porosity) in between the fibers (lighter color) is filled with a transparent epoxy. The porosity in the scaffold is mostly interconnected and there are few, if any, closed pores.

1.4.6 Hematoxylin and Eosin Stain (H&E)

The images of the 93B3 scaffold (four weeks *in-vivo*) stained with H&E in Fig 11, look significantly different from that in Fig 10. Soft tissue (purple) that has filled essentially all of the interconnected pores between the fibers, and the fibers (originally solid) have reacted with the body fluids and become hollow. The tissue throughout the scaffold is healthy with no sign of any significant immune reaction or foreign body reaction like a walling off of the entire scaffold or the individual fibers.

Figure 12A shows that blood vessels are present in both the soft tissue between the fibers and in the soft tissue that had grown into what were the hollow cores of the reacted fibers. The scaffold section in Fig 12A had fibers (F) that reacted and became hollow that subcutaneous tissue had grown inside. There is an ordered line of red blood cells at the center of the image in Fig 12A indicating a small blood vessel ~10μm in diameter (white arrows). The image in Fig 12B shows a larger blood vessel in the center of the image with significantly more red blood cells than in Fig 12A. The vessel lining is denoted by the white arrows, is approximately 30 to 40μm in diameter and contains numerous red blood cells.

Figures 13A and 13B are images of H&E stained sections of a 93B3 scaffold that had been implanted in the rat for four weeks. The two parallel purple regions marked (F) that run from the top left to bottom right of the image in Fig 13A are the outer edges of a reacted fiber, cut parallel to its longitudinal axis, to reveal a hollow core containing soft tissue (purple) and red blood cells (red dots) as indicated by the white arrow. Another fiber shown at the center of Fig 13B, which was cut perpendicular to its longitudinal axis, contains both soft tissue and red blood cells (vertical arrows) in what appears to be a blood vessel.

1.4.7 Verhoeff's Van Gieson Stain (VVG)

The images in Fig 14A and 14B are from a sectioned 93B3 scaffold, implanted in rat subcutaneous tissue for four weeks, which was stained with VVG (Verhoeff's Van Gieson) that stains specifically for elastic tissue, veins, arteries, and other vessels. The cell nuclei and blood vessel lining (elastin) stains black, collagen or other connective tissue is pink, and red blood cells are yellow.

The image in Fig 14A shows several reacted fibers (F) along with a circular shaped vessel in the center of the image (black arrow) and a black rim (elastin) filled with red blood cells (yellow dots). The image in Fig 14B, stained positive for a vessel, white arrow at center, in the hollow void of a reacted fiber (F), and there is connective tissue (pink) surrounding a black elastin ring (vessel wall) which contains red blood cells (yellow dots). A second vessel at the bottom center of Fig 14B, between two fibers, is shown by the black arrow. As is apparent from Figs. 14A and 14B, the dark color of the nuclei can make it difficult to determine whether or not there was a positive stain for elastic lining.

1.4.8 Periodic Acid Schiff Stain (PAS)

The images in Fig 15A and 15B are images of sections from a 93B3 scaffold implanted four weeks in a rat that were stained with Periodic Acid Schiff (PAS). The PAS stain bonds to glucose residue in tissue. Glucose is present in muscle, liver, and red blood cells, but vessel lining is also stained due to the diffusion of glucose from the red blood cells to the surrounding tissue. Connective tissue is light green, red blood cells are bright green, vessel lining is blue, macrophages are yellow or brown, and HA stains purple.

The vessels in Fig 15A are marked by arrows. Several of the vessels contain the bright green labeled red blood cells. There are also macrophages distributed throughout the section, as denoted by the black circles in the tissue surrounding the reacted fibers. Figure 15B shows a reacted fiber, cross sectioned perpendicular to its longitudinal axis, in the center of the image (dashed circle). There is a vessel (blue circle) with red blood cells (bright green) present in the hollow fiber (F) void as indicated by the black arrow.

1.5 DISCUSSION AND CONCLUSIONS

Upon removal of the 93B3 implanted scaffolds, soft tissue had penetrated deep into the scaffolds, and several blood vessels had grown adjacent to the scaffold surface as shown in Fig 13. There was no visible inflammation or infection surrounding the scaffolds and there was no sign of fibrous tissue that is typically present surrounding an object which the body considers a foreign body. This was an important indication that the scaffold was not being rejected by the animal. The lack of inflammation surrounding the scaffold upon excision agrees with work done by Richard using 45S5B1 glass particles in contact with bone [17].

The 93B3 scaffolds were no longer rigid when removed from the animals, as much of the original mechanical strength was lost when the glass converted to the porous HA. The soft tissue that had bonded to the fibers as it grew into the scaffold was holding the reacted fibers together. While a decrease in strength is not necessarily a desirable quality for bony defects, especially load bearing defects, the softening of the material may be an advantage for the treatment of soft tissue such as muscle and skin.

The XRD patterns from the 93B3 scaffolds implanted for four weeks matched HA, PDF card # 72-1243. The peaks are relatively broad due to the nano-sized crystals of HA shown in Fig 6D. The needle-like nanocrystals of HA that formed *in-vivo* from the 93B3 glass look similar to those from a silicate glass soaked in simulated body fluid (SBF) for 30 days indicating that the borate glass reacts in a similar manner as the well known and commercially used bioactive glasses [27]. The HA is carbonated similar to natural bone as shown by the micro raman in Fig 9.

The PAS stained sections in Figs 15A and 15B clearly show that blood vessels were present in both the open pores of the scaffold and inside the hollow core of reacted fibers. Macrophages were also identified, but, they were in the soft tissue and not specifically surrounding any of the HA from the reacted glass. The presence of macrophages in regenerating tissue is normal as they release growth factors required for tissue growth.

The histological staining proved that soft tissue had significantly penetrated the 93B3 scaffold in four weeks and had filled not only the open pores of the scaffold, but also the relatively large voids (50 to 150μm diameter) formed in the hollow fibers. The relatively low chemical durability of the 93B3 glass releases calcium when in contact

with body fluids and reacts with phosphate present in the body fluids to form hydroxyapatite on the surface of the glass fiber. This reaction continues until the glass fiber has fully degraded and released all of the calcium. The amount of calcium in the glass determines the HA wall thickness that is formed when reacted with body fluids.

The reacted fibers shown in Fig 5 and Fig 11 show that almost all of the fibers have become hollow, and most had soft tissue that had filled the hollow cavity. How the soft tissue got inside the cavity is not well understood, but the tissue may have gained access when the 93B3 fibers formed HA, lost mechanical strength, and fractured from the regular movement and activities of the animal. Regardless of how the tissue entered the hollow fiber cavities, both soft tissue and blood vessels were present. The fact that blood vessels entered the hollow fibers and grew in the direction of the hollow cavity indicated that these hollow fibers may have use as vascular or other tissue guides. Vessels were present in several of the hollow fibers and stained with either VVG or PAS for verification as shown in Figs 14, and 15.

One example of a vessel growing a significant distance (several hundred microns) along the hollow core of a fiber is shown in Fig 16A and 16B. The hollow fiber (F) of interest is the in the center of Fig 16A and has parallel dashed lines on either side of the vessel. Many of the HA fibers were debonded from the slide during the staining process and appear as white ellipses or circles depending upon the fiber orientation, but, the soft tissue was well adhered to the glass slide. Figure 16B is a magnified view of the reacted fiber in Fig 16A. The black horizontal arrows point to the blue vessel lining travelling from one end of the fiber to the other. The vessel has a diameter of about 20 to 30μm and

is approximately 700 to 800μm in length inside the hollow fiber. The exact length of the vessel could not be determined due to the orientation of the fiber when it was cut.

Boron, although not entirely understood, is hypothesized to play an important role in several developmental and biological functions. If boron is removed from the diet of a developing animal such as a rat, there is a significant decrease in the animal's size and the bones are not well developed [14]. Boron is in the diet of humans as it is found in most vegetables and nuts [1-3]. At low levels (1 to 20 mM BA) boron has been found to have a positive effect on mRNA uptake of human placental cells *in-vitro*, which means that the BA has a stimulatory effect on cell activity similar to a growth factor [39].

Assuming the 93B3 glass fibers reacted (lost weight) similarly to the way other borate glasses have been shown to do *in-vitro* [33], and the fibers were fully reacted in four weeks, it is possible to estimate the BA concentration in the adjacent tissue (tissue inside scaffold). In estimating the BA concentration, blood flow rates were used which were measurements of blood flow through rat adipose tissue [40]. The weight of the rats used in the present work was ~300g each.

The following is a description and background information required for making the BA concentration calculations. The 93B3 as-made scaffolds each weighed ~70mg prior to implantation. From Table 1, each scaffold was 53wt% B_2O_3 which means that a 93B3 scaffold contained 0.037 grams B_2O_3 or 0.066g BA (H_3BO_3), or $1.07E^{-3}$ moles of BA as that is the form boron takes in an aqueous environment such as body. Assuming it took four weeks, or 28 days, for the fibers to completely react and the fibers lost weight (reacted) linearly over the time period, the BA release was $3.82E^{-5}$ moles per day.

The Benchmark Dose Limit (BMDL) for boric acid as determined from a series of animal experiments is 55mg/kg/day [2]. A single 93B3 scaffold contained enough boron to produce 66mg of BA when fully reacted, which divided equally over 28 days is 2.36mg/day of BA. When the weight of a rat (300g) is taken into account, the release of H_3BO_3 from a scaffold is 7.87mg/kg/day. This simple calculation indicates that the concentration of BA in a single 300g rat should have been well below the BMDL. A 300g rat should be able to tolerate over seven times the mass of a single 93B3 scaffold (~500mg of glass) before any observable effect might be seen.

The concentration of BA in the vicinity of the infiltrated soft tissue was estimated to determine the concentration of BA present. The tissue inside the scaffold was estimated to be ~50mg just after the scaffold was removed by assuming complete reaction of the glass to HA (weight loss) and the weight of the scaffold and infiltrated tissue after removal from the subcutaneous tissue. The fluid flow through the scaffold was assumed to be due to blood flow, so the highest average (0.4ml/min/gram of tissue) and lowest (0.1ml/min/gram of tissue) flow rates from published data for rat adipose tissue were used in determining the concentration range of BA in the tissue [40]. The highest flow rate was measured while the rats were active and feeding, while the lowest was when the animals were sleeping.

Assuming the minimum flow rate for a 24 hour period, the amount of blood that would pass through the tissue in the scaffold was calculated to be 7.2ml. This number was calculated from Eqn 2.

$$\text{Vol. of blood} = \text{Blood flow rate} * \text{Mass of tissue} * \text{Time} \qquad (2)$$

The calculation for the minimum flow rate is shown below:

(1440min/day)(0.1ml/min*g)(1 day) (0.05g) = 7.2ml or 0.0072L

Taking the value calculated for the amount of BA released per day from a scaffold ($3.82E^{-5}$ moles/day) and dividing it by 0.0072L, the average concentration for an entire day is 5.29mM BA.

A similar calculation was made for the highest flow rate. Assuming the highest blood flow rate for a 24 hour period, the amount of blood that would pass through the soft tissue was 28.8ml. The four times greater volume of blood lead to a BA concentration that decreased by four times to the estimated concentration of 1.32mM BA.

The two concentrations calculated represent the highest and lowest BA concentration would reach, with the actual value fluctuating depending on the activity of the rats. The two calculated values have been compared to the *in-vitro* mRNA uptake data from human placental cells cultured with low levels of BA as shown in Fig 17. The total mRNA (nmol) uptake is plotted vs. concentration of BA in the culture media (mM), and the two calculated values from the present work are denoted by vertical red lines. The two concentrations fall in the stimulatory range (2 to 3X increase) BA had on the mRNA uptake of human placental cells. This could be an indicator that the BA released from the scaffolds may be having a positive effect on the nearby tissue. The increase in the mRNA with the human placental cells was described as similar to the effect of a growth factor would have on the cells, so the presence of BA in the tissue adjacent the scaffold could have enhanced growth characteristics.

Based on these simple calculations and information from the literature, it is likely that boron released from a scaffold could be expected to have a positive impact on the surrounding tissue. The hypothesis of a positive interaction between the boron released

from the 93B3 scaffolds and the soft tissue is confirmed by the histology in Figs 11 to 16. Soft tissue had filled the open pores of the 93B3 scaffolds, tissue had bonded with the reacted fibers, and blood vessels were growing not only in the open pores, but also inside the hollow cores of many of the reacted fibers.

In conclusion, scaffolds composed of randomly oriented, bioactive 93B3 fibers reacted with the body fluids in rat subcutaneous tissue to form a nanocrystalline carbonated HA. The interconnected and open pores in the scaffolds nearly filled with soft tissue after four weeks *in-vivo*. The initially solid glass fibers reacted in such a way that they became hollow. Soft tissue as well as blood vessels infiltrated the hollow core of the reacted fibers and the blood vessels tended to be oriented along the fiber axis. Scaffolds composed of bioactive borate glass fibers could have uses for future applications as tissue guides for blood vessels, bone, or other tissues.

Comparing published *in-vitro* data for the effect of BA on human placental cells with calculations from the present work on the estimated concentrations of BA in nearby tissue, the BA released from the 93B3 scaffolds falls in the range that was found to stimulate mRNA uptake in human placental cells. The calculated concentration of boron released from the 93B3 scaffolds is low compared to most published work studying the effects of BA concentration on biological interaction. The effects of BA concentrations in the range of those calculated (1 to 6mM) are still relatively unstudied, but could prove stimulatory and essential for biological functions.

Both the PAS and VVG stains positively stained vessels from the 93B3 scaffolds. The PAS stain appeared to be more useful as the colors of the vessel and the connective tissue were sufficiently different for vessel verification; but the color scheme of the PAS

was easier to interpret than the VVG. The PAS stain also positively stained macrophages which is important to make sure the foreign material is not causing an immune reaction.

ACKNOWLEDGEMENTS

The authors would like to thank Vernon Modglin for his assistance with the scaffold implantation and excision, Dr. Anne Maglia from S&T for her support and use of her histological equipment, Dr. Eric Bohannon from S&T for the X-Ray analysis, Dr. Vladimir Dusevich from the University of Missouri-Kansas City (UMKC) for help with the ESEM work, Penny McCormick from Phelps County Regional Medical Center (PCRMC) for the H&E staining, and Jackie Taylor from (UMKC) for the PAS and VVG staining.

1.6 REFERENCES

1. Smallwood C. Boron in Drinking-water. Volume 2. Geneva: W. H. O. 2003.
2. Price CJ, Strong PL, Marr MC, Myers CB, Murray FJ. Developmental Toxicity NOAEL and postnatal recovery in rats fed boric acid during gestation. Fund. Appl. Tox. 1996;32:179-193.
3. Smallwood CL, Lipscomb J, Swartout J, Teuschler L. Toxicological Report of Boron and Compounds. Washington D.C.: EPA; 2004.
4. Culver BD, Shen PT, Taylor TH, Lee-Feldstein A, Anton-Culver H, Strong PL. The Relationship of Blood and Urine-Boron to Boron Exposure in Borax-Workers and the Usefulness of Urine-Boron as an Exposure Marker. Environ. Health Perspec. 1994;102:133-137.
5. Draize JH, Kelley EA. The urinary excretion of boric acid preparations following oral administration and topical applications to intact and damaged skin of rabbits. Tox. Appl. Pharm. 1959;1:267-276.
6. Ku WW, Chapin RE, Moseman RF. Tissue disposition of boron in male Fischer rats. Tox. Appl. Pharm. 1991;111:145-151.
7. Becker RO, Spadaro JA, Berg EW. The Trace Elements of Human Bone. J. Bone and Joint. Surg. 1968;50:326-334.
8. Alexander GV, Nusbaum RE, MacDonald NS. The boron and lithium content of human bones. J. Bio. Chem. 1951;192:489-496.
9. Forbes RM, Cooper AR, Mitchell HH. On the occurrence of beryllium, boron, cobalt and mercury in human tissues. J. Bio. Chem. 1954;209:857-865.
10. Nielsen FH. Facts and fallacies about boron. Nutrition Today 1992;27:6-12.
11. Mertz W. Essential trace metals: new definition based on new paradigms. Nutr. Review 1993;51(10):287-295.
12. Devirian TA, Volpe SL. The physiological effects of dietary boron. Critical Reviews in Food Sci. and Nutr. 2003;43(2):219-231.
13. Bilezikian JP, Raisz LG, Rodan GA, editors. Principles of Bone Biology. San Diego CA: Academic Press; 1996.
14. Nielsen FH. Nutritional Requirements for Boron, Silicon, Vanadium, Nickel, and Arsenic: Current Knowledge and Speculation. FASEB Journal 1991;5:2661-2667.
15. Heindel JJ, Price CJ, Schwetz BA. The developmental toxicity of boric acid in mice, rats, and rabbits Environmental Health Perspectives 1994;102:107-112.
16. Huang W. Personal Communication. 2008.
17. Richard M. M.S. Thesis. Rolla, MO: University of Missouri-Rolla; 2000.
18. White JE. PhD Dissertation. Rolla, MO: University of Missouri-Rolla; 1995.
19. Conzone S. PhD Dissertation. Rolla, MO: University of Missouri-Rolla; 1999.
20. Conzone S. M.S. Thesis. Rolla, MO: University of Missouri-Rolla; 1996.
21. Han X. M.S. Thesis. Rolla, MO: University of Missouri-Rolla; 2003.
22. Vanderspiegel N. M.S. Thesis. Rolla, MO: University of Missouri-Rolla; 2004.
23. Fears K. M.S. Thesis. Rolla, MO: University of Missouri-Rolla; 2001.
24. Jai W-T, Zhang X, Luo S-H, Liu X, Huang W-H, Rahaman MN, Day DE, Zhang C-Q, Xie Z-P, Wang J-Q. Novel borate glass/chitosen composite as a delivery vehicle for teicoplanin in the treatment of chronic osteomyelitis. Acta Biomaterialia. 2009.

25. Liu X, Xie Z, Zhang C, Pan H, Rahaman MN, Zhang X, Fu Q, Huang W. Bioactive borate glass scaffolds: in vitro and in vivo evaluation for use as a drug delivery system in the treatment of bone infection. J. Mater. Sci.: Mater. Med. 2009;online.
26. Gorustovich AA, Lopez JMP, Guglielmotti M, Cabrini ML. Biological performance of boron-modified bioactive glass particles implanted in rat tibia bone marrow. Biomed. Mater. 2006;1:100-105.
27. Yamamuro T, Hench LL, Wilson J. Handbook of Bioactive Ceramics Vol. I - Bioactive Glasses and Glass-Ceramics. Boca Raton FL: CRC Press; 1990.
28. Merolli A, Tranquiilli P, Guidi PL, Gabbi C. Comparison in In Vivo Response Between a Bioactive Glass and a Non-Bioactive Glass. J. Mater. Sci.: Mater. Med. 2000;11:219-222.
29. Leach JK, Kaigler D, Wang Z, Krebsbach PH, Mooney DJ. Coating of VEGF-releasing scaffolds with bioactive glass for angiogenesis and bone regeneration. Biomaterials 2006;27:3249-3255.
30. Leu A, Leach JK. Proangiogenic Potential of Collagen/Bioactive Glass Substrate. Pharma. Res. 2008;25(5):1222-1229.
31. Jung SB, Day DE. Conversion kinetics of silicate, borosilicate, and borate bioactive glasses to hydroxyapatite. Phy. Chem. Glass. 2009;50(2):85-88.
32. Fu Q. PhD Dissertation. Rolla: Missouri University of Science and Technology; 2009.
33. Huang W, Day DE, Kittiratanapiboon K, Rahaman MN. Kinetics and Mechanisms of the Conversion of Silicate (45S5), Borate, and Borosilicate Glasses to Hydroxyapatite in Dilute Phosphate Solution J. Mater. Sci.: Mater. Med. 2006;17:583-596.
34. Pirhonen E, Moimas L, Haapanen J. Porous Bioactive 3-D Glass Fiber Scaffolds for Tissue Engineering Applications Manufactured by Sintering Technique. Key Eng. Mater. 2003;240-242:237-240.
35. Jung SB. M.S. Thesis. Rolla, MO: University of Missouri-Rolla; 2007.
36. Jung SB, Day DE, Brown RF. Comparison of self-bonded three dimensional bioactive glass fiber scaffolds after in-vivo implantation in rats. J. Am. Cer. Soc. 2009, accepted.
37. Huang W, Rahaman MN, Day DE, Li Y. Mechanisms for Converting Bioactive Silicate, Borate, and Borosilicate Glasses to Hydroxyapatite in Dilute Phosphate Solution. Phy. Chem. Glass 2006;47B(6):1-12.
38. Suzuki M, Kato H, Wakumoto S. Vibrational analysis by raman spectroscopy of the interface between dental adhesive resin and dentin. J. Dent. Res. 1991;70:1092-1097.
39. Dzondo-Gadet M, R M-N, Hess K, Nabet P, Belleville F, Dousset B. Action of Boron at the Molecular Level. Bio. Trace Element Res. 2002;85:23-33.
40. Herd JA, Goodman HM, Grose SA. Blood flow rates through adipose tissue of unanesthetized rats. Am. J. Phys. 1968;214:263-268.

TABLES

Table 1 – Nominal Bioactive Glass Compositions (wt%)

Glass	SiO_2	B_2O_3	Na_2O	CaO	MgO	K_2O	P_2O_5
45S5	45	0	24.5	24.5	0	0	6
45S5B1	0	45	24.5	24.5	0	0	6
13-93	53	0	6	20	5	12	4
93B3	0	53	6	20	5	12	4

FIGURES

Figure 1 – Optical micrograph of an as-made 93B3 scaffold after heating for 45 minutes at 575^{o}C. The scaffold has a nominal diameter and thickness of 7 ± 0.1mm and 2 ± 0.2mm, respectively, with an average open and interconnected porosity of 51 ± 2%, n=12.

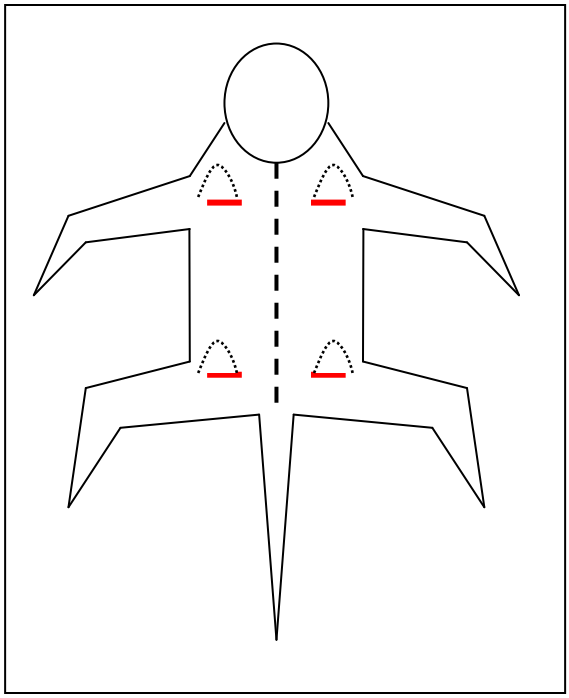

Figure 2 – Schematic showing scaffold implantation sites on the back of a rat. Implantation sites were approximately 15mm wide by 15mm long. The red line indicates the incision made in the skin, and the dotted arch represents the opening made under the skin.

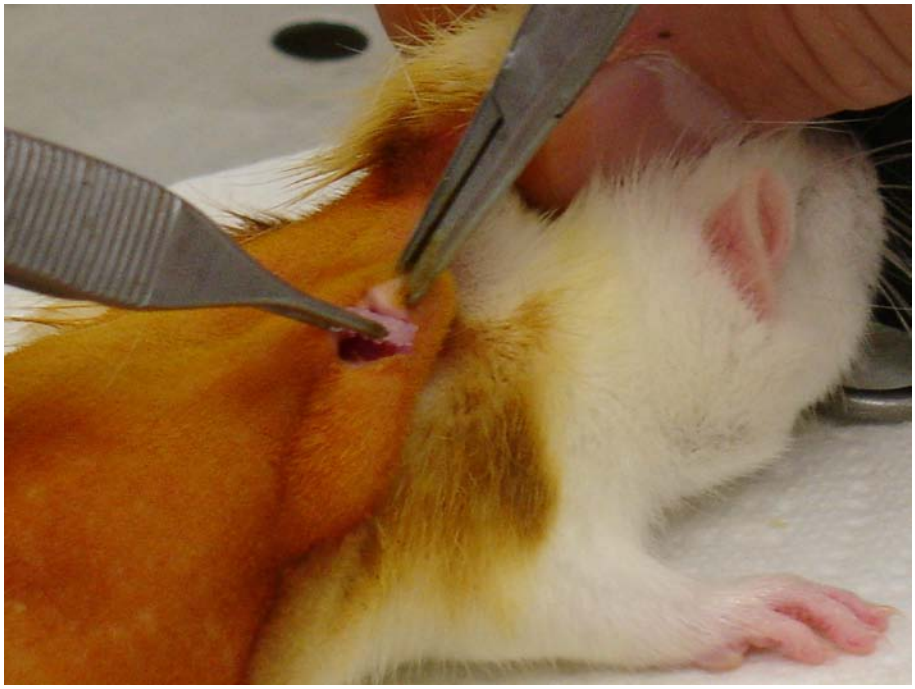

Figure 3 – Image showing the implantation of a 93B3 scaffold in the subcutaneous tissue. The hair was removed, and the skin has been cleaned and disinfected. The orange color on the back of the rat is from iodine.

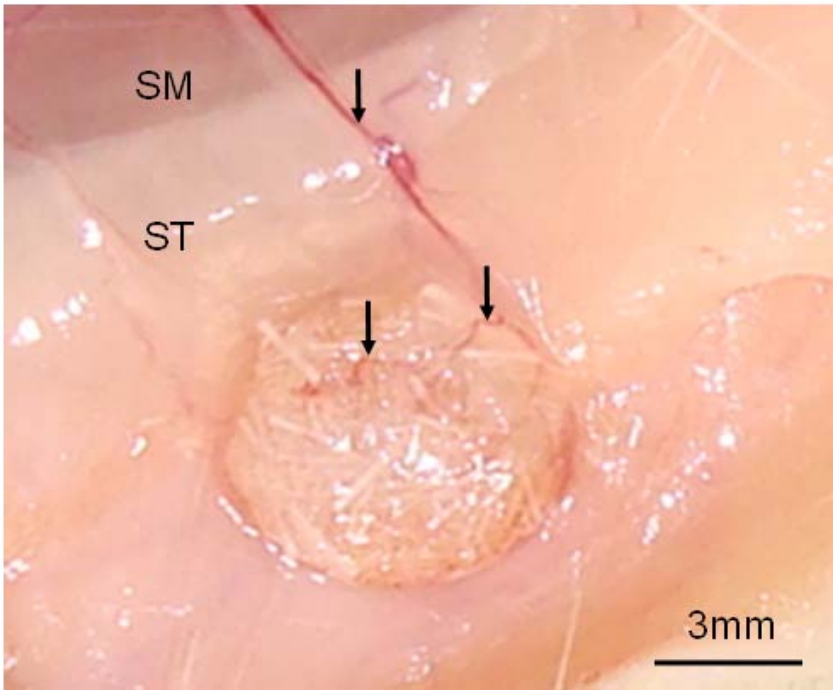

Figure 4 – Optical image of a 93B3 scaffold prior to removal from rat subcutaneous tissue. The skeletal muscle (SM) and subcutaneous tissue (ST) are labeled as well as vessels (black arrows) growing in the adjacent tissue. The scaffold was soft to the touch and the fibers were white indicating they had reacted with the body fluids.

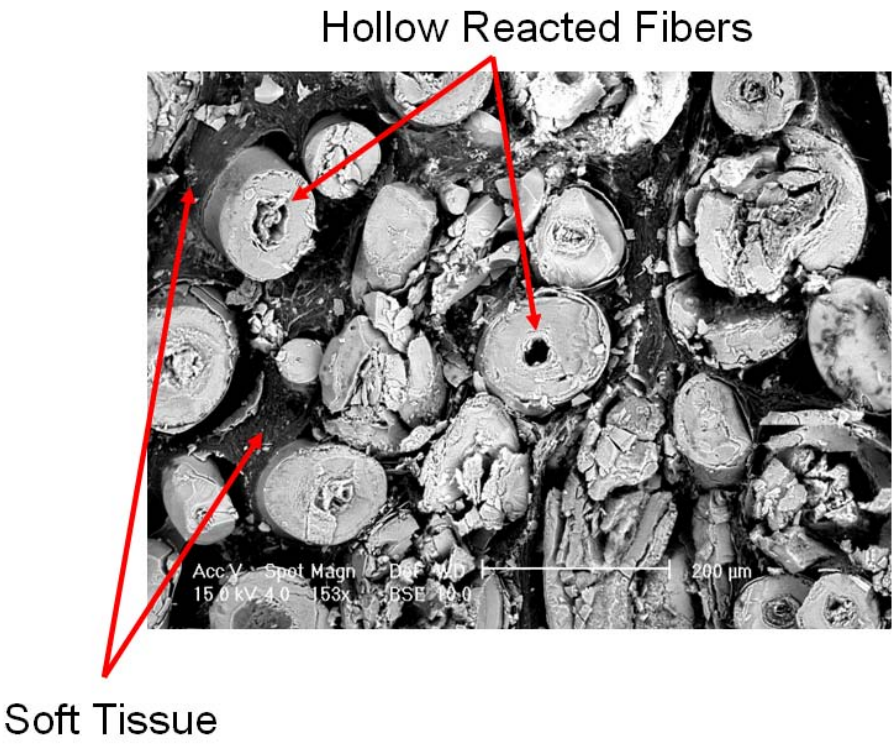

Figure 5 – SEMBSE micrograph of a cross section of a 93B3 scaffold after four weeks in the subcutaneous site in a rat. Soft tissue (dark gray) surrounds the reacted fibers (light gray). Many of the reacted 93B3 fibers have become hollow.

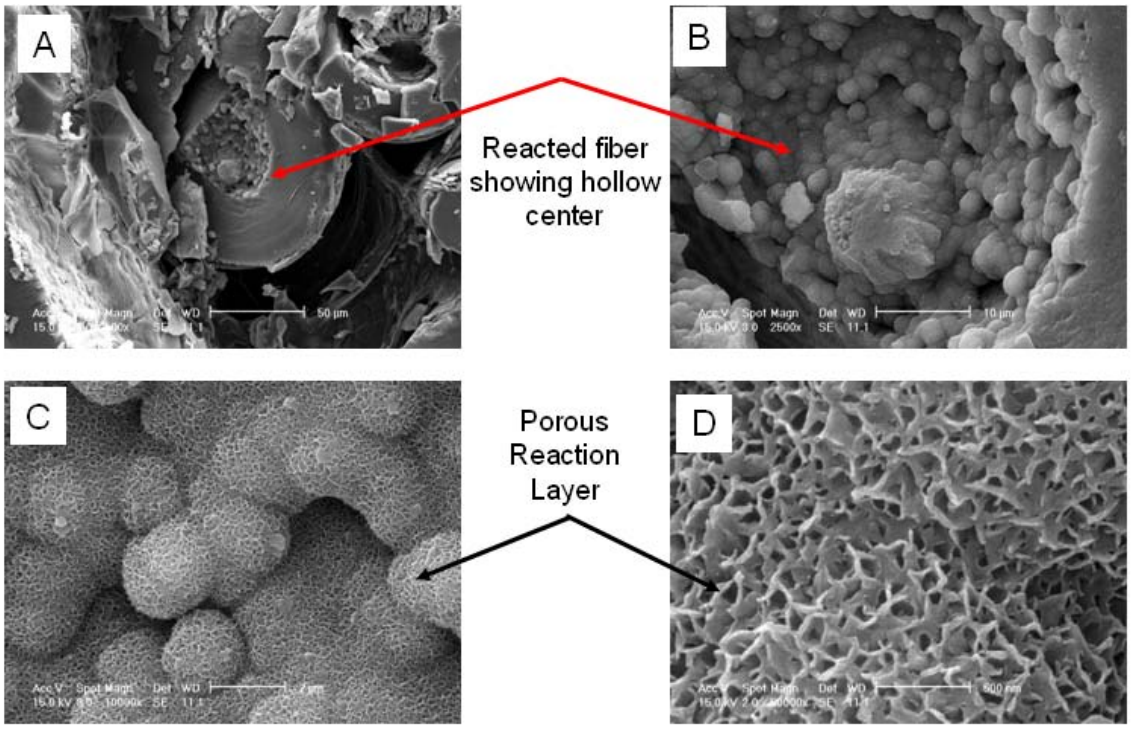

Figure 6 – A series of higher magnification SEM micrographs of reacted 93B3 fibers after four weeks in the subcutaneous site in a rat. Figure 6A shows the cross section of a reacted fiber having a hollow inner core. Figure 6B is a magnified view of the hollow core of the reacted 93B3 fiber in Fig 6A. Figure 6C is a magnified view of the nodules. Each nodule consists of a porous structure of nanocrystals and those are shown in Fig 6D.

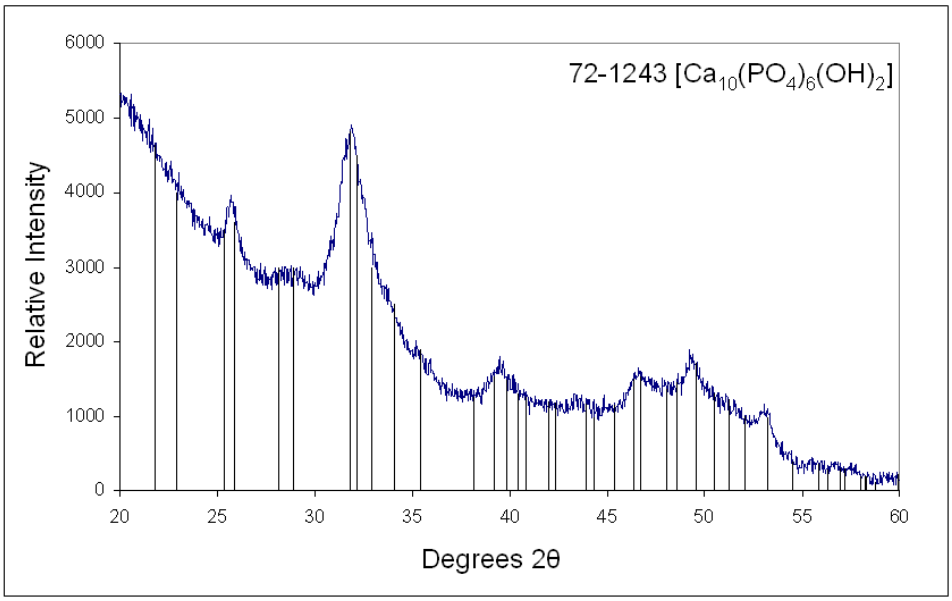

Figure 7 – XRD pattern for a 93B3 scaffold after four weeks *in-vivo*. The pattern matches hydroxyapatite, PDF card# 72-1243 (vertical lines). The peaks are relatively broad because of the nano sized hydroxyapatite crystals.

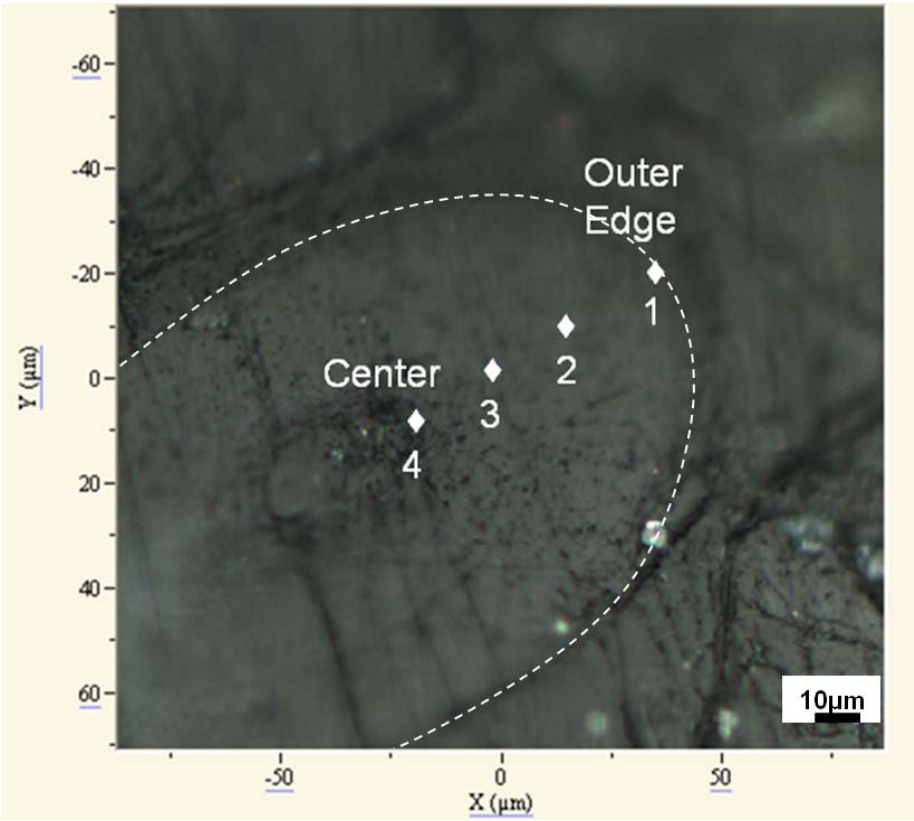

Figure 8 – Optical image of a 93B3 fiber reacted in rat subcutaneous tissue for four weeks, mounted in PMMA, and cross sectioned. The outer perimeter of the fiber is denoted by a dashed line, and the center and outer edge are labeled as indicated. The four locations inside the fiber were analyzed by micro raman and the spectra are shown in Fig 9.

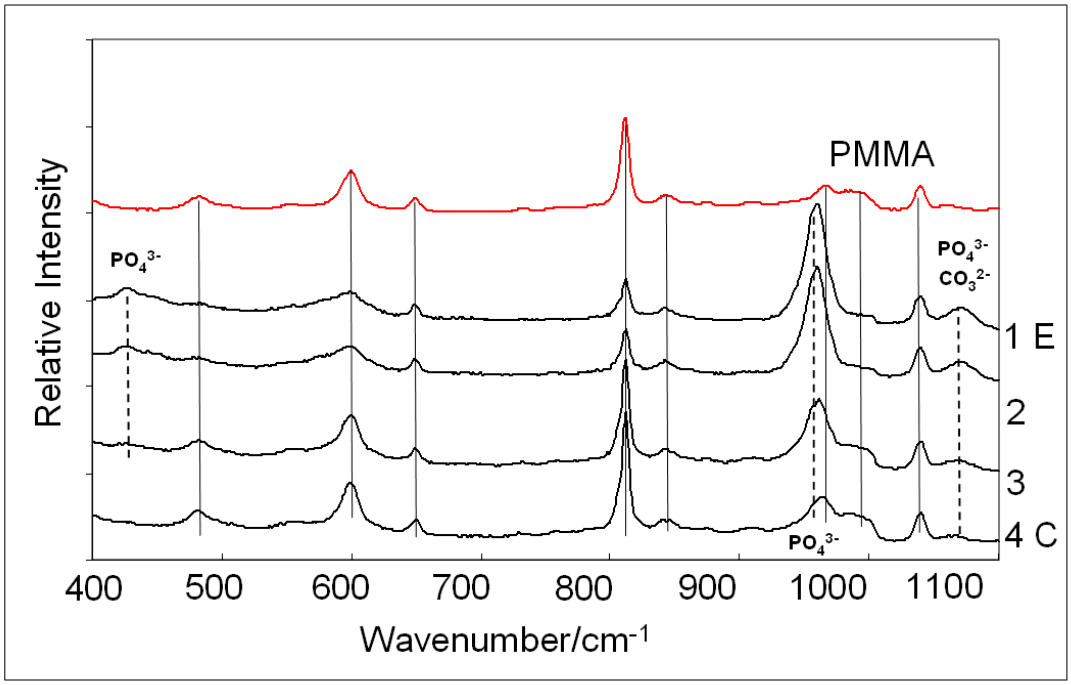

Figure 9 – Micro raman spectra for a 93B3 fiber that was implanted in rat subcutaneous tissue for four weeks. The peaks associated with HA are indicated by the dashed lines at (431cm^{-1} (PO_4^{3-} v2), 965cm^{-1} (PO_4^{3-} v1), 1065 to 1070cm^{-1} (CO_3^{2-} v1) and 1076cm^{-1} PO_4^{3-} v3) and the solid lines are for the mounting medium PMMA. At the top of Fig 9, the spectrum for PMMA mounting medium is shown. The spectrum for the outer edge of the reacted 93B3 fiber is labeled 1, and the center 4.

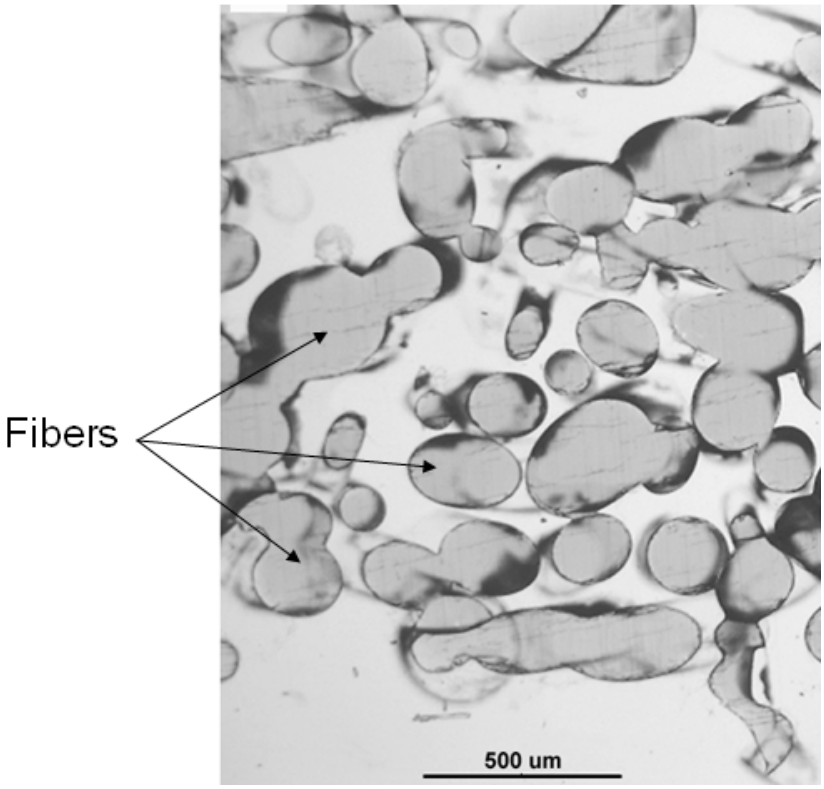

Figure 10 – Optical micrograph of the cross-section of an as-made 93B3 scaffold. The darker gray circular or ellipsoidal shapes are self-bonded, solid and unreacted, glass fibers and the light colored region is transparent epoxy.

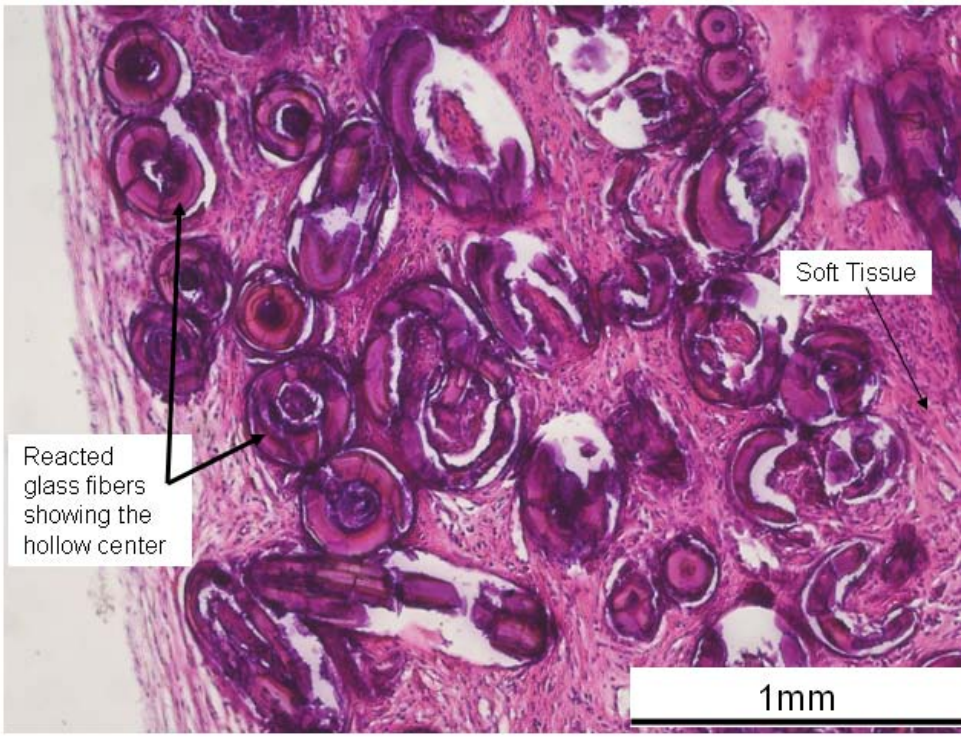

Figure 11 – Optical micrograph of an H&E stained section of a 93B3 scaffold that was implanted in rat subcutaneous tissue for four weeks. The 93B3 fibers have reacted with the rat body fluids and become hollow. Soft tissue (purple) has infiltrated nearly all of the open porosity within the scaffold, and several of the hollow fibers have soft tissue in the hollow core as well.

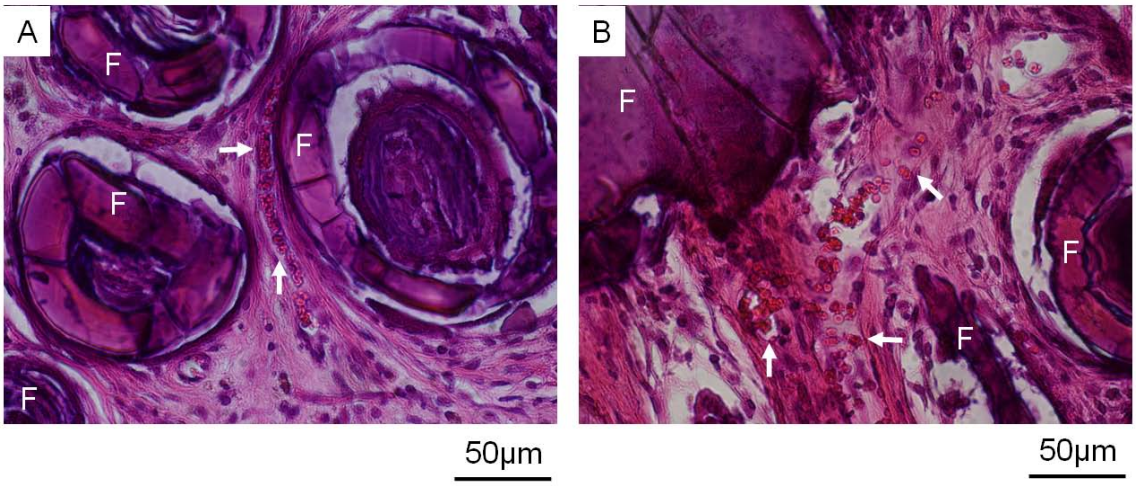

Figure 12 – Optical micrographs of H&E stained sections from a 93B3 scaffold implanted in the subcutaneous site in a rat for four weeks. Cell nuclei are blue, cytoplasm connective tissue and extra cellular matrix (ECM) are purple or red and red blood cells (RBC) are bright red. Figure 12A shows a section with multiple hollow fibers (F), some of which contain soft tissue (purple). There is also an organized line of red blood cells as pointed out by the arrows indicating a small blood vessel. Figure 12B shows a section with a larger vessel in the center of the image as indicated by the white arrows. There is a large amount of red blood cells (pink dots) in the vessel. The fibers (F) have significantly reacted to HA.

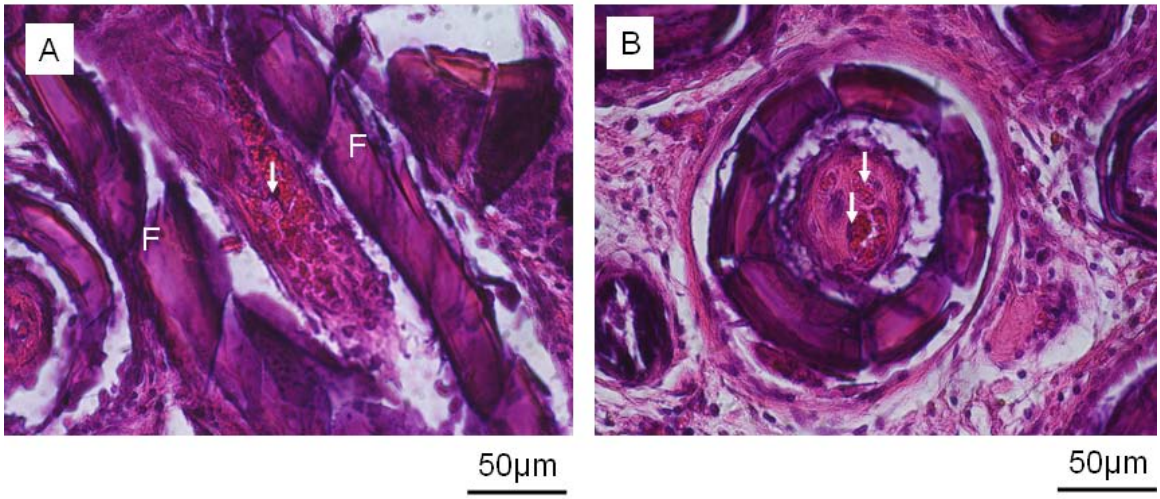

Figure 13 – Optical micrographs of H&E stained sections from a 93B3 scaffold implanted in a subcutaneous tissue for four weeks. Cell nuclei are blue, cytoplasm connective tissue and extra cellular matrix (ECM) are purple or red and red blood cells (RBC) are bright red. Figure 13A shows a reacted 93B3 fiber which has been cut parallel to the longitudinal fiber direction, and the sides of the fiber have been labeled with (F). There is soft tissue (purple) and red blood cells (white arrow) inside the hollow cavity of the fiber. Figure 13B has a fiber that has been cut perpendicular to the longitudinal fiber direction, and inside the fiber is soft tissue and red blood cells (arrows) indicating blood vessels are present inside the fiber.

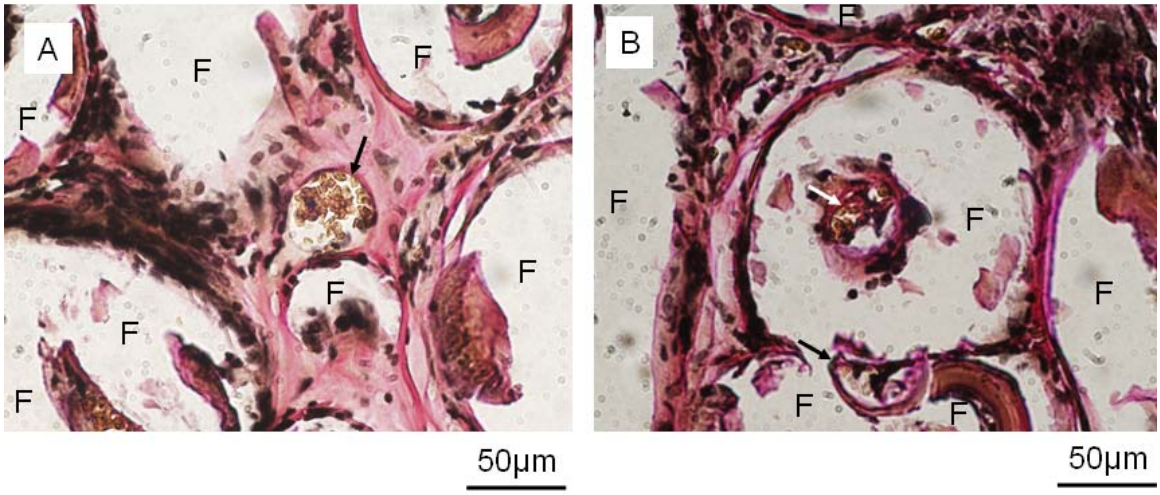

Figure 14 – Optical micrographs of VVG stained sections from a 93B3 scaffold implanted in a subcutaneous site for four weeks. Cell nuclei are brown to black, connective tissue is pink to red, and red blood cells (RBC) are yellow, and elastin is black. Several fibers, denoted by (F), are shown in Fig 14A; but much of the HA debonded during staining. There is a vessel in the center of the image (black arrow) as the elastin in the vessel is black, and there are several red blood cells in the center of the vessel (yellow). Figure 14B shows a hollow fiber (F) at the center of the image with a vessel in its hollow core (white arrow). There is a second vessel below, indicated by a black arrow that is in the void formed between two self-bonded fibers.

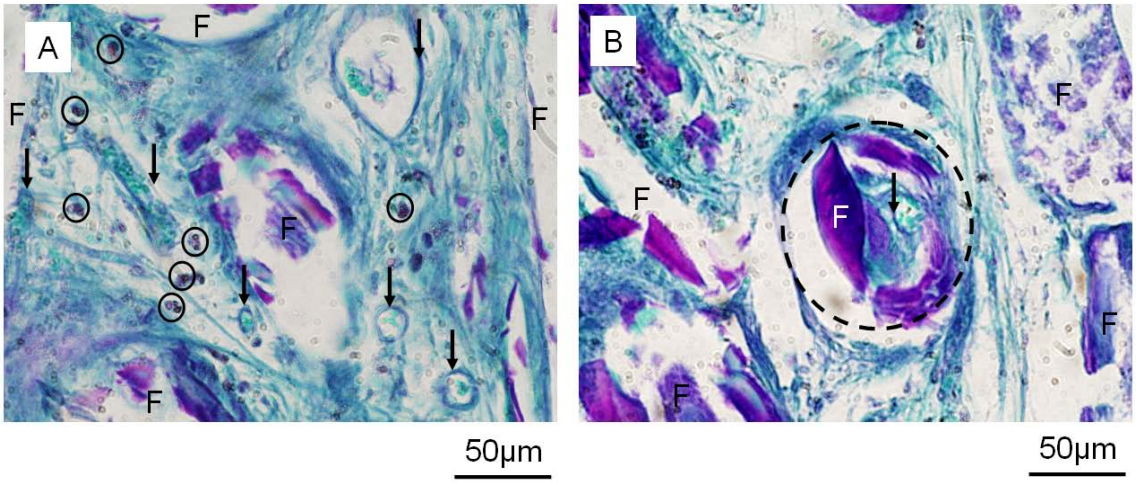

Figure 15 – Optical micrographs of PAS stained sections from a 93B3 scaffold implanted in a subcutaneous tissue for four weeks. Connective tissue is light green, and red blood cells (RBC) are bright green, vessel lining is blue, hydroxyapatite is purple, and macrophages are brown. Figure 15A has stained positive for several blood vessels (arrows) as the blue rings are surrounding bright green RBC. There are several macrophages throughout the tissue, circled; however they are not congregating around the scaffold material (F). Figure 15B has a hollow fiber (F) in the center of the image (dashed circle) with a vessel inside the void (arrow).

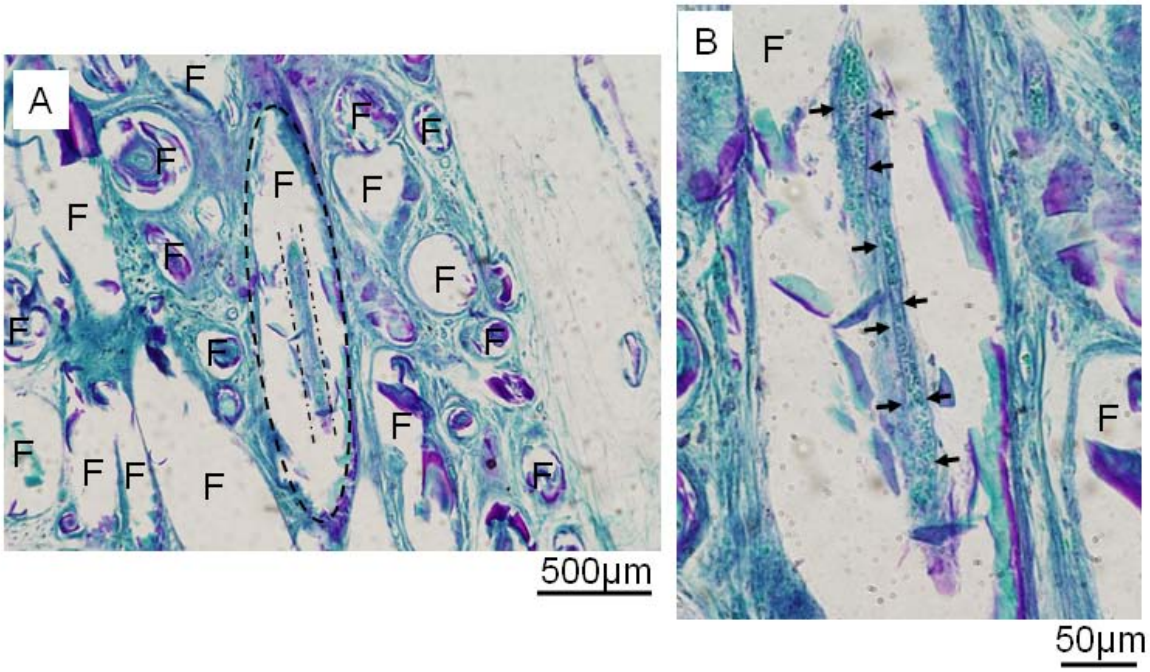

Figure 16 – Optical micrographs of PAS stained sections from a 93B3 scaffold implanted in a subcutaneous tissue for four weeks. Connective tissue is light green, and red blood cells (RBC) are bright green, vessel lining is blue, hydroxyapatite is purple, and macrophages are brown. Figure 16A shows has several fibers denoted by (F), however much of the HA washed off during staining. The hollow fiber in the center of the image has a vessel that grew 700 to 800µm down the hollow void of the reacted 93B3 fiber. Figure 16B shows a magnified view of the vessel, and the lining has been indicated by a series of arrows. The vessel has a significant number of red blood cells (RBC) present inside it.

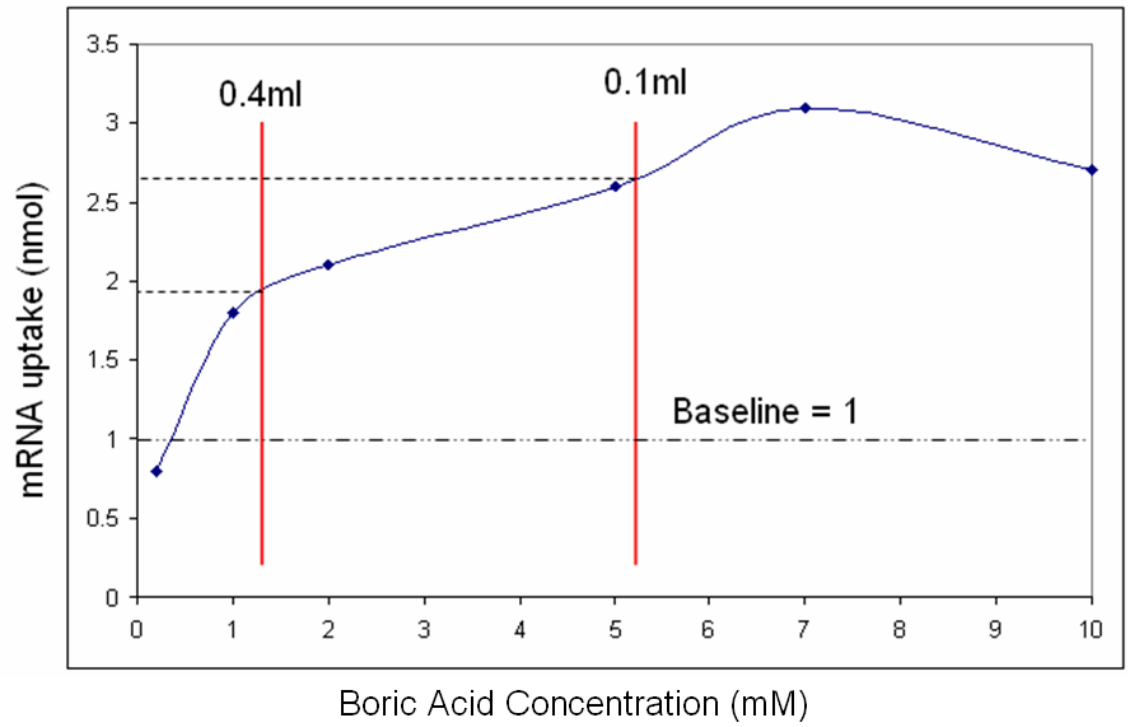

Figure 17 - Effect of mRNA uptake compared to boric acid concentration for human placental cells compared to the estimated boric acid concentrations from a reacting 93B3 scaffold in a sleeping (0.1ml/min*g) and active rats (0.4ml/min*g). According to the estimated boric acid concentrations from the scaffolds, and the effect seen from *in-vitro* cell culture experiments [39], there could be a stimulatory growth effect similar to a growth factor from the reacting 93B3 scaffolds.

2. POTENTIAL TOXICITY OF BIOACTIVE BORATE GLASSES *IN-VITRO* AND *IN-VIVO*

Steven B. Jung[1], Delbert E. Day[1], Roger F. Brown[2], and Linda F. Bonewald[3]

[1]Graduate Center for Materials Research, Materials Science and Engineering Department, Missouri University of Science and Technology, Rolla, MO, 65409-1170

[2]Department of Biological Sciences, Missouri University of Science and Technology, Rolla, MO, 65409-1170

[3]Department of Oral Biology, School of Dentistry, University of Missouri Kansas City, Kansas City, MO 64108-2784

2.1 ABSTRACT

The potential toxicity of a bioactive borate glass was evaluated using *in-vivo* animal models in soft tissue and bone and from *in-vitro* cell culture experiments using MLOA5 late osteoblast/early osteocytes cells. No toxicity was found between bioactive borate glass and subcutaneous tissue, in the liver, and nothing beyond normal incidental changes in rat kidney. Bone growth across porous scaffolds composed randomly oriented borate glass fibers was significantly higher than for a scaffold composed of a borosilicate glass or a silicate bioactive glass (13-93) fibers after 12 weeks *in-vivo*, $p<0.05$. *In-vitro* cell culture testing of bioactive glasses showed that under static culture conditions, borate glass disks tended to inhibit the growth of MLOA5 late osteoblast/early osteocyte cells, but when the disks were pre-reacted (in culture medium or a dilute phosphate solution) the cell proliferation is significantly increased to levels similar to 45S5 bioactive glass. The present work, along with data from the literature, show that bioactive borate glasses are biocompatible *in-vivo* and are not toxic to adjacent hard or soft tissues, or internal systemic organs such as the kidney and liver, were unaffected at the relatively high, estimated concentrations tested (<~126mg/kg/day). Based on the present results and

literature data, boron released from the borate glasses in the form of boric acid was not toxic in a dynamic environment such as the body and should be considered for use in humans and other mammals for soft and hard tissue engineering applications.

2.2 INTRODUCTION

Silicate based bioactive glasses such as 45S5 (Table 1) have been known to bond to bone and soft tissue for almost 40 years [1]. Bioactive silicate glasses are useful materials for tissue engineering due to their high degree of biocompatibility in the body. The rate at which silicate bioactive glasses convert to hydroxyapatite (HA) is relatively slow, on the order of months to years depending upon the size of the bioactive glass particle and its composition [2]. Due to this slow reaction rate, bioactive glasses containing boron have been developed which react significantly faster with body fluids than silicate glasses [3].

The effect of boron on cells and animals has been studied *in-vitro* and *in-vivo* to determine its physiological role [4]. Boron has not been linked to any specific biological function, but there is evidence that the absence of boron changes growth patterns in animals and stimulates cell growth *in-vitro* [4, 5]. Determining the effect that a bioactive borate glass has on cells and living tissue is a controversial issue due to the difference in the experimental parameters. Typically, *in-vitro* cell cultures are static systems in which cells are seeded, covered with culture medium, and depending on the experiment, not disturbed for several days. The human body is a dynamic system where heavily buffered fluids, relatively constant pH, are constantly moving and being replenished.

Using a static culture environment to determine *in-vivo* biocompatibility for a non-reactive material is trivial. As long as the material is un-reactive, the pH remains relatively constant, and nothing changed in the system by the material, so the material does not directly affect cell attachment and growth. When the material of interest is reactive, differences between the static culture environment and *in-vivo* (dynamic) become apparent. With a reactive material, the solution pH, the composition of the media, and the material being studied may all be changing, and, thereby affect cell attachment and growth. In a static environment, especially in regions adjacent to the reactive material, there are no means of equilibration. Therefore, comparisons between the static culture and *in-vivo* environments may not be representative.

The schematic in Fig 1 shows the conditions that have been used to evaluate potential toxicity of a borate glass *in-vitro* and *in-vivo*. The *in-vitro* method has been used mostly with static culture, but dynamic culture (continual or repetitious agitation) has yielded some interesting improvements in cell proliferation [6]. Marion et al found that pre-reaction of a bioactive borate glass also increased the *in-vitro* culture of cells [7].

In-vivo studies of the biocompatibility of borate based bioactive glasses are limited, but animal studies where the potential toxicity of boric acid (BA) has been studied are also relevant. Soft and hard tissues and internal organs of mice, rats, and rabbits dosed with BA have been studied and the maximum limits to avoid toxicity in adult and fetal animals have been determined [8]. It should be noted that there is a relatively wide range of minimum toxicity limits between different animal species, so for simplification, hereafter, the lowest toxicity level of a given group will be the assumed toxic level for the entire group.

The BA levels acceptable for ingestion by animals or added to cell culture are shown in Fig 2 and the data and sources are listed in Table 2 [5, 6, 8-12]. The data in Fig 2 is labeled as non-toxic (green), if inhibition or toxicity is reported in animals (fade from green to red), and red where extreme inhibition or cell death occurred. The static culture of the cells had the lowest level of BA toxicity at 62mg/kg/day, or 1mM [6]. The conversion from 1mM to mg/kg was made using 62g/mole for boric acid (H_3BO_3), and dividing by 1000 to get 62mg/mM. An aqueous solution of boric acid is mostly water, and one liter of water weighs 1kg, therefore, a 1mM solution of boric acid is equivalent to 62mg/kg.

One reason why static cell culture on reactive materials, such as bioactive borate glasses, may not be the best method of determining *in-vivo* performance is illustrated by the schematic in Fig 3. Three different conditions are simulated, *in-vitro* static, *in-vitro* dynamic or pre-reacted, and *in-vivo* dynamic. The *in-vitro* dynamic or pre-reacted conditions were grouped together because the toxicity gradients from each are thought to be similar (i.e. a smaller potentially toxic region). As indicated by the dashed circle and the color gradient, the area of cell inhibition in a static culture is in the liquid immediately surrounding the material, for this example a glass disk (G). The majority of the culture medium could be only minimally affected by the reaction of the glass with the culture media.

In the dynamic *in-vitro* condition, the material dissolving from the glass becomes diluted and is ideally distributed throughout the culture medium. This solution reduced the potential toxicity of the reactive material and its effect on proliferation. The final condition, *in-vivo* dynamic, shows a minimal gradient as the leached ions are transported

from the glass surface by the fluids in the adjacent tissue and the blood flow. The BA is removed from the body and high concentrations do not build up locally in the tissue adjacent to the glass.

Borate glasses of the composition used in the present work react quickly, within a few hours, with an aqueous solution like a phosphate solution or cell culture medium. Weight loss data for a soda lime borate glass of is shown in Fig 4 [7]. Initially, the glass loses almost 25wt% in the first 24 hours, but the rate decreases by a factor of four between 30 and 120 hours due to the formation of calcium phosphate on the glass surface. The weight loss in the first day is primarily due to the dissolution of sodium and boron from the glass. This explains why pre-reaction of a bioactive borate glass for just a few hours prior to a cell culture experiment can improve cell growth. Eliminating the initially large influx of alkali and boron in the culture media and forming a calcium phosphate layer on the glass surface helps to better simulate how cells might interact during the more representative condition of the cells growing on a calcium phosphate coated glass.

The objective in the present work was to evaluate the potential toxicity of bioactive borate glass fiber scaffolds *in-vivo*. Like almost anything, toxicity has to do with the amount or quantity of something ingested or the overall concentration that leads to a negative outcome. Therefore, bioactive borate glass fiber scaffolds were implanted *in-vivo* in soft and hard tissue of rats followed by a comprehensive histological analysis. As a reference, comparisons with well known silicate based bioactive glasses were included when appropriate.

2.3. MATERIALS AND METHODS

2.3.1 Scaffold and Disk Preparation

Reagent grade chemicals of SiO_2, H_3BO_3, $CaCO_3$, K_2CO_3, $MgCO_3$, P_2O_5, and Na_2CO_3 were used to prepare the bioactive glasses (Table 1). The raw materials were weighed (±0.01), thoroughly dry mixed, and melted in a platinum crucible at temperatures ranging from 1050 to 1400^oC for one to two hours depending on the composition. The glass was stirred with a silica rod several times to achieve a chemically homogeneous melt.

Rods of 45S5, 13-93, 13-93B1, and 13-93B3 glass (Table 1) were cast into graphite molds with an internal diameter of 10mm and annealed at temperatures between 450 and 550^oC for two hours before slow cooling to room temperature. The rods were cut into 1mm thick disks with a slow speed saw which were used for cell culture experiments. The disks were rinsed with ethanol and acetone and stored in a dessicator until used.

Fibers 100 to 300μm in diameter were hand pulled from the melt and broken into 2 to 3mm lengths (Fig 5A) which were used to manufacture porous, three dimensional, randomly oriented fiber scaffolds. Seventy milligrams of glass fibers were weighed for each scaffold and placed with a random orientation in a 7mm inside diameter ceramic (mullite) cylindrical mold (Fig 5B). The molds were placed in a preheated oven at selected temperatures between 575 to 695^oC for 45 minutes, depending on the glass composition, to allow the fibers to soften and thermally bond. The molds were then removed from the oven and cooled to room temperature. Once cool, the scaffolds were

removed from the molds and stored in an air tight desiccator. The as-made scaffolds had nominal dimensions of 7mm in diameter and 2mm thick, see Fig 5C.

Prior to implantation or cell culture, the scaffolds and disks were dry heat sterilized by placing them in a silica glass vial, covering the vial with aluminum foil, and heating the vial to 300^{o}C for four hours in an oven. The scaffolds or disks were slow cooled to room temperature. Once cool the scaffolds or disks were ready for use.

2.3.2 Growth of MLOA5 Cells on Bioactive Glass Disk

MLOA5 late osteoblast/early osteocyte cells were cultured on as-cut (unpolished) disks of 45S5, 13-93, 13-93B1, and 13-93B3 for 24 hours on un-reacted disks and pre-reacted disks (four hours in culture media) at 37^{o}C, 5%CO_2 atmosphere. The cells were fixed, collected, and counted for comparison with the control (50,000 MLOA5 cells cultured on the bottom of a single well of a 24 well plate). The cell culture experiments were completed at the University of Missouri –Kansas City (UMKC) School of Dentistry Department of Bone Biology [13].

2.3.3 Subcutaneous Scaffold Implantation

The schematic in Fig 7 shows the four implant sites in which a scaffold was implanted in a Sprague Dawley rat above each shoulder and above each hind leg between the subcutaneous tissue and the skeletal muscle. Since the scaffolds were implanted in multiples of four, each site contained between one and four scaffolds. No scaffolds were implanted in the control animals.

2.3.4 Subcutaneous Scaffold and Organ Removal, Tissue Processing, and Histology Slide Preparation

After four weeks, the scaffolds from the experimental group, a lobe of the liver, and the left kidney from each rat were excised, photographed, and fixed in 10% formalin for four days.

2.3.5 Tissue Processing and Histology Slide Preparation

After the tissues were fixed, they were dehydrated with a series of ethanol solutions ranging from 70 to 100% ethanol [14] and a microwave irradiation technique [15]. Each scaffold, kidney, or liver was submerged in a glass vial with 10ml of ethanol solution, packed into an ice bath, placed in the microwave (EBSciences H2850 Microwave Processor) for 2.5 minutes at a power of 65% at 37±4^{o}C, and after removal, set at room temperature for at least 15 minutes. This process was followed for each tissue in each ethanol solution.

As a control, a 13-93B3 fiber scaffold was embedded in a transparent epoxy and cross sectioned to show an un-reacted fiber scaffold without any and is shown in Fig 11. The glass fibers are circular or elliptical depending on the fiber orientation. Several of the fibers have bonded together in the plane of the cross section, to form complex geometrical shapes.

Each kidney, liver, and fiber scaffold was embedded with paraffin for histological analysis with a tissue processor (AutoTechnicon Model 2A) filled with paraffin mounting wax (Paraplast Tissue Embedding Medium, McCormick Scientific LLC) at 45^{o}C for four hours. The infiltrated tissue was mounted in a wax block with a paraffin mounting system (Leica EG 1150H). Histological sections 18μm thick were cut of the recovered scaffold to better keep in tact the reacted fibers with a microtome (Leica

RM 2235 microtome) with TBS Shur/sharp blades. The kidney and liver sections were cut 6μm thick to improve the clarity of the sections. Each section was floated on a water bath (Lipshaw Electric Tissue Float, model number 375, Detroit MI) at 40^{o}C prior to mounting the section on a glass slide (Fisher Brand Superfrost, St. Louis MO). Between two and four tissue sections were mounted on each slide and dried over night (Fisher Scientific slide warmer, St. Louis MO). Each of the tissues (scaffold, kidney, liver) was stained with H&E stain (Phelps Country Regional Medical Center in Rolla MO). A detailed protocol for the H&E staining procedure is available elsewhere [10].

2.3.6 Tissue Assessment

The kidney and liver sections were labeled generically and sent to Charles River Research Animal Diagnostic Services Center (Wilmington, MA) for a blinded pathological analysis. The scaffold sections were used to assess tissue infiltration and the extent of the fiber reaction.

2.3.7 Calvaria Implant Experiment

Porous scaffolds composed of 13-93B3 fibers, 13-93B1 fibers, 13-93 fibers, and particles of 45S5 glass (100 to 200μm in diameter) were implanted in a 4mm rat calvaria defect (n=4) for 12 weeks. The growth of the bone was monitored in-situ with micro-CT (computer tomography) analysis. The calvaria implant experiment was conducted at the dental school at UMKC.

2.4. RESULTS

2.4.1 *In-vitro* MLOA5 Cell Culture (As-made and Pre-reacted)

Data for the proliferation for MLOA5 cells after culture on as-made 45S5, 13-93, 13-93B1, 13-93B3, and the control (empty well) is shown in Fig 6 [13]. The control was

not significantly different ($p<0.05$) from 45S5, 13-93, and 13-93B1 disks which means there is almost no difference between those glasses in a static culture. Compared to the control, 13-93B3 had ~1/3 the cells and was significantly less ($p<0.001$) indicating that the culture conditions inhibited cell growth when compared to the other glasses.

After incubating (pre-reacting) the as-made discs in the culture media for four hours and then transferring the discs to fresh culture media, a similar proliferation analysis was completed at 24 hours as shown in Fig 6 [13]. The number of MLOA5 cells on the pre-reacted disks of each glass was higher than the as-made disks, but the cell count on the 13-93B3 disks was noticeably higher.

2.4.2 13-93B3 Scaffold and Tissue Removal

2.4.2.1 Assessment of Scaffold after Four Weeks *In-Vivo*

Figure 8 shows a representative image of the 13-93B3 scaffolds during removal from the subcutaneous tissue. Numerous blood vessels were visible at the outer edge (perimeter) of several of the scaffolds as indicated by the arrows. All of the 160 scaffolds implanted in the 16 rats were recovered. The particular rat in Fig 8 had a total of 12 scaffolds implanted, thus the site in Fig 8 has three scaffolds (S) present. The scaffolds have soft tissue completely surrounding them and blood vessels are present at the perimeter of the scaffolds (arrows). There was no inflammation or infection detected in the vicinity of the scaffolds which indicated biological compatibility. The scaffolds had lost their original rigidity indicating that they had reacted with body fluids. There was no detectable change in the size or volume of the scaffolds after four weeks *in-vivo*.

A representative image of the reacted scaffolds stained with H&E is shown in Fig 12. The H&E stained section of a 13-93B3 scaffold reacted for four weeks in

subcutaneous tissue is shown in Fig 12A. The scaffold is >90% filled with soft tissue and the fibers that once looked like those in Fig 11 are now reacted. Magnified views of two portions of the scaffold, box B at the center and box C at the outer edge in Figs 12B and 12C show the fibers were fully reacted throughout the scaffold.

2.4.2.2 Assessment of Kidney and Liver

A representative image of a liver and kidney from rats with zero to 16 scaffolds implanted is shown in Figs 9 and 10, respectively. Each liver and kidney is labeled with the number of scaffolds that were implanted in the rat. There were no noticeable difference in the size or color between the control and livers from rats implanted with 13-93B3 scaffolds (Fig 9), and no spots or other differences were seen at the surface of the organs. No hardening or texture differences were noticeable in the livers. There was no difference in size or color, and no spots or other noticeable differences on any kind were noticed between the kidneys from animals implanted with up to sixteen 13-93B3 scaffolds and the control as shown by the images in Fig 10.

No pathological differences were reported between the control rats (no scaffolds) and the rats implanted with up to sixteen 13-93B3 scaffolds (Table 3). An example of a liver section from each condition (number of scaffolds) is shown in Fig 15.

The pathological report on the kidneys (Table 3) showed that 13 of 16 of the scaffold implanted animals and 3 of 4 control animals showed at least one of the following findings: tubular degeneration, protein casts, and nephrocalcinosis. All of these findings were graded as minimal severity and the findings were described as normal incidental changes not uncommon for adult rats. The tubular degeneration described included one or more of the following changes; decreased epithelial eosinophilia,

minimally dilated tubules, gold/brown pigment in tubules, and minimal infiltrates of mononucleated inflammatory cells. These minor changes were not observed in the control tissues, but the changes were described as minor. The nephrocalcinosis and protein casts are considered frequent histological occurrences in rats as three of four of the control animals had protein casts present. The findings described were either focal, present in one spot, or multi focal, present in a few spots. None of the findings were described as diffuse, (present throughout the much of the section), which is the most severe gradation for a specific findings occurrence. An example of a kidney section with no pathological abnormalities is shown in Fig 16. Examples of the observed pathological changes are preserved in the appendix.

2.5. DISCUSSION

2.5.1 *In-vivo* Analysis of Potential Boron Toxicity from Bioactive Borate Glass Scaffolds

From the present work, no boron toxicity was observed in rat subcutaneous tissue, or in systemic organs such as the kidney and liver at or below the estimated BA concentration of ~126mg/kg/day. The estimated BA concentration was based on all the boron being released as BA from sixteen scaffolds (70mg each) at a constant rate over a 28 day period. Conservatively speaking, the reaction was assumed to be finished in approximately four weeks, but if the 13-93B3 scaffolds reacted in two weeks, the BA concentration in the rats would have been ~250mg/kg/day. Regardless of the length of time required for the scaffolds to fully react, the fact that there was no toxicity observed in the liver, kidney, or in the subcutaneous tissue at the implant sites in the rats with up to sixteen 13-93B3 scaffolds is the most significant point.

As shown in Fig 17, the 13-93B3 bioactive borate glass scaffold implanted in rat calvaria for 12 weeks supported significantly more bone growth ($p<0.05$) than silicate based bioactive glass 13-93. The amount of bone growth into a scaffold is not a direct measure of toxicity, but in-directly, the increase in bone growth in borate glass scaffolds over well studied and clinically used silicate bioactive glasses would not be expected if the scaffold was measurably toxic. A histomorphometry analysis of the bone tissue surrounding the 13-93B3 scaffolds showed no evidence of an immune reaction (increased presence of macrophages or immune cells) or necrotic tissues [16].

2.5.2 Subcutaneous Scaffold Removal

The scaffolds removed from the subcutaneous tissue looked similar to those described by Jung et al in a previous experiment when 13-93B3 fiber scaffolds were implanted in subcutaneous tissue for four weeks [10]. The scaffolds were infiltrated with subcutaneous tissue and blood vessels were present in the surrounding and adjacent tissues. The scaffolds lost their original rigidity and had reacted to form carbonated hydroxyapatite (HCA) [10].

2.5.3 Histological Analysis of Tissues

The absence of any negative findings in the liver sections was not unexpected. The importance of the liver to the functions of the body warranted the analysis, but, Janku et al found no histological differences in borocaptate dosed animals when compared to the control [17]. Heindel et al gave rats upwards of 330mg/kg/day of BA, which is almost three times the estimated dose given in the present work, and no histological changes were reported [8].

The kidney was found to have incidental changes that are common in adult rats. These changes occurred in the rats with 16 scaffolds and in the control rats indicating that the boron released from the 13-93B3 glass, at the levels administered, had no immediate effects on the kidneys. Heindel et al dosed rats with 330mg/kg/day and found that after a histological analysis of the tissues there was no correlation between nephropathy and BA dose [8]. Only a few of the animals showed signs of minimal histological changes from the control and were considered normal changes [8].

The kidney was the organ that was originally considered to be at the highest risk since >90% of BA is removed from the body through urine [18, 19]. No long term effects would be expected since BA is removed from the body almost entirely after 96 hours of ingestion [18, 19]. A study of borax workers exposed to airborne borax found that over the course of a single work week that boron was removed from the body daily through urination and there was no progressive daily increase of boron concentration in blood or urine [9]. Therefore, once the 13-93B3 glass has fully reacted, the boron concentration of the body should decrease to normal levels within a few days.

2.5.4 Bone Response to Bioactive Glasses in Rat Calvaria

In the rat calvaria, the 13-93B3 scaffolds performed statistically better ($p<0.05$) than the 13-93 or 13-93B1 glasses at promoting bone growth. Since about 50% more new bone grew on the 13-93B3 glass scaffold as compared to 13-93 scaffold, the 13-93B3 glass had a stimulatory effect on bone growth. It was not surprising to find that the 13-93B3 glass scaffold promoted bone growth statistically as well in rat calvaria as 45S5 and better than 13-93. Richard found previously that particles of the borate analog of

45S5 (denoted 45S5-3B) also promoted bone growth as well as the 45S5 glass at 30 and 60 days in rat tibia [12].

2.5.5 *In-vitro* Analysis of Potential Boron Toxicity from Bioactive Borate Glass Disks

Comparing the results of the as-made disks and the pre-reacted disks (Fig 6), it is apparent that the reactivity of the glass disk and the ionic concentration adjacent to the seeded cells affect the cell proliferation *in-vitro*. By leaching some of the alkali and boron from the 13-93B3 disks prior to seeding the cells, the glass went from the lowest number of cells after 24 hours to the highest, a 4-fold increase in cell number. Based on weight loss data, the 13-93 is the slowest reacting glass followed by 13-93B1 and 45S5 which are about the same, and then the 13-93B3 glass which is the most reactive. Increasing the pre-reaction time may continue to improve the proliferation rates of the 13-93B3 glass, but at some point the benefit will likely stop. Marion et al showed that pre-reacting a soda lime borate glass improved cell proliferation of human mesenchymal stem cells over the as-made glass, but complete reaction to HA did not promote cell growth as much as the partially reacted glass [7]. It was found that the release of some ions from the glass improved cell proliferation [7].

Three glasses, the well known 45S5, the borate analog of 45S5 known as 45S5-3B (Table 1), and a pre-reacted 45S5-3B glass were all cultured under static conditions for four days. As shown in Fig 18, the 45S5 glass disk had the most cells (as measured by total DNA), and the as-made 45S5-3B glass had significantly less cells present after four days, $p<0.01$. In contrast, the pre-reacted 45S5-3B glass disks supported cell growth almost as well as the less reactive 45S5 glass [6].

In another experiment, a static culture was compared to dynamic culture for 45S5 and three borate containing glasses (45S5-1B, 45S5-2B, and 45S5-3B, Table 1). As shown in Fig 19 the greatest difference between the static and dynamic conditions was seen for the borate glass (45S5-3B) [6]. The static cell growth for the borate containing glasses (1B, 2B, and 3B**)** decreases as the boron level and reaction rate increases. An interesting result for the dynamic condition was the dramatic improvement in cell growth (DNA) for all of the borate containing glasses. Only the borate glass (3B) was statistically lower than the 45S5 glass after four days [6]. The two experiments (Figs 18 and 19) show how the experimental conditions (static vs. dynamic) can influence cell culture data when bioactive glasses are being measured, especially higher reactive glasses such as the borate glasses.

In Table 2, the 0.002M BA concentration caused a 40% decrease in cell number according to Brown et al, but Richard reported an increase in cell proliferation. The experiments conducted by Brown were static as were those by Richard, but Richard counted cells every day for four days. The movement of the fluids that likely occurred during the cell counting procedure by Richard may explain why the data disagree. The dynamic environment in the culture dish while counting cells may have been enough to significantly modify the proliferation of the cells.

2.5.6 Correlation between the Sprague Dawley (SD) Rat Model and Humans

Heindel et al found that of the SD rat, Swiss CD-1 mouse, and New Zealand rabbit, the SD rat had the lowest tolerance for BA ingestion [8] and is therefore determined to be the best of the three mammalian models for human comparison. The fact that SD rats dosed with 16 scaffolds (1.12g of 13-93B3 glass, or 1.05g BA in body

fluids assuming all boron from glass becomes BA) had no negative histological changes in the kidney or liver when compared to the control indicates that bioactive borate glass 13-93B3 is not toxic to most mammals at or below estimated concentration (126mg/kg/day) of BA. Using the estimated levels of BA administered to the SD rat and assuming humans have equal tolerance to the 13-93B3 glass, the graph in Fig 20 was made to show the amount of 13-93B3 glass a human could have implanted and be at the same concentrations as in the rat experiment. The weight percent of glass used in the calculations, determined by the 4, 8, 12, or 16 scaffolds per rat, was 0.09, 0.19, 0.28, and 0.37%, respectively, by assuming the weight of each scaffold was 70mg the weight of the rat was fixed at 300g.

From the graph in Fig 20, ~170 grams (~1/3 pound) of 13-93B3 glass would need to be implanted in a 100 pound person to reach the same BA concentration in their body as the 300g SD rat containing 1.12 grams of 13-93B3 glass (16 scaffolds). For a person weighing 200 pounds, the person could have almost 340g (~3/4 pound) of 13-93B3 glass implanted (Fig 20) without exceeding the BA concentration of ~126mg/kg/day (concentration equal to 16 scaffolds in a SD rat). The amount of bioactive glass used for treatment in bone or periodontal defects is typically less than 10 grams which is ~15 to 30 times less than the levels described here.

Young children and developing new born babies may be more susceptible to potential boron toxicity. Animal experiments have reported decreased weights in unborn SD rats when the mother was given a BA dose exceeding 78mg/kg/day [8]. There is no work to the author's knowledge of BA doses given to developing animals that were healthy when born to determine if the no adverse effect level (NOAEL) changes from

prenatal to postnatal. *In-vitro* cell cultures (static) also begin to become inhibited cell growth at 1mM concentration [6] (~62mg/kg/day of BA). Assuming a new born could consume ~62mg/kg/day, (equivalent to 8 scaffolds in a 300g SD rat), an eight pound baby could have ~6.7g of 13-93B3 glass implanted, which is approximately what an adult might expect for most periodontal applications [20].

2.6. CONCLUSIONS

Boron toxicity has been analyzed from multiple *in-vitro* cell culture conditions and compared with animal toxicity reports. The present experiments were conducted to determine what levels of boron are acceptable or potentially toxic. *In-vitro* data were found to be highly dependent on the culture environment, static or dynamic, and the condition of the glass (as-made or pre-reacted) and the glass composition. Therefore it is suggested that *in-vitro* cell culture experiments be conducted in a dynamic or semi-dynamic system where the culture media is circulated similar to conditions *in-vivo*, especially when working with highly reactive materials such as bioactive borate glasses.

In-vivo experiments with Sprague Dawley rats with up to 16 bioactive borate glass 13-93B3 fiber scaffolds (70mg each) implanted for four weeks in subcutaneous tissue fully reacted and the boron released caused no detectable histological changes in the kidney or liver. Each SD rat remained healthy and no signs of inflammation or infection were seen at the implant sites after four weeks. There were no negative histological findings in the liver and only minor changes which were noted as incidental changes normal for an adult rat, were noted in the kidneys. The open interconnected pores of the 13-93B3 scaffolds were filled with soft tissue and there was no inflammation

in the tissue adjacent to the scaffolds during the scaffold removal. Blood vessels had grown next to the outer surface of the scaffolds and were seen in the adjacent tissue during scaffold removal.

Scaffolds composed of 13-93B3, 13-93B1, 13-93 glass fibers, and loose particles of 45S5 in rat calvaria for 12 weeks produced no adverse reactions. The rats were monitored regularly, and no rats became sick or died due to the implantation of the scaffolds. The 13-93B3 scaffold was found to have statistically more bone ($p<0.05$) than both the 13-93 and 13-93B1 scaffolds by histomorphometry analysis and the bone adjacent the reacted 13-93B3 scaffolds showed no signs of immune response or necrotic tissue after 12 weeks. Therefore, bioactive borate glasses such as 13-93B3 should be strongly considered for use in humans for hard and soft tissue engineering applications.

Acknowledgements

The authors would like to thank Vernon Modglin for his help during the surgical procedures, Dr. Anne Maglia for providing the histological equipment, and Penny McCormick of Phelps County Regional Medical Center for staining the H&E sections.

2.7 REFERENCES

[1] Hench LL, Paschall HA. Direct chemical Bond of Bioactive Glass-Ceramic Materials to Bone and Muscle. Journal of Biomedical Materials Research 1973;4:25.

[2] Asikainen AJ, Hagstrom J, Sorsa T, Noponen J, Kellomaki M, Juuti H, Lundqvist C, Hietanen J, Suuronen R. Soft Tissue Reactions to Bioactive Glass 13-93 Combined with Chitosen. Journal of Biomedical Materials Research 2007;83A:530.

[3] Huang W, Day DE, Kittiratanapiboon K, Rahaman MN. Kinetics and Mechanisms of the Conversion of Silicate (45S5), Borate, and Borosilicate Glasses to Hydroxyapatite in Dilute Phosphate Solution Journal of Materials Science: Materials in Medicine 2006;17:583.

[4] Nielsen FH. Boron in Human and Animal Nutrition. Plant and Soil 1997;193:199.

[5] Dzondo-Gadet M, R M-N, Hess K, Nabet P, Belleville F, Dousset B. Action of Boron at the Molecular Level. Biological Trace Element Research 2002;85:23.

[6] Brown RF, Rahaman MN, Dwilewicz AB, Huang W, Day DE, Li Y, Bal BS. Effect of borate glass composition on its conversion to hydroxyapatite and on the proliferation of MC3T3-E1 cells. Journal of Biomedical Materials Research 2008;88A:392.

[7] Marion NW, liang W, Reilly G, Day DE, Rahaman MN, Mao JJ. Borate Glass Supports the In Vitro Osteogenic Differentiation of Human Mesenchymal Stem Cells. Mechanics of Advanced Materials and Structures 2005;12:1.

[8] Heindel JJ, Price CJ, Schwetz BA. The developmental toxicity of boric acid in mice, rats, and rabbits Environmental Health Perspectives 1994;102:107.

[9] Culver BD, Shen PT, Taylor TH, Lee-Feldstein A, Anton-Culver H, Strong PL. The Relationship of Blood and Urine-Boron to Boron Exposure in Borax-Workers and the Usefulness of Urine-Boron as an Exposure Marker. Environmental Health Perspectives 1994;102:133.

[10] Jung SB, Day DE, Brown RF. Preliminary evaluation of bioactive borate glass fiber scaffolds for mammalian tissue regeneration. Rolla, MO: Missouri University of Science and Technology, 2010. p.42.

[11] Ning J, Yao A, Wang D, Huang W, Fu H, Liu X, Jiang X, Zhang X. Synthesis and invitro bioactivity of a borate-based bioglass. Materials Letters 2007;61:5223.

[12] Richard M. Bioactive behavior of a borate glass. Ceramic Engineering, vol. M.S. Rolla: University of Missouri-Rolla, 2000. p.140.

[13] Bonewald L. MLOA5 Cell Growth on Bioactive Glass Disks. 2010.

[14] Jung SB, Day DE, Brown RF. Comparison of self-bonded three dimensional bioactive glass fiber scaffolds after in-vivo implantation in rats. Journal of the American Ceramic Society 2009.

[15] Laboux O, Dion N, Arana-Chavez V, Ste-Marie L-G, Nanci A. Microwave Irradiation of Ethanol-fixed Bone Improves Preservation, Reduces Processing Time, and Allows Both Light and Electron Microscopy on the Same Sample. Journal of Histochemistry and Cytochemistry 2004;52:1267.

[16] Bonewald L. Histomorphometry Analysis of Bone Growth in Bioactive Glass Scaffolds Implanted in Rat Calvaria. 2010.
[17] Janku I, Buchar E, Jiricka Z. Nephrotoxicity of borocaptate after short-term administration in rabbits. Toxicology 1993;79:99.
[18] Smallwood CL, Lipscomb J, Swartout J, Teuschler L. Toxicological Report of Boron and Compounds. In: Agency USEP, editor. Washington D.C.: EPA, 2004. p.134.
[19] Smallwood C. Boron in Drinking-water. vol. 2. Geneva: World Health Organization, 2003.
[20] Froum SJ, Weinberg MA, Tarnow D. Comparison of bioactive glass synthetic bone graft particles and open debridement in the treatment of human periodontal defects. A clinical study. Journal of Periodontology 1998;69:698.

TABLES

Table 1 – Bioactive Glass Compositions (wt%)

Glass	SiO_2	B_2O_3	CaO	P_2O_5	MgO	K_2O	Na_2O
45S5	45.0	0	24.5	6.0	0	0	24.5
45S5-1B	30.0	15.0	24.5	6.0	0	0	24.5
45S5-2B	15.0	30.0	24.5	6.0	0	0	24.5
45S5-3B	0	45.0	24.5	6.0	0	0	24.5
13-93	53.0	0	20.0	4.0	5.0	12.0	6.0
13-93B1	35.3	17.7	20.0	4.0	5.0	12.0	6.0
13-93B2	17.7	35.3	20.0	4.0	5.0	12.0	6.0
13-93B3	0	53.0	20.0	4.0	5.0	12.0	6.0

Table 2 – Toxicity Effect of BA Concentration *In-vitro* and *In-vivo*

BA Concentration (mg/kg/day)	Experiment and Findings	Reference
~1	BA inhaled by humans working with borate materials (non-toxic)	Culver et al [9]
12.4 to 620	Human Placental Cells (growth increase)*	Dzondo-Gadet et al[5]
~8	~BA release from a single 13-93B3 Scaffold In-vivo (non-toxic)	Jung et al [10]
62	0.001M BA addition to MC3T3-E1 cell culture (growth inhibited)*	Brown et al [5]
78	Fetal Toxicity Limit (SD Rat)	Heindal [8]
<111	Extract from a bioactive borate glass with goat bone marrow stroma cells (no change in cell number)*	Ning et al [11]
124	0.002M BA addition to MC3T3-E1cell culture (growth increase)**	Richard [12]
124	0.002M BA addition to MC3T3-E1cell culture (cell number decreased 40%)*	Brown et al [6]
125	Fetal Toxicity Limit (NZ Rabbit)	Heindal [8]
~126	~BA release for up to sixteen 13-93B3 scaffolds in Adult SD Rat: adjacent subcutaneous tissue, kidney and liver (non-toxic)	Present Work
160	Maternal Toxicity Limit (SD Rat)	Heindal [8]
248	Fetal Toxicity Limit (CD-1 Mice)	Heindal [8]
250	Maternal Toxicity Limit (NZ Rabbit)	Heindal [8]
452	Maternal Toxicity Limit (CD-1 Mice)	Heindal [8]
618	0.01M BA addition to MC3T3-E1 cell culture (no change in cell number)**	Richard [12]
3090	0.05M BA addition to MC3T3-E1 cell culture (cell death)**	Richard [12]
15450	0.25M BA addition to MC3T3-E1 cell culture (cell death)**	Richard [12]

Green – non toxic
Yellow – no change in cell number or minimum toxicity in-vivo
Red – cell death
* Static Cell Culture
** Semi-Dynamic Culture

Table 3 – Histological Results for Sprague Dawley Rats Implanted with 13-93B3 bioactive Glass Fiber Scaffolds (70mg) for Four Weeks

# of Scaffolds per Animal	16	16	16	16	12	12	12	12	8	8
Tissue Finding										
Kidney	+	+	+	-	+	+	-	+	+	+
Degeneration, tubular	1M	1M	-	-	-	-	-	-	1M	-
Protein casts, tubular	1M	1M	1M	-	-	1M	-	-	1M	1M
Nephrocalcinosis	1M	-	-	-	1F	-	-	1M	1F	-
Liver	-	-	-	-	-	-	-	-	-	-

# of Scaffolds per Animal	8	8	4	4	4	4	Control	Control	Control	Control
Tissue Finding										
Kidney	-	+	+	+	+	+	-	+	+	+
Degeneration, tubular	-	-	-	-	1M	1M	-	-	-	-
Protein casts, tubular	-	1M	1M	1M	1M	1M	-	1M	1M	1M
Nephrocalcinosis	-	-	-	-	-	-	-	-	-	-
Liver	-	-	-	-	-	-	-	-	-	-

Key: - =negative/no significant finding; + = positive/finding present; 1 = minimal severity; 2 = mild severity; 3 =moderate severity; 4 = marked severity; F = focal; M = multifocal; D = diffuse.

FIGURES

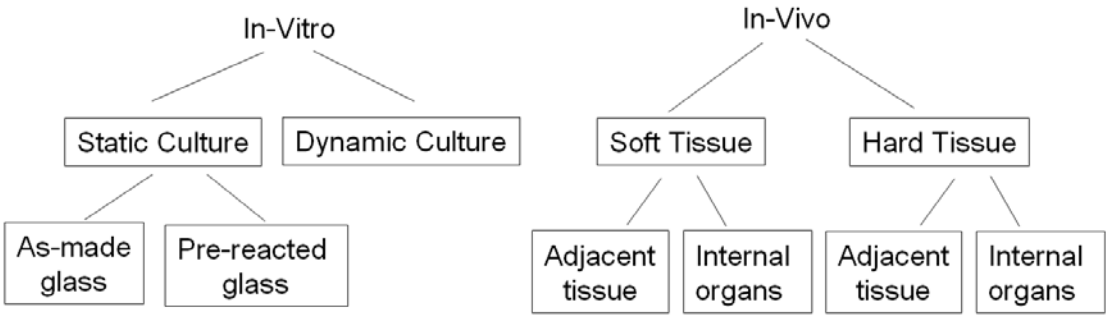

Figure 1 – Methods and testing conditions for boron toxicity *in-vitro* and *in-vivo*.

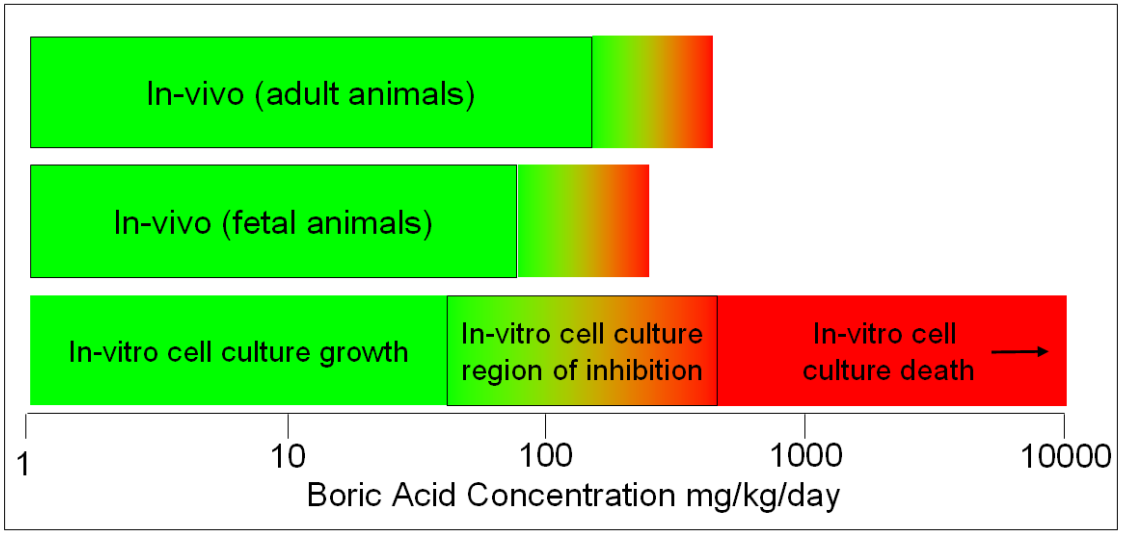

Figure 2 – *In-vitro* and *in-vivo* data for boric acid toxicity in mg/kg/day. The green regions represent no toxicity, the green to red fade regions show where inhibition begins, and all red shows where cell death occurs.

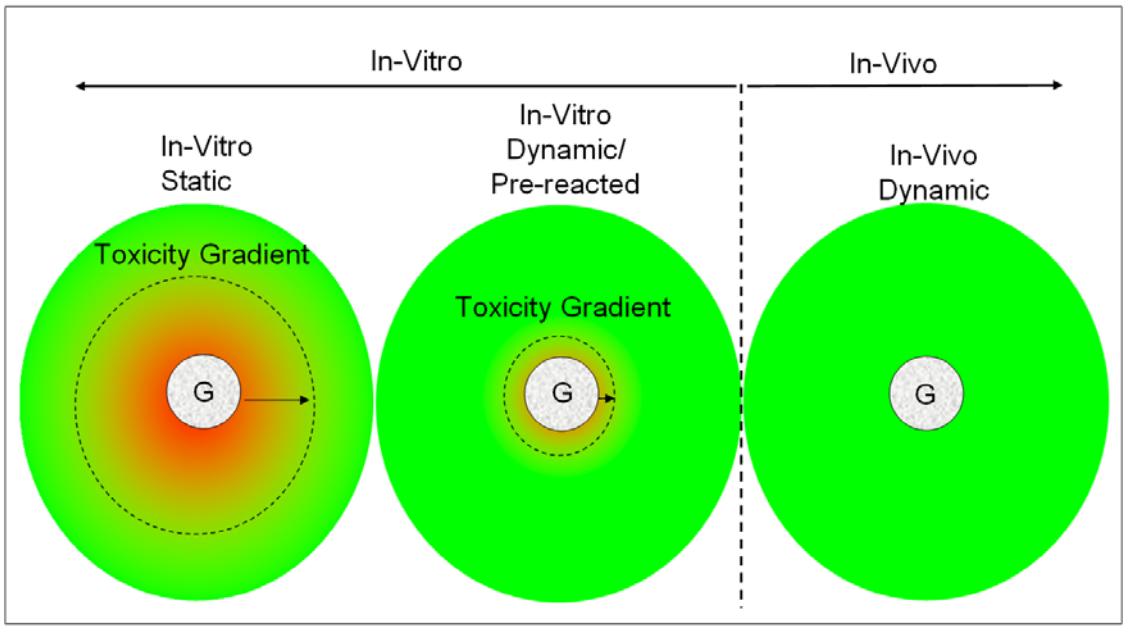

Figure 3 – Schematic showing how toxic conditions could develop (pH, B concentration, etc) and affect the immediate surroundings of a highly reactive material during *in-vitro* static conditions, *in-vitro* dynamic or pre-reacted conditions, or *in-vivo*. The circle labeled (G) represents a glass disk, fiber, sphere, or particle.

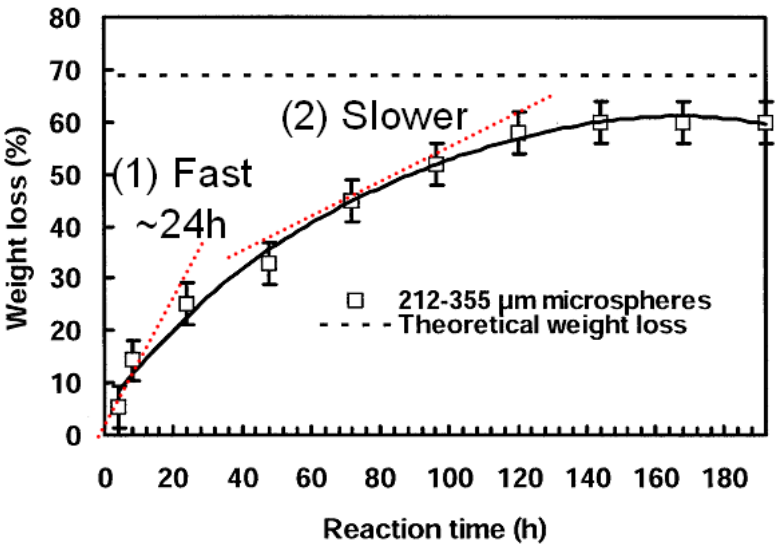

Figure 4 – Weight loss data for a soda lime borate glass showing the initial fast weight loss (24 hrs), followed by a decreasing weight loss which was attributed to the precipitation of calcium phosphate on the glass surface [7].

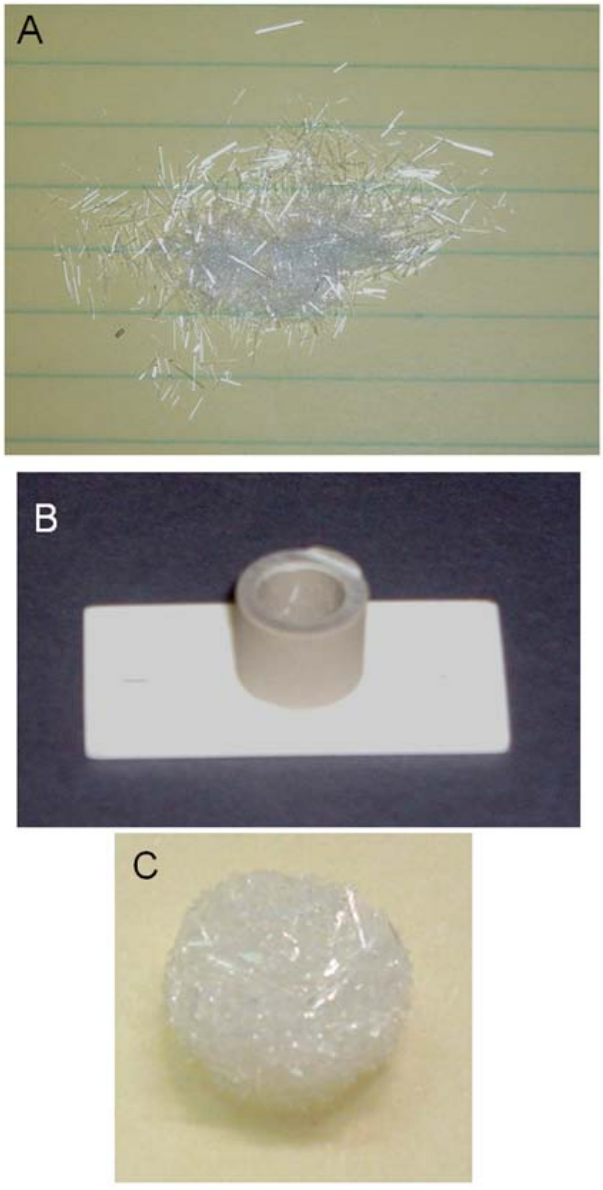

Figure 5 – Steps in manufacturing a scaffold composed of randomly oriented glass fibers. The as-made fibers (100 to 300μm diameter, 2 to 3mm long) are shown in (A). The mold used for holding the fibers (70mg) during the heat treatment (575^{o}C to 690^{o}C depending on glass composition, for 45 minutes) is shown in (B). An as-made scaffold (nominal dimensions of 7mm diameter, 2mm thick) composed of self bonded randomly oriented fibers is shown in (C).

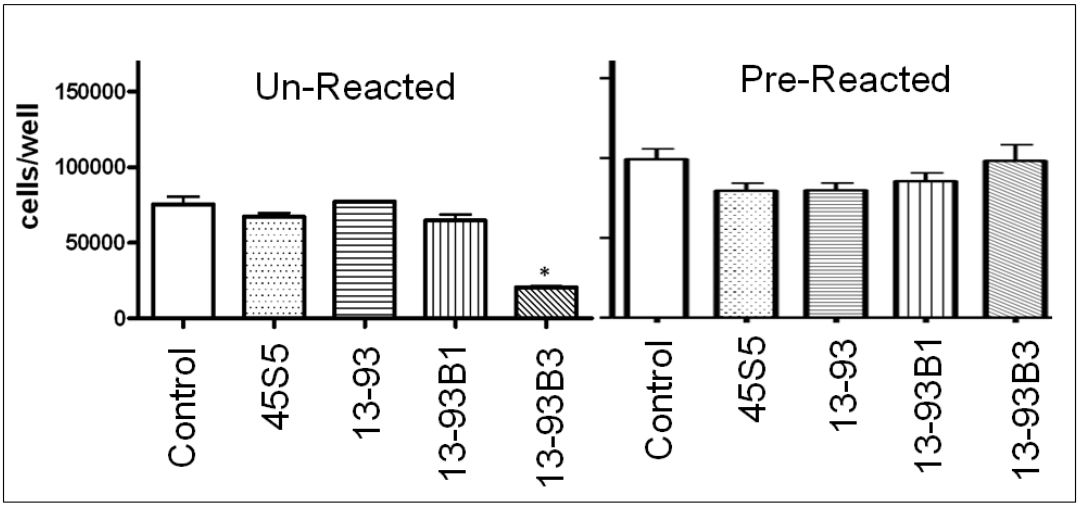

Figure 6 – Proliferation of MLOA5 cells after 24 hours at 37^{o}C on unpolished as-cut bioactive glass disks and pre-reacted bioactive glass disks. [13]. * $p<0.001$ when compared to control.

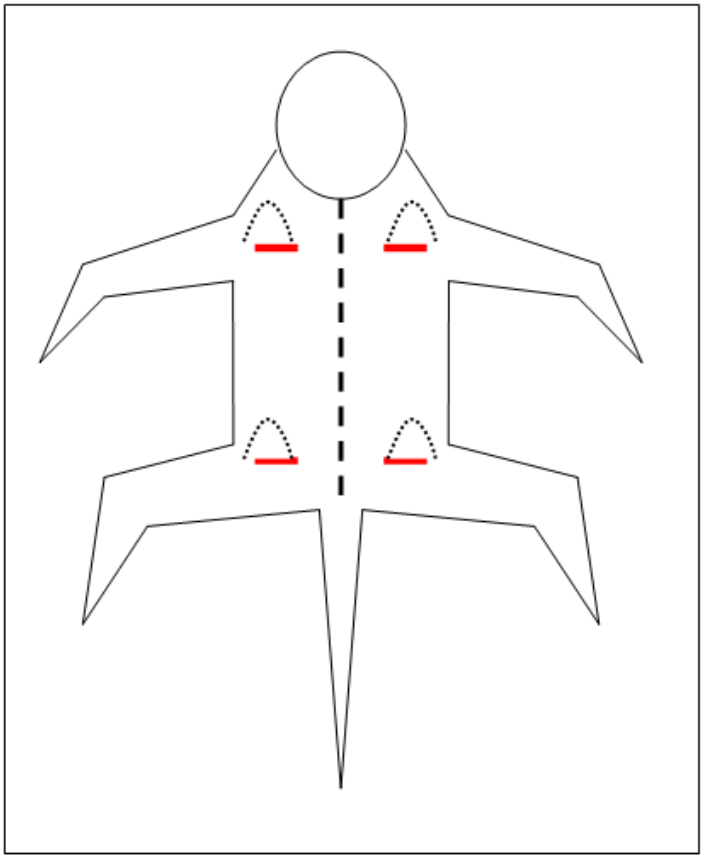

Figure 7 – Schematic showing the implant sites located on the back of a rat. The red lines are sites where the skin was cut (15mm) and the dotted line represent the approximate implant site (20mm long). Up to 16 borate glass fiber scaffolds, four per site, were implanted in a rat.

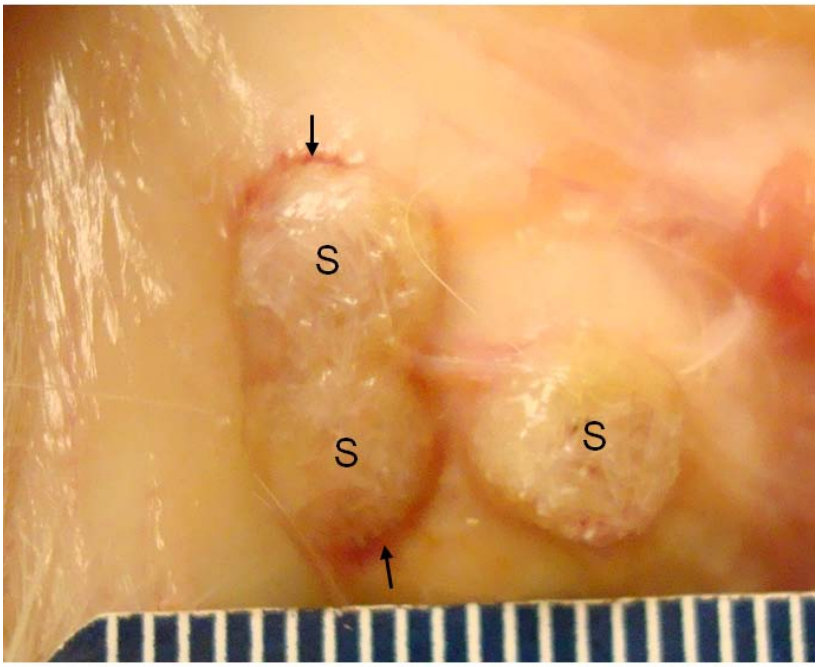

Figure 8– Appearance of a subcutaneous site containing three 13-93B3 scaffolds after four weeks in subcutaneous tissue. The scaffolds are labeled with an S and arrows point to tissue rich with blood vessels surrounding two of the scaffolds (red tissue).

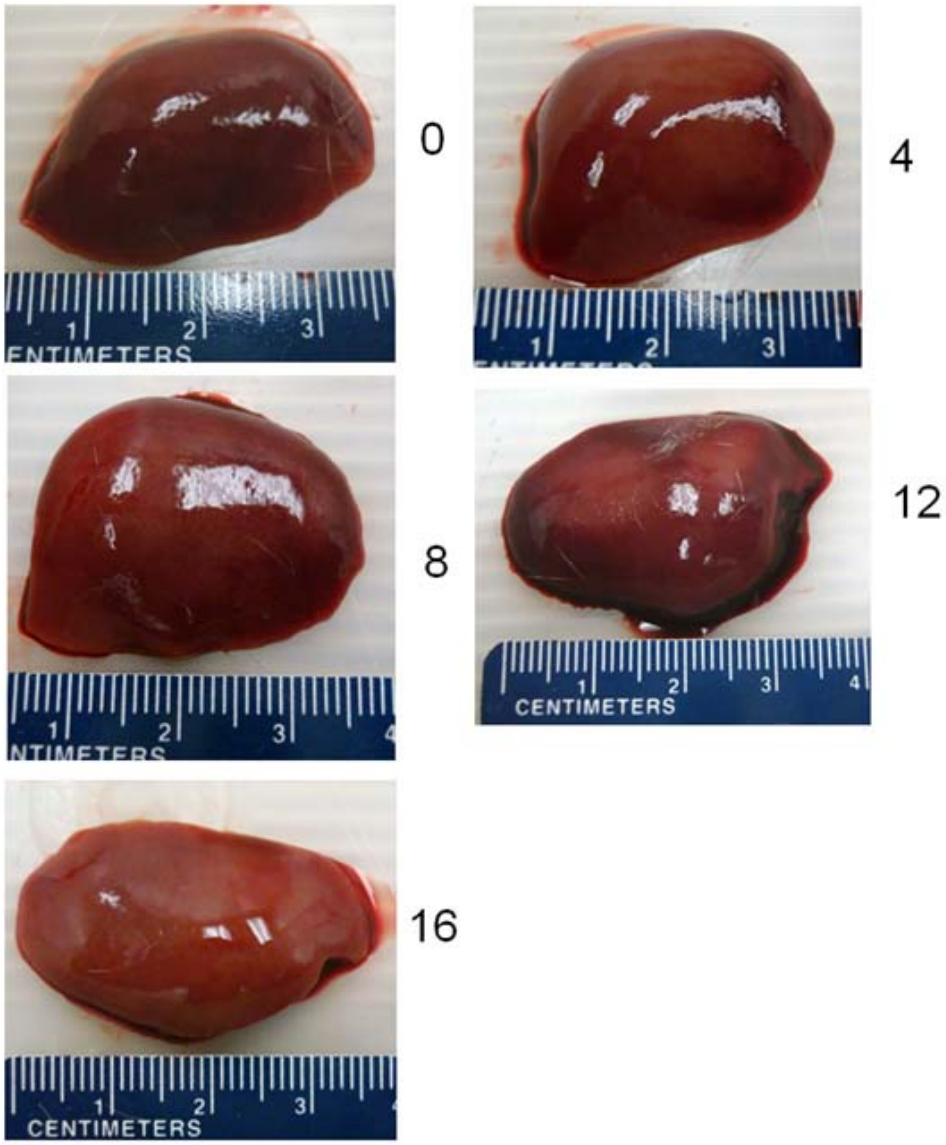

Figure 9– Representative photographs of the livers recovered from rats implanted with up to sixteen 13-93B3 fiber scaffolds (70mg each). The number at the side of each image corresponds to the number of 13-93B3 fiber scaffolds implanted in the rat; control (0), (4), (8), (12), and (16).

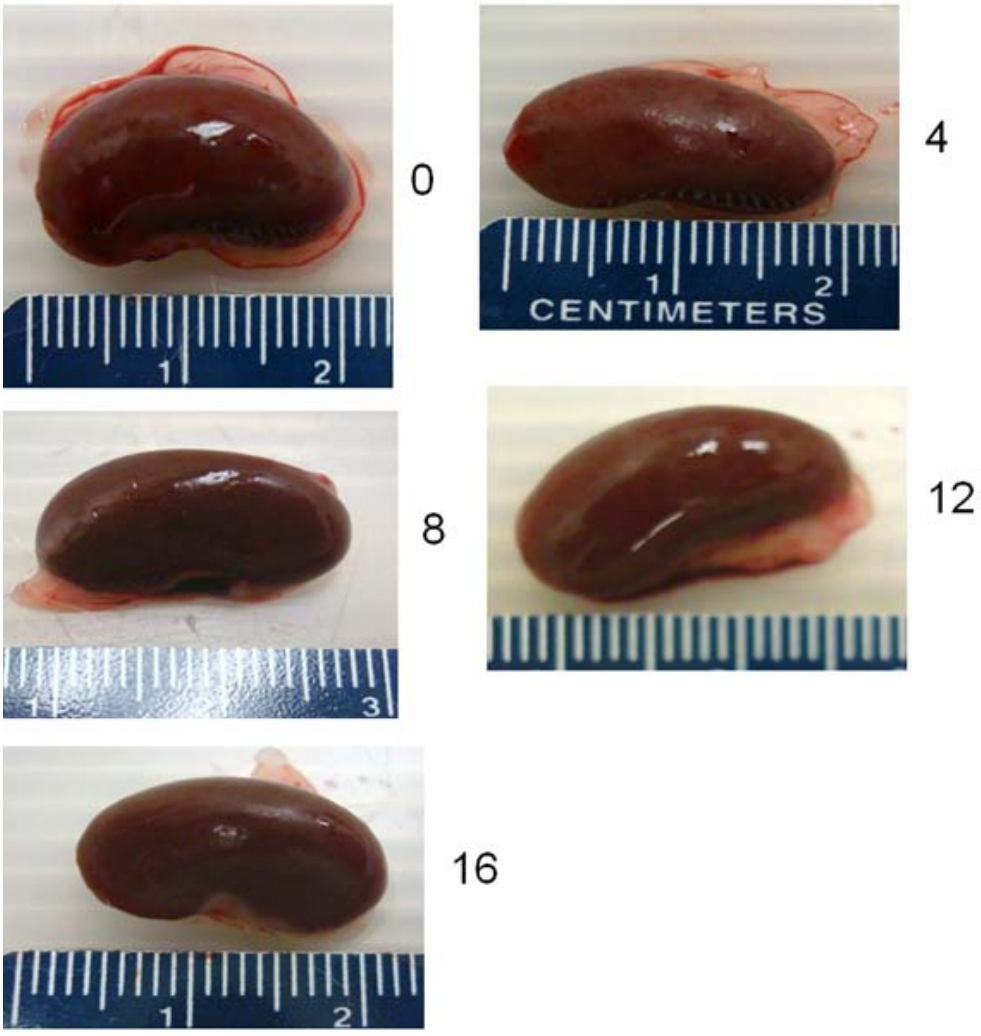

Figure 10 – Representative photographs of the kidneys recovered from rats implanted with up to sixteen 13-93B3 fiber scaffolds (70mg each). The number at the side of each image corresponds to the number of 13-93B3 fiber scaffolds implanted in the rat; control (0), (4), (8), (12), and (16).

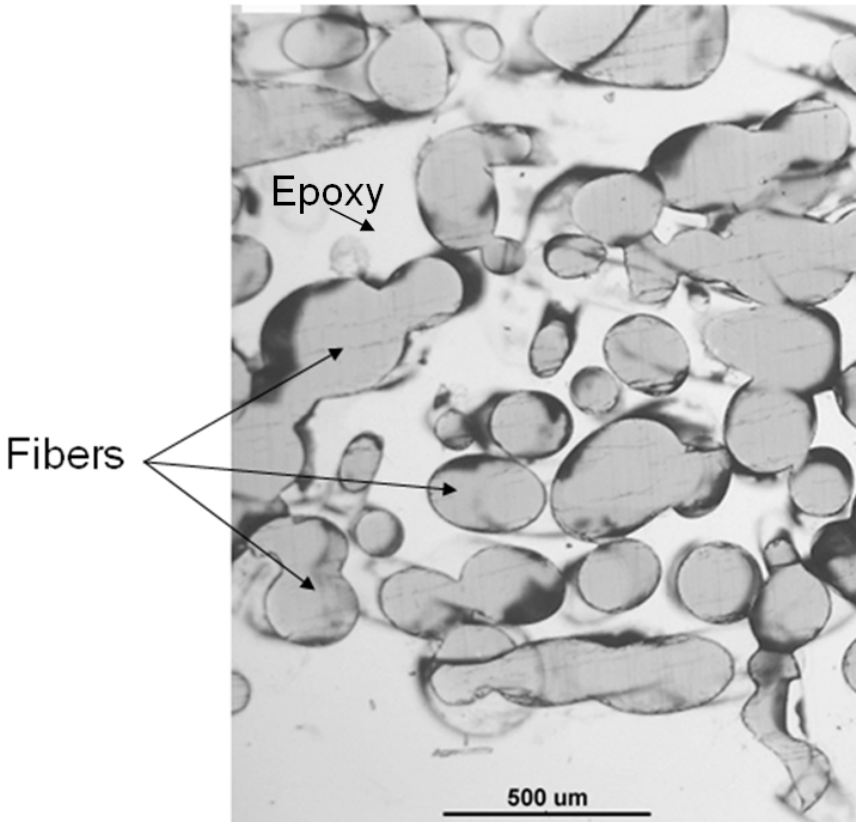

Figure 11 – Cross section of a glass scaffold composed of randomly oriented bioactive glass fibers that have been infiltrated with transparent epoxy which provides a reference for the histological images. The fibers (gray) are circular or elliptical depending on the orientation, and the fibers that have bonded to other fibers in the plane of the cross section look like complex geometrical shapes. The epoxy occupies what were initially open, interconnected pores of the scaffold.

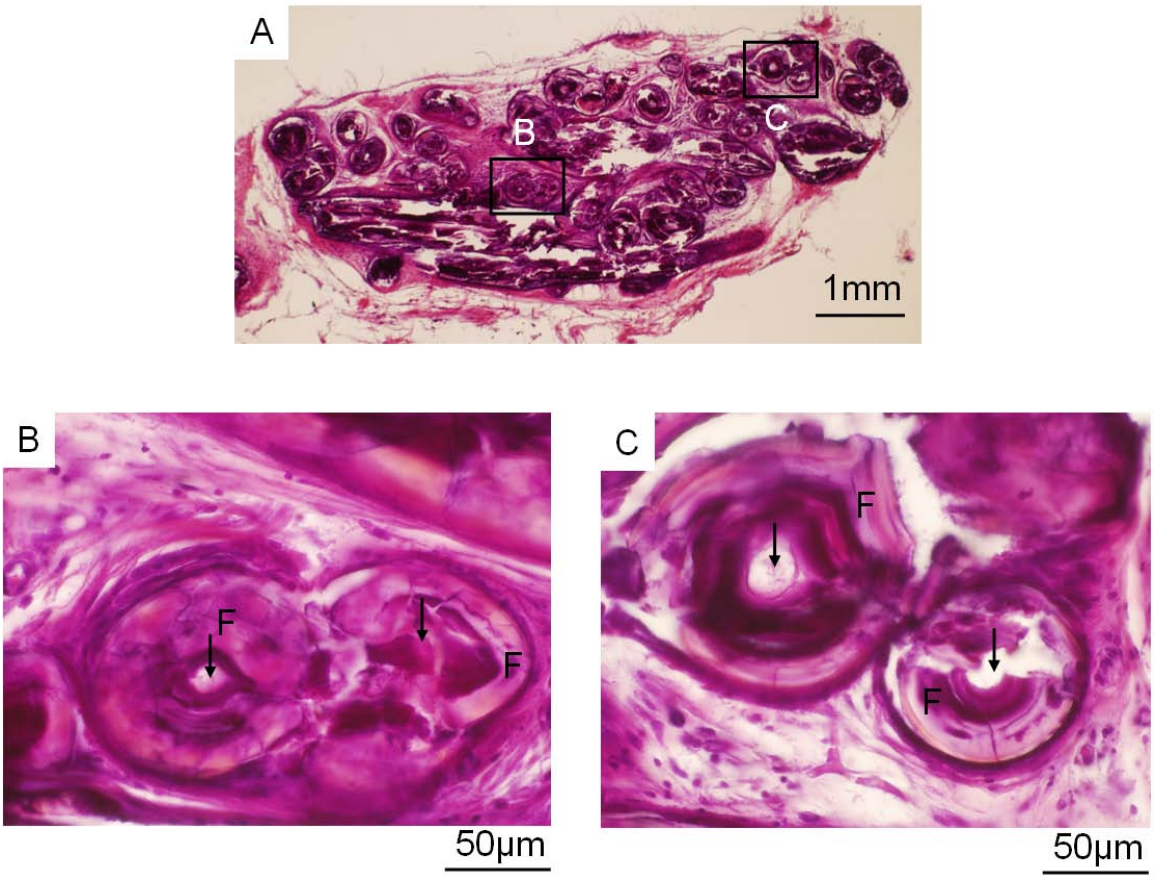

Figure 12 – H&E stained section of a 13-93B3 scaffold implanted in subcutaneous tissue for four weeks (A). The section is >90% filled with soft tissue and the fibers have all reacted. A magnified view of box B, located at the center of the scaffold, is shown in (B). There are two fibers that have reacted as indicated by the arrows pointing to the center of the fibers. Healthy soft tissue has attached to the inner and outer surfaces of the fibers. A magnified view of the scaffold at the outer edge is shown in (C), where two fibers that have reacted and are surrounded by soft tissue.

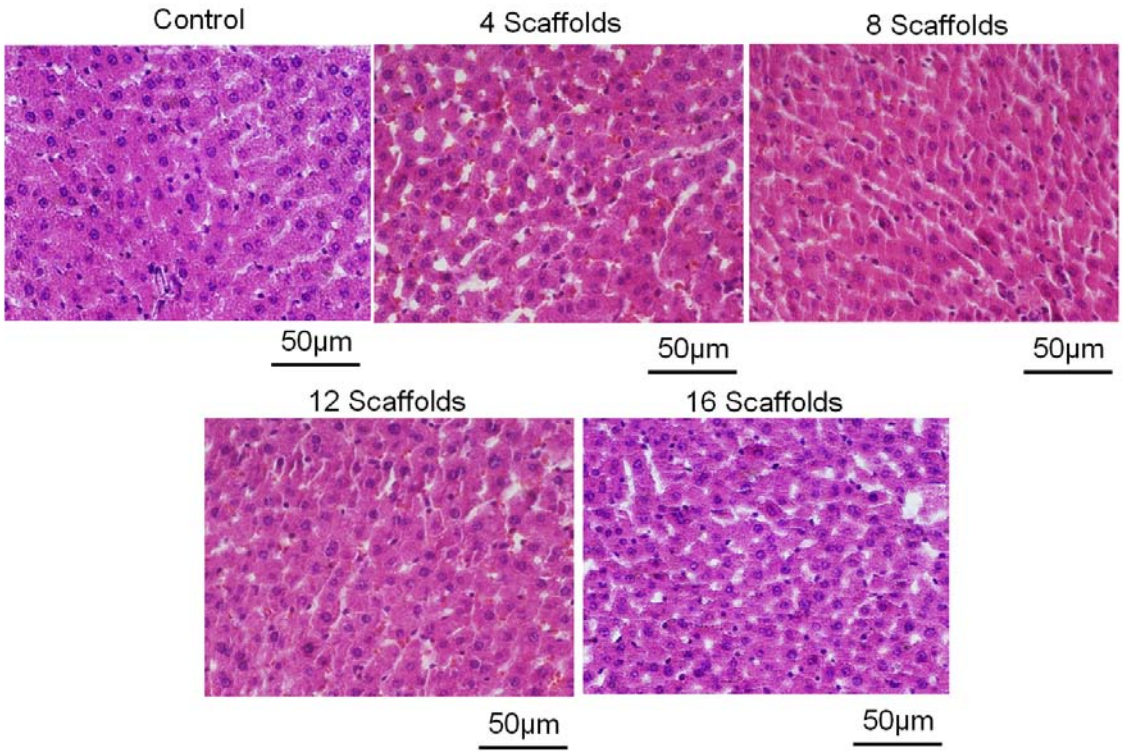

Figure 13 – H&E stained section of a control liver and a liver section from a rat with four to sixteen 13-93B3 scaffolds (70mg each) implanted in subcutaneous tissue. The estimated boric acid concentration present in the rat with 16 scaffolds was 126mg/kg/day.

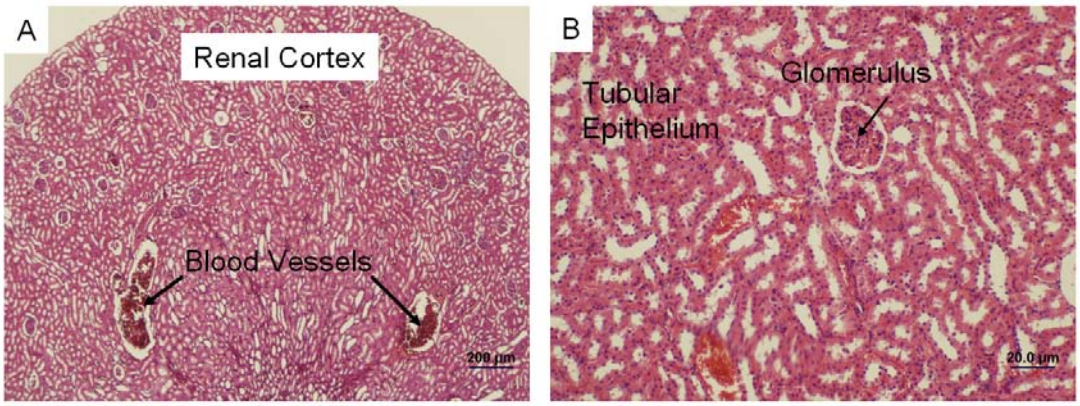

Figure 14 – Photomicrograph of an H&E stained section of the renal cortex from a control rat (A). Figure 14B is a magnified view of the renal cortex showing the tubular epithelium and a glomerulus (a capillary tuft where blood begins the filtering process to form urine).

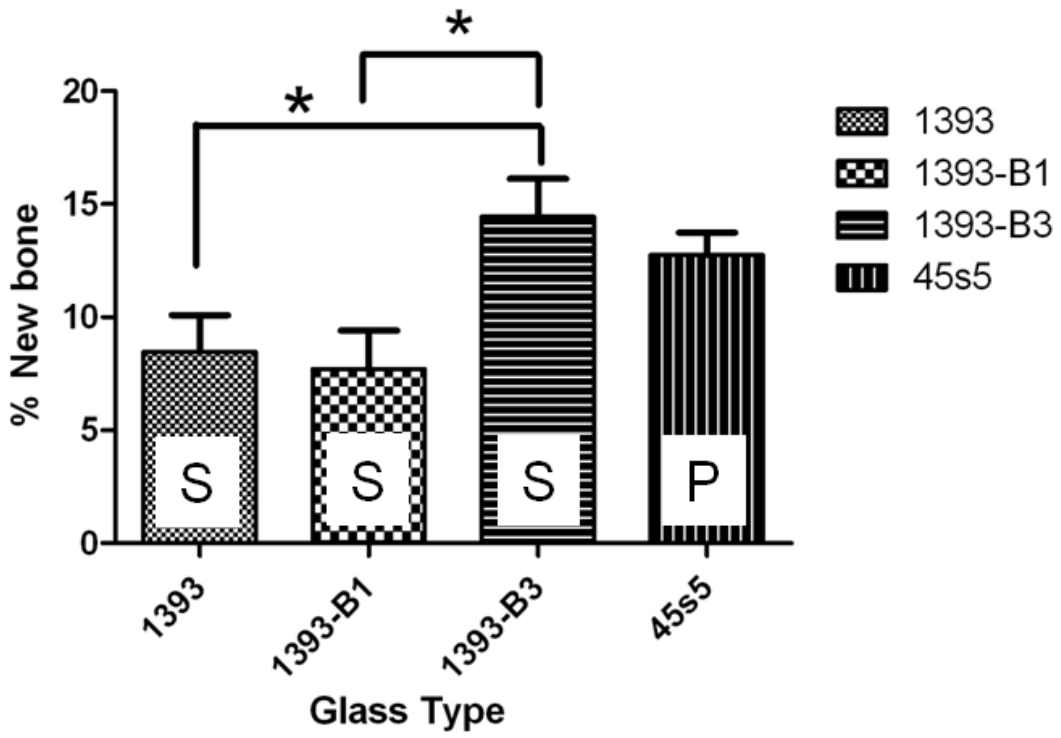

Figure 15 – Total bone growth into randomly oriented porous bioactive glass scaffolds (S), (45S5 was loose particulate (P) form (100 to 200µm)) after 12 weeks in rat calvaria (n=4) as determined by histomorphometry analysis. The 13-93B3 scaffolds generated twice as much bone as the 13-93 or 13-93B1 scaffolds and had statistically more bone *($p<0.05$), personal communication [16].

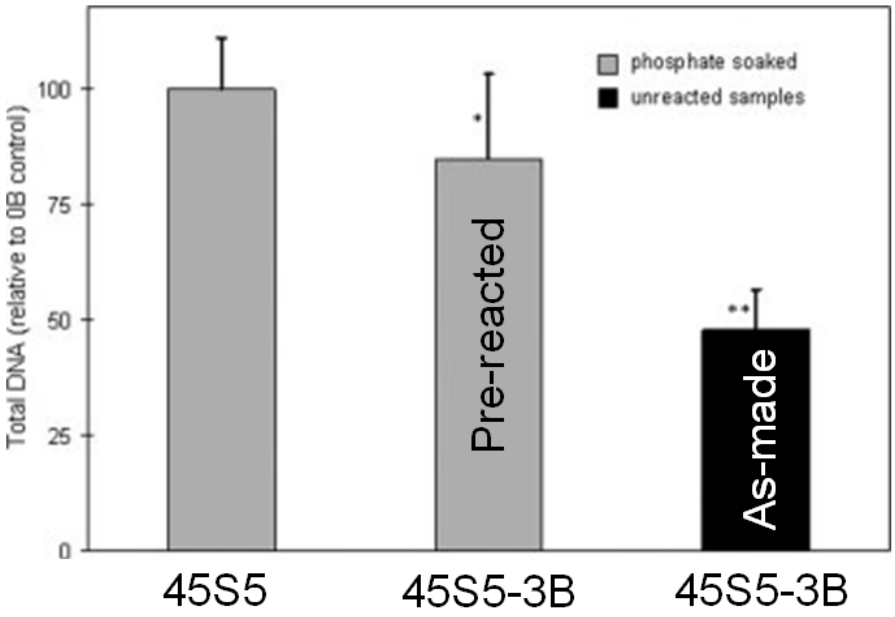

Figure 16 – Quantitative measurement of DNA produced by MC3T3-E1 cells cultured for four days on as-made disks of 45S5 (0B), pre-reacted 45S5-3B, and as-made 45S5-3B glass disks after four days of culture. The pre-reacted 45S5-3B glass contained ~2x the DNA as the as-made glass [6]. * $p<0.05$, ** $p<0.01$ as compared to 45S5.

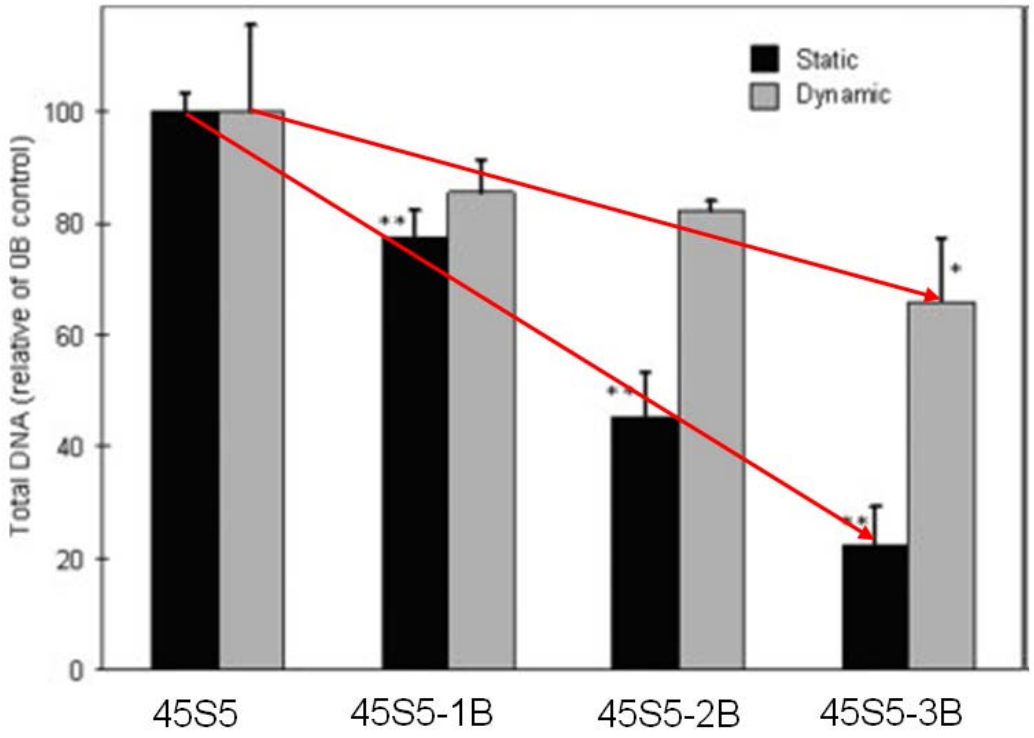

Figure 17 – Quantitative measurement of DNA from MC3T3-E1 cells for 45S5 (0B), 45S5-1B, 45S5-2B, and 45S5-3B glass disks after four days of culture under static (black) and dynamic conditions (gray). The dynamic condition significantly improved the amount of viable cells for all the boron containing glasses after four days of culture as indicated by the red lines [6]. * $p<0.05$, ** $p<0.01$ as compared with 45S5.

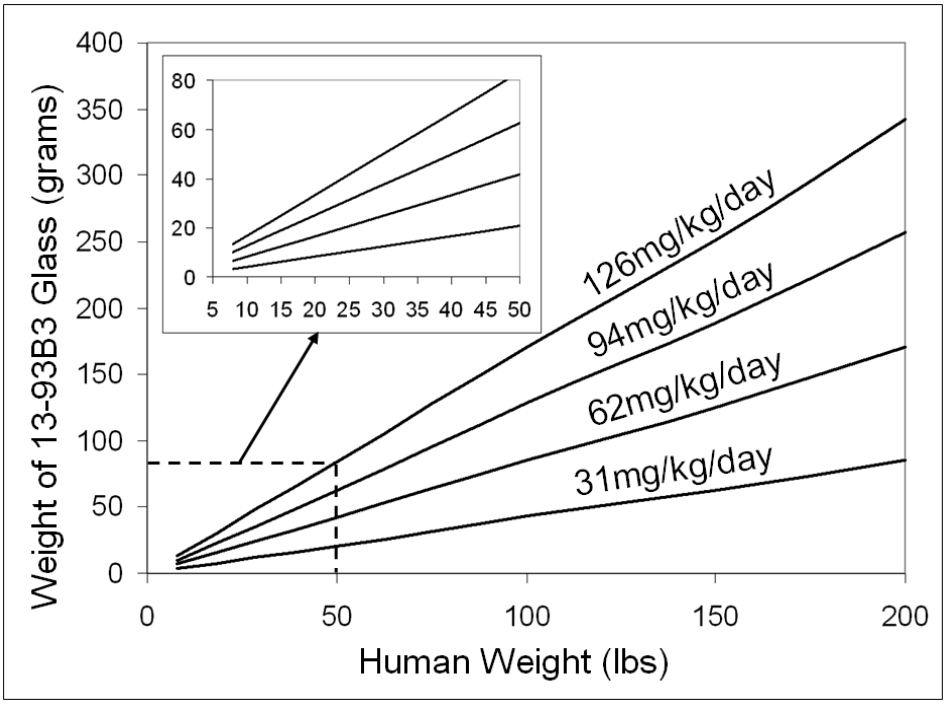

Figure 18 – Estimation of how much 13-93B3 glass could be implanted in a human based off of the histological analysis of the kidney and liver from Sprague Dawley rats. Eight to 50 pounds was magnified to make reading the graph at lower weights easier.

3. ANGIOGENIC BIOACTIVE BORATE GLASSES

Steven B. Jung[1], Delbert E. Day[1], and Roger F. Brown[2]

[1]Graduate Center for Materials Research, Materials Science and Engineering Department, Missouri University of Science and Technology, Rolla, MO, 65409-1170

[2]Department of Biological Sciences, Missouri University of Science and Technology, Rolla, MO, 65409-1170

3.1 ABSTRACT

Porous scaffolds composed of randomly oriented bioactive borate glass fibers doped with copper, strontium, zinc and iron were implanted in laboratory rats for up to six weeks to study the biological and angiogenic response. No inflammation or infection was detected at any of the implant sites with a CuO concentration at or below 0.4wt%. Scaffolds made from fibers containing (0.1 to 2wt%) CuO had a marked increase in blood vessels surrounding the scaffolds after two and four weeks *in-vivo*. After six weeks, a blinded histological blood vessel analysis (PAS) of the tissue present in the scaffolds showed that 0.4wt% CuO produced a statistically significant increase in blood vessel area compared to the un-doped scaffold. It was also found that seeding the scaffolds with mesenchymal stem cells also increased the number of blood vessels present in the subcutaneous implants. In a second experiment, the angiogenic effect of strontium, zinc, and iron was evaluated in scaffolds doped with 0.4wt% CuO. Upon retrieval of the scaffolds, significant numbers of blood vessels were present in the adjacent tissues and an analysis of the infiltrated tissues showed that the addition of zinc to the copper doped bioactive glass produced a significant increase ($p<0.05$) on the number of blood vessels present.

3.2. INTRODUCTION

Bioactive glasses were first introduced by Hench in 1969 with the well known silicate based 45S5 (Table 1) [1]. Since then, several silicate based bioactive glasses such as 45S5, 13-93, S53P4 (Table 1), and other compositions have been widely studied for bone [1-4] and soft tissue [2, 5] applications. Some of these applications include replacement of bones in the middle ear [6], treatment of periodontal defects [6, 7], and periodontal implants [6].

In the last 10 years, three dimensional porous scaffolds composed of bioactive glass [8-14], calcium phosphates such as hydroxyapatite [15-18], and carbonates such as calcium carbonate [17, 18] have been studied for bone augmentation. Unfortunately, the inability to promote vascularization in many of these materials has limited their use [19]. *In-vitro* performance of porous scaffolds in a regularly agitated culture dish or in a perfusion chamber are not necessarily a good estimate of what may be expected *in-vivo* since the nutrients are constantly being replenished to the cells [19]. The approximate diffusion limit for oxygen and most nutrients is 100 to 200μm from a blood capillary [19], therefore successful *in-vivo* performance of a scaffold requires a vascular network that can provide an adequate blood supply [19].

In general, porous scaffolds for tissue regeneration have not performed as well as hoped [19]. Current scaffolds made from materials such as titanium, hydroxyapatite, or even bioactive glass such as 45S5 lack the ability to stimulate angiogenesis (blood vessel formation), which is the key component required for tissue regeneration [19]. Several methods of improving the vascularization of scaffolds have been investigated including attaching vascular endothelial growth factor [20], coating scaffolds with copper

containing salts [21, 22], *in-vitro* pre-vascularization [19], and *in-vivo* pre-vascularization [19].

Unfortunately, all of the previously mentioned methods of promoting angiogenesis have drawbacks. Growth factors are expensive and have limited usefulness in treating wounds as several growth factors are required at specific time points for enhanced healing, but only a few growth factors are approved by the Food and Drug Administration (FDA) for clinical use [23]. *In-vitro* procedures are time consuming and must be planned in advance of the surgery. *In-vivo* pre-vascularization requires multiple surgeries which increases the possibility of infection and also requires a significant amount of planning and time. The dissolution of copper containing salts, while shown to promote blood vessel growth [21], has the potential to dissolve too quickly, especially in large scaffolds, and dissipate before the full beneficial effect of copper has occurred.

Of the previously discussed methods for promoting angiogenesis in scaffolds, the release of metal ions such as copper, is effective, relatively inexpensive, and requires a single surgical procedure. The role and requirement of copper ions for angiogenesis has been well documented *in-vitro* and *in-vivo*. Hu et al showed that copper ions in the concentration of 5 to 500μM promoted the growth and proliferation of human endothelial cells *in-vitro* [24]. The addition of metal ions such as copper and tin to cell culture media has been shown to promote endothelial cell migration [25]. Barralet et al increased the vascular density inside a calcium phosphate scaffold by releasing copper sulfate. Copper ions released from a hyaluronan based hydrogel promoted blood vessel formation in soft tissue [22]. The addition of copper chelators (blockers) has a negative effect on tumors,

essentially decreasing the microvascular density and decreasing the amount of copper stimulated enzymes available for tumor growth [26].

Other trace elements such as zinc, boron, strontium, and iron have been studied for specific biological responses and are elements found in human cadaver bone [27]. Zinc serves as a cofactor responsible for keratinocyte migration during wound healing which promotes re-epithelialization and also improves epithelial cell resistance to apoptosis [28]. Zinc oxide has also been shown to decrease blood clotting time *in-vitro* [29]. Boron, in the form of boric acid, added in the concentration of 1 to 10mM to cultures of human placental cells caused a significant increase in mRNA uptake that was described as similar to what would be expected of a growth factor [30].

Greater than 99% of the strontium in the human body is located in the skeleton [31]. Rats given strontium in quantities >4g/l in food and water showed signs of disturbed bone mineralization, and it is speculated that this is due to the larger size of strontium compared to calcium [31]. Strontium in relatively low doses, <4g/l of food and water had increased bone formation rates and increased trabecular bone density [31]. Iron is a constituent of several enzymes, bone marrow, and red blood cells [32], and a deficiency of iron in the body can lead to anemia [32]. Iron oxide may also be useful in increasing blood clot formation rates [29].

In the present work, four of the most abundant minor elements found in human bone have been systematically doped into the 13-93B3 glass for the purposes of promoting angiogenesis. With the exception of copper, the amounts of the trace elements was based on the relative abundance of the trace elements in human cadaver bone [27]. The elements were added to the 13-93B3 glass consecutively, copper (C or Cu), copper +

strontium (CS), copper + strontium+ zinc (CSZ), and copper + strontium + zinc + iron (CSZF). Fibers of each glass were thermally bonded to form porous scaffolds that were implanted in the subcutaneous tissue of rats for six weeks. The scaffolds were removed after durations between two and six weeks and the tissue analyzed for the presence of blood vessels.

3.3. MATERIALS AND METHODS

3.3.1 Glass Melting and Scaffold Preparation

The borate glass compositions present in Table 1 were made from homogeneous mixtures of reagent grade chemicals which were melted in a platinum crucible at 1065^{o}C for one hour. Fibers, with a diameter ranging from 100 to 300μm, were pulled, by hand, from the melt. These fibers were broken into 2 to 3mm lengths which were used to prepare porous scaffold composed of randomly oriented fibers.

Approximately 70mg of fiber was placed in a cylindrical ceramic mold (mullite) with an internal diameter of 7mm. The molds were placed in an oven at 575^{o}C for 45 minutes, after which the molds were removed and cooled to room temperature. Once cool, the scaffolds were removed from the molds and were ready for use. Examples of the as-made scaffolds doped with up to 2wt% CuO have the nominal dimensions of 7mm in diameter and 2mm thick are shown in Fig 1.

Prior to implantation of the as-made scaffolds or cell seeding with mesenchymal stem cells (MSCs), the scaffolds were dry heat sterilized. The scaffolds were placed in a silica glass vial, covered with a loose fitting aluminum foil top, heated in an oven to

300^{o}C for four hours, and cooled to room temperature. Once cool, the scaffolds were ready for either cell seeding with MSCs or implantation.

3.3.2 Scaffold Seeding with Mesenchymal Stem Cells (MSC)

Mesenchymal stem cells were recovered from the long bones of sacrificed Fisher 344 rats. The cells were cultured *in-vitro* to separate the stem cells from bone marrow prior to seeding the scaffolds. Half of the scaffolds were seeded with 50,000 MSCs, the other half were unseeded. The cells were cultured on the scaffolds for approximately 12 hours to allow the cells to attach to the glass fibers prior to the implantation.

3.3.3 Scaffold Implantation

Five scaffolds made from each type of glass seeded with MSCs and five unseeded as-made scaffolds were implanted in subcutaneous tissue of Fisher 344 rats for six weeks. The scaffolds were implanted randomly to remove any bias from a single rat. Each rat had four implant sites, two above the shoulders and two above the back legs, which contained a single scaffold for a total of four scaffolds per rat. The back of each rat was shaved with clippers to remove hair from the implant sites and washed with iodine and then 70% ethanol to disinfect the rats prior to surgery. During surgery, the rats were anesthetized with isoflourine.

An incision approximately 20mm in length was made completely through the cutaneous tissue perpendicular to the spine with a pair of surgical scissors. Next, a clamp was inserted into the incision and gently opened to form an opening between the cutaneous tissue and the skeletal muscle. The opening was made approximately 15 to 20 mm long. The scaffold was then inserted toward the back of the cutaneous opening and the skin was closed with superglue.

After all four scaffolds were implanted; each rat was injected with 0.2ml of penicillin (0.1ml per hind leg). The ears of each rat were labeled and they were placed on a heating pad in a cage with access to fresh air during recovery. Two rats were caged together, had access to food pellets and tap water, and were on a light schedule of 12 hours light, 12 hours dark.

3.3.4 Scaffold Removal

After two, four, or six weeks, respectively, the rats were sacrificed by CO_2 inhalation and the scaffolds were removed for analysis. The scaffolds were placed in 5ml of 10% formalin solution for four days to fix the tissue.

3.3.5 Tissue Processing

After the scaffolds were fixed, they were dehydrated with a series of ethanol solutions by a microwave dehydration technique (EBSciences H2850 Microwave Processor) [33]. The microwave was operated at 70% power, and sample temperature was set to 37 ± 4^{o}C, for 2.5 minutes for each solution. Each scaffold was immersed in each ethanol solution for a minimum of 15 minutes including microwave time.

3.3.6 Histology Slide Preparation

The dehydrated scaffolds were placed in a tissue processor (AutoTechnicon Model 2A) filled with fluid paraffin mounting wax (Paraplast Tissue Embedding Medium, McCormick Scientific LLC) at 45^{o}C for four hours for wax infiltration of the scaffold and tissue. Each scaffold was mounted in wax for histological sectioning with a paraffin mounting system (Leica EG 1150H). Sections 18µm thick were cut with a histological microtome (Leica RM 2235 microtome) with TBS Shur/sharp blades, (Triangle Biomedical Sciences, Durham NC). The cut sections were floated on a water

bath (Lipshaw Electric Tissue Float, model number 375, Detroit MI) (40^{o}C) prior to mounting on a glass slide (Fisher Brand Superfrost microscope slides, St. Louis MO). Three to four tissue sections were placed on a single glass slide, and dried overnight (Fisher Scientific slide warmer, St. Louis MO). Stained slides were viewed with a microscope (Olympus BX50, Olympus Optical Co) at magnifications of 40, 100, and 400X and imaging software (DP Controller, Olympus Optical Co) was used for image capture.

A scaffold composed of randomly oriented fibers was embedded in poly methyl methacrylate (PMMA) for use as a reference for the histology sections. The plastic embedded fiber scaffold was sectioned with a slow speed saw and a diamond coated blade and polished with 320, 400, 600, 800, and 1200 grit silicon carbide paper. An image of the polished scaffold section is shown in Fig 6. The fibers appear round if the longitudinal axis of the fiber is perpendicular to the plane of the image and ellipsoidal if the fiber is cut at an angle to its longitudinal axis.

3.3.7 Histological Assessment

3.3.7.1 Blood Vessel Analysis after Six Weeks *In-Vivo* – Copper Additions

Scaffolds of 13-93B3, B3 Cu-1 and B3 Cu-3, seeded with MSCs and implanted for six weeks in subcutaneous tissue, were sectioned 18μm thick, and stained with hematoxylin and eosin stain (H&E), procedure described in detail elsewhere [34], for a blood vessel analysis. The blood vessels present in each tissue section were counted in 20 randomly selected spots, which predominantly encompassed soft tissue, to determine the number of vessels present and to calculate the average blood vessel diameter.

Blood vessel formation was assessed from a blinded analysis of tissue sections from the seeded (msc) and unseeded 13-93B3, B3 Cu-1, and B3 Cu-3 scaffolds implanted in subcutaneous tissue for six weeks. Each type of scaffold, n=3, was stained with Periodic Acid Schiff stain (PAS) and was analyzed as illustrated in Fig 9, where the center of the scaffold was examined across its middle (dashed line) with a 200x objective. The blood vessels in each track of tissue were counted and each blood vessel diameter measured. The data from each scaffold was compared by the student t test. An example of the PAS stained tissue is shown in Fig 10.

3.3.7.2 Blood Vessel Analysis – Minor Element Additions (H&E)

Three scaffolds of each composition (B3 Cu-3, CS, CSZ, CSZF) were stained with H&E and the number of blood vessels seen in the soft tissue were counted. Three lines from each histological tissue section (parallel to the thickness (2mm) direction and at least 1mm apart) were viewed at 400x magnification and the blood vessels counted. An example of one scaffold section and the three tracks of tissue analyzed are shown in Fig 11 and the remaining sections are shown in the appendix.

3.4. RESULTS

3.4.1 Scaffold Removal

Photographs of the unseeded, copper containing scaffolds taken as they were removed after two weeks in subcutaneous tissue are shown in Fig 2. It is apparent from these pictures that the release of copper from the glasses, especially B3 Cu-3 to B3 Cu-5, produced a noticeable increase in the number of blood vessels growing toward and into the scaffolds when compared to the copper-free 13-93B3 scaffold. The B3 Cu-5 scaffold

has at least six blood vessels growing toward the scaffold and blood vessels are visible inside the scaffold are marked with arrows. The blue color of the scaffolds containing, 0.2 to 2wt% CuO is still visible, which indicates that some portion of the copper ions are still in the glass fibers.

After four weeks *in-vivo*, there appears to be more blood vessels surrounding the scaffolds with 0.1wt% CuO (B3 Cu-1) than the copper free 13-93B3 scaffold, which have been circled for easier viewing (Fig 3). There are a few visible vessels at the surface of the 13-93B3 scaffold, but the B3 Cu-1 scaffold had three red areas (arrows) which indicate the presence of red blood cells and likely blood vessels. The B3 Cu-3 scaffold in Fig 3 has two areas (dark spots) that are attributed to numerous blood vessels. The side of the B3 Cu-3 scaffold that was attached to the subcutaneous tissue was separated and lifted from the tissue, and in doing so, the blood vessels were cut which extended from the subcutaneous tissue into the scaffold (arrows), which may account for the dark spots. Several blood vessels surround the B3 Cu-4 and B3 Cu-5 scaffolds, and in four weeks, fibrous tissue appears to have formed around the scaffolds containing greater than 1wt% CuO.

Based on the results from the four week scaffolds, four scaffolds (13-93B3 as the control, B3 Cu-1, B3 Cu-3, and B3 Cu-5) were chosen for a six week *in-vivo* experiment. Each of these four scaffolds had a set, n=4, that were seeded with 50,000 MSCs and a set, n=4, that were unseeded, for a total of 32 scaffolds in eight rats. The scaffolds were randomly implanted so that no rat contained a single set of scaffolds.

Representative images of scaffolds after six weeks *in-vivo* are shown in Fig 4. The B3 Cu-3 scaffolds were more red than the 13-93B3 scaffolds indicating more blood

vessels, and the MSC seeded scaffolds appeared to have more vessels present than the corresponding non-seeded scaffolds. The fibers in the scaffolds after six weeks *in-vivo* (13-93B3, B3 Cu-1 and B3 Cu-3) had lost their blue color which was present at two and four weeks. This loss in color is considered to indicate that the fibers had fully reacted with the body fluids and all of the copper ions originally in the glass fibers had been released. There was also no significant change in diameter or thickness of the scaffolds.

After six weeks *in-vivo*, the B3 Cu-5 scaffolds (2wt% CuO) were not biologically compatible. During removal, the B3 Cu-5 scaffolds were found to be surrounded by tissue approximately 15mm in diameter (twice the original diameter of the scaffolds) as indicated by the arrow in Fig 12A. The tissue was cut across the top (oval in Fig 12B), and a thick yellow fluid was inside. Further dissection of the tissue revealed a wall about 4mm thick that surrounded the B3 Cu-5 scaffold (Fig 12C). The scaffold was removed, Fig 12D, and had decreased in size to about 3mm in diameter. All eight of the B3 Cu-5 scaffolds, had the same appearance and reactions with the body as shown in Fig 12.

3.4.2 Histology

3.4.2.1 Histology – 4 Weeks (H&E)

After four weeks, many of the copper doped scaffolds had not fully reacted as previously indicated, but it was possible to cut sections at the outer edge of the 13-93B3, B3 Cu-1, and a B3 Cu-5 scaffolds. The stained section of the unseeded 13-93B3 scaffold in Fig 13A shows that the fibers are fully reacted and several contain soft tissue. Figures 13B and 13C show two magnified areas of tissue adjacent to reacted 13-93B3 fibers (F) with infiltrated soft tissue that contain blood vessels (arrows).

A section of B3 Cu-1 scaffold after four weeks *in-vivo* is shown in Fig 14A. There appears to be more blood vessels in the tissue at the outer edge of the scaffold in Figs 14B and 14C as indicated by the arrows. The majority of the fibers toward the center of the scaffold were not fully reacted as indicated by the presence of unreacted glass fibers. The B3 Cu-5 scaffold had more vessels present than either the 13-93B3 or the B3 Cu-1 scaffolds as shown by the histological section in Fig 15A. The magnified images of the B3 Cu-5 scaffold in Figs 15B and 15C show several blood vessels (V) in the soft tissue, and several of the blood vessels contain red blood cells (pink dots).

3.4.2.2 Blood Vessel Analysis – 6 Weeks (H&E)

After six weeks *in-vivo,* the number and diameter of the blood vessels were measured in a randomly chosen, seeded section of a 13-93B3, B3 Cu-1 and B3 Cu-3 scaffold to estimate the blood circulation inside the scaffolds. The color of the box on the tissue H&E stained sections indicates the number of vessels counted, so a green box is 1 to 2 vessels, yellow 3 to 4, light blue 5 to 6, orange 7 to 8, dark blue 9 to 10, and red 11 to 12. Examples of blood vessels in an H&E stained section shown in Fig 8 where each blood vessel has an arrow showing its location. For reference, the image in Fig 8 is from spot three in the B3 Cu-3 scaffold (Fig 7C). The total number of blood vessels found in the 20 spots from the 13-93B3, B3 Cu-1 and B3 Cu-3 scaffolds, were 66, 92, and 145, respectively (Fig 7).

3.4.2.3 Histology and Vessel Analysis – 6 Weeks (PAS)

The PAS staining technique is useful for a blood vessel analysis because it stains tissue light blue that is high in glycogen. Glycogen is a material that is carried by red blood cells and distributed throughout the body for cell metabolism. It diffuses through

the lining of blood vessels; therefore blood vessels tend to be relatively high in glycogen. Connective tissue stains light green, red blood cells bright green, blood vessel lining blue, and macrophages yellow or brown.

The results of the statistical analysis for the blinded blood vessel study using the PAS staining technique are given in Table 2 and an example of the PAS stained tissue is shown in Fig 10. The blood vessel area was measured as area percent of the entire section analyzed. The data for each scaffold is shown in Fig 16 along with selected comparisons which are indicated by the brackets and the p values shown.

3.4.2.4 Blood Vessel Analysis – Minor Elements Addition (H&E)

An example of the H&E histology sections used for the blood vessel analysis is shown in Fig 11. Several blood vessels throughout the three tissue sections have been identified by arrows to guide the reader. The average number of blood vessels counted in each of the scaffold types (Cu-3, CS, CSZ, and CSZF), n=3, are plotted in Fig 17 and were compared by the student t test for statistical significance (Table 3). There was a statistically significant increase in the total number of vessels in the zinc containing scaffolds (CSZ and CSZF) when compared to the Cu-3 scaffold, see Table 3. The CS scaffold had no statistically significant improvement over the Cu-3 scaffold although the average number of blood vessels increased about 30%. The addition of iron in the CSZF scaffold showed no significant increase in blood vessels as compared to the CSZ scaffold. The addition of the zinc to the scaffold (0.4wt% CuO) produced the most significant improvement in the angiogenic effect of the scaffolds.

3.5. DISCUSSION

3.5.1 Scaffold Removal and *In-vivo* Biocompatibility

During the removal of the scaffolds from the rats, it was apparent that the mechanical strength was decreased. The scaffolds were soft to the touch indicating that the fibers had reacted significantly with the animal fluids. The relatively high number of blood vessels present in the soft tissue surrounding the scaffolds and the change in color of the fibers were signs that the trace elements released from the scaffolds had an angiogenic effect. Subcutaneous skin tissue has relatively few blood vessels compared to other tissues like muscle or bone [35].

There were no signs of inflammation surrounding the scaffolds, infection at the implant site, or rejection of the scaffolds from the rats except the previously mentioned B3 Cu-5 scaffolds after six weeks *in-vivo*, which were doped with 2wt% CuO. These scaffolds are thought to have had the negative biological response due to the release of excessive copper to the surrounding tissues. Bioactive borate glasses not doped with CuO have been implanted in hard and soft tissue of rats, and there were no reports of necrotic tissue, increases in the presence of macrophages, or inflammation [12, 34, 36-39]. The systemic internal organs of rats such as the kidney and liver have also been screened for lesions and other tissue degeneration after implantation of 13-93B3 borate fiber scaffolds [40]. There was no marked difference between the rats implanted with sixteen (70mg) scaffolds versus the control rats, and any recorded finding was at the lowest severity and considered normal in adult rats [40].

3.5.2 Angiogenic Analysis of *In-Vivo* Scaffolds - Blood Vessel Analysis Six Weeks (H&E) and (PAS)

The diameter of each blood vessel in the three scaffolds described in Fig 7 was measured to find the average blood vessel diameter in each scaffold type. The average blood vessel diameter was calculated by measuring the diameter of each vessel at its smallest diameter, summing the diameters, and dividing by the total number of blood vessels. The shortest distance across each blood vessel was measured to have a conservative and consistent measurement technique for blood vessels that were cut at an angle different from perpendicular to the longitudinal axis in the histological sections.

The total blood vessel area for each scaffold was calculated by assuming the blood vessels were circular, so the area of a circle was used. The average blood vessel diameters were used to calculate the average area for the blood vessels for the 13-93B3, B3 Cu-1 and B3 Cu-3 scaffolds which were 205, 175, and 283μm^2, respectively. Figure 18 shows the average blood vessel area (dashed line) plotted vs. the left y-axis and the total number of vessels (dash and dot line) plotted vs. the right y-axis.

After six weeks *in-vivo*, the number of blood vessels in the B3 Cu-1 scaffold (0.1wt% CuO) increased ~50% over the 13-93B3 scaffold, but the average blood vessel diameter decreased by 30μm^2 (~15%). The decrease in blood vessel diameter from the 13-93B3 to the B3 Cu-1 could be coincidental to the scaffolds analyzed since n=1 for this analysis. Another possibility could be that the copper ions stimulated formation of vessels at more locations, but not enough copper was present to recruit significant amounts of endothelial cells that were required to increase the average blood vessel diameter.

The total vascular area was calculated by multiplying the average blood vessel area by the total number of vessels per scaffold type. The total vascular areas for the 13-93B3, B3 Cu-1 and B3 Cu-3 scaffolds, were ~13,000, ~17,000, and ~40,000μm^2, respectively, as shown in Fig 19. The addition of 0.4wt% CuO to the B3 Cu-3 scaffold increased the vascular area by ~300%, which is assumed to increase the blood flow through the scaffold by a similar amount.

The blinded analysis of the six week *in-vivo* PAS stained sections of 13-93B3, B3 Cu-1 and B3 Cu-3 scaffolds, n=3, confirmed the findings of the H&E blood vessel analysis that the release of copper from a bioactive glass promoted angiogenesis in the surrounding tissues. The B3 Cu-3 scaffold with and without seeded MSCs had significantly more vessels ($p<0.05$) than the unseeded 13-93B3 scaffold. Copper is known to have a role in blood vessel formation as Harris et al reported copper as a requirement for angiogenesis [41], and the addition of copper in various forms to calcium phosphate scaffolds [21] and a hyaluronan based hydrogel [22] stimulated blood vessel formation. This however, is the first time that copper had been released from a bioactive glass and stimulated an angiogenic response *in-vivo*.

The addition of MSCs to the 13-93B3 bioactive borate fiber scaffolds also significantly improved the vascular growth ($p<0.05$) over the unseeded 13-93B3 scaffolds (Fig 16) without the expense of multiple surgeries or growth factors. Mesenchymal stem cells can differentiate into a variety of connective tissues including blood vessels, cartilage, and bone given the correct combination of biological signals and growth factors [35]. From this analysis, it was apparent that the 13-93B3 scaffolds

seeded with MSC's were in the presence of the correct combination of biological signals *in-vivo* to differentiate into blood vessels.

As additional evidence that copper released from bioactive glass is angiogenic, Brown et al counted the number of blood vessels present in the soft tissue that infiltrated porous 13-93 silicate scaffolds, 13-93B3 scaffolds, and B3 Cu-3 scaffold containing 0.4wt% CuO after two weeks in rat subcutaneous tissue [42]. The scaffolds were not fully reacted, particularly the slower reacting 13-93 silicate scaffolds, so the scaffolds were mounted in PMMA for sectioning and stained with Sanderson Bone Stain to differentiate the blood vessels from the other soft tissue. Ten random locations were analyzed from each scaffold section as shown by the arrows in Fig 20. Data from each scaffold type, n=2, was compared by the student t test to determine any significant statistical differences ($p<0.05$). There was no statistically significant difference in the number of blood vessels found ($p<0.6535$) in the copper free silicate (13-93) and borate (13-93B3) scaffolds, but the difference between B3 Cu-3 scaffold containing 0.4wt% CuO and copper free 13-93 was statistically significant as $p<0.0021$. After only two weeks *in-vivo*, copper released from borate glass was stimulating vascular growth better than a silicate based bioactive glass.

3.5.3 Blood Vessel Analysis of Scaffolds Doped With Selected Metal Ions

The bioactive borate scaffolds composed of B3 Cu-3 glass fibers contained a larger number of blood vessels when compared to 13-93B3 glass fiber scaffolds. Since copper had such a dramatic effect on vascular growth, copper was added to all of the minor element doped scaffolds to see what the effect, if any, occurred by the addition of strontium, zinc, or iron. Both scaffold types containing zinc (CSZ and CSZF) proved to

significantly increase the number of blood vessels ($p<0.05$), when compared to the B3 Cu-3 scaffold (Table 3). Having two sets of scaffolds (CSZ and CSZF), both containing equal amounts of zinc, and both statistically outperforming the B3 Cu-3 scaffold acts as a check and secondary data point confirming that the addition of zinc to the glass promoted an increased angiogenic response.

Zinc is well known to promote soft tissue reactions such as keratinocyte migration during wound healing which promotes re-epithelialization [28]. Keratinocytes are the cells that make up the majority of the epidermis [35], which includes blood vessels, so assuming the release of zinc from the scaffold increased the migration rate of the keratinocytes and promoted epithelialization inside the scaffold, the increase in blood vessels may be explained by the overall promotion of tissue growth.

3.6. CONCLUSIONS

The present work shows that ions important to stimulating angiogenesis can be released from bioactive glass to promote the important biological function. Scaffolds composed of bioactive borate glass fibers doped with copper, strontium, zinc, and iron, were used to promote angiogenesis in the subcutaneous tissue of rats. The copper doped borate glass (0.4wt% CuO) seeded and unseeded with MSCs produced significantly more blood vessels when compared to the copper free 13-93B3 glass fiber scaffold.

The addition of zinc to bioactive borate scaffolds doped with copper significantly increased the number of blood vessels in the subcutaneous tissue of rats when compared to bioactive borate scaffolds doped with copper only after six weeks *in-vivo*. Of the materials added for the promotion of angiogenesis, strontium and iron had little impact,

but copper and zinc significantly increased the vascularity in the scaffolds they were added. It was also found that the addition of MSCs to a scaffold further enhanced the *in-vivo* angiogenic response.

Acknowledgements

The authors would like to thank Vernon Modglin for his assistance with the surgical procedures, Dr. Anne Maglia of MS&T for access to histological equipment, Dr. Vladimir Dusevich of UMKC for the ESEM analysis, Penny McCormick of PCRMC for the H&E histological staining and Jackie Taylor from (UMKC) for the PAS staining and blood vessel analysis.

3.7 REFERENCES

[1] Hench LL, Hench JW, Greenspan DC. Bioglass: A short history and bibliography. . J. Aust. Cer. Soc. 2004;40:1.

[2] Yamamuro T, Hench LL, Wilson J. Handbook of Bioactive Ceramics Vol. I - Bioactive Glasses and Glass-Ceramics. Boca Raton FL: CRC Press, 1990.

[3] Pirhonen E, Niiranen H, Brink M, Tormala P. Manufacturing, mechanical characterization, and in-vitro performance of bioactive glass 13-93 fibers. J. Biomed. Mater. Res. 2006;77B:227.

[4] Peltola MJ, Aitasalo KMJ, Suonpaa JTK, Yli-Urpo A, Laippala PJ. In Vivo Model for Frontal Sinus and Calvarial Bone Defect Obliteration with Bioactive Glass S53P4 and Hydroxyapatite. J. Biomed. Mater. Res. 2001;58:261.

[5] Asikainen AJ, Hagstrom J, Sorsa T, Noponen J, Kellomaki M, Juuti H, Lundqvist C, Hietanen J, Suuronen R. Soft Tissue Reactions to Bioactive Glass 13-93 Combined with Chitosen. J. Biomed. Mater. Res. 2007;83A:530.

[6] Hench LL. Bioceramics. Journal of the American Ceramic Society 1998;81:1705.

[7] Froum SJ, Weinberg MA, Tarnow D. Comparison of bioactive glass synthetic bone graft particles and open debridement in the treatment of human periodontal defects. A clinical study. J. Period. 1998;69:698.

[8] Fu Q, Rahaman MN, Bal BS, Brown RF, Day DE. Mechanical and InVitro Performance of 13-93 Bioactive Glass Scaffolds Prepared By a Polymer Foam Replication Technique. Acta Biomaterialia 2008;4:257.

[9] Rahaman MN, Day DE, Brown RF, Fu Q, Jung SB. Nanostructured Bioactive Glass Scaffolds for Bone Repair. 32nd Inter. Conf. Adv. Cer. Comp. 2008.

[10] Moimas L, Biasotto M, Lenarda RD, Olivo A, Schmid C. Rabbit pilot study on the resorbability of three-dimensional bioactive glass fibre scaffolds. Acta Biomaterialia 2006;2:191.

[11] Malasoma A, Fritsch A, Kolhauser C, Brynk T, Vitale-Brovarone C, Pakiela Z, Eberhardsteiner J, Hellmich C. Micromechanics of Bioreseorbable Porous CEL2 Glass Ceramic Scaffolds For Bone Tissue Engineering. Adv. Appl. Cer. 2008;107:277.

[12] Liu X, Xie Z, Zhang C, Pan H, Rahaman MN, Zhang X, Fu Q, Huang W. Bioactive borate glass scaffolds: in vitro and in vivo evaluation for use as a drug delivery system in the treatment of bone infection. J. Mater. Sci.: Mater. Med. 2009;online.

[13] Pirhonen E, Moimas L, Haapanen J. Porous Bioactive 3-D Glass Fiber Scaffolds for Tissue Engineering Applications Manufactured by Sintering Technique. Key Eng. Mater. 2003;240-242:237.

[14] Chen QZ, Thompson ID, Boccaccini AR. 45S5 Bioglass-derived glass-ceramic scaffolds for bone tissue engineering. Biomaterials 2006;27:2414.

[15] Fu Q. PhD Dissertation. Rolla: Missouri University of Science and Technology, 2009.

[16] Ebaretonbofa E, Evans JRG. High Porosity Hydroxyapatite Foam Scaffolds for Bone Substitutes. J. Porous Mater. 2002;9:257.

[17] Ohgushi H, Okumura M, Yoshikawa T, Inoue K, Senpuka N, Tamai S. Bone Formation Process in porous Calcium Carbonate and Hydroxyapatite. J. Biomed. Mater. Res. 1992;26:885.
[18] Vuola J, Goransson H, Bohling T, Asko-Scljavaara S. Bone marrow induced osteogenesis in hydroxyapatite and calcium carbonate implants. Biomaterials 1996;17:1761.
[19] Rouwkema J, Rivron NC, Blitterswijk CAv. Vascularization in Tissue Engineering. Trends in Biotech. 2008;26:434.
[20] Leach JK, Kaigler D, Wang Z, Krebsbach PH, Mooney DJ. Coating of VEGF-releasing scaffolds with bioactive glass for angiogenesis and bone regeneration. Biomaterials 2006;27:3249.
[21] Barralet J, Gbureck U, Habibovic P, Vorndran E, Gerard C, Doillon CJ. Angiogenesis in calcium phosphate scaffolds by inorganic copper ion release. Tissue Eng. 2009;15:1.
[22] Giavaresi G, Torricelli P, Fornasari PM, Giardino R, Barbucci R, Leone G. Blood vessel formation after soft tissue implantation of hyaluronan-based hydrogel supplemented with copper ions. Biomaterials 2005;26:3001.
[23] Singer AJ, Clark RAF. Cutaneous Wound Healing. The New Eng. J. Med. 1999;341:738.
[24] Hu G-f. Copper Stimulates Proliferation of Human Endothelial Cells Under Culture. J. Cell. Biochem. 1998;69:326.
[25] McAuslan BR, Reilly W. Endothelial Cell Phagokinesis in Response to Specific Metal Ions. Exp. Cell Res. 1980;130:147.
[26] Lowndes SA, Harris AL. The Role of Copper in Tumour Angiogenesis. J. Mammary Gland Bio. Neo. 2005;10:299.
[27] Becker RO, Spadaro JA, Berg EW. The Trace Elements of Human Bone. J. Bone and Joint Surg.1968;50:326.
[28] Lansdown ABG, Mirastschijski U, Stubbs N, Scanlon E, Agren MS. Zinc in Wound Healing: Theoretical, Experimental, and Clinical Aspects. Wound Repair Regen. 2006;15:2.
[29] Ostomel TA, Shi Q, Stoimenov PK, Stucky GD. Metal Oxide Surface Charge Mediated Hemostasis. Lang. 2007;23:11233.
[30] Dzondo-Gadet M, R M-N, Hess K, Nabet P, Belleville F, Dousset B. Action of Boron at the Molecular Level. Biological Trace Element Research 2002;85:23.
[31] Cabrera WE, Schrooten I, Broe MED, D'Haese PC. Strontium and Bone. J. Bone Min. Res. 1999;14:661.
[32] Goldhaber SB. Trace Element Risk Assessment: Esentiality vs. Toxicity. Reg. Tox. Pharma. 2003;38:232.
[33] Laboux O, Dion N, Arana-Chavez V, Ste-Marie L-G, Nanci A. Microwave Irradiation of Ethanol-fixed Bone Improves Preservation, Reduces Processing Time, and Allows Both Light and Electron Microscopy on the Same Sample. J. Histochem. Cytochem. 2004;52:1267.
[34] Jung SB, PhD Dissertation, Chapter 1. Rolla, MO: Missouri University of Science and Technology, 2010.
[35] Cormack DH. Ham's Histology. Philadelphia PA: J. B. Lippincott Company, 1987.

[36] Conzone S. PhD Dissertation. Rolla: University of Missouri-Rolla, 1999.
[37] Richard M. M.S. Thesis. Rolla, MO: University of Missouri-Rolla, 2000.
[38] Jai W-T, Zhang X, Luo S-H, Liu X, Huang W-H, Rahaman MN, Day DE, Zhang C-Q, Xie Z-P, Wang J-Q. Novel borate glass/chitosen composite as a delivery vehicle for teicoplanin in the treatment of chronic osteomyelitis. Acta Biomaterialia 2009.
[39] Bonewald L. Personal Communication. 2010.
[40] Jung SB, PhD Dissertation, Chapter 2. Rolla, MO: Missouri University of Science and Technology, 2010.
[41] Harris ED. A Requirement for Copper in Angiogenesis. Nutri. Rev. 2004;62:60.
[42] Brown RF. Personal Communication. 2010.

TABLES

Table 1 – Compositions of Bioactive Glasses (wt%)

Glass	B_2O_3	Na_2O	CaO	K_2O	MgO	P_2O_5	SiO_2	CuO	SrO	ZnO	Fe_2O_3
45S5	0	24.50	24.50	0	0	6.00	45.00	0	0	0	0
13-93	0	6.00	20.00	12.00	5.00	4.00	53.00	0	0	0	0
S53P4	0	21.50	21.50	0	0	4.00	53.00	0	0	0	0
13-93B3	53.00	6.00	20.00	12.00	5.00	4.00	0	0	0	0	0
B3 Cu-1	52.95	5.99	19.98	11.99	5.00	4.00	0	0.10	0	0	0
B3 Cu-2	52.89	5.99	19.96	11.98	4.99	3.99	0	0.20	0	0	0
B3 Cu-3	52.79	5.98	19.92	11.95	4.98	3.98	0	0.40	0	0	0
B3 Cu-4	52.47	5.94	19.80	11.88	4.95	3.96	0	1.00	0	0	0
B3 Cu-5	51.94	5.88	19.60	11.76	4.90	3.92	0	2.00	0	0	0
CS	51.73	5.86	19.52	11.71	4.88	3.90	0	0.40	2.00	0	0
CSZ	51.20	5.80	19.32	11.59	4.83	3.86	0	0.40	2.00	1.00	0
CSZF	50.88	5.76	19.20	11.52	4.80	3.84	0	0.40	2.00	1.00	0.40

Table 2 – Statistical Analysis for PAS Blood Vessel Analysis of CuO Doped Bioactive Borate Glasses (6 weeks *In-vivo*)

Scaffold Comparison		p value	Significance
13-93B3	B3 Cu-1	0.4302	No
13-93B3	B3 Cu-3	0.0472	Yes
B3 Cu-1	B3 Cu-3	0.0607	No
13-93B3 msc	B3 Cu-1 msc	0.3798	No
13-93B3 msc	B3 Cu-3 msc	0.0802	No
B3 Cu-1 msc	B3 Cu-3 msc	0.3533	No
13-93B3	13-93B3 msc	0.0406	Yes
13-93B3	B3 Cu-1 msc	0.1105	No
13-93B3	B3 Cu-3 msc	0.0282	Yes

msc - denotes the scaffolds was seeded with 50,000 mesenchymal stem cells

Table 3 – Student t Test Results for Blood Vessel Analysis

Scaffold Comparison		Student t Test Result	Significant ($p<0.05$)
B3 Cu-3	CS	0.386	No
B3 Cu-3	CSZ	0.0443	Yes
B3 Cu-3	CSZF	0.0456	Yes
CS	CSZ	0.0698	No
CS	CSZF	0.0738	No
CSZ	CSZF	0.5325	No

FIGURES

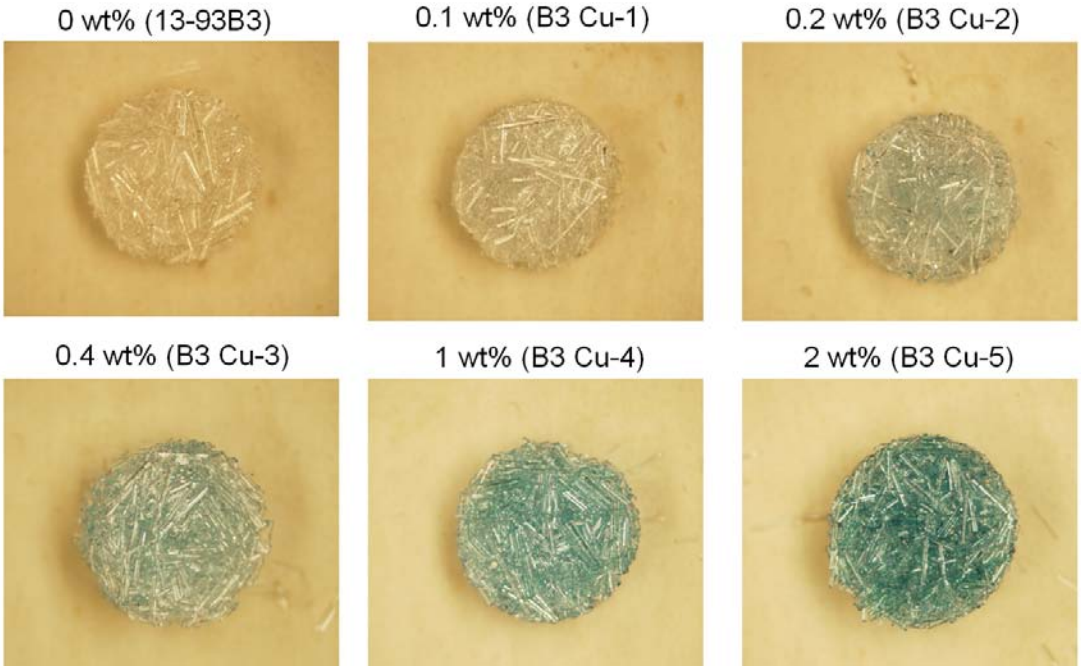

Figure 1– Examples of as-made bioactive borate glass scaffolds doped with CuO in amounts from 0.1wt% to 2wt%. Each scaffold was 7mm in diameter and 2mm thick.

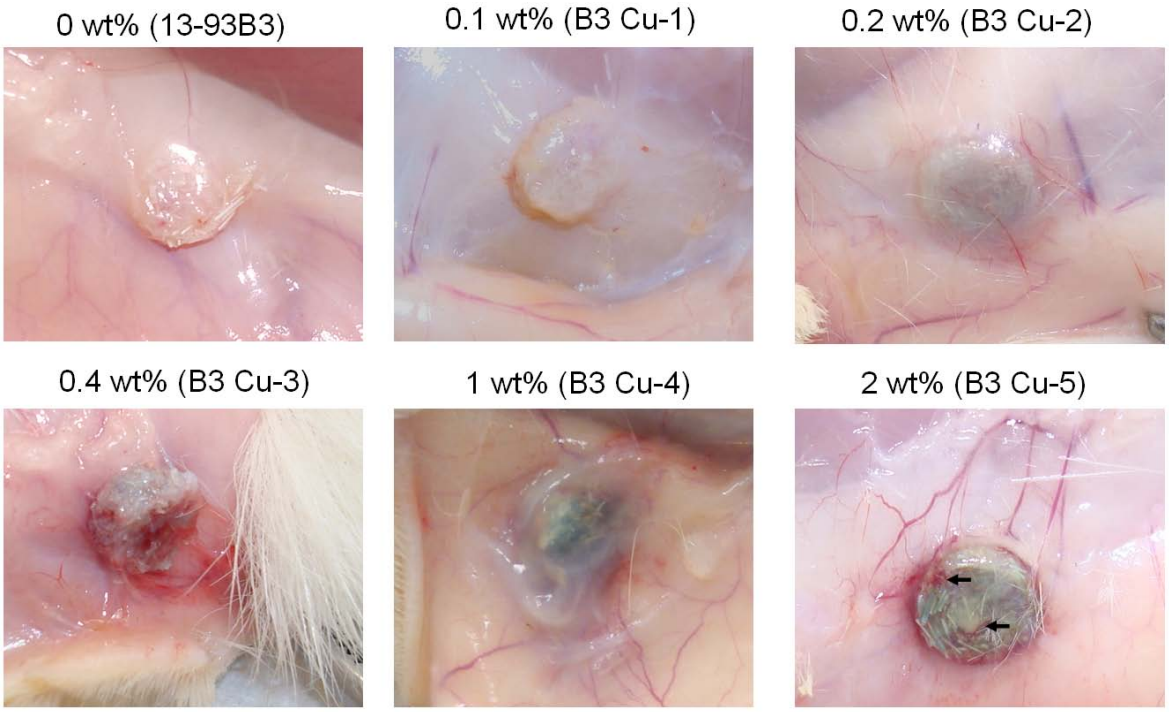

Figure 2 –Appearance of bioactive borate scaffolds doped with CuO, after two weeks in subcutaneous sites in rats, for evaluation of vascular growth (unseeded).

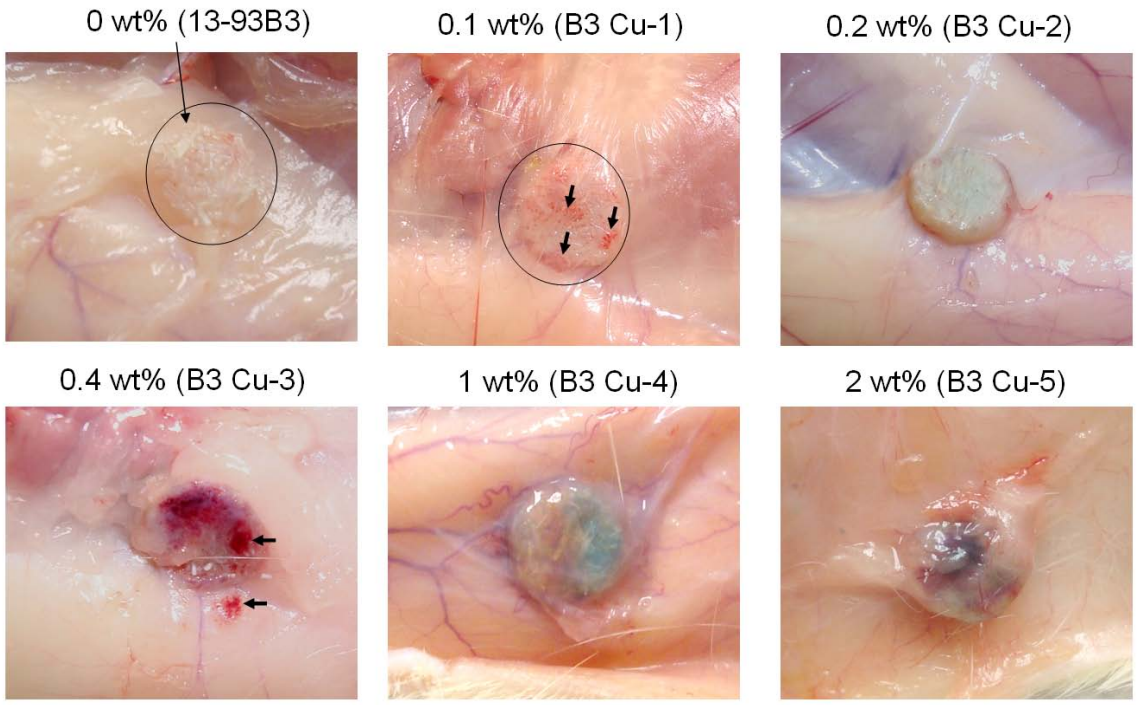

Figure 3 – Bioactive borate scaffolds doped with increasing amounts of CuO, implanted in subcutaneous sites in rats (four weeks) for evaluation of vascular growth (unseeded). The circles are to guide the eye.

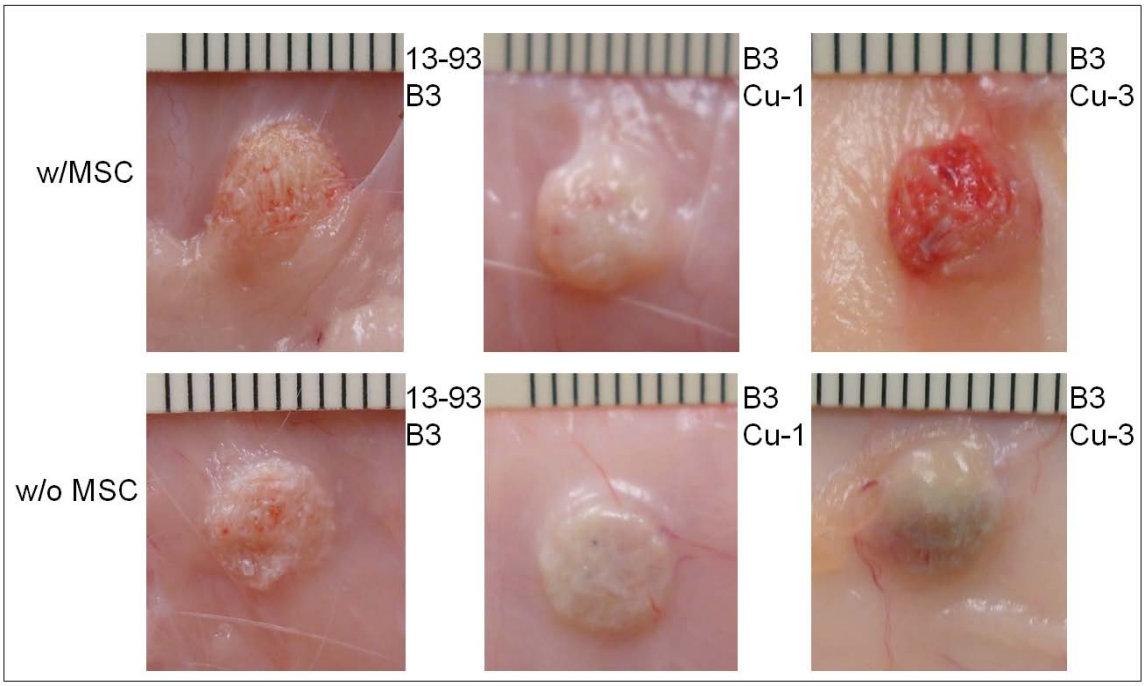

Figure 4 – Appearance of 13-93B3, B3 Cu-1, and B3 Cu-3 borate glass fiber scaffolds with and without 50,000 seeded mesenchymal stem cells after a six week implantation in a subcutaneous site.

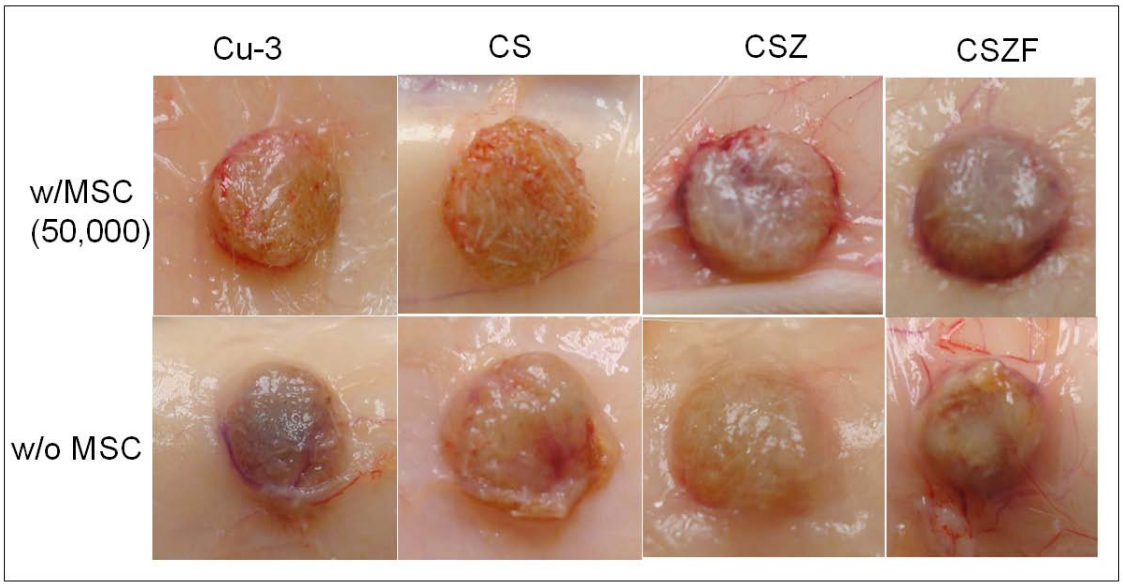

C or *Cu* – Copper, *S* – Strontium, *Z* – Zinc, *F* – Iron, MSC – Mesenchymal stem cells

Figure 5 – Digital micrographs of borate glass scaffolds (original dimensions – 7mm diameter, 2mm thick) doped with 0.40% CuO, 2.0% SrO, 1.0% ZnO, and 0.4% Fe_2O_3 (wt%) after six weeks in a subcutaneous site. The top row of scaffolds was seeded with 50,000 mesenchymal stem cells (MSC) and the bottom row was unseeded.

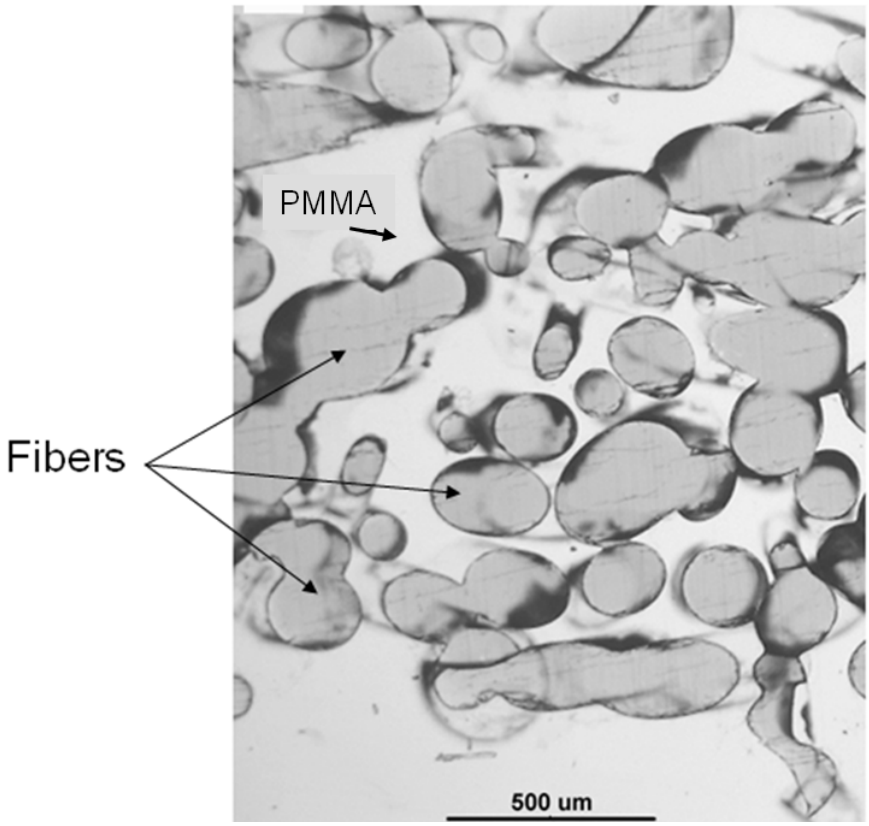

Figure 6 – Optical micrograph of the cross section of an as-made randomly oriented fiber scaffold infiltrated with PMMA. The due to the fiber orientation, many of the fibers look ellipsoidal, and several fibers fused together during the heat treatment.

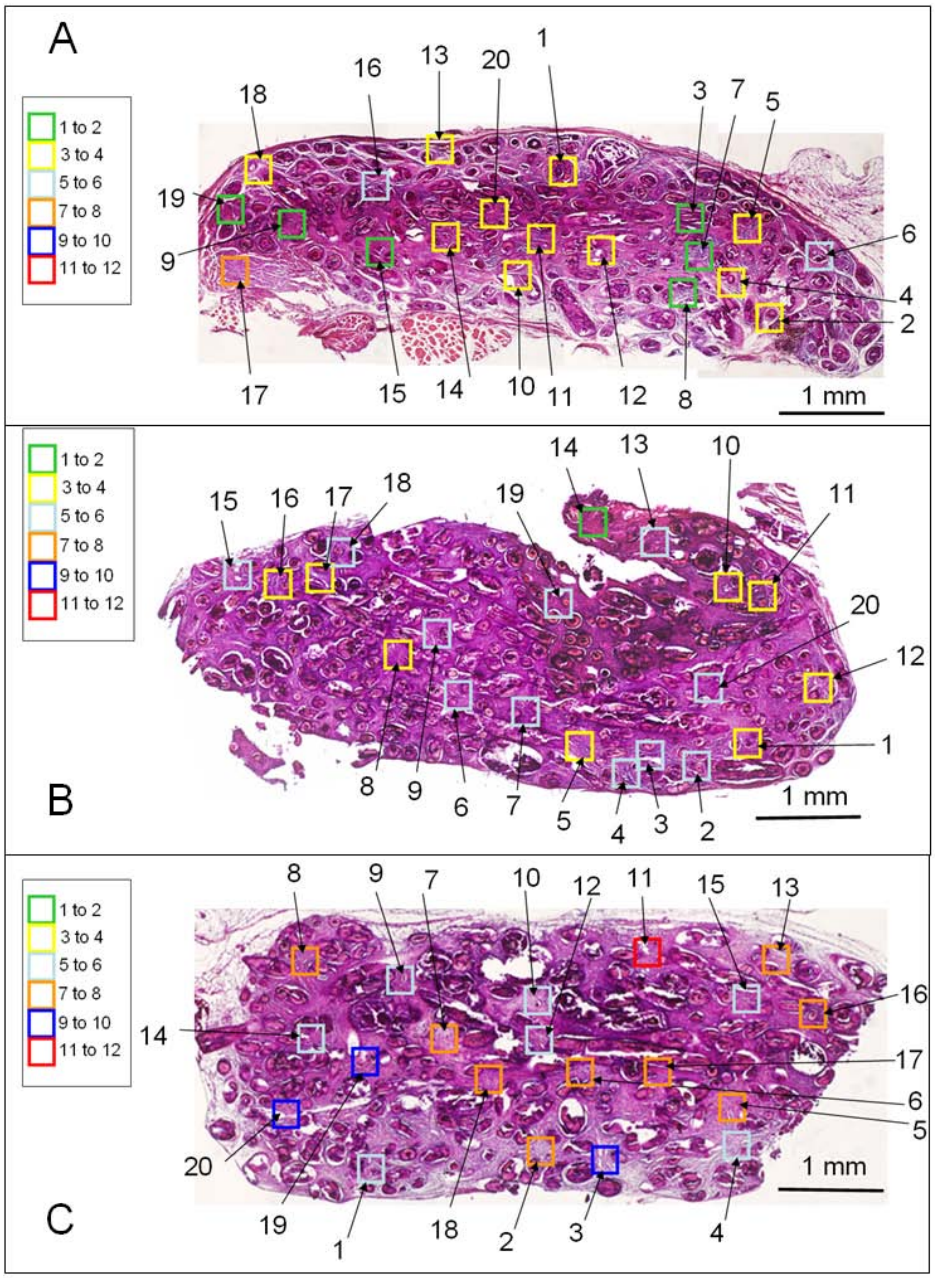

Figure 7 – H&E stained sections of the six week subcutaneously implanted 13-93B3 (A), B3 Cu-1 (B), and B3 Cu-3 (C) scaffolds seeded with 50,000 mesenchymal stem cells. The colored boxes (left) are an indication of the number of blood vessels present in each of the areas.

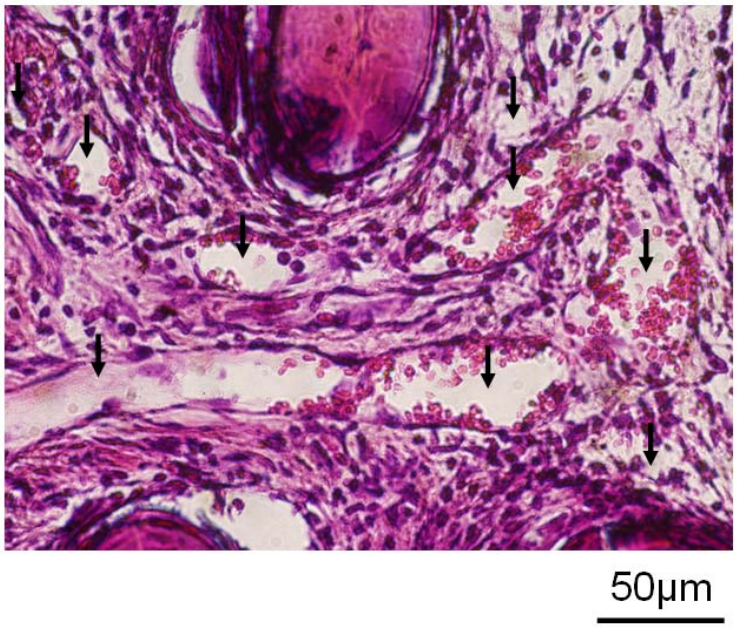

Figure 8 – An example of an H&E stained tissue section with blood vessels marked (black arrow), and often have red blood cells inside (red or pink). Blood vessels have a purple defining edge.

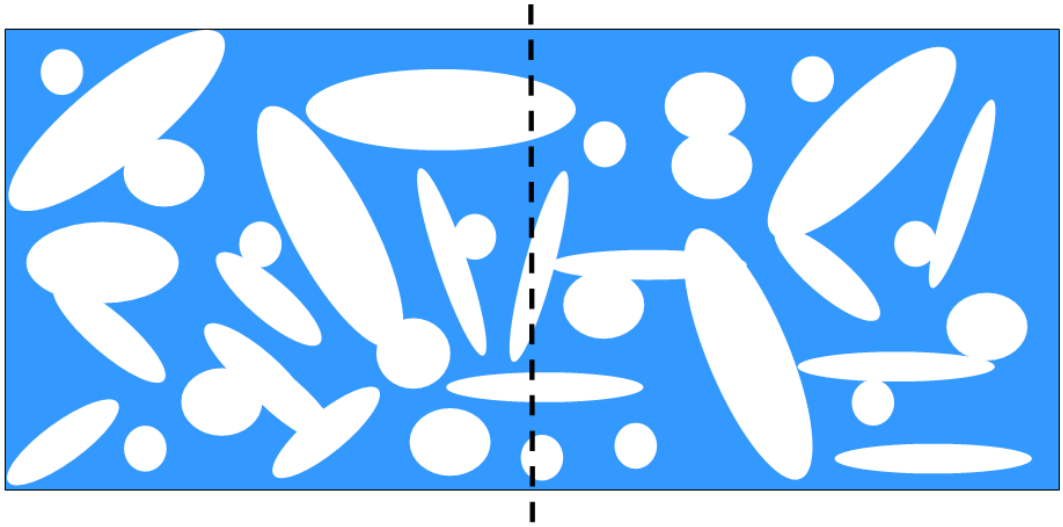

Figure 9 – Schematic showing how the PAS stained tissue sections (CuO doped) were analyzed. The dashed line represents the section of tissue analyzed, typically close to the center of the section, used for blood vessel analysis. As indicated by the schematic, reacted fibers (white) were often in the line of tissue analyzed and since the scaffolds were approximately the same porosity, no correction was required.

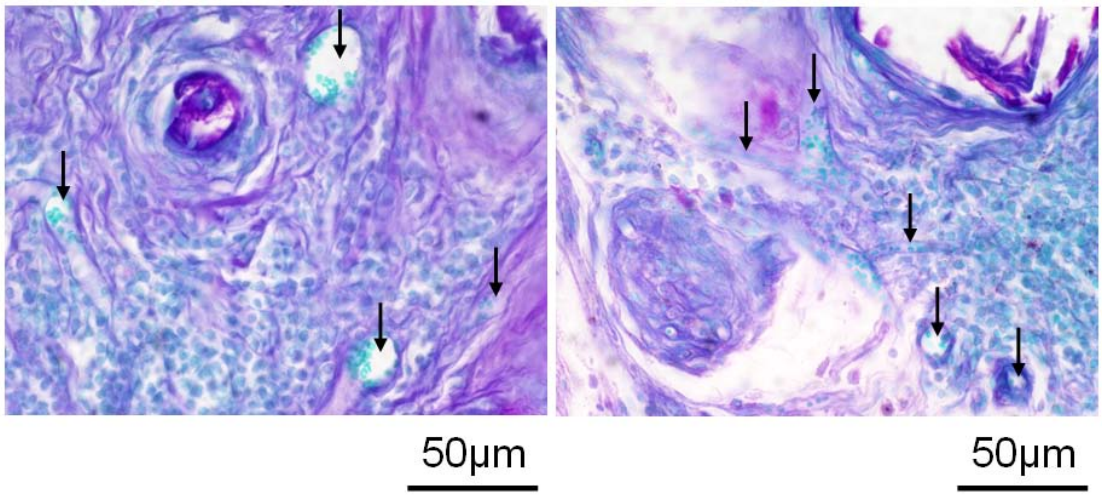

Figure 10 – Optical micrographs of PAS stained tissue section from a B3 Cu-3 bioactive glass fiber scaffold implanted six weeks. The arrows point to blood vessels (purple ring) and the objects in the vessels are stained red blood cells (green).

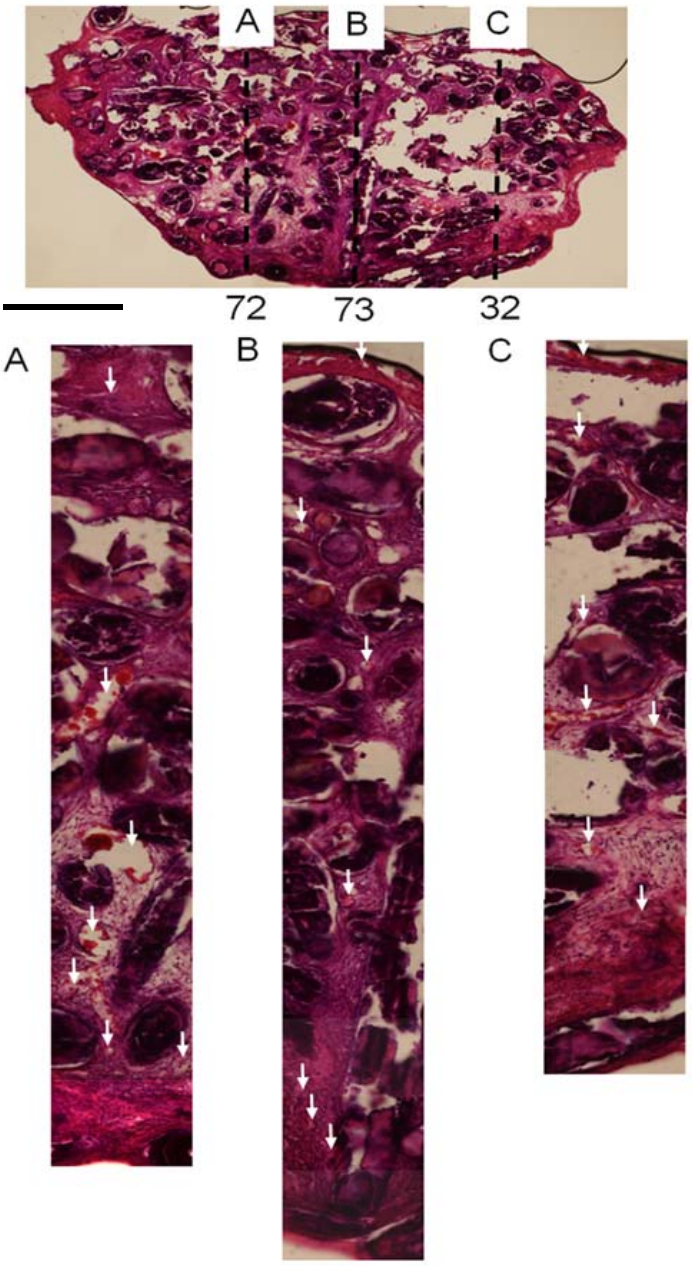

Figure 11 – Example of an H&E section used for the blood vessel analysis (H&E). The dashed lines in the top image show the areas across the scaffold that were analyzed, and the total number of vessel for each line of tissue are shown (72, 73, and 32, respectively). The individual tissue sections are shown below (A to C) and several of the largest blood vessels are pointed out with arrows to guide the reader. Bar = 1mm.

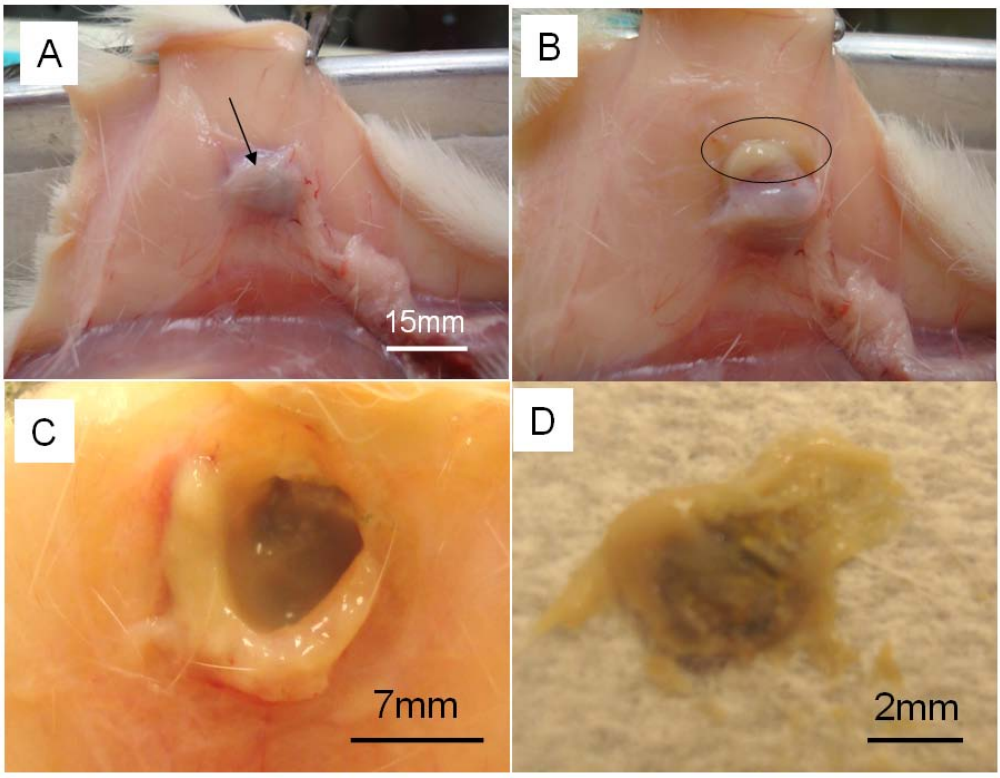

Figure 12 – Optical images showing a B3 Cu-5 scaffold after six weeks walled off in subcutaneous tissue, Fig 12A. A thick fluid was present inside the site, Figs. 12B and 12C, and the remainder of the scaffold removed from the site is shown in 12D. All images come from the same rat.

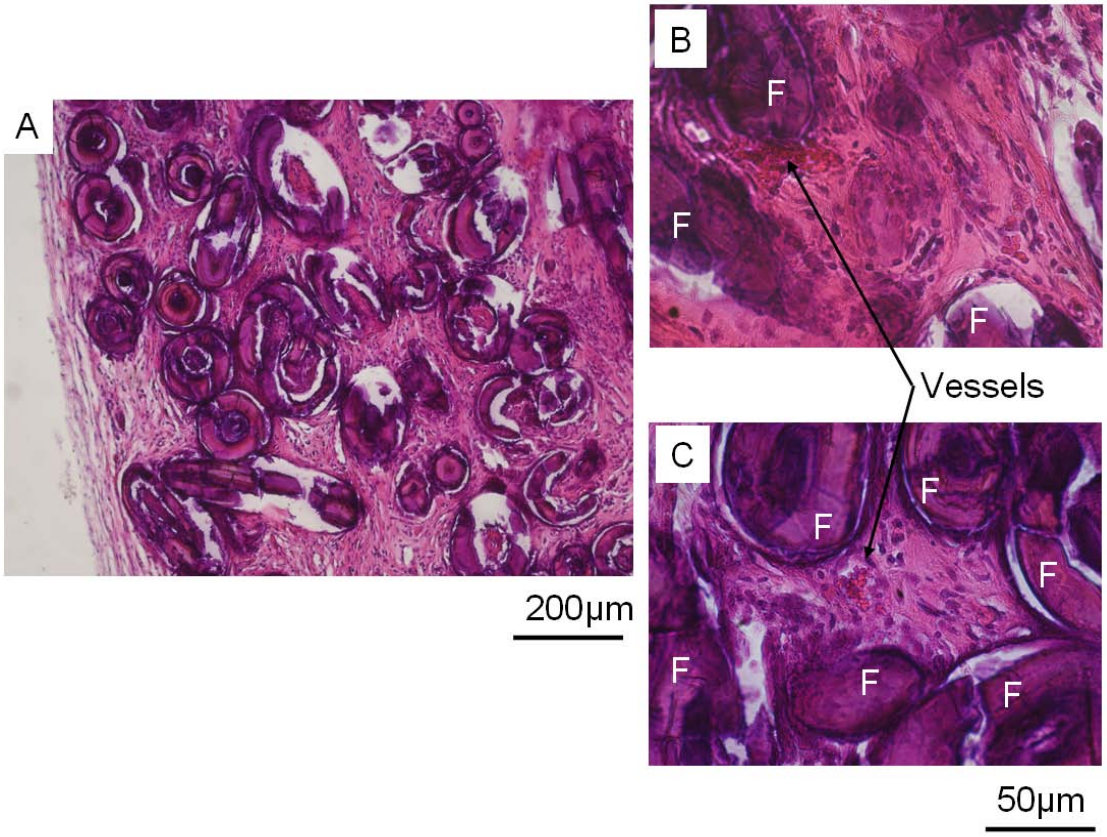

Figure 13 – Optical micrographs of stained sections (H&E) from a 13-93B3 scaffold after four weeks *in-vivo*. Many of the fibers (F) are reacted, and some contain tissue.

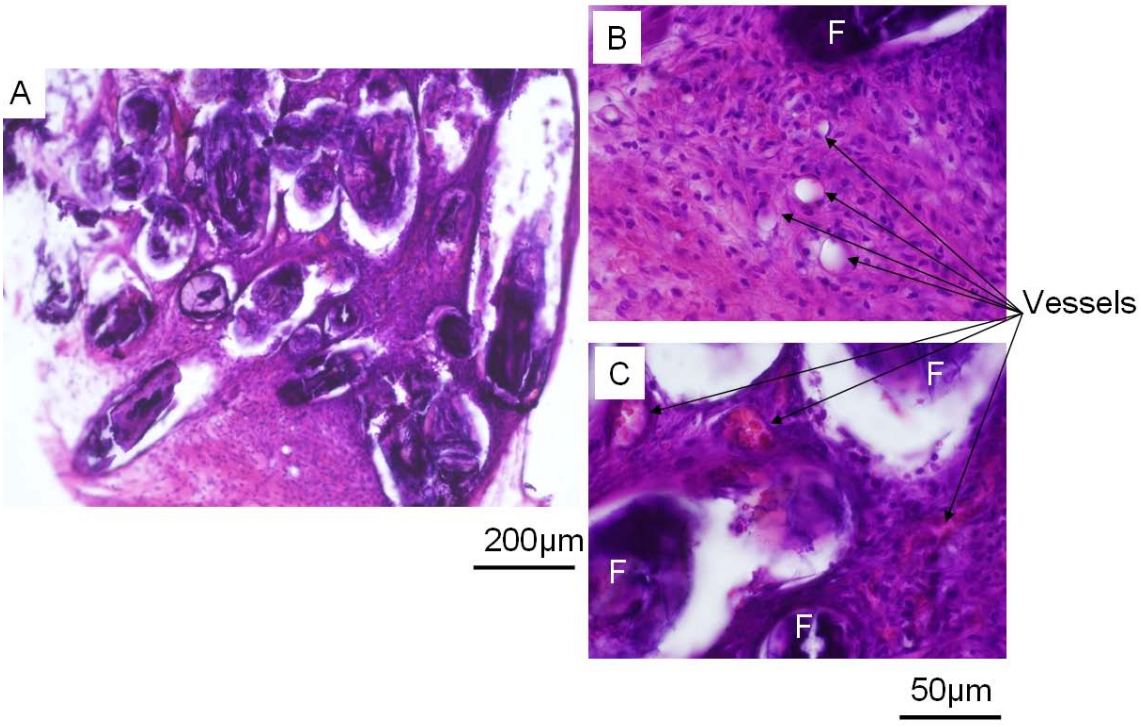

Figure 14 – Optical micrographs of B3 Cu-1 scaffold sections (H&E) that were removed from rat subcutaneous tissue after four weeks *in-vivo* and stained with H&E stain. Many of the fibers (F) are hollow, and some contain tissue.

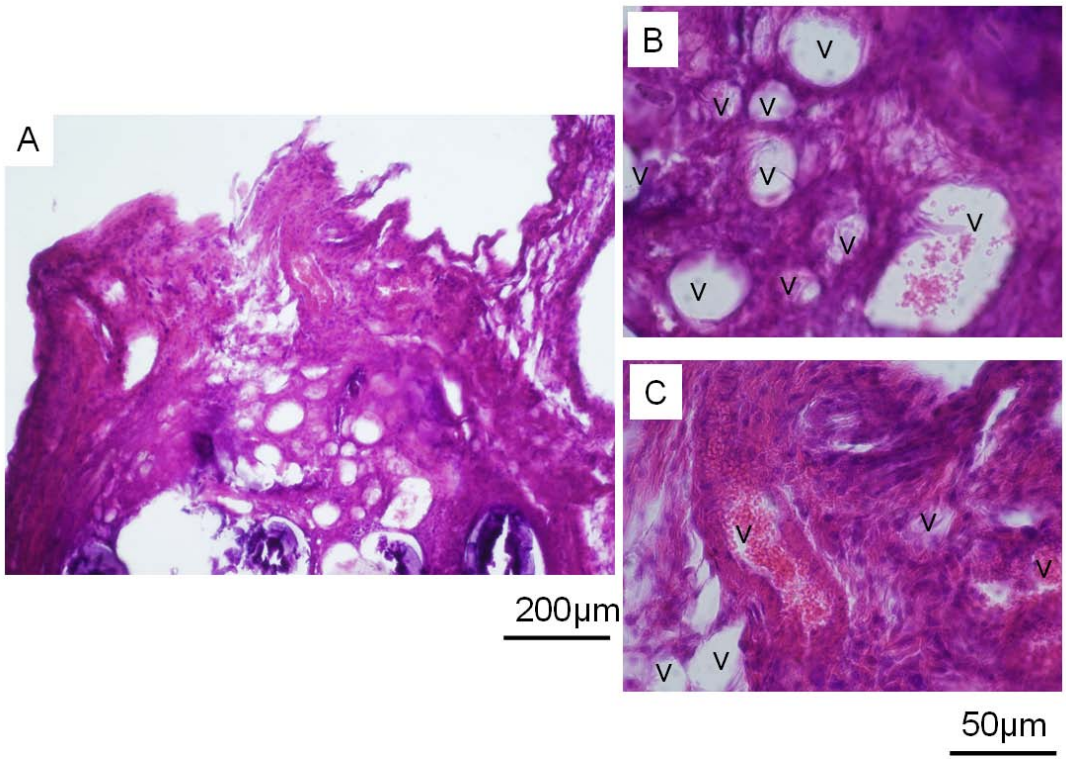

Figure 15 – Optical micrographs of B3 Cu-5 scaffold sections (H&E) that were removed from rat subcutaneous tissue after four weeks *in-vivo* and stained with H&E stain. Large blood vessels (V) have been identified throughout the tissue.

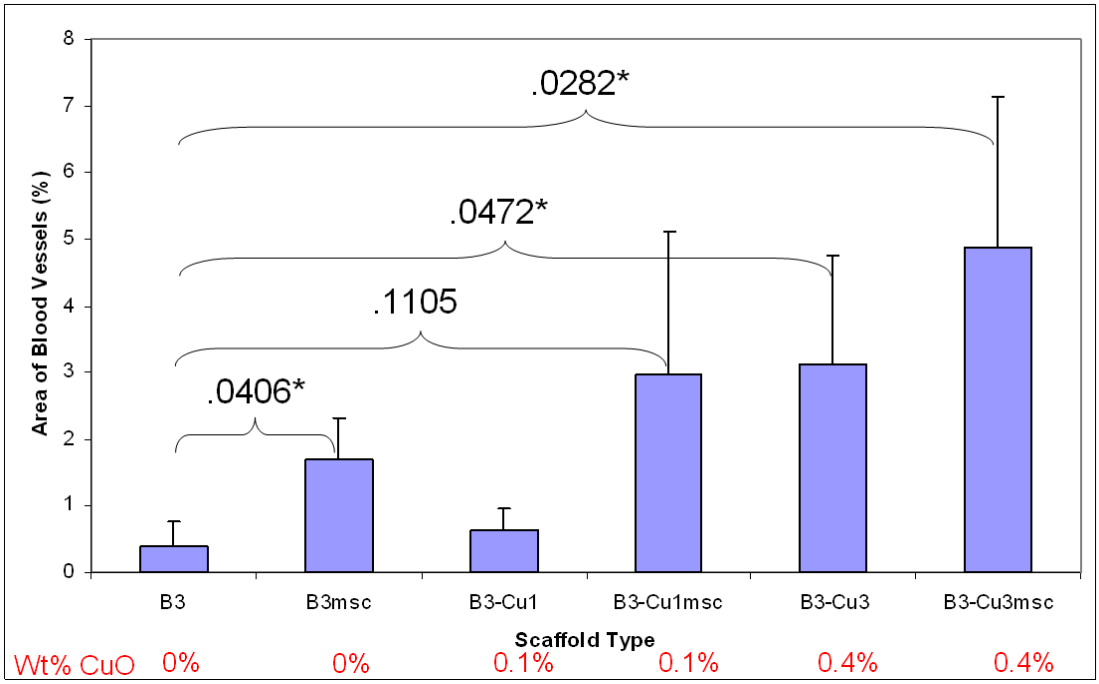

Figure 16 – Area % of blood vessels measured from PAS stained tissue sections from bioactive borate glass scaffolds (doped with CuO) after six weeks *in-vivo*. N=3. Differences considered significant if *($p<0.05$).

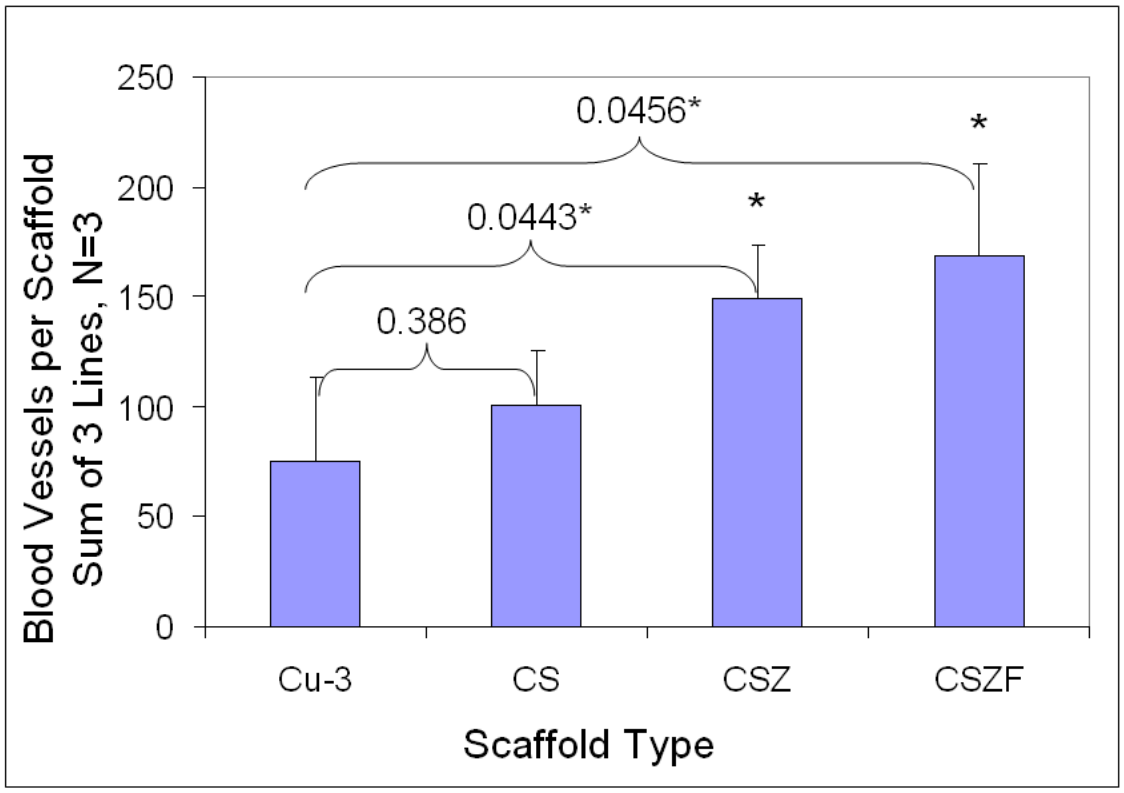

Figure 17 – Total number of blood vessels measured for H&E stained borate glass scaffold tissue sections doped with minor elements (Cu of C = copper, S = Strontium, Z = Zinc, and F = iron) after six weeks *in-vivo*. * $p<0.05$, N=3.

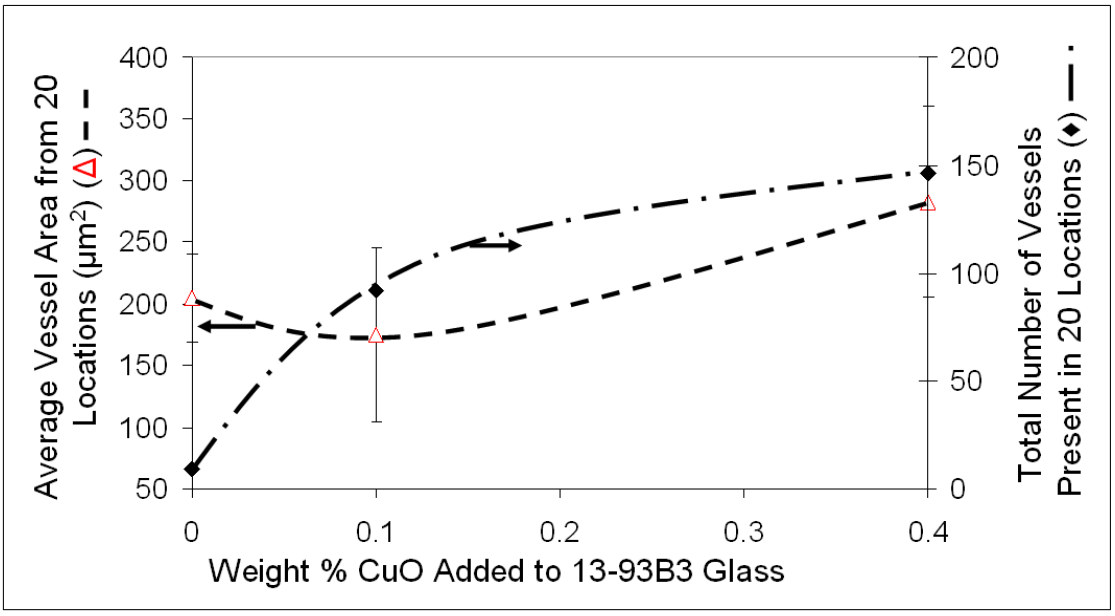

Figure 18 – Average area for vessels in 20 randomly selected boxes across an H&E stained histology section for the borate glass fiber scaffold, 13-93B3 (no CuO), B3 Cu-1 (0.1wt% CuO), and B3 Cu-3 (0.4wt% CuO) (left side, red triangle). The total number of vessels measured for each scaffold is plotted on the right hand y-axis (black diamonds).

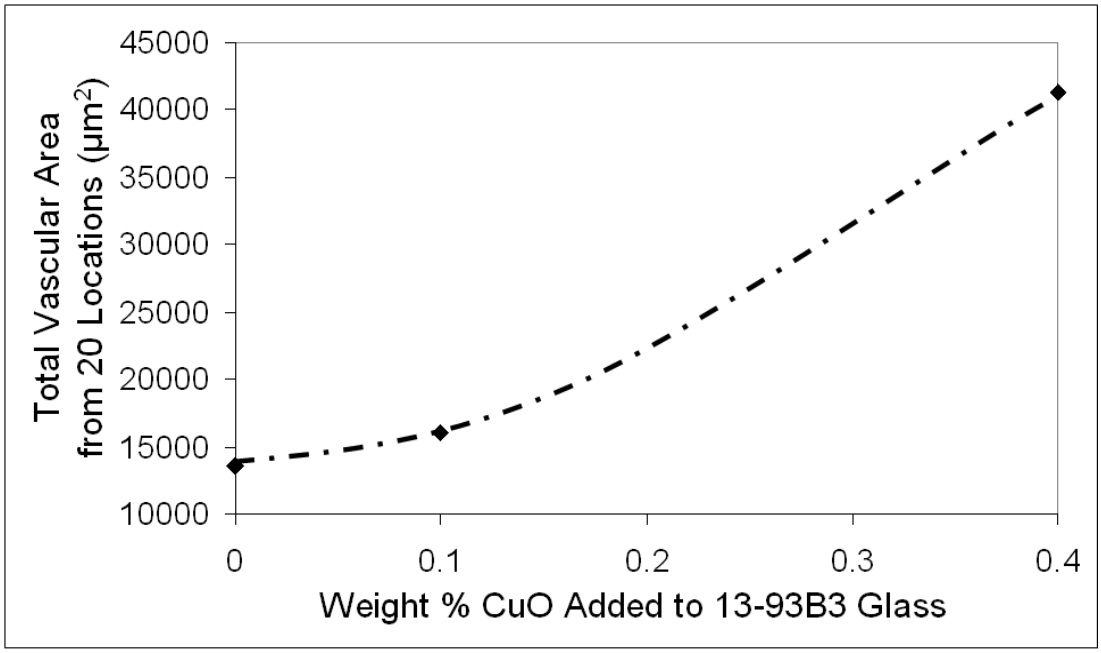

Figure 19 – Total vascular area calculated from 20 randomly chosen areas in H&E stained sections for the 13-93B3 (0wt% CuO), B3 Cu-1 (0.1wt% CuO), and B3 Cu-3 (0.4wt% CuO) scaffolds.

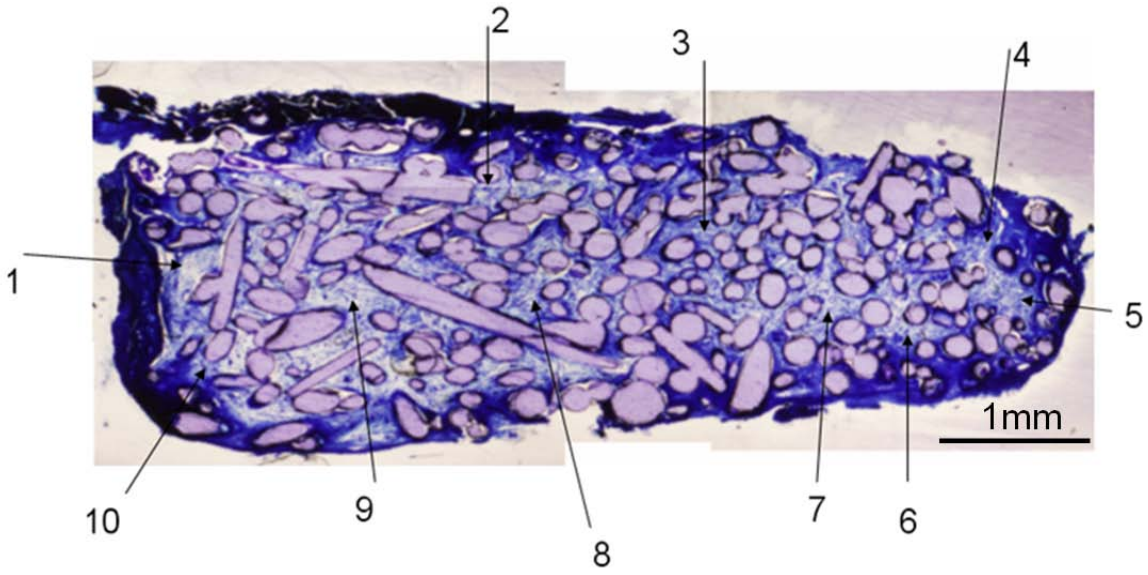

Figure 20 – Cross section of a 13-93 fiber scaffold that had been implanted in subcutaneous tissue of a rat for two weeks. Ten areas of tissue examined for blood vessels are indicated by the arrows. The section was stained with Sanderson Bone Stain. Personal communication [42].

4. BONE GROWTH ON BIOACTIVE BORATE GLASS SCAFFOLDS

Steven B. Jung[1], Delbert E. Day[1], Roger F. Brown[2], and Linda F. Bonewald[3]

[1]Graduate Center for Materials Research, Materials Science and Engineering Department, Missouri University of Science and Technology, Rolla, MO, 65409-1170

[2]Department of Biological Sciences, Missouri University of Science and Technology, Rolla, MO, 65409-1170

[3]Department of Oral Biology, School of Dentistry, University of Missouri Kansas City, Kansas City, MO 64108-2784

4.1 ABSTRACT:

Bone growth was investigated on bioactive borate glass fiber scaffolds and was assessed by two models, the rat calvaria model for osteoconduction and a subcutaneous rat model for osteoinduction. Porous bioactive glass scaffolds composed of randomly oriented fibers and loose particulates (100 to 200μm) were placed in calvaria defects (4mm diameter) of rats for 12 weeks to compare borate, borosilicate, and two silicate based bioactive glasses (45S5 and 13-93) effect on bone growth. Micro-CT analysis of the scaffolds after 12 weeks showed that on average, n=4, the borate glass scaffold had the highest bone coverage of the four glasses tested on both the top and bottom of the scaffold. Histomorphometry analysis of the calvaria implanted scaffolds showed that the borate glass scaffold had significantly more bone ($p<0.05$) than the borosilicate or silicate based bioactive glass scaffolds.

In a separate experiment, borate based bioactive glass scaffolds doped with minor elements present in bone (copper, strontium, zinc, and iron) were seeded with mesenchymal stem cells and implanted in subcutaneous tissue of rats to determine if the scaffolds could foster osteoinductive bone growth. No inflammation or infection was

observed at any of the implant sites. Upon retrieval of the scaffolds, significant numbers of blood vessels were present in the adjacent tissues. Analysis of the tissue for mineralized bone-like material showed that none of the unseeded scaffolds formed osteoid or bone-like tissue. At least one of every type of the MSC seeded scaffolds stained positive for mineralized bone-like tissue indicating that the bioactive borate scaffolds are osteoinductive.

4.2 INTRODUCTION

Bioactive glasses such as 45S5 (Table 1) have been known to bond with hard and soft tissue since 1969 [1, 2]. Bioactive glasses and glass-ceramics have been used in clinical applications including periodontal repair [3], replacement of bones in the inner ear [4], and filler for bone cement [5, 6]. Three dimensional scaffolds composed of bioactive glasses in a variety of microstructures have recently been under investigation for bone defects for load bearing and non-load bearing applications [7-11]. Silicate based bioactive glasses however have been shown to react relatively slowly *in-vivo* taking months to years to fully react to hydroxyapatite (HA) [12].

Due to the relatively slow reaction of silicate based bioactive glasses, a new family of faster reacting bioactive glasses was developed. Borate based bioactive glasses submerged in phosphate solutions convert to HA similar to silicate based bioactive glasses [13-15]. For example, an *in-vitro* study comparing the reaction rate of silicate based bioactive glass (45S5) to two borosilicate glasses (1/3 and 2/3 of silica replaced by boron) and a borate based bioactive glass (all silica from 45S5 replaced by boron), the borate glass converted to HA five times faster than the silicate glass [13, 16].

Richard et al was the first to implant particles of a 45S5 borate analog (complete exchange of boron for silica) in rat femurs. The glass converted to HA at a significantly accelerated rate and bone grew in and attached to the borate glass particles [17]. No negative immune response was reported from the histological analysis of the borate based particles.

Jai et al. [18] made pellets from borate glass particles (<50μm) mixed with teicoplanin (4 and 8wt%) for the treatment of osteomyelitis. *In-vitro* experiments showed that approximately 80% of the teicoplanin was released within 15 days. The compressive strength of the scaffolds decreased from 22 MPa to 12 MPa after being submerged for six days in PBS solution. *In-vivo* experiments with New Zealand White rabbits confirmed the previously described *in-vitro* work, as the teicoplanin exhibited a controlled release and the implants had sufficient load bearing strength. There was no reported *in-vivo* toxicity in the bone adjacent to the bioactive borate glass as the glass converted to HA and supported the growth of new bone in the scaffolds.

Liu et al. [19] treated osteomyelitis located in the tibia of New Zealand White rabbits with a scaffold made of bioactive borate glass particles bonded together with a polymer binder loaded with Vancomycin. After eight weeks *in-vivo*, the implant sites had no observable tissue damage or inhibition of bone growth. After eight weeks, approximately 80% of the osteomyelitis infected tibia tested negative for the infection. Vascular growth adjacent to the scaffolds was reported to have been participating in the bone regeneration.

Bioactive glass 13-93B3 (Table 1) was used to make porous scaffolds composed of randomly oriented fiber which were implanted in the subcutaneous tissue of Sprague

Dawley rats for four weeks [20]. The 13-93B3 fibers fully reacted to carbonated hydroxyapatite, and the fibers formed porous tubes [20]. Soft tissue and blood vessels were present in the open pores of the scaffold and at the center of many of the reacted 13-93B3 fibers. There was no noticeable inflammation due to the implantation of the scaffold indicating that the 13-93B3 glass was compatible with rat subcutaneous tissue [20].

In the present work, porous scaffolds made from randomly oriented fibers composed of borate glass fibers, borosilicate glass fibers, silicate based bioactive glass fibers (13-93) and loose particles of 45S5 glass were implanted in 4mm rat calvaria defects to compare bone growth between scaffolds and loose particles, and to determine if silicate or borate glasses promote the most bone growth. Additionally, a series of bioactive borate glass scaffolds doped with copper, strontium, zinc, and iron were seeded with mesenchymal stem cells (MSC's) and implanted in subcutaneous tissue to determine if the scaffolds were osteoinductive. The amount of each of the minor elements was based off the relative abundance of the trace elements in human bone [21].

4.3 MATERIALS AND METHODS

4.3.1 Glass Melting, Scaffold Preparation, and Sterilization

The borate glass compositions present in Table 1 were made from reagent grade chemicals and melted in a platinum crucible. The batch materials were melted at 1050 to 1400^{o}C for one to two hours depending upon the composition. Fibers of each glass with a diameter ranging from 100 to 300μm were pulled from the melt. The fibers were

broken into 2 to 3mm lengths for the preparation of porous randomly oriented fiber scaffolds.

For the subcutaneous implants, approximately 70mg of fiber was placed in a cylindrical ceramic mold with an internal diameter of 7mm. The molds were placed in an oven preheated to 575^{o}C and heated for 45 minutes, after which the molds were removed and cooled to room temperature. Once cool, the scaffolds were removed from the molds and were ready for use. The nominal dimensions of the as-made scaffolds were 7mm in diameter and 2mm thick.

The scaffolds for the calvaria implantation experiment were made using a graphite mold (~50mm long) with 4mm diameter holes machined longitudinally. The holes were filled with glass fibers, placed in an oven at room temperature, and heated to the bonding temperature of; 575^{o}C, 625^{o}C, and 690^{o}C for the 13-93B3, 13-93B1, and 13-93, respectively, at a rate of 20^{o}C/min and held for 20 minutes. After the heat treatment, the mold was removed from the oven and cooled to room temperature. Once cool, the scaffolds (~40mm long) were removed from the mold and infiltrated with molten wax. Once the wax solidified, the scaffolds were cut with a slow speed saw with a diamond wafer blade to a nominal thickness of 1.5mm. After cutting, the scaffolds were submerged in xylene to dissolve the wax and were stored in a desiccator until needed.

Prior to implantation or seeding with MSCs, the as-made scaffolds were dry heat sterilized. The scaffolds were placed in a glass vial, covered with a loose fitting aluminum foil top, heated to 300^{o}C for four hours, and cooled to room temperature. Once cool, the scaffolds were ready for seeding with MSCs or implantation.

4.3.2 Calvaria Defect Model

4.3.2.1 Scaffold Porosity

The interconnected open porosity of the scaffolds used for the calvaria implantation experiment was measured by a liquid displacement method. The equation used to calculate the open porosity (P_o) is shown as Eqn 1. The dry weight of the scaffolds was measured with a digital scale (Mettler Toledo XS105 ±0.00001g) to obtain a dry weight (M_1). The scaffolds were submerged in kerosene and placed under vacuum for one hour to fill the open, interconnected, pores and then weighed while suspended in kerosene (M_2) and while saturated with kerosene in air (M_3). The open porosity (P_o) of the scaffold was calculated from Eqn 1.

$$P_o = \frac{M_3 - M_1}{M_3 - M_2} \times 100\% \quad (1)$$

The average open porosity from an n=12 from eqn 1 for each type of scaffolds was 47 ± 4%, 47 ± 3%, and 51 ± 2% for the 13-93, 13-93B1, and 13-93B3, scaffolds, respectively.

4.3.2.2 Scaffold Implantation in Rat Calvaria

Fiber scaffolds of 13-93, 13-93B1, and 13-93B3 glasses (see Table 1) and 100 to 200μm diameter loose particles of 45S5 were implanted in 4mm diameter calvaria defects of rats for 12 weeks. The rats were anesthetized with intravenous drugs prior to the surgery. Two 4mm diameter defects were made with a high speed dental bur and placed on each side of the sinus as shown in the schematic in Fig 1. The fiber scaffolds or loose particles of 45S5 were implanted in the defects, and the skin was closed. The calvaria implantation and micro-CT measurements were done at the University of Missouri – Kansas City School of Dentistry. Histomorphometry of the 12 week scaffolds

and loose particles for quantization total bone growth was compared by one-way analysis of variance (ANOVA).

4.3.2.3 Micro-CT Analysis of *In-Situ* Scaffolds

After 12 weeks the rats were sacrificed and the bone growth across the top and bottom of the implanted scaffolds was determined with micro-CT. The rats were anaesthetized and the implant areas scanned to determine bone growth at the implant sites.

4.3.3 Subcutaneous Model

4.3.3.1 Scaffold Seeding with Mesenchymal Stem Cells

Mesenchymal stem cells were recovered from the long bones of sacrificed Fisher 344 rats. The cells were cultured *in-vitro* to separate the stem cells from bone marrow prior to seeding the scaffolds. Half of the scaffolds were seeded with 50,000 MSCs, the other half were unseeded. The cells were cultured on the scaffolds for approximately 12 hours prior to the implantation to allow the cells to attach to the scaffolds/fibers.

4.3.3.2 Scaffold Implantation

Five scaffolds of each type (Cu-3, CS, CSZ, CSZF, Table 1) were seeded with MSCs and five were left unseeded. These scaffolds were implanted in subcutaneous sites of Fisher 344 rats for a total of 40 implants in 10 rats. The scaffolds were implanted randomly to remove any bias from a single rat. A schematic of the implant sites is shown in Fig 2. Each rat had four implant sites, two above the shoulders and two above the back legs, where a single scaffold was implanted for a total of four scaffolds per rat. The back of each rat was shaved with clippers and washed with iodine and then 70% ethanol to

disinfect the skin prior to the surgery. During the surgery, the rats were anesthetized with isoflourine.

An incision was made about 20mm in length completely through the cutaneous tissue, perpendicular to the spine, with a pair of surgical scissors. Next, a surgical clamp was inserted into the incision and opened to separate the cutaneous tissue from the skeletal muscle. The implant site was made approximately 15 to 20 mm long. The scaffold was then placed at the back of the cutaneous opening and the skin closed. Any air that entered the implantation site was removed by gently pressing the cutaneous tissue against the skeletal muscle. The wound was closed by mechanically bonding the skin with super glue.

After scaffold implantation, the rat was injected with 0.2ml of penicillin (0.1ml per hind leg) and placed on a heating pad in a clean cage with access to fresh air to recover. The ears of each rat were marked to differentiate the rats. Two rats were caged together during the length of the experiment and had free access to food pellets and tap water and the light schedule was 12 hours light, 12 hours dark.

4.3.3.3 Scaffold Removal and Tissue Processing

After six weeks, the rats were sacrificed by CO_2 inhalation and the scaffolds were removed for analysis. The scaffolds were placed in 5ml of 10% formalin solution for four days to fix the tissue. Once the tissue attached to the scaffolds was chemically fixed, the scaffolds were dehydrated with a series of ethanol solutions by a microwave dehydration technique [22]. The microwave used was a microwave tissue processor (EBSciences H2850 Microwave Processor). The microwave was set to 70% power, the

sample temperature was set to 37±4^{o}C, and microwave was on for 2.5 minutes for each solution. A scaffold was in each ethanol solution for a minimum of 15 minutes.

4.3.3.4 Histology Slide Preparation and Histological Assessment

The dehydrated scaffolds were placed in a tissue processor (AutoTechnicon Model 2A) filled with fluid paraffin mounting wax (Paraplast Tissue Embedding Medium, McCormick Scientific LLC) at 45^{o}C for four hours for wax infiltration of the scaffold and tissue. Each scaffold was mounted in wax for histological sectioning with a paraffin mounting system (Leica EG 1150H). Sections 18µm thick were cut with a histological microtome (Leica RM 2235 microtome) with TBS Shur/sharp blades, (Triangle Biomedical Sciences, Durham NC). The cut sections were floated on a water bath (Lipshaw Electric Tissue Float, model number 375, Detroit MI) (40^{o}C) prior to mounting on a glass slide (Fisher Brand Superfrost microscope slides, St. Louis MO). Three to four tissue sections were placed on a single glass slide, and dried overnight on a slide warmer (Fisher Scientific slide warmer, St. Louis MO). Slides were stained with Sanderson Rapid Bone Stain to determine if the scaffolds were osteoinductive. Stained slides were viewed with a microscope (Olympus BX50, Olympus Optical Co) at magnifications of 40, 100, and 400X and imaging software (DP Controller, Olympus Optical Co) was used for image capture.

A scaffold composed of randomly oriented and self bonded fibers was embedded in PMMA for use as a reference for the fibers present in the cross sectioned histology sections. The plastic embedded randomly oriented fiber scaffold was sectioned with a slow speed saw and a diamond coated blade and polished with 320, 400, 600, 800, and 1200 grit silicon carbide paper. The polished cross section of a scaffold is shown in Fig 3

The fibers appear round if the longitudinal axis of a fiber is perpendicular to the plane of the image and ellipsoidal if the fiber is oriented at an angle to the section.

4.3.3.5 Bone-like Material Analysis

Sections from four scaffolds of each type, seeded and unseeded with MSC's, were stained with Sanderson Rapid Bone Stain at 50^{o}C for 60 to 75 seconds. The sections rinsed with DI water and checked under a microscope to ensure the tissue stained to an appropriate level. The sections were counter stained with an acid fuchsin solution (99mL DI water, 1mL concentrated acetic acid, 1.0 gram of acid fuchsin) at room temperature (22^{o}C) for 30 to 45 seconds. The sections were viewed under the microscope again to check the counterstain. The sections were then coated with a transparent resin and coverslipped. Each section was viewed at 10X and 40X with an Olympus MI transmitted light microscope (Olympus Corporation, Japan).

4.3.3.6 Scanning Electron Microscopy Analysis (SEM)

An FEI environmental scanning electron microscope ESEM (FEI, Hillsboro, OR) was used for SEM imaging of cross sectioned scaffolds. Each scaffold was embedded with poly methyl methacrylate (PMMA) and sectioned in half with a slow speed diamond saw. The surface imaged by SEM was polished with silicon carbide polishing paper to 1200 grit, coated with ~100nm of Au/Pd for conduction prior to SEM analysis. Backscattered SEM was used to identify areas of mineralized bone-like material.

4.4 RESULTS

4.4.1 Calvaria Defect Experiment

Micro-CT was used to image the bone that had grown across the top and bottom of each scaffold as shown by Fig 4. The area of scaffold not covered by bone was

subtracted from the original defect area to determine the defect closure. The average percent closure for each implant type is shown in Fig 5. The 13-93B3 glass had the highest average percent bone regeneration on top and bottom of the scaffold when compared to the other implants. The 45S5 silicate glass had the least amount of bone regeneration on the top and bottom after 12 weeks.

4.4.2 Bone Growth in Bioactive Glass Scaffolds Implanted in Rat Calvaria (12 Weeks)

Total bone growth in the 12 week calvaria scaffolds was quantified by a histomorphometric analysis [23] and the results are shown in Fig 6. The 13-93B3 borate scaffolds contained the most new bone of any of the glasses, about twice as much bone as the 13-93 and 13-93B1 scaffolds. A one-way ANOVA analysis of the histomorphometry data concluded that the 13-93B3 scaffolds contained significantly more bone ($p<0.05$) than the 13-93 or 13-93B1 scaffolds.

4.4.3 Subcutaneous Implantation Experiment – Doped Scaffolds

4.4.3.1 Scaffold Removal

After six weeks *in-vivo*, each scaffold was removed from the subcutaneous tissue of each rat. None of the rats died during the experiment, and none exhibited any signs of sickness or infection. The images in Fig 7 show the appearance of seeded (MSC's) and unseeded scaffolds, while still attached to the subcutaneous tissue. Several blood vessels were visible in the tissue adjacent each scaffold. Most scaffolds had what appeared to be a red or pink tissue inside the scaffold indicating that blood vessels had grown inside the open and interconnected pores in the scaffold.

4.4.3.2 Osteoinductivity of Scaffolds (Sanderson Rapid Bone Stain)

The ability to foster the differentiation of stem cells to a bone-like material is known as osteoinductivity. Half of the scaffolds implanted in the subcutaneous tissue were seeded with 50,000 MSCs recovered from rat femurs. If MSCs differentiate into a bone-like material in the presence of the scaffold that has been implanted away from a bone site, then the scaffold may be considered an appropriate device for bone regeneration in a bony defect. Sections stained with Sanderson Rapid Bone Stain (SBS) appear as follows: cell nuclei are dark blue for bone and soft tissue, cytoplasm stains a light blue, osteoid (bone precursor composed of proteins secreted by osteoblast cells) is purple, mineralized bone and hydroxyapatite is pink to red, and soft tissue is dark blue.

4.4.3.3 Histology of Un-Seeded Scaffolds

An example of each unseeded scaffold type stained with the Sanderson Rapid Bone Stain (SBS) is shown in Fig 8 and the tissue analysis results are present in Table 2. All of the scaffolds were filled with soft tissue (dark blue) in the interconnected pore space. No osteoid (bone precursor) or mineralized bone-like material was detected in any of the unseeded scaffolds as expected. The arrows in Fig 8B point to air bubbles that formed when the cover slip was glued to the section. The color of the stained sections varied as the sections were stained individually by hand and were not stained as precisely as they would have been in an automated system.

4.4.3.4 Histology of MSC Seeded Scaffolds

A cross section of a representative Cu-3 scaffold seeded with MSCs, and stained with SBS is shown in Fig 9A. Soft tissue (dark blue) is visible throughout almost the entire scaffold, filling the interconnected pores between the reacted Cu-3 fibers (red).

The area magnified in Fig 9B was chosen because it shows several reacted fibers (F) with purple osteoid tissue (O) that grew adjacent with the surface of the reacted Cu-3 fibers (red). Several blood vessels are indicated with white arrows showing the integration of blood vessels within the osteoid. Figure 9C shows a mixture of bone-like (red) and osteoid tissue (purple) next to reacted Cu-3 fibers at the outer edge of the scaffold. The bone-like material was located toward the outer surface of the scaffolds. Osteoid was present throughout the seeded (MSC) scaffolds and was often intermixed with tissue that stained positive for bone-like material. The osteoid material contained blood vessels which is important for bone metabolism.

Figure 10A is the backscattered SEM micrograph of a seeded Cu-3 scaffold after six weeks in subcutaneous tissue. The fibers are significantly reacted as most have formed hollow voids toward their center. The pore space between the fibers appears black since the soft tissue filling the interconnected pores has a low average atomic number. The ellipsoidal fibers in the image are due to the random orientation of the fibers as previously mentioned. There is a material surrounding some of the reacted fibers as indicated by the arrow in Fig 10A which has been magnified in Fig 10B. This material could be bone matrix (calcium phosphate) as its contrast in the BSE image is similar to the HA (calcium phosphate) of the reacted fiber. The material is not recognizable as bone at this point, but the formation of this material could be from the differentiation of the seeded MSCs.

The cross section of an MSC seeded CS scaffold is shown in Fig 11. There is significant soft tissue (dark blue) infiltration of the once empty pores as shown in Fig 11A. Figure 11B is a magnified view of the outer portion (box B) of the CS scaffold that

has a mixture of bone-like and osteoid tissues (B-O). The image in Fig 11C is a higher magnified view of the bone-like and osteoid tissues adjacent to some reacted CS fibers (F) in box C.

The fibers comprising the seeded CS scaffold in Fig 12 had reacted after six weeks as most of the fibers had areas that appeared hollow near or at the center of the fibers. Those fibers marked with an arrow at the bottom left of Fig 12, which were near the center of the scaffold, had not fully reacted, but the majority of the fibers are fully reacted. No recognizable bone-like material was found in Fig 12 since there was no mineralized material attached to any of the reacted fibers or in the interconnected pore space.

A section from a seeded (MSC) CSZ scaffold, implanted in rat subcutaneous tissue for six weeks, and stained with SBS is in Fig 13. Soft tissue (dark blue) was present throughout the scaffold as indicated in Fig 13A. The material in box B, Fig 13B, contained bone-like (red) and osteoid material (purple) next to a reacted CSZ fiber (F) that was close to the outer edge of the scaffold. The bone-like material (B) toward the bottom of Fig 13B contains osteocytes (circled purple dots) surrounded by mineralized matrix (red). Another area of the CSZ scaffold, box C, contains a mixture of osteoid and bone-like material (B-O) and soft tissue (S) next to reacted CSZ fibers is shown in Fig 13C. There are several circular and ellipsoidal shapes indicative of blood vessels between the two reacted fibers in Fig 13C (red arrows). The blood vessels adjacent to the mixture of bone-like and osteoid tissue indicated that the adjacent tissues had sufficient oxygen and nutrient supply needed for cellular metabolism.

The backscattered SEM image in Fig 14 shows a MSC seeded CSZ scaffold after six weeks in rat subcutaneous tissue. The outer edge of the scaffold is at the upper right corner of the image and the center of the scaffold is located toward the lower left. Some of the CSZ fibers were only partially reacted, as they contained residual glass at the center (arrows) of the fiber. The fibers at the outer edge are reacted, but, did not form hollow fibers as was observed for the Cu-3 and the CS fibers. The center of many of the reacted fibers had a calcium rich core (horizontal arrows) that has been described in detail elsewhere [24]. There was no detectable bone-like material attached to the reacted fibers.

A section from a seeded (MSC) CSZF scaffold, implanted in rat subcutaneous tissue for six weeks, and stained with SBS, is shown in Fig 15. The only section of the four seeded CSZF scaffolds to stain positive for a bone-like material when stained with SBS is shown in Fig 15A. Soft tissue was present throughout the scaffold, but the only bone-like material was present near the outer surface of the scaffold, boxes B and C. A mixture of osteoid and mineralized bone-like tissue formed along the outer portion of the scaffold, and two examples of tissue that stained positive for osteoid and bone-like material next to reacted CSZF fibers are shown in Figs 15B and 15C.

Figure 16 is a SEMBSE micrograph of the reacted cross section of a seeded CSZF scaffold implanted in rat subcutaneous tissue for six weeks. The fibers are all reacted since the once homogeneous fibers are now composed of noticeably different layers as can be seen in Fig 16. The reacted CSZF fibers have white cores similar to the CSZ fibers in Fig 14. There was no evidence of any mineralized bone-like material attached to the reacted fibers as there was no mineralized material surrounding any of the fibers or present in the interconnected pore space.

4.5 DISCUSSION

4.5.1 Calvaria Bone Regeneration

The present study is the first to compare similar scaffold microstructures composed of borate and silicate glasses. On the average, the scaffold with the most bone regenerated across the scaffold top and bottom surfaces after 12 weeks as measured by micro-CT was the 13-93B3, and 13-93B3 the only scaffold type to have bone completely cover the bottom side of a scaffold. The 13-93B3 scaffold had significantly more bone than the 13-93 or 13-93B1 scaffolds by histomorphometry analysis (1 way ANOVA).

The 45S5 glass was implanted in particulate form because the glass is difficult to heat treat and form a porous scaffold without crystallization [9]. The objectives of the calvaria experiment were to determine the effect of glass composition on bone growth and to determine if a scaffold with interconnected pores was better for bone growth than loose particles. The facts of the experiment are that the borate glass had significantly more bone ($p<0.05$) than the borosilicate or silicate glass scaffolds and the borate scaffold had on the average more bone than the 45S5 loose particles (Fig 6). Porous, three dimensional scaffolds are becoming popular for tissue engineering of bone and soft tissue because they can be made with a tailorable porosity, pore structure, and some bioactive glass scaffolds can withstand considerable load (~140MPa) which loose particles can not [25].

4.5.2 Gene Expression Triggered By Bioactive Glass

Several researchers have studied the effect of the dissolution products from 45S5 glass on bone cells *in-vitro* and *in-vivo* and found that extracts containing calcium and silica promote the up-regulation or activation of seven families of genes associated with

the osteoprogenitor cell and these activities lead to enhanced bone growth [26]. The families of genes that are activated belong to transcription factors and cell cycle regulators, DNA synthesis, repair and recombination, apoptosis regulators, growth factors and cytokines, cell surface antigens and receptors, signal transduction molecules, and extracellular matrix compounds. Each of these families of genes contains multiple genes that have been reported to be stimulated between 160 and 700% when in the presence of the 45S5 dissolution products [26].

Glasses such as 45S5, 13-93, and the 13-93B1 all contain silica and calcium, which has been shown to stimulate genes and promote bone growth [27]. The absence of SiO_2 in the 13-93B3 glass does not disprove the importance of SiO_2 in bone regeneration, but in the present work, the borate based 13-93B3 scaffolds promoted bone growth statistically better than the silicate containing scaffolds. This promotion of bone growth comes as no surprise because boron has been hypothesized to have several biological roles including bone mineralization and development [28].

Animals fed boron deficient diets had decreased or inhibited bone growth when compared to animals fed a normal diet [29]. There has been no study done to prove that boron can promote bone growth or activate genes if administered at levels above physiological levels. Boron does not affect the calcium or phosphorus levels in bone, but affects the levels of trace elements in bone such as zinc, magnesium, copper and potassium [29]. Therefore, boron indirectly affects bone formation by altering the physiological levels of other elements that have direct roles in bone formation [29].

The reaction rate of the 13-93B3 glass is ~10 times faster than 13-93 *in-vivo* based on data from glass fibers reacted in rat subcutaneous tissue [7, 20]. Calcium was

also previously mentioned as a gene stimulator, so assuming the boron had no effect on bone growth, the increased rate in calcium released from the 13-93B3 scaffold could be one reason why more bone grew in the borate scaffold than in the silicate (13-93) glass scaffold.

The 13-93B1 scaffold is an interesting data point because if boron was stimulating the bone growth, then the borosilicate glass arguably should have had the most growth since it was releasing silica, calcium, and boron. The 13-93B1 glass and the 13-93 glass grew almost identical amounts of bone after 12 weeks (Fig 20). From *in-vitro* reaction of 45S5 glass particles modified with boron [13], the weight loss of the borosilicate glass (1/3 replacement of silica with boron) and the silicate glass were almost identical, so a similar reaction rate and release of calcium from the 13-93B1 and 13-93 glasses would be expected. This is more evidence that the release of calcium may have been the driving force behind the increased bone growth.

In-vitro testing of MC3T3-E1 pre-osteoblast cells with added calcium ions showed that the calcium ions (up to 4.8mM) stimulated DNA synthesis and chemotaxis (cellular movement caused by a chemical gradient) of the cells [30]. The local release of calcium from a material such as a bioactive glass is thereby hypothesized to stimulate migration and proliferation of osteoblasts *in-vivo*.

Fast reacting bioactive glasses such as the 13-93B3 glass release calcium at a higher rate than 13-93 or 45S5 and increase the chemical gradient of calcium in the adjacent tissue. The increase in chemical gradient could potentially increase cellular migration which could increase the rate of bone regeneration. The increased release of calcium due to the faster reaction rate of the silica-free 13-93B3 scaffold is therefore

offered as an explanation as to why the 13-93B3 scaffold had more bone present after 12 weeks than the slower reacting silica containing scaffolds.

4.5.3 Potential Toxicity of the Boron Containing Glasses

Borate glasses tested *in-vitro* have inhibited cell proliferation and decreased cell number during static culture [31]. Dynamically cultured cells [31] or pre-reaction of the borate glasses [32] have improved the *in-vitro* proliferation as these techniques have been done to more closely mimic the *in-vivo* environment. The boron released from the borate scaffolds in the rat calvaria caused no increase in macrophages or other inflammatory cells in the adjacent tissue, and no necrotic tissue was reported [23]. No necrosis was expected in systemic organs such as the kidney and liver since rats with up to sixteen 13-93B3 scaffolds (70mg each) were implanted in a single rat and there were no pathological differences between the control rats and those implanted with sixteen scaffolds. Any recorded finding was at the lowest level of severity and considered normal in adult rats [33].

4.5.4 Osteoinductive Bone-like Tissue Formation Analysis

The SBS sections of the doped scaffolds indicated that at least one of the analyzed scaffolds from all four scaffold types seeded with MSCs promoted the differentiation of the MSCs to a bone-like material when implanted in rat subcutaneous tissue. The bone-like tissue formed at the outer edge of the scaffolds according to the SBS staining. There was no SEMBSE evidence to confirm the presence of a mineralized material except in the Cu-3 scaffold. It is unknown why there was little bone-like tissue formation toward the center of the scaffolds, but it may have to do with where the MSC cells attached during the initial cell seeding or perhaps there was insufficient supply of nutrients at the

center of the scaffolds after the initial implantation to sustain the MSC's. The MSC's may also still have been in the process of differentiating, although previous work with 13-93 fiber scaffolds seeded with MSC's and implanted in rat subcutaneous tissue had bone-like material present after four weeks [34].

Blood vessels present next to soft and bone-like tissues, as shown in Figs 9B and 13C are examples of blood vessels adjacent to the osteoid and or bone-like tissues. Jung et al modified the 13-93B3 glass composition with CuO to release copper ions to the surrounding tissue similar to copper salts, but in a controlled manner [35]. The addition of 0.4wt% of CuO to the 13-93B3 glass increased the amount of vessels present in rat soft tissue that had infiltrated the open pores of the scaffolds [35]. It took the scaffolds approximately six weeks to fully react in the subcutaneous tissue of the rats and there was no negative immune response in any of the glasses containing 0.4wt% CuO or less [35].

4.6 CONCLUSIONS

Borate glass 13-93B3 scaffolds promoted bone growth in rat calvaria significantly better than scaffolds with a similar microstructure composed of the silicate based 13-93 bioactive glass scaffolds after 12 weeks *in-vivo*. The explanation offered as to why the borate scaffold had more bone present is because of the faster reaction of the borate glass which increased the release rate of calcium, which is known to promote osteoblastic migration and proliferation.

Borate based bioactive glass fiber scaffolds doped with small amounts of copper, strontium, zinc, and iron, each of which is present in human bone, were seeded with mesenchymal stem cells and incubated in a soft tissue site to allow for the differentiation

of a bone-like material. Each of the types of doped scaffolds had at least one scaffold that stained positive for bone-like material. Blood vessels were seen throughout the infiltrated soft tissue, but it is unclear if the doped glasses promoted the differentiation of mesenchymal stem cells into osteoblastic type cells able to make bone-like material.

All rats remained healthy during the course of their given experiment; there were no signs of sickness in the rats, infection at the implant sites (bony or subcutaneous), or increase in macrophages or other inflammatory cells in the rat calvaria. These favorable results make borate based bioactive glasses and scaffolds important for future development of biomaterials for hard and soft tissue applications.

Acknowledgements

The authors would like to thank Vernon Modglin for his assistance with the surgical procedures, Dr. Anne Maglia of MS&T for access to histological equipment, and Dr. Vladimir Dusevich of UMKC for the ESEM analysis.

4.7 REFERENCES

[1] Hench LL. The story of Bioglass. Journal of Materials Science: Mater. Med. . 2006;17:967.

[2] Yamamuro T, Hench LL, Wilson J. Handbook of Bioactive Ceramics Vol. I - Bioactive Glasses and Glass-Ceramics. Boca Raton FL: CRC Press, 1990.

[3] Froum SJ, Weinberg MA, Tarnow D. Comparison of bioactive glass synthetic bone graft particles and open debridement in the treatment of human periodontal defects. A clinical study. J. Perio. 1998;69:698.

[4] Hench LL, Hench JW, Greenspan DC. Bioglass: A short history and bibliography. J. Aust. Cer. Soc. 2004;40:1.

[5] Sanus GZ, Tanriverdi T, Kafadar AM, Ulu MO, Uzan M. Use of Cortoss for reconstruction of anterior cranial base: a preliminary clinical experience. Eur. J. Plast. Surg. 2005;27:371.

[6] Larsson S. Cement Augmentation in Fracture Treatment. Scand. J. Surg. 2006;95:111.

[7] Jung SB, Day DE, Brown RF. Comparison of self-bonded three dimensional bioactive glass fiber scaffolds after in-vivo implantation in rats. J. Am. Cer. Soc. 2009, accepted.

[8] Fu Q, Rahaman MN, Bal BS, Brown RF, Day DE. Mechanical and InVitro Performance of 13-93 Bioactive Glass Scaffolds Prepared By a Polymer Foam Replication Technique. Acta Biomaterialia 2008;4:257.

[9] Chen QZ, Thompson ID, Boccaccini AR. 45S5 Bioglass-derived glass-ceramic scaffolds for bone tissue engineering. Biomaterials 2006;27:2414.

[10] Pirhonen E, Moimas L, Haapanen J. Porous Bioactive 3-D Glass Fiber Scaffolds for Tissue Engineering Applications Manufactured by Sintering Technique. Key Eng. Mater. 2003;240-242:237.

[11] Rahaman MN, Day DE, Brown RF, Fu Q, Jung SB. Nanostructured Bioactive Glass Scaffolds for Bone Repair. 32nd Int. Conf. Adv. Cer. Comp. 2008.

[12] Moimas L, Biasotto M, Lenarda RD, Olivo A, Schmid C. Rabbit pilot study on the resorbability of three-dimensional bioactive glass fibre scaffolds. Acta Biomaterialia 2006;2:191.

[13] Huang W, Day DE, Kittiratanapiboon K, Rahaman MN. Kinetics and Mechanisms of the Conversion of Silicate (45S5), Borate, and Borosilicate Glasses to Hydroxyapatite in Dilute Phosphate Solution J. Mater. Sci.: Mater. Med. 2006;17:583.

[14] Fears K. M.S. Thesis. Rolla, MO: University of Missouri-Rolla, 2001.

[15] Fu Q. PhD Dissertation. Rolla, MO: Missouri University of Science and Technology, 2009.

[16] Jung SB, Day DE. Conversion kinetics of silicate, borosilicate, and borate bioactive glasses to hydroxyapatite. Phy. Chem. Glass. 2009;50:85.

[17] Richard M. M.S. Thesis. Rolla, MO: University of Missouri-Rolla, 2000.

[18] Jai W-T, Zhang X, Luo S-H, Liu X, Huang W-H, Rahaman MN, Day DE, Zhang C-Q, Xie Z-P, Wang J-Q. Novel borate glass/chitosen composite as a delivery vehicle for teicoplanin in the treatment of chronic osteomyelitis. Acta Biomaterialia 2009.
[19] Liu X, Xie Z, Zhang C, Pan H, Rahaman MN, Zhang X, Fu Q, Huang W. Bioactive borate glass scaffolds: in vitro and in vivo evaluation for use as a drug delivery system in the treatment of bone infection. J. Mater. Sci.: Mater. Med. 2009;online.
[20] Jung SB, PhD Dissertation, Chapter 1. Rolla, MO: Missouri University of Science and Technology, 2010.
[21] Becker RO, Spadaro JA, Berg EW. The Trace Elements of Human Bone. J. Bone Joint Surg. 1968;50:326.
[22] Laboux O, Dion N, Arana-Chavez V, Ste-Marie L-G, Nanci A. Microwave Irradiation of Ethanol-fixed Bone Improves Preservation, Reduces Processing Time, and Allows Both Light and Electron Microscopy on the Same Sample. J. Histochem. Cytochem. 2004;52:1267.
[23] Bonewald L. Personal Communication. 2010.
[24] Jung SB, PhD Dissertation, Chapter 5. Rolla, MO: Missouri University of Science and Technology, 2010.
[25] Jung SB, Day DE. United States Patent Publication, Scaffolds For Bone and Tissue Repair In Mammals. US 2010/0179667.
[26] Hench LL, Polak JM. A Genetic Basis for Design of Biomaterials For In Situ Tissue Regeneration. Key Eng. Mater 2008;377:151.
[27] Jugdaohsingh R. Silicon and Bone Health. J. Nutri. Health and Aging 2007;11:99.
[28] Nielsen FH. Boron in Human and Animal Nutrition. Plant and Soil 1997;193:199.
[29] Gorustovich AA, Steimetz T, Nielsen FH, Guglielmotti MB. A Histomorphometric Study of Alveolar Bone Modelling and Remodelling in Mice Fed A Boron-Deficient Diet. Arch. Oral Bio. 2008;53:677.
[30] Yamaguchi T, Chattopadhyay N, Kifor O, Robert R. Butters J, Sugimoto T, Brown EM. Mouse Osteoblastic Cell Line (MC3T3-E1) Expresses Extracellular Calcium (Ca^{2+}) Sensing Receptor and Its Agonists Stimulate Chemotaxis and Proliferation of MC3T3-E1 Cells. J. Bone and Min. Res. 1998;13:1530.
[31] Brown RF, Rahaman MN, Dwilewicz AB, Huang W, Day DE, Li Y, Bal BS. Effect of borate glass composition on its conversion to hydroxyapatite and on the proliferation of MC3T3-E1 cells. J. Biomed. Mater. Res. 2008;88A:392.
[32] Marion NW, liang W, Reilly G, Day DE, Rahaman MN, Mao JJ. Borate Glass Supports the In Vitro Osteogenic Differentiation of Human Mesenchymal Stem Cells. Mech. Adv. Mater. Struct. 2005;12:1.
[33] Jung SB, PhD Dissertation, Chapter 2. Rolla, MO: Missouri University of Science and Technology, 2010.
[34] Jung SB. M.S. Thesis. Rolla, MO: University of Missouri-Rolla, 2007.
[35] Jung SB, PhD Dissertation, Chapter 3. Rolla, MO: Missouri University of Science and Technology, 2010.

TABLES

Table 1 – Bioactive Glass Compositions (wt%)

Glass	B_2O_3	Na_2O	CaO	K_2O	MgO	SiO_2	P_2O_5	CuO	SrO	ZnO	Fe_2O_3
45S5	0	24.50	24.50	0	0	45.00	6.00	0	0	0	0
13-93	0	6.00	20.00	12.00	5.00	53.00	4.00	0	0	0	0
13-93B1	17.67	6.00	20.00	12.00	5.00	35.33	4.00	0	0	0	0
13-93B3	53.00	6.00	20.00	12.00	5.00	0	4.00	0	0	0	0
Cu-3	52.79	5.98	19.92	11.95	4.98	0	3.98	0.40	0	0	0
CS	51.73	5.86	19.52	11.71	4.88	0	3.90	0.40	2.00	0	0
CSZ	51.20	5.80	19.32	11.59	4.83	0	3.86	0.40	2.00	1.00	0
CSZF	50.88	5.76	19.20	11.52	4.80	0	3.84	0.40	2.00	1.00	0.40

Table 2 – Results of Bone-like Tissue Formation (Sanderson Rapid Bone Stain)

Scaffold Type	Seeded MSC Cells	Soft Tissue	Osteoid	Bone-Like Tissue
Cu-3	No	4/4	0/4	0/4
Cu-3	Yes	4/4	4/4	3/4
CS	No	4/4	0/4	0/4
CS	Yes	4/4	4/4	2/4
CSZ	No	4/4	0/4	0/4
CSZ	Yes	4/4	4/4	3/4
CSZF	No	4/4	0/4	0/4
CSZF	Yes	4/4	3/4	1/4

Scaffolds seeded with MSC cells were seeded with 50,000 MSC cells.

FIGURES:

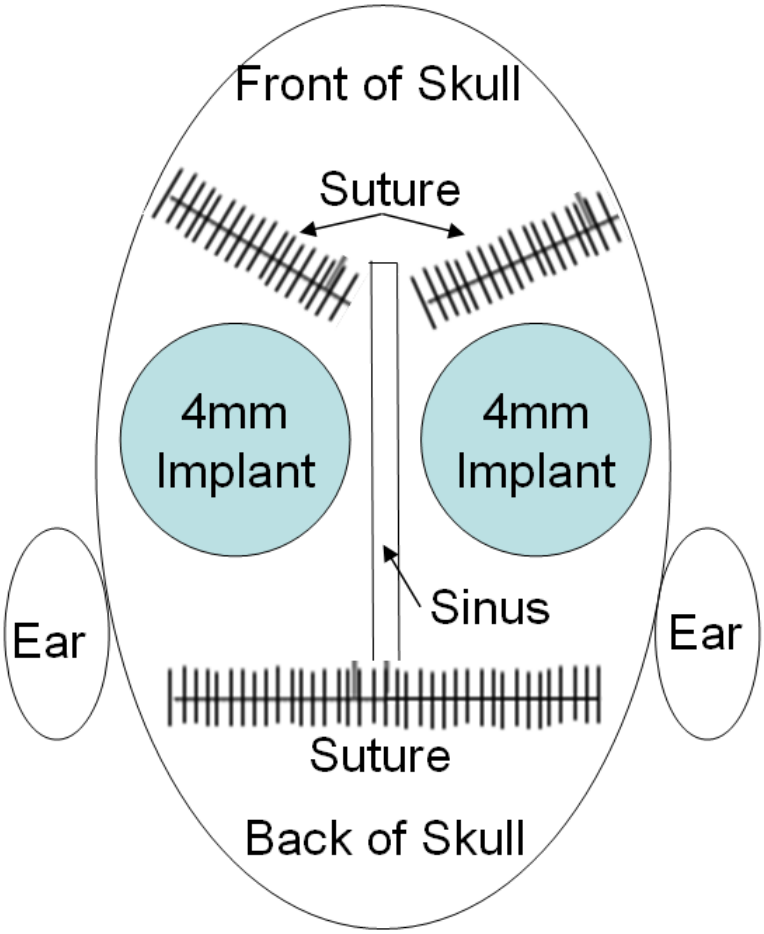

Figure 1 – Schematic showing the scaffold placement in the calvaria of a rat. The scaffolds implanted measured 4mm in diameter and 1.5mm thick as shown in Fig 1. Each scaffold was placed between the surrounding sutures and the sinus was avoided to reduce surgical complications.

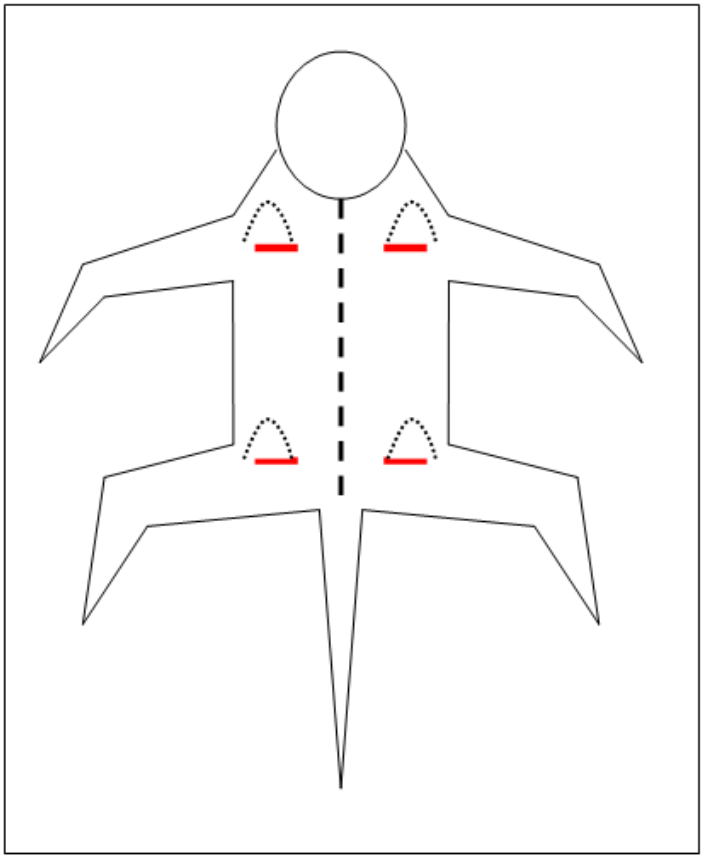

Figure 2 – Schematic showing the subcutaneous scaffold implant sites located on the back of a rat. A scaffold was placed above each of the front shoulders and above both hind legs as indicated. The incision (red line) made in the skin was approximately 20mm wide and the pocket made under the skin (dotted line) is about 20mm long. The dashed line represents the spine as a reference.

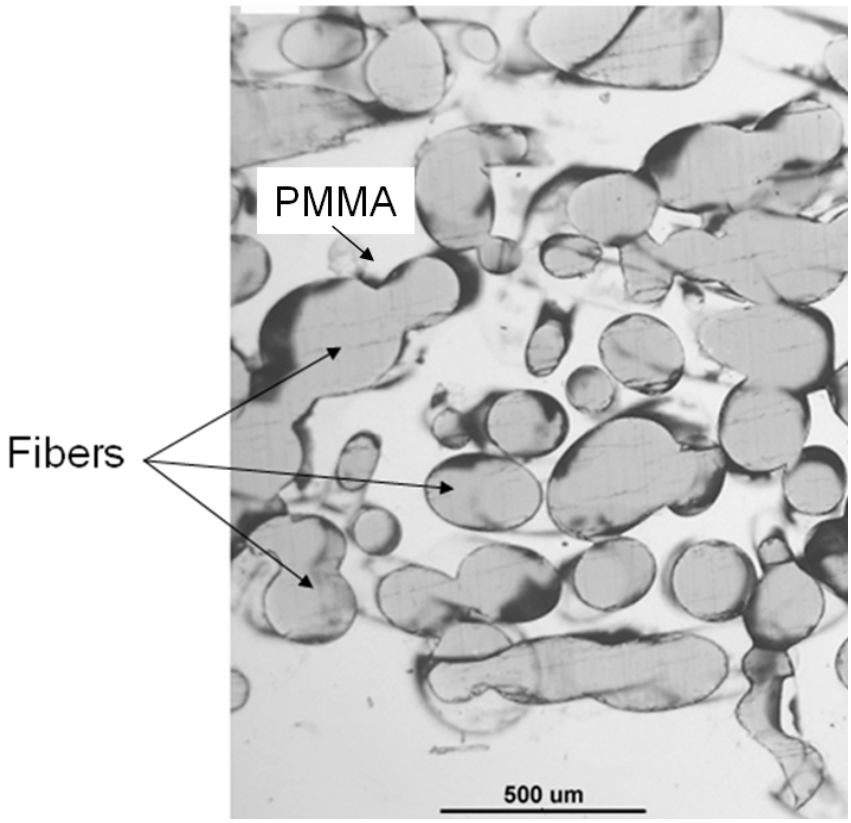

Figure 3 – Optical micrograph of a cross sectioned randomly oriented bioactive glass fiber scaffold. The fibers are gray and look like circular or elliptical depending on the fiber orientation.

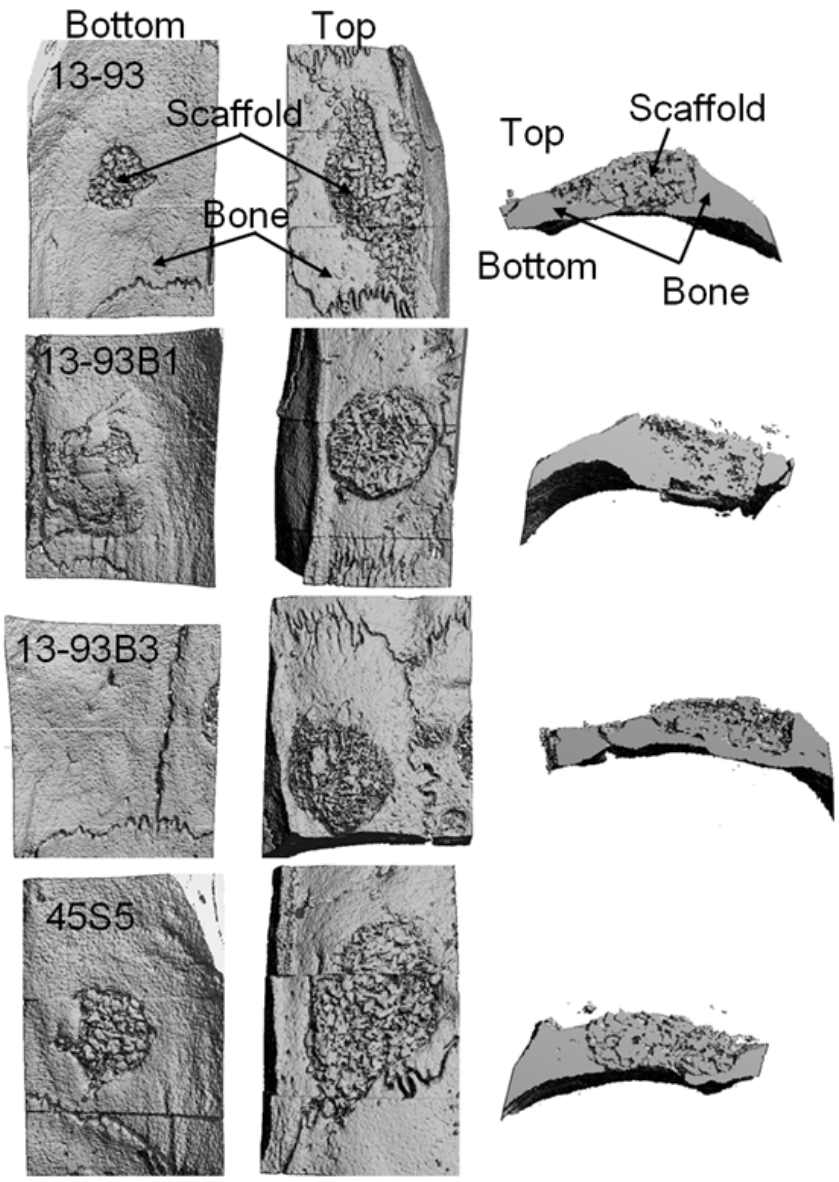

Figure 4 – Micro-CT images of the top and bottom of porous randomly oriented fiber scaffolds composed of bioactive glass fibers (13-93, 13-93B1, 13-93B3) and 45S5 particulates (100 to 200μm) after 12 weeks in 4mm rat calvaria defects. The scaffold and bone are labeled for the 13-93 scaffold for the top, bottom, and cross sectioned views. Note that the 13-93B3 scaffold is not visible in the bottom image (left). Bone had completely grown across the bottom of the 13-93B3 scaffold [23].

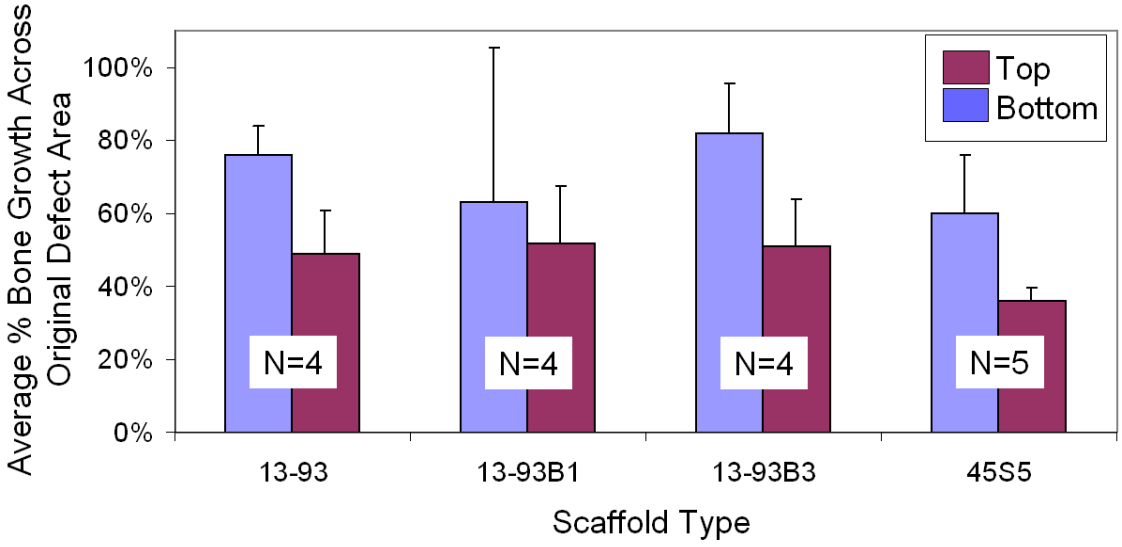

Figure 5 – Average bone growth across the top and bottom of the implanted scaffolds or particulates (45S5) after 12 weeks in rat calvaria (4mm original defect). Scaffold porosity was ~50% for each scaffold.

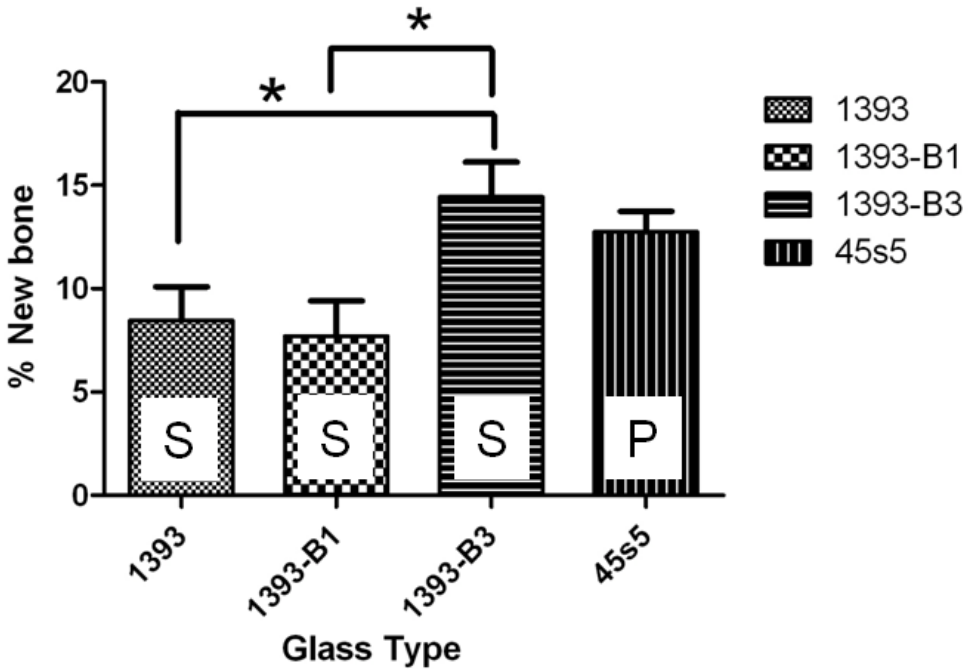

Figure 6 – Total bone growth into porous bioactive glass scaffolds (S), (45S5 was in particulate (P) form (100 to 200μm)) after 12 weeks in rat calvaria (n=4) as determined by histomorphometry analysis. Statistical significance represented by *($p<0.05$), [23].

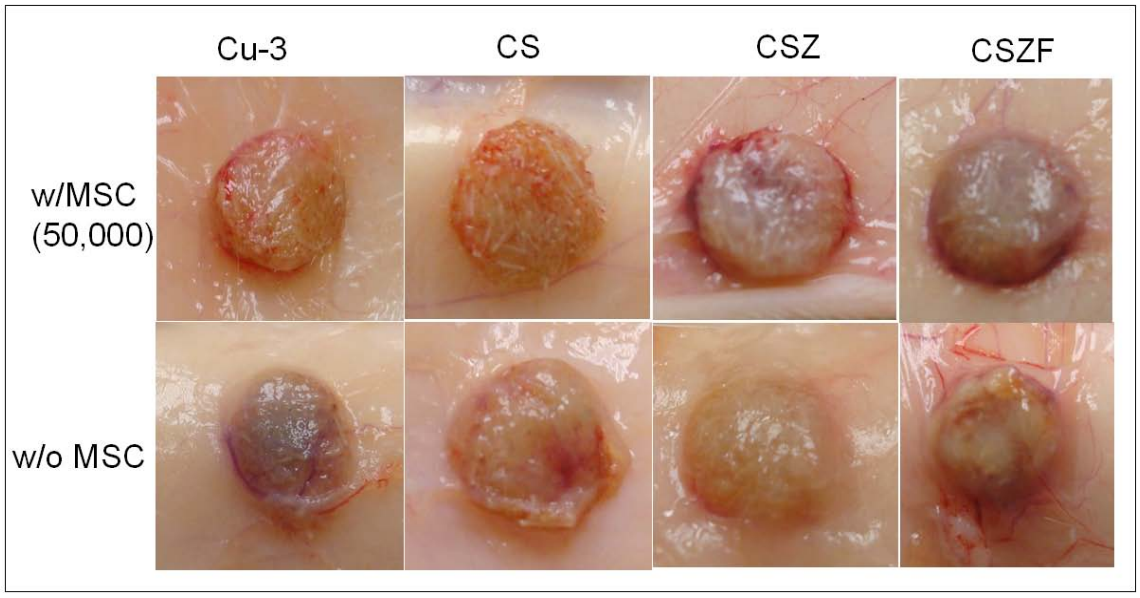

Figure 7 – Bioactive borate glass scaffolds doped with minor elements after six weeks in rat subcutaneous tissue. The top row shows scaffolds seeded with 50,000 MSCs, and the bottom row shows unseeded scaffolds.

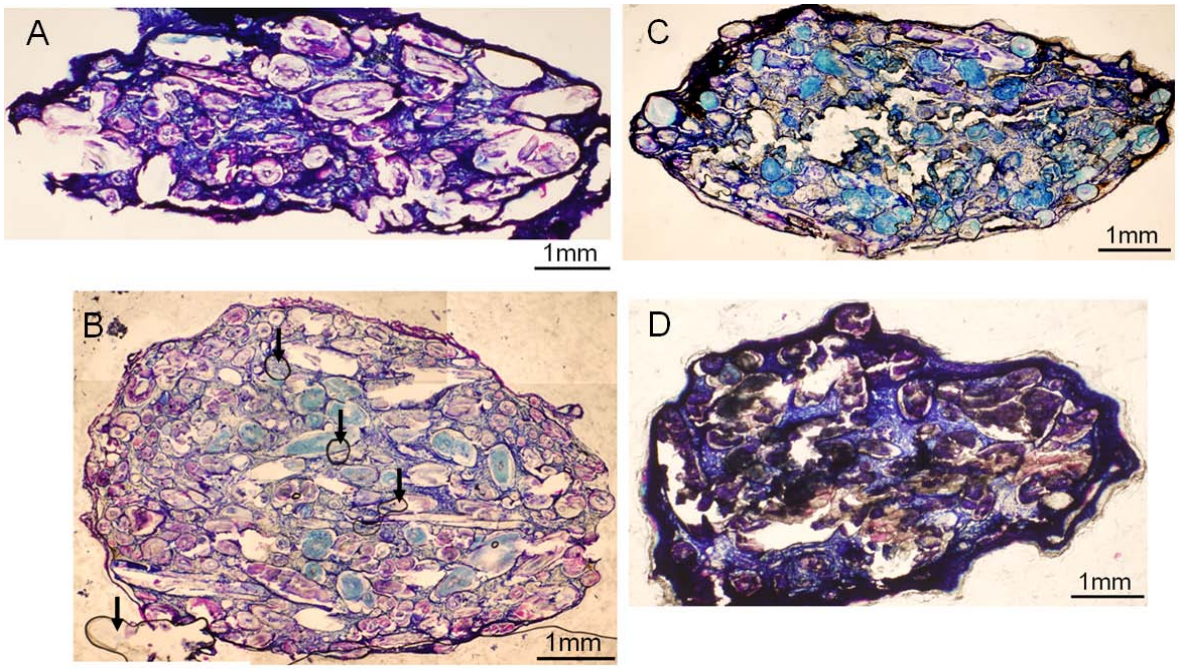

Figure 8 – Histological sections from a Cu-3 (A), CS (B), CSZ (C), and CSZF (D) unseeded scaffold after six weeks in subcutaneous tissue, stained with Sanderson Rapid Bone Stain and counterstained with acid fuchsin. The arrows in Fig 7B indicate the presence of air bubbles.

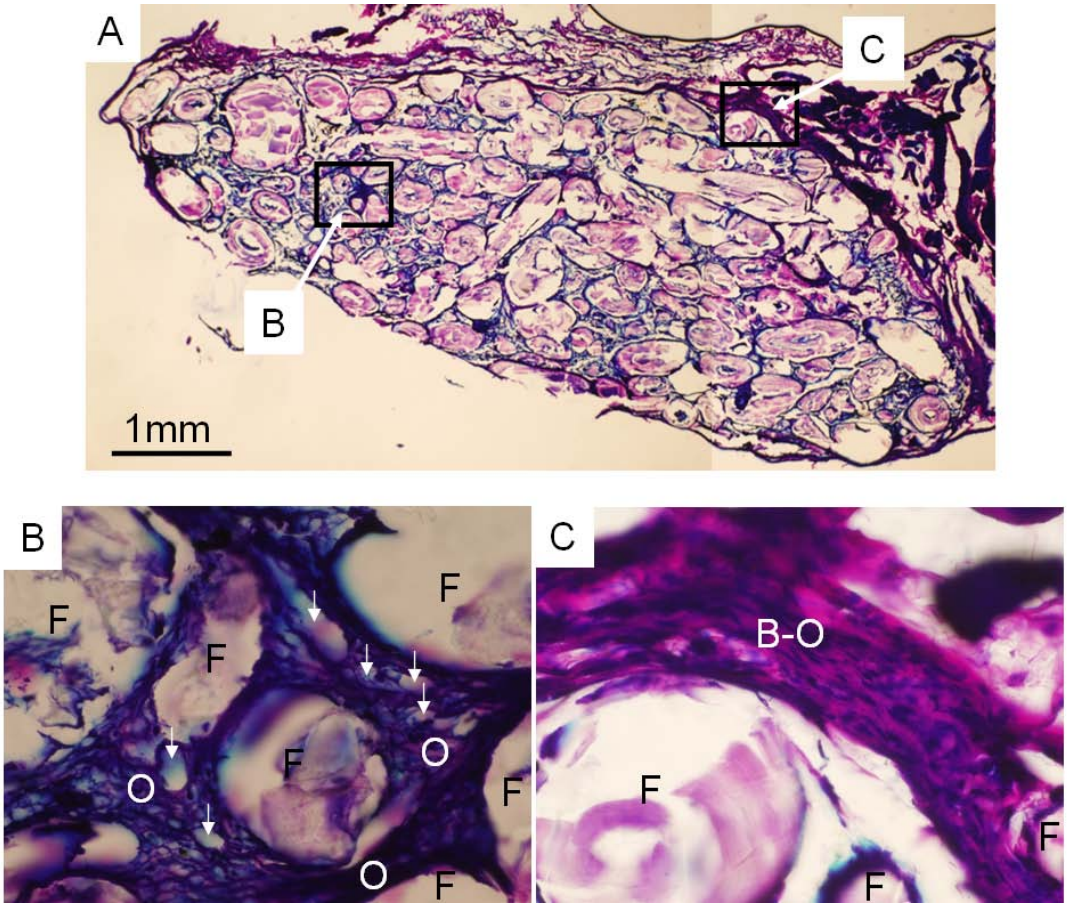

Figure 9 – Fig 9A is a representative image of a Cu-3 scaffold, seeded with 50,000 MSCs, after six weeks in subcutaneous tissue, stained with Sanderson Rapid Bone Stain and counterstained with acid fuchsin.

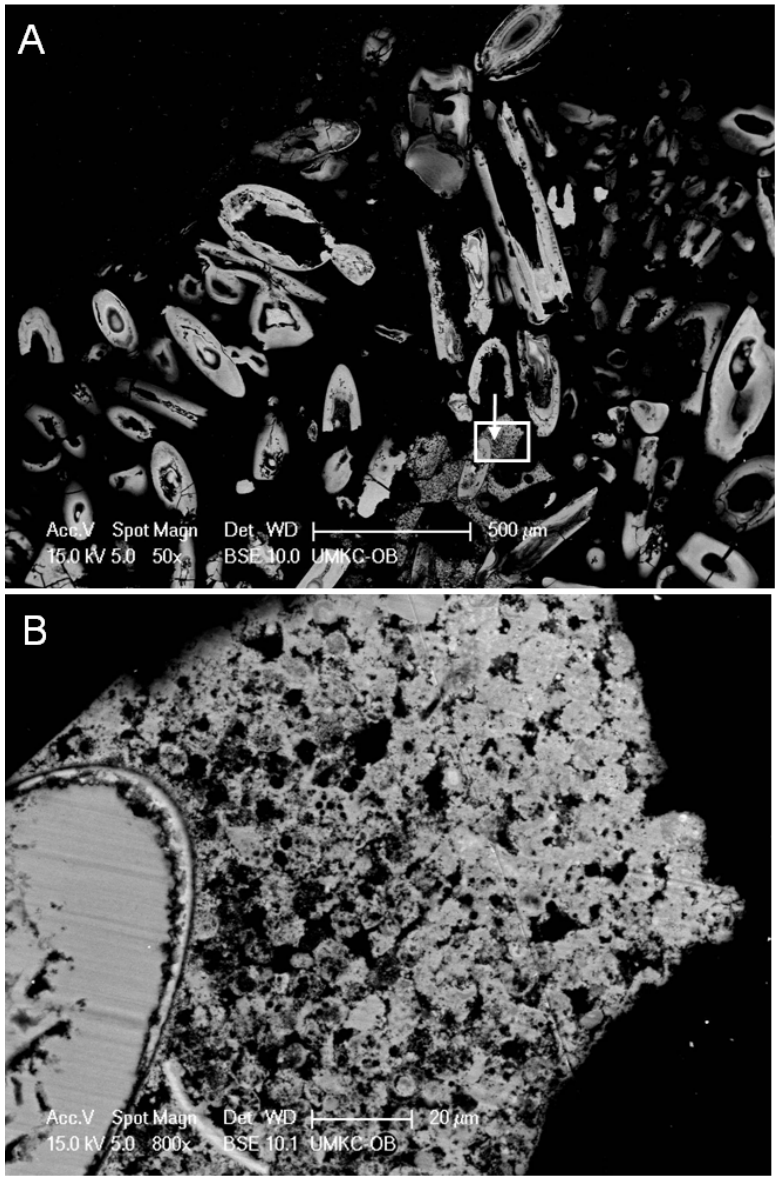

Figure 10 - SEMBSE image of the cross section of a seeded Cu-3 fiber scaffold (Fig 10A) that had been implanted in the subcutaneous tissue of a rat for six weeks.

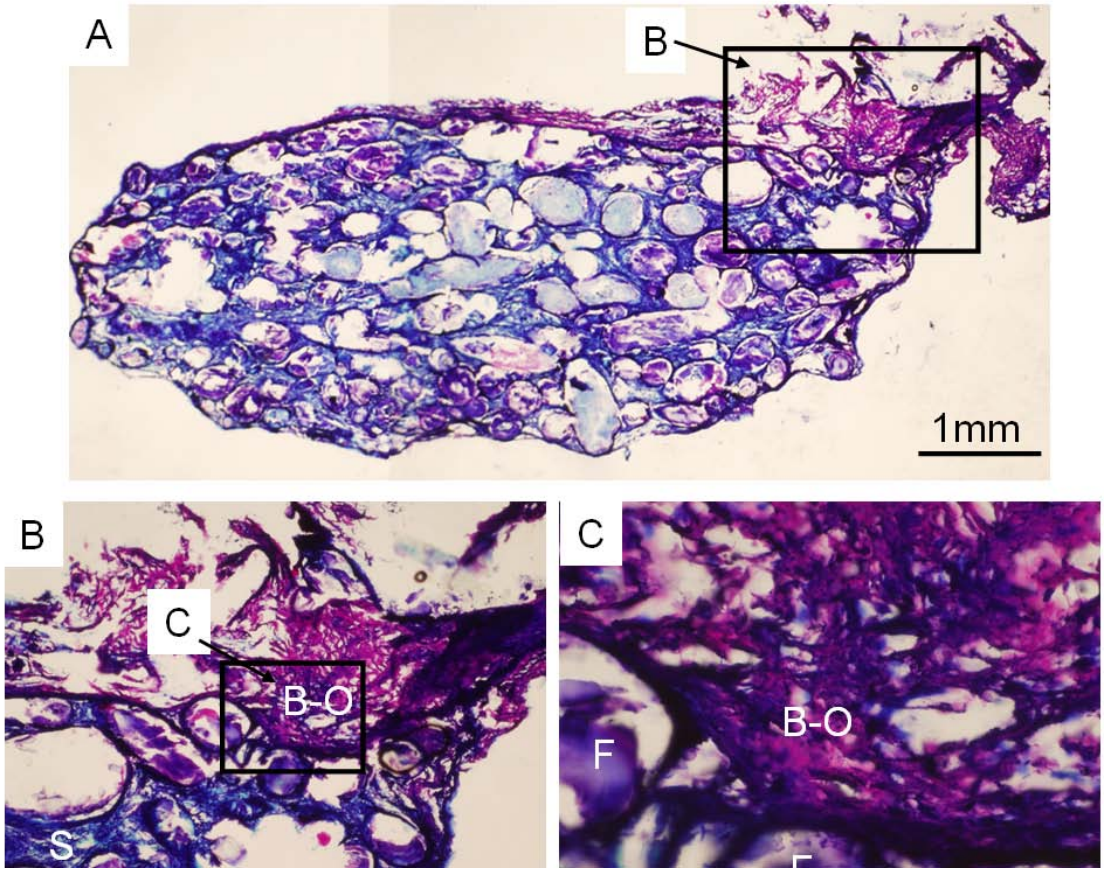

Figure 11 – Fig 11A is a representative image of the cross section of a seeded CS scaffold after six weeks in subcutaneous tissue, stained with Sanderson Rapid Bone Stain and counterstained with acid fuchsin.

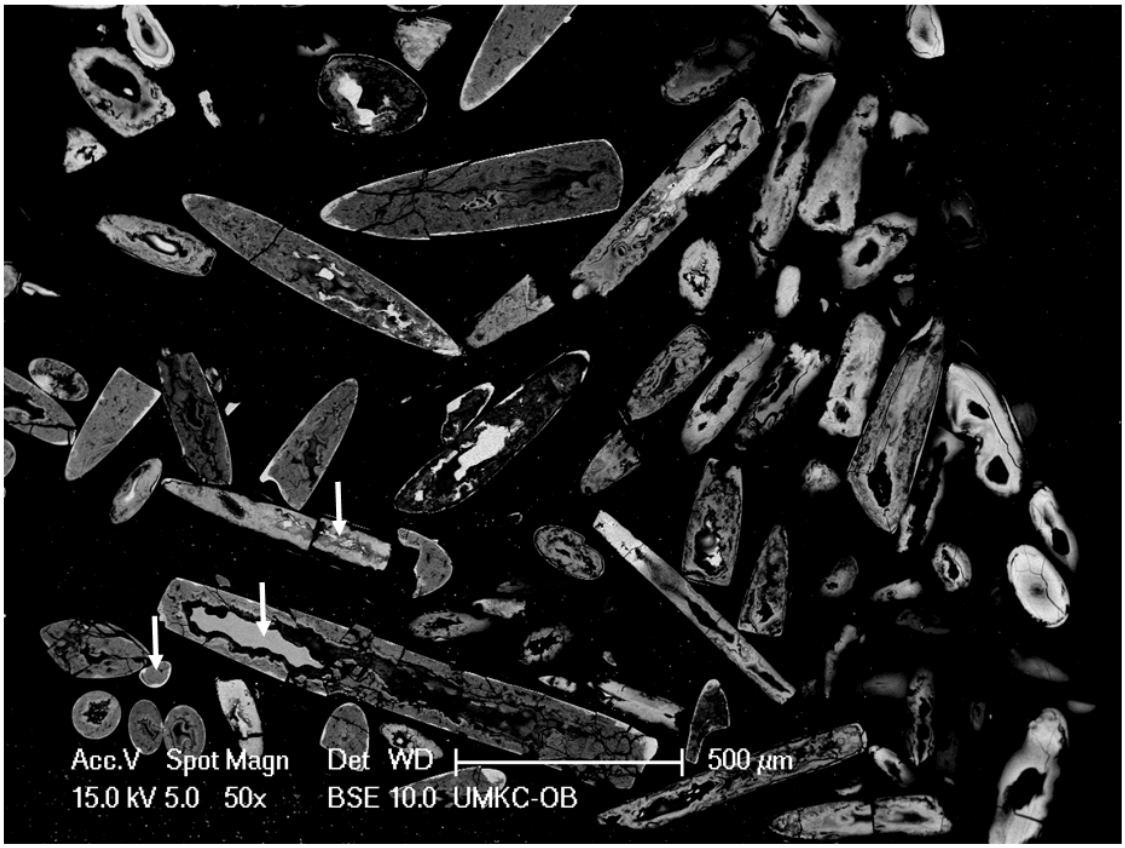

Figure 12 - SEMBSE image of a cross section of a seeded CS fiber scaffold and implanted subcutaneously in the back of a rat for six weeks. Arrows denote unreacted glass.

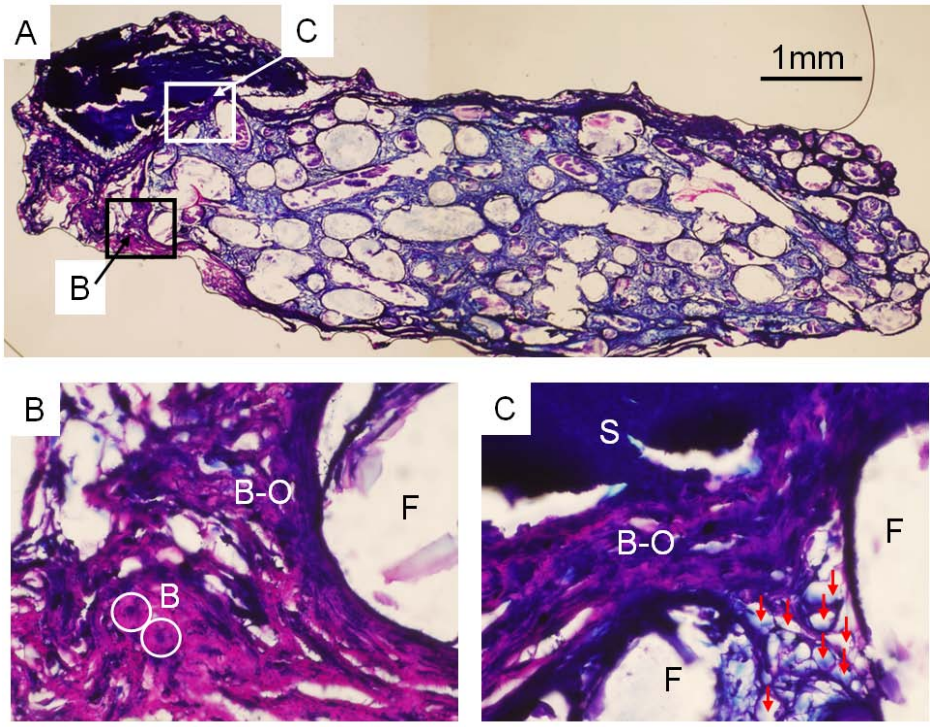

Figure 13 – Fig 13A is a representative image of a CSZ scaffold, seeded with 50,000 MSCs, after six weeks in subcutaneous tissue, stained with Sanderson Rapid Bone Stain and counterstained with acid fuchsin. Box B shows osteoid mixed with bone-like material (B-O) next to a reacted fiber (F). The two circles in Fig 13B are surrounding osteocytes that have become completely surrounded by mineralized matrix. The (B-O) mixture in Fig 13C shows bone-like material in the presence of reacted fibers (F) and soft tissue (S).

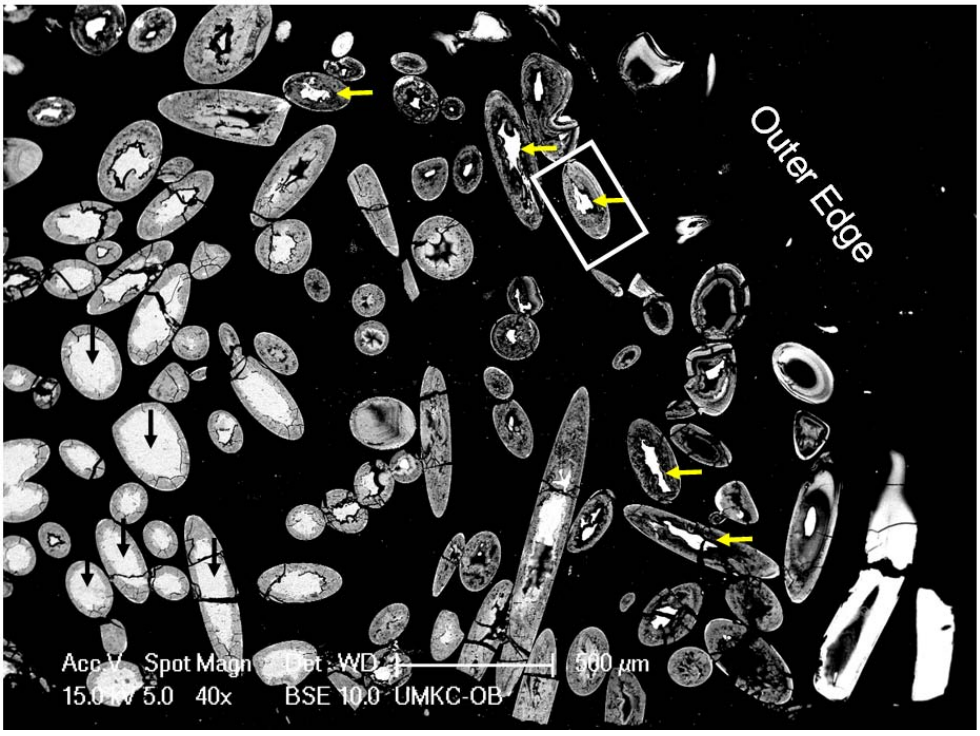

Figure 14 - SEMBSE image of a cross section of a seeded CSZ fiber scaffold that was implanted subcutaneously in the back of a rat for six weeks.

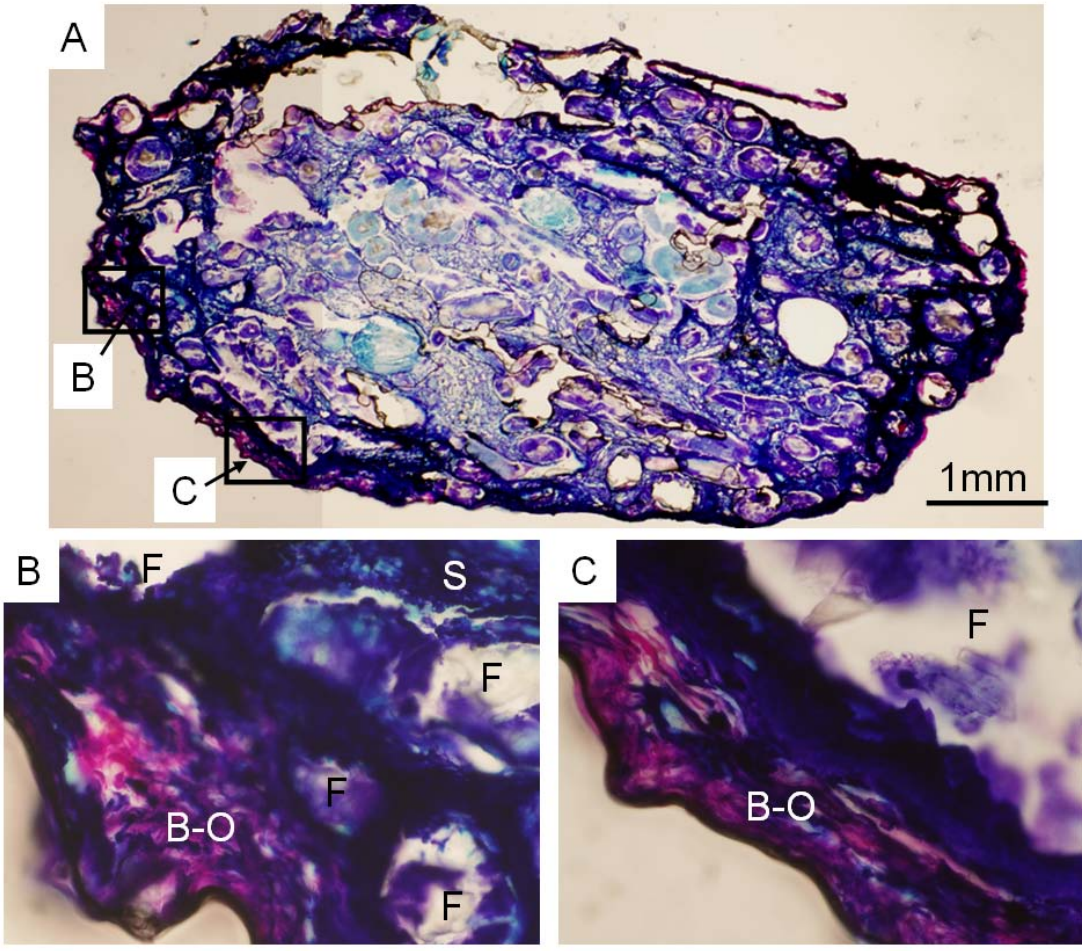

Figure 15 – Fig 15A is a representative image of a seeded CSZ scaffold after six weeks in subcutaneous tissue, stained with Sanderson Rapid Bone Stain and counterstained with acid fuchsin.

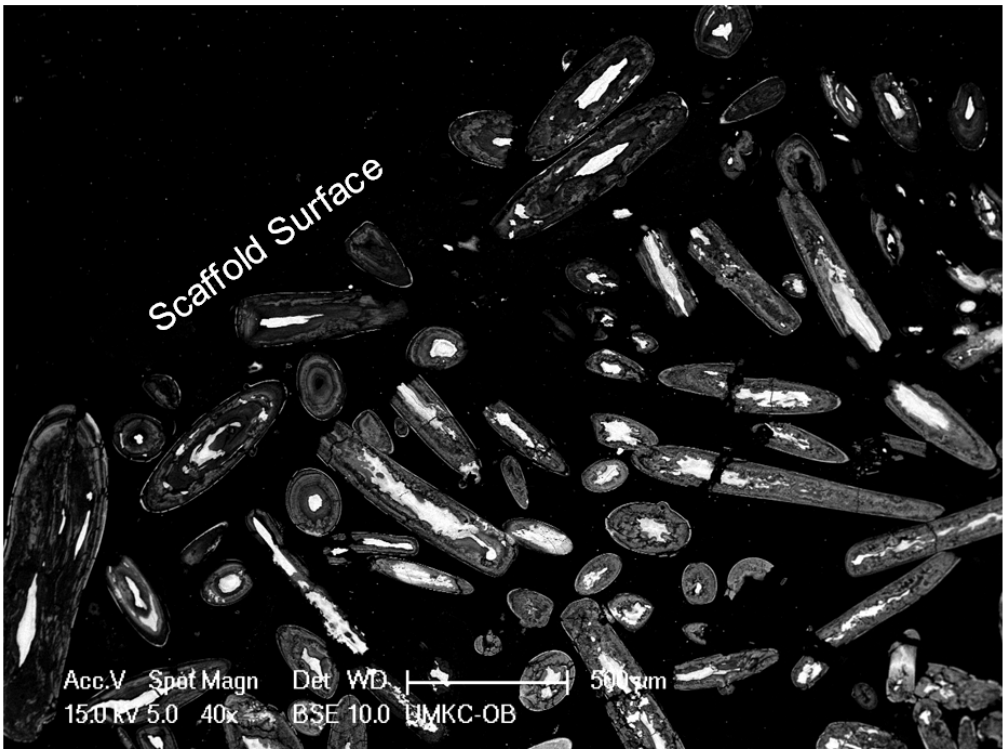

Figure 16 - SEMBSE image of a cross sectioned CSZF fiber scaffold that was seeded with 50,000 mesenchymal stem cells (MSC) and implanted subcutaneously in the back of a rat for six weeks. The majority of the fibers have fully reacted and formed a multilayered fiber made of two distinct materials, center white and outer edge gray.

5. IN-VIVO REACTION OF BIOACTIVE BORATE GLASSES DOPED WITH SELECTED METAL IONS

Steven B. Jung[1], Delbert E. Day[1], and Roger F. Brown[2]

[1]Graduate Center for Materials Research, Materials Science and Engineering Department, Missouri University of Science and Technology, Rolla, MO, 65409-1170

[2]Department of Biological Sciences, Missouri University of Science and Technology, Rolla, MO, 65409-1170

5.1 ABSTRACT

The *in-vivo* reaction of three dimensional scaffolds composed of randomly oriented, borate glass fibers doped with copper, strontium, zinc, and iron were investigated after being implanted in a subcutaneous site in laboratory rats for up to six weeks. No inflammation or infection was observed at any of the implant sites. Upon retrieval of the scaffolds, blood vessels were observed adjacent to new tissue. Evidence of the minor elements in the scaffolds after six weeks was confirmed by XRF. The minor elements were either present in the adjacent tissues or in the reacted fibers. Analysis of the reacted fibers by scanning electron microscopy (SEM) and x-ray diffraction (XRD) showed that the majority of the un-doped fibers were fully converted to hydroxyapatite (HA) after four weeks. The addition of the minor elements slowed the conversion of the bioactive glass fibers to HA. The scaffold containing copper doped fibers converted to HA, but at a slower rate than the un-doped glass. The addition of copper and strontium to the glass significantly decreased the PO_4^{3-} peak intensities associated with HA as determined by micro-raman measurements, but still had broad peaks for HA according to XRD. The addition of zinc to the copper and strontium caused the formation of calcium carbonate in the form of calcite at the middle of the reacted fibers. Iron added to the

fibers doped with copper, strontium, and zinc further decreased the amount of HA formed in the fiber and increased the size of the calcite core in the reacted fibers. This is believed the first instance where calcium containing bioactive glasses transformed *in-vivo* into materials (calcite) other than HA.

5.2. INTRODUCTION

Bioactive glasses such as 45S5 (Table 1) have been known to bond to hard and soft tissues for more then four decades [1, 2] and have been used in clinical applications for periodontal repair [3], repair of bones in the inner ear [4], and fillers for bone cement [5, 6]. Bioactive glasses convert to the mineral known as hydroxyapatite (HA), whose stoichiometric composition is $Ca_{10}(PO_4)_6(OH)_2$, when in contact with body fluids. Carbonated hydroxyapatite (HCA), whose composition is $Ca_{10}(PO_4,CO_3)_6(OH)_2$, is the same mineral that is present in the inorganic part of bone, and bone will strongly bond to synthetic HA or HCA. Three dimensional porous scaffolds composed of bioactive glasses have recently been under investigation by several researchers to repair large bone defects [7-11]. Silicate based bioactive glasses, however, have been shown to react relatively slowly *in-vivo*, requiring several months to fully react [12].

Typically, calcium containing borate glasses submerged in phosphate solutions convert to HA in a manner similar to silicate based bioactive glasses [13-15]. An *in-vitro* study of the reaction rate of a bioactive silicate 45S5 glass, two borosilicate glasses, and a bioactive borate glass, showed they all converted to HA, but at different rates [13, 16].

Richard et al implanted particles (300 to 355μm) of a 45S5 borate analog (complete exchange of boron for silica) in rat femurs and the glass converted to HA at a

significantly higher rate and bone grew around and attached to the glass particles [17]. Jai et al [18] made pellets of borate glass particles (<50μm) mixed with teicoplanin (4 and 8wt%) for the purpose of treating the bone disease osteomyelitis. The bioactive borate glass converted to HA *in-vivo* and supported the growth of new bone.

A bioactive borate glass, designated 13-93B3 in Table 1, was used to construct porous scaffolds composed of randomly oriented fibers which were placed in the subcutaneous tissue of laboratory rats [19]. After four weeks, the 13-93B3 fibers had fully reacted to form porous tubes composed of HCA which were filled with soft tissue and blood vessels [19].

In the present work, four of the most abundant minor elements found in human cadaver bone that have positive effects on bone formation were systematically added to the 13-93B3 glass for subcutaneous implantation for the purpose of determining their effect on the formation of HA *in-vivo*. The concentration of the minor elements selected were chosen from the amount of copper found to have a stimulatory effect on blood vessel formation from previous work [20] and the relative abundance of trace elements in human cadaver bone [21]. The elements were added to the 13-93B3 glass in the order, copper (C), copper + strontium (CS), copper + strontium+ zinc (CSZ), and copper + strontium + zinc + iron (CSZF). After six weeks, the scaffolds were removed from the subcutaneous tissue of Fisher 344 rats and evaluated by XRD, SEMBSE and SEMEDS, and XRF.

5.3 MATERIALS AND METHODS

5.3.1 Glass Melting and Scaffold Preparation

Bioactive borate glasses, whose compositions are given in Table 1, were made from reagent grade chemicals and melted in a platinum crucible. The melts were heated to 1065^{o}C for one hour in a furnace. Fibers of each glass, with a diameter ranging from 100 to 300µm, were hand pulled from the melt. The un-annealed fibers were broken into 2 to 3mm lengths which were used to prepare porous scaffolds composed of randomly oriented fibers.

Approximately 70mg of fiber (Fig 1A) was placed in a cylindrical ceramic (mullite) mold (Fig 1B) with an internal diameter of 7mm. The mold was placed in an oven preheated to 575^{o}C for 45 minutes, after which the mold was removed and cooled to room temperature. Once cool, the scaffold was removed from the mold and was ready for sterilization.

An example of an as-made 13-93B3 and Cu-3 scaffold are shown in Figs. 1C and 1D, respectively. The scaffolds had nominal dimensions of 7mm in diameter and 2mm thick. The doped scaffolds such as Cu-3 are blue due to the addition of CuO to the glass. The three dimensional scaffold composed of randomly oriented and self bonded fibers had an open, interconnected porosity of 50±2% [22].

Prior to implantation the scaffolds were dry heat sterilized. The scaffolds were placed in a silica glass vial, covered with a loose fitting aluminum foil top, heated in an oven to 300^{o}C for four hours, and cooled to room temperature. Once cool, the scaffolds were ready for implantation.

5.3.2 Scaffold Implantation

Each type of bioactive borate scaffold (five types total) was implanted in subcutaneous tissue of Fisher 344 rats, n=5, for either four or six weeks. The scaffolds were implanted randomly to remove any bias from a single rat. A schematic of the implant sites is shown in Fig 2. Each rat had four implant sites, two above the shoulders and two above the back legs, where a single scaffold was implanted in each site, for a total of four scaffolds per rat. The back of each rat was shaved with clippers and washed with iodine and then 70% ethanol to disinfect the skin prior to surgical work. During the surgery, the rats were anesthetized with isoflourine.

An incision 20mm in length was made through the cutaneous tissue perpendicular to the spine with a pair of surgical scissors. The cutaneous tissue was separated from the skeletal muscle by inserting a clamp and gently opening it to make an opening ~20 mm long. A scaffold was inserted at the back of the cutaneous opening of the skin and closed with super glue. Once all four scaffolds were implanted; the rat was injected with 0.2ml of penicillin (0.1ml per hind leg) prior to complete recovery. The rats had free access to food pellets and tap water and were on a light schedule of 12 hours light, 12 hours dark.

5.3.3 Scaffold Removal

After either four or six weeks, the rats were sacrificed by CO_2 inhalation and the scaffolds were removed for analysis. The scaffolds were placed in 5ml of 10% formalin solution for four days to fix the tissue.

5.3.4 Scaffold Processing

Once the scaffolds were fixed, they were dehydrated with ethanol solutions by a microwave dehydration technique [23]. A microwave tissue processor (EBSciences

H2850 Microwave Processor) was set to 70% power, the sample temperature was set to 37±4^{o}C, and microwave was on for 2.5 minutes for each solution. Each scaffold was in each ethanol solution for at least 15 minutes.

The recovered scaffolds were embedded in poly methyl methacrylate (PMMA) by first submerging them in methyl methacrylate (MMA) monomer for 24 hours which was stirred with a magnetic stir bar. Next, the scaffolds were infiltrated with MMA containing 50% of the polymerizing agent Perkodox 15 for 24 hours. The final infiltration with MMA containing all of the required polymerizer, and was stirred for four hours. The scaffolds were removed from the MMA, placed on a pre-polymerized bed of PMMA, and covered with the final solution of MMA. The MMA was polymerized at low temperature, ~4^{o}C until solid.

An unreacted as-made scaffold composed of randomly oriented fibers was embedded in PMMA for use as a reference for the fibers present in the cross sectioned histology sections. The PMMA embedded scaffold was sectioned with a slow speed saw with a diamond coated blade and polished with silicon carbide paper from 320 to 1200 grit. The fibers appear round or ellipsoidal depending on the fiber orientation.

5.3.5 X-Ray Diffraction (XRD)

X-ray diffraction patterns of the recovered scaffolds after four or six weeks *in-vivo* were obtained with a PANalytical X'Pert Multipurpose diffractometer. Cu Kα radiation (0.15418 nm) was used with a counting time of 150 seconds and a step size of 0.0263 degrees. The scaffolds were placed in the diffractometer after dehydration and x-rayed in their as-recovered form rather than being ground to a powder.

5.3.6 Scanning Electron Microscopy Analysis (SEM)

An environmental scanning electron microscope (ESEM) (FEI, Hillsboro, OR) was used for SEM imaging of cross sectioned scaffolds. The 13-93B3 scaffold implanted for four weeks was not embedded with polymer or wax but was instead sectioned with a razor blade. Each scaffold doped with the selected metal ions was embedded with PMMA and sectioned in half with a slow speed diamond saw. The surface examined by SEM was polished with silicon carbide polishing paper to 1200 grit, and coated with ~100nm of Au/Pd to SEM analysis. Backscattered SEM, SEMBSE, energy dispersive spectroscopy (EDS), and SEM phase mapping were used to the characterize the scaffolds.

5.3.7 Micro-Raman Analysis

Micro Raman spectroscopy was used to analyze fibers that had been *in-vivo* for six weeks, LabRAM ARAMIS (Horiba Jobin Yvon). A 50x objective was used to view the fibers and the LABSpec5 software was used to capture the image and analyze the spectra. A diode laser (785nm) was used with and the collection time was five seconds.

5.3.8 X-ray Fluorescence (XRF)

X-ray fluorescence spectra of as-made glass and scaffolds implanted for six weeks were obtained with a SPECTRO XEPOS XRF (Spectro Analytical Instruments, Germany). The scaffolds were ground to a fine powder and pressed into a 30mm tablet. Spectra were collected for 300 seconds from 6.0 to 10.5 E/kV using a molybdenum target at 40kV and 0.88mA. Spectra between 13.0 and 17.0 E/kV were collected using an aluminum target at 49.5kV, 0.70mA for 300 seconds. The XRF software used for peak analysis was X-LAB Pro software.

5.4 RESULTS

5.4.1 Sectioned As-Made Scaffold Composed of Randomly Oriented Fibers for SEM Reference

A scaffold composed of randomly oriented glass fibers embedded in PMMA is shown in Fig 3. The fibers are dark gray and the PMMA is light gray. Depending on the fiber orientation, the fibers are circular (longitudinal axis perpendicular to the plane of the image) or ellipsoidal (not perpendicular to the plane of the image) shapes. During the heat treatment at 575^{o}C the glass fibers, soften and fuse (bond) together forming a three dimensional scaffold of self bonded randomly oriented fibers. This is evident from Fig 3 as there are several instances where multiple fibers have bonded. The light gray area between the fibers is the interconnected open porosity. This cross section of an unreacted as-made scaffold serves as a guide for the changes that occurred to both the glass fibers and the interconnected pore space during the *in-vivo* experiment.

5.4.2 Evaluation of Scaffolds As Recovered from Subcutaneous Tissue

None of the rats died during four or six week experiments, nor did any exhibit signs of sickness or infection. The images in Fig 4 show the appearance of each scaffold type while it was still attached to the subcutaneous tissue. Several blood vessels are visible in the tissue adjacent to each scaffold. The scaffolds containing the copper were blue prior to implantation (Fig 1D), so the darker color of the reacted scaffolds could be due to some un-reacted glass or an increase in the number of blood vessels. Most of the scaffolds had what appeared to be red or pink tissue inside the scaffold indicating that blood vessels had grown inside the open pores.

5.4.3 X-ray Diffraction (XRD)

The XRD patterns obtained from the scaffolds implanted in rat subcutaneous tissue for four to six weeks are shown in Fig 5. The patterns for the 13-93B3, Cu-3 and CS scaffolds contained identifiable peaks for HA (powder diffraction file (PDF) 72-1243), but, the peaks were broad and diffuse, most likely due to the nanocrystalline HA [19]. The HA peak heights decreased in the Cu-3 and CS scaffold patterns. The CSZ scaffold had broad peaks attributed to HA and much smaller peaks associated with calcium carbonate in the form of calcite (pdf card 05-0586). The XRD pattern for the CSZF scaffold contained stronger peaks for calcite only, and no peaks for HA were detectable. A second CSZ and CSZF scaffolds was x-rayed and the presence of calcite was confirmed in both scaffolds (patterns not shown).

5.4.4 Microstructure Analysis of Reacted 13-93B3 Fibers (Four weeks *In-Vivo*)

An SEMBSE image in Fig 6 shows the cross section of a 13-93B3 scaffold after four weeks *in-vivo*. The soft tissue that had grown into the scaffold is dark gray, while the reacted fibers are a lighter gray. Several of the reacted fibers were broken into smaller pieces during the sectioning procedure; but many of the fibers remained intact.

The center portion of a fully reacted 13-93B3 fiber is shown in Fig 7. The image in Fig 7A shows the inside surface of the exposed end of a reacted fiber. The center of the fiber has a relatively rough surface and no original glass is detectable. Figure 7B is a magnified view of the interior surface of the hollow fiber where nodules can be seen covering the inside surface of what is believed to be HA (from XRD pattern in Fig 5). The magnified view of the nodules in Fig 7C, shows that the nodules are composed of a porous network of nanocrystals, which are magnified in Fig 7D. The needle-like

structure of the crystals is consistent with that of HA. The crystals are ~50nm in length, and the microstructure of the crystals is highly porous.

Figure 8 shows another area of the cross section of a reacted 13-93B3 scaffold. Many of these fibers have a hollow core as was found for the fibers in Fig 7. The two fibers in the box in Fig 8, marked with arrows, were magnified to examine their cross sections in more detail. The reacted fiber in Fig 9A, overall diameter of ~170µm, is surrounded by soft tissue (dark material) and has a layered structure that is especially prevalent close to the center. The magnified view of the layered structure in Fig 9B shows ~50 layers in the ~40µm of fiber perpendicular to the hollow center. Ten to twelve layers are magnified in Fig 9C, and it is apparent that the layers are composed of a nanocrystalline material. The box in Fig 9C is magnified in Fig 9D, and the individual layers, ~500nm thick) have a system of struts ~20nm in diameter (arrows) that are oriented perpendicular to the layers that connect the entire nanostructure.

A magnified view of the smaller fiber (~100µm) in the box in Fig 8 shown in Fig 10 reveals a layered microstructure that is different from that of the fiber in Fig 9. The layers are thicker and fewer are present. As shown in the magnified view in Fig 11A, the layers are ~1µm thick and the distance between is ~1µm. Each layer is connected by a series of struts (~1µm thick) oriented perpendicular to the layer orientation as indicated by the arrow in Fig 11A. A single layer is magnified in Fig 11B and the crystals look similar to those seen in the reacted fiber in Fig 7D.

5.4.5 Chemical Analysis of Reacted Scaffolds (Four or Six Weeks *In-Vivo*)

The cross section of reacted scaffolds shown in Fig 12 is the backscattered SEM micrograph of the Cu-3 scaffold after six weeks in subcutaneous tissue. The fibers are

significantly reacted and many appear partially hollow at the center. The ellipsoidal fibers in the image are due to the random orientation of the fibers.

The fibers composing the CS scaffold in Fig 13 had reacted significantly after six weeks. Some of the fibers in the bottom left corner of the image in Fig 13, (white arrows) had a reacted surface that surrounded unreacted glass (gray center), but the majority of the fibers were fully reacted. Most of the CS fibers had voids at their center similar to the Cu-3 fibers in Fig 8.

A randomly selected fiber located at the outer edge of the CS scaffold is magnified in Fig 14. The fiber has reacted with body fluids and has a relatively dense outer surface, but a less dense center where a layered structure similar to an onion skin or spider web is visible. The three spots (numbered) in Fig 14 were analyzed by SEM EDS. Calcium and phosphorus were formed at each spot and the calcium to phosphorus (Ca/P) ratio for spot 1, 2 and 3 is 1.86, 2.00, and 1.71, respectively (Fig 14). These Ca/P ratios are reasonably close to that for stoichiometric HA (1.67).

The backscattered SEM image in Fig 15 shows a CSZ scaffold after six weeks *in-vivo*. The outer edge of the scaffold is on the right side of the image, and the center of the scaffold is located toward the lower left. The CSZ fibers at the outer edge of the scaffold are significantly reacted as there is no detectable glass remaining, but they did not form partially hollow fibers as did the Cu-3 and the CS fibers. There is a distinct white material located at the center of many of the CSZ fibers. The CSZ fibers toward the center of the scaffold (lower left of Fig 15) are not fully reacted, consist of a reacted surface layer surrounding a solid glass core (black arrows).

One of the partially reacted CSZ fibers with three distinctly different regions was chosen (see box in Fig 15) for further analysis (Fig 16). The outer surface of the fiber is solid (light gray), then there is a relatively thick region that is more porous and has some layers present (darker gray and layered). The center of the fiber contains a white material. The Ca/P ratios for the spots 1, 2, 3, and 4 were 27, 2.67, 3.00, and 1.56, respectively (Fig 16). Spot 4 was the only spot where the Ca/P ratio (1.56) was similar to that for HA (1.67).

The CSZF fibers shown in Fig 17 were all significantly reacted since the fibers contained a white material at their center similar to the CSZ fibers. There appears to be more of the white material in the CSZF fibers, Fig 17, than in the CSZ fibers, Fig 15. The fiber in the box in Fig 17 was arbitrarily selected for further analysis and a EDS phase map for calcium, phosphorus, potassium, magnesium, and strontium is shown in Fig 18. Calcium is present in a thin layer on the outer surface of the fiber, but the strongest calcium signal is at the center of the fiber. The phosphorus map shows a similar strong ring close to the outer edge of the fiber, but decreases toward the center, which contains noticeably less phosphorus.

The elements mapped were magnesium, potassium, and strontium, but none of these elements were present in detectable amounts. The CSZF fibers only contained 2wt% SrO, so the strontium concentration may have been too low to detect. However, the absence of the much larger amounts of sodium, potassium, and magnesium in the CSZF fibers is attributed to their being leached from the fibers while *in-vivo*.

The fiber in the box in Fig 17 was analyzed by EDS at four spots. The Ca/P ratios for spots 1, 2, 3, and 4 were 29, 1.60, 1.40, and 1.28, respectively. Spot 2 was in the

range of Ca/P ratio for HA found in the body (~1.5 to 1.7), but spots 1 was mostly calcium, and spots 3 and 4 were similar to the Ca/P ratio for octacalcium phosphate (OCP), $Ca_8H_2(PO_4)_6$-5(H_2O), which is 1.33.

5.4.6 Micro-Raman of *In-Vivo* Reacted Fibers

A 13-93B3 fiber that had been reacted four weeks *in-vivo* was analyzed at four points by micro raman across the cross section of the fiber diameter as shown in Fig 20. A dashed line has been added to outline the perimeter of the fiber to guide the reader. The micro-raman spectra for the four spots are shown in Fig 21. Spot 1 is at the outer edge of the fiber and spot 4 is at the center of the reacted fiber. Since the scaffold was mounted in PMMA, many of the peaks, denoted by the solid vertical lines, are from PMMA [24], but peaks reported for HA were also present [25]. The peaks associated with HA (431cm^{-1} (PO_4^{3-} v2), 965cm^{-1} (PO_4^{3-} v1), 1065 to 1070cm^{-1} (CO_3^{2-} v1) and 1076cm^{-1} PO_4^{3-} v3) [24] are denoted by dashed lines.

Spots 3 and 4 located near the center of the reacted 13-93B3 fiber in Fig 20 have the highest intensity for the phosphate and carbonate peaks of the four spots analyzed. Spot 1 was intended to measure the edge of the fiber, but the measured spot may have been partially off the fiber (on the PMMA) which would have decreased the intensity of the peaks associated with the fiber and magnified the intensity of the PMMA peaks. The presence of a carbonate peak at 1065 to 1070cm^{-1} (CO_3^{2-} v1) indicates that the fibers are carbonated, similar to the HA in natural bone.

The Cu-3 fiber (six weeks *in-vivo*) shown in Fig 22 was analyzed by micro-raman at seven spots across the fiber cross section. As shown by the spectra in Fig 23, the intensity of the HA peaks in spectra 1 to 5 are almost identical indicating no significant

change in the material from the outer edge to the center. The phosphate peaks in spectra 6 and 7 are noticeably smaller than the other peaks in spectra 1 to 5, which is likely due to the measurements being made in the partially hollow center of the fiber. There was also an increase in the intensity of the PMMA peak at 600cm^{-1} in spectra 6 and 7 further providing evidence that the beam was in contact with more of the PMMA than the fiber itself. The presence of CO_3^{2-} peaks in the spectra indicate that the HA is carbonated similar to natural bone.

As shown in Fig 24 the CS fiber was analyzed by micro-raman at five spots across the fiber. The spectra in Fig 25 may have low intensity peaks for HA located at 428cm^{-1} (PO_4^{3-} v2) and the broad peak at 1065-1080 which encompasses 1065 and 1070cm^{-1} (CO_3^{2-} v1), and 1076cm^{-1} (PO_4^{3-} v3), but the 965cm^{-1} (PO_4^{3-} v1) peak for HA was not present in any of the spectra.

The CSZ fiber was measured in ten spots as indicated in Fig 26 and the spectra are in Fig 27. Spectra 1 to 5 are from the outer edge to the interface between the porous calcium phosphate and the calcium rich center had no detectable peaks associated with HA present in the micro-raman spectra. Two new peaks are present in spectra 6 to 10, at 711cm^{-1} and 1085cm^{-1}. These peaks are associated with CO_3^{2-} in calcium carbonate in the form of calcite [26].

The CSZF fiber was analyzed at six spots by micro-raman (Fig 28) and the spectra are shown in Fig 29. Again, no peaks associated with HA were observed in the spectra. The peaks for calcite at 711cm^{-1} and 1085cm^{-1} were detected at the points inside the calcium rich center (spots 4 to 6).

5.4.7 X-ray Fluorescence (XRF) of Fibers After *In-Vivo* Reaction

The as-made glass fibers were analyzed with XRF to verify the presence of the minor elements (copper, strontium, zinc, and iron). The spectra for the four as-made glasses verify the presence of iron, copper, and zinc (Fig 30A) and strontium (Fig 30B). The amount of copper was almost identical for all four glasses as expected. Iron was only added to the CSZF glass, but it was detected in each glass due to impurities in the batch materials. The spectra for zinc in the CSZ and CSZF glasses overlap as shown in Fig 30A. The amount of strontium present in the three glasses it was added overlap in Fig 30B. The peak at 7.4E/kV, marked with an arrow, was due to the organic binder in which the samples were pressed.

The XRF spectra for the six week implanted scaffolds are shown in Figs 31A and 31B. Copper, strontium, zinc and iron were all detected in the scaffolds in which they were originally added after six weeks *in-vivo*. The Cu-3 scaffold, which contained small amounts of strontium, zinc, and iron as impurities (Fig 30), contained similar concentrations for each impurity after six weeks *in-vivo*. Copper was almost completely absent from the Cu-3 scaffold reacted *in-vivo* (Fig 31A), the copper concentration had decreased by over 90% of the original concentration (Fig 30A).

The as-made CS scaffolds contained low concentrations of zinc or iron as impurities in the as-made scaffolds as shown green lines in the XRF spectra in Fig 30. After six weeks *in-vivo*, the copper and strontium concentrations in the CS scaffold decreased by ~90% (blue lines in Fig 31) while the zinc and iron (impurities) remained similar to the original concentrations.

Prior to implantation, the as-made CSZ scaffolds contained a low concentration of iron as an impurity which did not change after the six weeks *in-vivo*. The concentration of copper and strontium decreased by 75%, and the zinc concentration decreased by only ~20% from the as-made scaffolds.

The as-made CSZF scaffold had nearly identical concentrations of copper, strontium, and zinc when compared to the as-made CSZ scaffold, but the iron concentration (red lines in Figs 30 and 31) was significantly higher than the impurity levels from the other three scaffolds (Fig 30). After six weeks *in-vivo*, the metal ion concentration in the CSZF scaffolds had decreased ~80% for copper, ~75% for strontium, and ~5% for zinc. The iron concentration was nearly the same in the as-made glass. The release of metal ions (copper, strontium, and zinc) from the CSZF and the CSZ scaffolds were similar in comparison.

5.5 DISCUSSION

5.5.1 Scaffold Evaluation and Tissue Analysis during Scaffold Removal

During the removal of the scaffolds from the rats, it was apparent that the mechanical strength had decreased. The originally rigid scaffolds were soft to the touch indicating that the fibers had reacted with the body fluids and became pliable. There were no signs of inflammation or infection at the implant site, or rejection of the scaffolds from the rats.

Previously, bioactive borate glasses have been studied *in-vitro* with osteoblasts for cell proliferation, and the number of cells decreased with increasing time [27]. The most toxic environment for the cells was observed in static *in-vitro* cultures. A dynamic culture of MC3T3-E1 osteoblast cells on disks of bioactive borate glass showed a much

milder effect on cell proliferation which is thought to be more similar to the *in-vivo* environment [27].

Experiments with bioactive borate glasses *in-vivo* have shown excellent integration of bone into defects filled with particles of bioactive borate glass [17, 18, 28, 29]. Scaffolds composed of the 13-93B3 glass fibers had significantly more bone ($p<0.05$) after 12 weeks in rat calvaria defects than scaffolds with the similar microstructure and interconnected porosity composed of 13-93 bioactive glass fibers (Table 1) [22, 30]. No necrotic tissue or increase in macrophages or other inflammatory cells was reported in the bone tissue encasing the reacted bioactive borate glass fibers [22, 30]. Systemic toxicity of the kidney and liver has also been studied by *in-vivo* by implantation of up to sixteen (70mg each) 13-93B3 fiber scaffolds in Sprague Dawley rats. No pathological changes were reported in the liver when compared to the control, and only incidental changes normal in adult rats were reported in the kidney [31].

The relatively high number of blood vessels present in the soft tissue surrounding the scaffolds upon removal after six weeks *in-vivo* (Fig 4) can be explained by the release of copper and zinc from the metal ion containing scaffolds. Jung et al. showed that scaffolds doped with copper and zinc significantly increased the number of blood vessels in tissue adjacent to bioactive borate glass fiber scaffolds implanted in the soft tissue of rats for six weeks [20].

5.5.2. Reaction of Metal Ion Doped Borate Scaffolds *In-Vivo*

This is believed to be the first time that bioactive glasses containing calcium have been found to convert to a material other than a calcium phosphate such as HA when reacted *in-vivo*. Conzone and White reacted rare earth containing borate glasses *in-vivo*

and formed rare earth phosphate materials, but those glasses contained no calcium [29, 32]. The XRD patterns of the reacted scaffolds in Fig 5 show a progressive change from HA to calcite as the strontium, zinc, and iron were added to the bioactive borate glass. The minor elements having the largest negative effect on the conversion of the glass to HA were zinc and iron. The first XRD peaks for calcite appeared with the addition of zinc in the CSZ scaffold. With the addition of 0.4wt% Fe_2O_3, there were no detectable peaks for HA in the XRD pattern for the CSZF scaffold, Fig 5. The only detectable crystalline material present was calcium carbonate (calcite).

Calcite is a polymorph of calcium carbonate that can be found in nature in both seashells and coral [33]. Degradable scaffolds composed of calcite have been shown to promote bone marrow induced osteogenesis better than a comparable hydroxyapatite scaffold [33]. Calcite has been reported to remodel at a faster rate than natural or synthetic HA [34] and tricalcium phosphate [35] through *in-vitro* osteoclast excavation experiments. Bone cement filled with calcite powder has also been made for biomedical use [36]. The presence of calcite in the reacted CSZ and CSZF fibers is therefore thought in general to be good for tissue engineering of bone and other tissues.

The copper addition to 13-93B3, Cu-3 glass, increased the time required to fully convert a scaffold of similar size and microstructure from four weeks to six weeks, but the micro-raman spectra for the Cu-3 glass showed carbonate and phosphate peaks indicative of HCA [25]. The increase in time required for the conversion of the glass may be explained by previous work by Madsen where copper was found to slow the formation of calcium phosphates *in-vitro* [37]. The addition of strontium to the CS glass completely eliminated the 965cm^{-1} (PO_4^{3-} v1) raman peak (Fig 28) indicating that the

formation of calcium phosphate was being inhibited. The addition of zinc eliminated the remaining phosphate peaks in the CSZ fiber. Instead of becoming partially hollow like the Cu-3 and CS fibers, the CSZ fibers formed a calcite center. This change in reaction may be explained by the strong inhibition zinc has on HA formation [38]. The CSZ glass contained copper which likely caused the decreased formation of calcium phosphate initially, and the addition of strontium and zinc further inhibited HA formation (Fig 5). The combination of these three elements (Cu, Sr, Zn) could also have enhanced the inhibition of HA formation due to multiple mechanisms of inhibition working together. The CSZF fibers contained more calcite present in their center than the CSZ fibers. This is likely due to the addition of a fourth known calcium phosphate inhibiting element Fe^{2+} and/or Fe^{3+} [38].

The formation of calcium carbonate at the center of the CSZ and CSZF fibers is not surprising if there are free calcium ions that are not bonded to phosphorus. There are carbonates in body fluids [39], and in aqueous solutions, calcium carbonate is sparingly soluble (6.6mg/L) in aqueous solutions like body fluids [40]. Hydroxyapatite has a solubility of ~5mg/L at pH = 7.3, and there are no other calcium compounds with a calcium solubility between HA and calcite [40].

The pH that is present in the fluids inside the reacted fibers is not known, but as with calcium phosphate crystallization, pH is a factor in the material formed (example, calcium carbonate) or the phase of the material (example, calcite, aragonite, or vaterite). Calcite and aragonite have the same reported aqueous solubility (6.6mg/L) [40] but calcite is the favored phase at pH 7.3. Vaterite has a solubility of 11mg/L [40], and therefore is a less preferable phase for precipitation than either calcite or aragonite.

The scaffolds that converted to a mixture of HA and calcite (CSZ and CSZF) retained most of the metal ions in either the soft tissue or the reacted fibers as determined by XRF. The EDS spectra for calcium rich portion of the CSZ and CSZF fibers (not shown) had small peaks for strontium. A solid solution of strontium calcium carbonate does exist, and has its highest intensity XRD peak is at 29.879 degrees 2θ (PDF card 84-0591) as opposed to 29.430 degrees 2θ for calcite (PDF card 05-0586). A slight shift in the XRD pattern of the CSZ and CSZF patterns would be difficult to interpret since the patterns were relatively low in intensity and the peaks were broad (Fig 5). Therefore, strontium may have been substituting in the calcium sites in the calcite structure and forming a solid solution.

The release of the elements into the surrounding soft tissue would be an important finding as the doped glasses could be used to promote healing of wounds by controlled ion release. Evidence that the ions were released from the glass and promoted a positive biological response in the surrounding tissue is shown by the vascular growth adjacent to and inside the minor element doped scaffolds (Fig 4).

5.5.3 Microstructure Analysis of Reacted Bioactive Borate Glass Fibers (Layered Microstructure)

After four weeks *in-vivo*, the 13-93B3 fibers were fully reacted and converted to a carbonated HA. The reaction of the fibers is interesting in that the microstructure of the calcium phosphate changes from forming a thick monolayer of HA to a multilayered structure. The thickness and periodicity in the layered structure also appear to be linked to the original fiber diameter. The larger the fiber diameter (~170μm) had about 50 layers (500nm thick) with a ~500nm periodicity (Fig 9). The smaller diameter fiber

(~100μm) had only about seven to eight layers with a layer thickness of ~1μm with a ~1μm distance between the layers (Fig 10).

The microstructure similar to those in Figs 8 to 11 and Fig 14 has been seen in reacted bioactive borate glasses *in-vivo* [17, 19, 29] and *in-vitro* [29, 41]. Conzone [29] suggested the formation of the layered structure could result from convection currents of fluids at the glass to dysprosium phosphate (DyP) layer interface. After ~ 3 to 5μm of layer formation, the glass core was hypothesized to detach from the DyP layer and start the layer forming process again.

A reaction similar to that reported by Conzone [29] occurred in the fiber shown in Fig 9, but the layer thickness was only ~500nm and there are struts connecting the layers which contradict the shell formation by convection current model. The layers in Fig 10 are also connected, but with larger struts than in Fig 9. The well defined thickness of the nanocrystalline layers and the almost fixed distance between the layers could be due to the deposit of an amorphous calcium phosphate gel that, in the process of crystallizing, shrinks in size while the next layer of calcium phosphate gel has already started forming. The formation of the struts could be due to epitaxial growth of crystals from the crystallized layer to the amorphous gel layer since the surface of the crystallized layer could promote crystal growth from its surface. The strut could also act as a seed crystal for the crystallization of the next layer.

The process of deposition and precipitation through a porous material should remain similar as the body fluids flow and could be an explanation for the layered microstructure. The difference in the layer thickness for different diameter fibers could be due to the differences in diffusion of phosphate from the body fluids through the fiber.

As the fiber diameter increases, thinner layers might be expected if the phosphate had to diffuse a longer distance. The smaller diameter fibers would have more phosphate available in a shorter distance, hence form fewer and thicker layers.

Both the Cu-3 and CS fibers reacted to form microstructures similar to 13-93B3 *in-vivo*. Evidence that a change had occurred in the reaction of the minor element doped glass fibers was first noticed in the microstructure of the CSZ fibers. The distinctly different material at the center of the fiber as shown by the SEMBSE image in Fig 15 and the diffuse calcium phosphate layers surrounding it was different from any reacted bioactive glass microstructure seen before.

The reacted CSZF fiber in Fig 32 had a similar structure to the CSZ fiber in Fig 15 in that it first formed a surface layer of calcium phosphate, but only about 2μm thick, and then began forming a highly porous and low density calcium phosphate that eventually changed to a porous layered structure. This porous layered structure is significantly different from the relatively thick mono layer at the surface of the 13-93B3 fiber (Fig 10). The layered structure started in the porous HA region of the fiber and continued into the calcium rich center. The thicknesses of the calcium rich layers in the CSZF fiber (Fig 35) were noticeably thicker than the calcium phosphate layers adjacent. The varied thickness of the layers could be due to differences in the precipitation of HA versus the calcite.

5.5.4 Reaction of Metal Ion Doped Bioactive Glasses

There is little published work in the area of bioactive glasses doped with metal ions. Glasses such as the well known 45S5 have been doped with up to 20wt% zinc [42] and after 30 days in simulated body fluid, two phases in separate calcium phosphate

layers were discovered, a normal HA layer, and a zinc containing calcium phosphate phase $CaZn_2(PO_4)_2$-$2H_2O$ [43]. Tape cast 45S5 bioactive glass soaked with a silver containing solution formed HA [44]. Pan et al found that adding strontium to borosilicate glass significantly reduced the cytotoxic effects of the glasses *in-vitro*, and the glasses converted to HA. Fluorine has been added to silicate based bioactive glass but HA was formed [45]. Boron has been added as a minor constituent (3wt%) to silicate based bioactive glasses [2], as a glass former in a borosilicate bioactive glass [13, 46], and as the major glass former in borate based bioactive glasses [13, 15, 19, 46], and all converted to HA.

5.5.5 Role of Metal Ions in Calcium Phosphate Formation

Madsen studied the influence foreign metal ions had on the conversion of brushite ($CaHPO_4$-$2H_2O$) to OCP and to HA. He found that several transition metal ions decrease the conversion rate or significantly poison the reaction [38]. Both Cu^{2+} and Zn^{2+} were found to be strong inhibitors to HA crystal growth. Sr^{2+}, Fe^{2+}, and Fe^{3+} were described as intermediate as opposed to strong, but nonetheless act as inhibitors during HA crystallization [38]. Bigi et al. found that Mg^{2+} and Sr^{2+} are important in determining what calcium phosphate phase is formed as pH varies in a simulated aqueous solution [47]. TenHuisen et al studied the effect Mg^{2+} on HA formation *in-vitro*, and found that concentrations of Mg^{2+} below 1mM had no effect on HA crystallization [48]. Concentrations of Mg^{2+} between 1mM and 2.5mM changed the shape of the HA crystals formed but not the kinetics, and concentrations greater than 2.5mM slowed the overall reaction kinetics [48]. Madsen found that Cu^{2+} ions initially inhibit calcium phosphate precipitation on a brushite substrate in dilute phosphate solution by surface adsorption

[37]. The Cu^{2+} coated surface layer eventually diffuses into the interior of the brushite crystal clearing the surface to nucleate and grow calcium phosphate [37].

Not all metal ions inhibit the growth of HA. Nickel and lead have been found to promote HA formation *in-vitro* [38]. The Ni^{2+} and Pb^{2+} ions can substitute for calcium ions in calcium phosphates and act as nucleating agents, however, Ni^{2+} ions have been reported to promote the growth of irregular crystals [38]. Chromium ions (Cr^{3+}) have been suggested as both a strong inhibitor [38] and a strong promoter [49] of calcium phosphate growth, but, the two experiments were completed at different pH values and chromium concentrations.

To better understand why certain ions inhibit or promote HA formation, the ionic radius of several ions (6 - coordinated) [50] were plotted against an arbitrary scale of 0 to 5 in Fig 33, where 0 represents no HA inhibition, and 5 represent severe HA inhibition as reported in the literature [38]. The inhibition of HA appears to trend with decreasing atomic radius as compared to the radius of calcium. This helps to explain why aluminum, which has a small radius (0.53 Å) has been reported as a poison to HA formation in bioactive glass [2], and why the CSZ and CSZF glasses from the present work, which have zinc (0.75Å) and iron (0.61Å for $Fe^{2+}$and 0.65Å for Fe^{3+}) stopped forming HA and formed another calcium compound, calcite.

5.6 CONCLUSIONS

Scaffolds composed of randomly oriented bioactive borate glass fibers, some doped with copper, strontium, zinc and iron were implanted in subcutaneous tissue of rats fully and reacted with body fluids for four to six weeks. Each rat remained healthy during the course of the experiment; there were no signs of sickness in the rats or

infection at the implant sites. The metal ions in the doped scaffolds were released to the surrounding tissues and/or incorporated into the calcium containing reaction products as the glasses reacted with body fluids.

For the first time, a calcium containing bioactive glass converted to a non-calcium phosphate when implanted *in-vivo*. Calcium carbonate in the form of calcite was deposited at the center of the CSZ and CSZF bioactive glass fibers. The calcite formation was likely due to inhibition of calcium to bond with phosphorus caused by the addition of the metal ions. The formation of calcite could be an improvement in scaffold resorption as osteoblasts can remodel calcite faster that HA into new bone.

Acknowledgements

The authors would like to thank Vernon Modglin for his assistance with the surgical procedures, Dr. Anne Maglia of MS&T for access to histological equipment, Dr. Vladimir Dusevich of UMKC for the ESEM analysis, and Tamara Weimer from Mo-Sci Corporation for the XRF analysis.

5.7 REFERENCES

[1]. Hench LL. The story of Bioglass. J. Mater. Sci.: Mater. Med. 2006;17(11):967-978.

[2]. Yamamuro T, Hench LL, Wilson J. Handbook of Bioactive Ceramics Vol. I - Bioactive Glasses and Glass-Ceramics. Boca Raton FL: CRC Press; 1990.

[3]. Froum SJ, Weinberg MA, Tarnow D. Comparison of bioactive glass synthetic bone graft particles and open debridement in the treatment of human periodontal defects. A clinical study. J. Perio. 1998;69:698-709.

[4]. Hench LL, Hench JW, Greenspan DC. Bioglass: A short history and bibliography. J. Aust. Cer. Soc. 2004;40:1-42.

[5]. Sanus GZ, Tanriverdi T, Kafadar AM, Ulu MO, Uzan M. Use of Cortoss for reconstruction of anterior cranial base: a preliminary clinical experience. Eur. J. Plastic Surg. 2005;27:371-377.

[6]. Larsson S. Cement Augmentation in Fracture Treatment. Scand. J. Surg. 2006;95:111-118.

[7]. Jung SB, Day DE, Brown RF. Comparison of self-bonded three dimensional bioactive glass fiber scaffolds after in-vivo implantation in rats. J. Am. Cer Soc. 2009, accepted.

[8]. Fu Q, Rahaman MN, Bal BS, Brown RF, Day DE. Mechanical and InVitro Performance of 13-93 Bioactive Glass Scaffolds Prepared By a Polymer Foam Replication Technique. Acta Biomaterialia 2008;4(6):257-293.

[9]. Chen QZ, Thompson ID, Boccaccini AR. 45S5 Bioglass-derived glass-ceramic scaffolds for bone tissue engineering. Biomaterials 2006;27(11):2414-2425.

[10]. Pirhonen E, Moimas L, Haapanen J. Porous Bioactive 3-D Glass Fiber Scaffolds for Tissue Engineering Applications Manufactured by Sintering Technique. Key Eng. Mater. 2003;240-242:237-240.

[11]. Rahaman MN, Day DE, Brown RF, Fu Q, Jung SB. Nanostructured Bioactive Glass Scaffolds for Bone Repair. 32nd Int. Conf. Adv. Cer. Comp. 2008.

[12]. Moimas L, Biasotto M, Lenarda RD, Olivo A, Schmid C. Rabbit pilot study on the resorbability of three-dimensional bioactive glass fibre scaffolds. Acta Biomaterialia 2006;2(2):191-199.

[13]. Huang W, Day DE, Kittiratanapiboon K, Rahaman MN. Kinetics and Mechanisms of the Conversion of Silicate (45S5), Borate, and Borosilicate Glasses to Hydroxyapatite in Dilute Phosphate Solution J. Mater. Sci.: Mater. Med. 2006;17:583-596.

[14]. Fears K. M.S. Thesis. Rolla, MO: University of Missouri-Rolla; 2001.

[15]. Fu Q. PhD Dissertation. Rolla, MO: Missouri University of Science and Technology; 2009.

[16]. Jung SB, Day DE. Conversion kinetics of silicate, borosilicate, and borate bioactive glasses to hydroxyapatite. Phy. Chem. Glass. 2009;50(2):85-88.

[17]. Richard M. M.S. Thesis. University of Missouri-Rolla; 2000.

[18]. Jai W-T, Zhang X, Luo S-H, Liu X, Huang W-H, Rahaman MN, Day DE, Zhang C-Q, Xie Z-P, Wang J-Q. Novel borate glass/chitosen composite as a delivery vehicle for teicoplanin in the treatment of chronic osteomyelitis. Acta Biomaterialia 2009.

[19]. Jung SB, PhD Dissertation, Chapter 1. Rolla, MO: Missouri University of Science and Technology; 2010.
[20]. Jung SB, PhD Dissertation, Chapter 2. Rolla, MO: Missouri University of Science and Technology; 2010.
[21]. Becker RO, Spadaro JA, Berg EW. The Trace Elements of Human Bone. J. Bone Joint Surg. 1968;50:326-334.
[22]. Jung SB, PhD Dissertation, Chapter 4. Rolla, MO: Missouri University of Science and Technology; 2010.
[23]. Laboux O, Dion N, Arana-Chavez V, Ste-Marie L-G, Nanci A. Microwave Irradiation of Ethanol-fixed Bone Improves Preservation, Reduces Processing Time, and Allows Both Light and Electron Microscopy on the Same Sample. J. Histochem. Cytochem. 2004;52(10):1267-1275.
[24]. Suzuki M, Kato H, Wakumoto S. Vibrational analysis by raman spectroscopy of the interface between dental adhesive resin and dentin. J. Dental Res. 1991;70:1092-1097.
[25]. Mul FFMd, Hottenhuis MHJ, Bouter P, Greve J, Arends J, Bosch JJt. Micro-raman line broadening in synthetic carbonated hydroxyapatite. J. Dent. Res. 1986;65:437-440.
[26]. Kontoyannis CG, Vagenas NV. Calcium carbonate phase analysis using XRD and FT-Raman spectroscopy. The Analyst 2000;125:251-255.
[27]. Brown RF, Rahaman MN, Dwilewicz AB, Huang W, Day DE, Li Y, Bal BS. Effect of borate glass composition on its conversion to hydroxyapatite and on the proliferation of MC3T3-E1 cells. J. Biomed. Mater. Res. 2008;88A:392-400.
[28]. Liu X, Xie Z, Zhang C, Pan H, Rahaman MN, Zhang X, Fu Q, Huang W. Bioactive borate glass scaffolds: in vitro and in vivo evaluation for use as a drug delivery system in the treatment of bone infection. J. Mater. Sci.: Mater. Med. 2009;online.
[29]. Conzone S. PhD Dissertation. Rolla, MO: University of Missouri-Rolla; 1999.
[30]. Bonewald L. Personal Communication. 2010.
[31]. Jung SB, PhD Dissertation, Chapter 2. Rolla, MO: Missouri University of Science and Technology; 2010.
[32]. White JE. PhD Dissertation. Rolla, MO: University of Missouri-Rolla; 1995.
[33]. Vuola J, Goransson H, Bohling T, Asko-Scljavaara S. Bone marrow induced osteogenesis in hydroxyapatite and calcium carbonate implants. Biomaterials 1996;17:1761-1766.
[34]. Redey SA, Razzouk S, Rey C, Bernache-Assollant D, Leroy G, Nardin M, Cournot G. Osteoclast adhesion and activity on synthetic hydroxyapatite, carbonated hydroxyapatite, and natural calcium carbonate: Relationship to surfaces energies. J. Biomed. Mater. Res. 1999;45:140-147.
[35]. Monchau F, Lefevre A, Descamps M, Belquin-myrdycz A, Laffargue P, Hildebrand HF. In Vitro studies of human and rat osteoclast activity on hydroxyapatite, Beta-tricalcium phosphate, calcium carbonate. Biomol. Eng. 2002;19:143-152.
[36]. Tas AC. Porous, biphasic $CaCO_3$-calcium phosphate biomedical cement scaffolds from calcite ($CaCO_3$) powder. Int. J. Appl. Cer. Tech. 2007;4:152-163.

[37]. Madsen HEL. Heterogeneous nucleation of calcium phosphates. II. Inhibition by cupric ions. Acta Chemica Scand. A 1975;29:277-281.
[38]. Madsen HEL. Influence of foreign metal ions on crystal growth and morphology of brushite ($CaHPO_4$, $2H_2O$) and its transformation to octacalcium phosphate and apatite. J. Cry. Growth 2008;310:2602-2612.
[39]. Muller L, Muller F. Preparation of SBF with Different HCO_3^- Content and Its Influence on the Composition of Biomimetic Apatites. Acta Biomaterialia 2006;2:181-189.
[40]. Lide DR, editor. CRC Handbook of Chemistry and Physics. 89 ed. Volume 8: Taylor and Francis Group LLC; 2009.
[41]. Pan HB, Zhao XL, Zhang X, Zhang KB, Li LC, Li Y, Lam WM, Lu WW, Wang DP, Huang WH and others. Strontium Borate Glass: Potential Biomaterial for Bone Regeneration. J. Royal Soc. Inter. 2009;online.
[42]. Aina V, Perardi A, Bergandi L, Malavasi G, Menabue L, Morterra C, Ghigo D. Cytotoxicity of Zinc-containing Bioactive Glasses in Contact with Human Osteoblasts. Chemico-Bio. Inter. 2007;167:207-218.
[43]. Linati L, Lusvardi G, Malavasi G, Menabue L, Menziani MC, Mustarelli P, Segre U. Qualitative and Quantitative Structure - Property Relationships Analysis of Multicomponent Potential Bioglasses. J. Phy. Chem. 2005;109B:4989-4998.
[44]. Clupper DC, Hench LL. Bioactive Response of Ag-doped Tape Cast Bioglass 45S5 Following Heat Treatment. J. Mater. Sci.: Mater. Med. 2001;12:917-921.
[45]. Fujiu T, Ogino M, Kariya M, Ichimura T. New explination for the bonding behaviour of fluorine containing bioglass. J. Non-Cryst. Solids 1983;56:417-422.
[46]. Huang W, Rahaman MN, Day DE, Li Y. Mechanisms for Converting Bioactive Silicate, Borate, and Borosilicate Glasses to Hydroxyapatite in Dilute Phosphate Solution. Phy. Chem.Glass. 2006;47B(6):1-12.
[47]. Bigi A, Marchetti F, Ripamonti A, Roveri N, Foresti E. Magnesium and strontium interaction with carbonate-containing hydroxyapatite in aqueous medium. J. Inorg. Biochem. 1981;15:317-327.
[48]. TenHuisen KS, Brown PW. Effects of magnesium on the formation of calcium deficient hydroxyapatite from $CaHPO_4$ - $2H_2O$ and $Ca_4(PO_4)_2O$. J. Biomed. Mater. Res. 1997;36:306-314.
[49]. Wakamura M, Kandori K, Ishikawa T. Influence of chromium(III) on the formation of calcium hydroxyapatite. Polyhedron 1997;16:2047-2053.
[50]. Shannon RD, Prewitt CT. Effective Ionic Radii in Oxides and Fluorides. Acta Crystallographica 1969;B25:925-946.

TABLES

Table 1 – Bioactive Glass Compositions (wt%)

Glass	B_2O_3	Na_2O	CaO	K_2O	MgO	SiO_2	P_2O_5	CuO	SrO	ZnO	Fe_2O_3
45S5	0	24.50	24.50	0	0	45.00	6.00	0	0	0	0
13-93	0	6.00	20.00	12.00	5.00	53.00	4.00	0	0	0	0
13-93B3	53.00	6.00	20.00	12.00	5.00	0	4.00	0	0	0	0
Cu-3	52.79	5.98	19.92	11.95	4.98	0	3.98	0.40	0	0	0
CS	51.73	5.86	19.52	11.71	4.88	0	3.90	0.40	2.00	0	0
CSZ	51.20	5.80	19.32	11.59	4.83	0	3.86	0.40	2.00	1.00	0
CSZF	50.88	5.76	19.20	11.52	4.80	0	3.84	0.40	2.00	1.00	0.40

FIGURES:

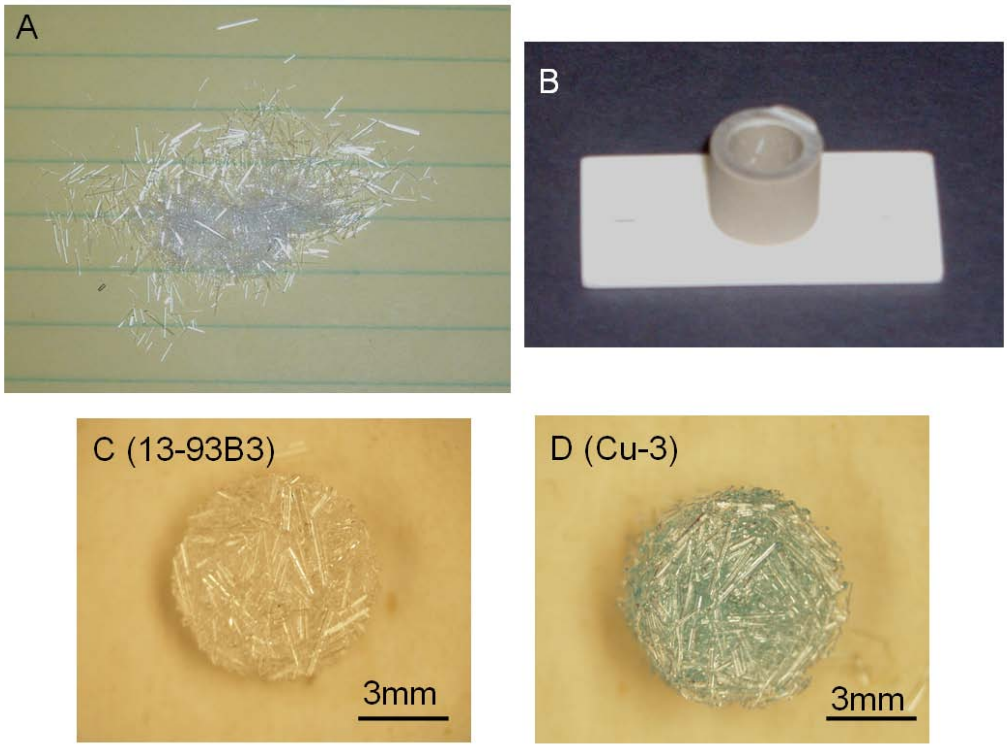

Figure 1 – Figure 1A shows some chopped fiber 2 to 3mm in length, 100 to 300µm in diameter, used for making scaffolds. Figure 1B shows a ceramic mold used to hold the fibers during the heat treatment. Figures 1C and 1D are examples of an as-made 13-93B3 and Cu-3 scaffolds that weighs 70mg and has dimensions of 7mm in diameter and 2mm thick. Scaffold porosity is 50±2%.

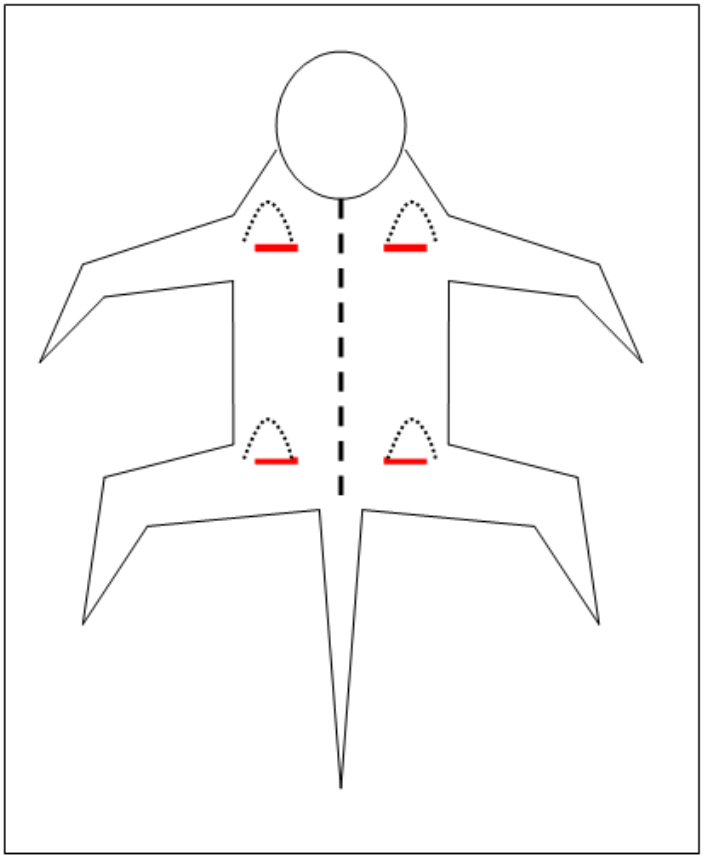

Figure 2 – Schematic showing the four subcutaneous scaffold implant sites located on the back of a rat. The dashed line represents the spine as a reference.

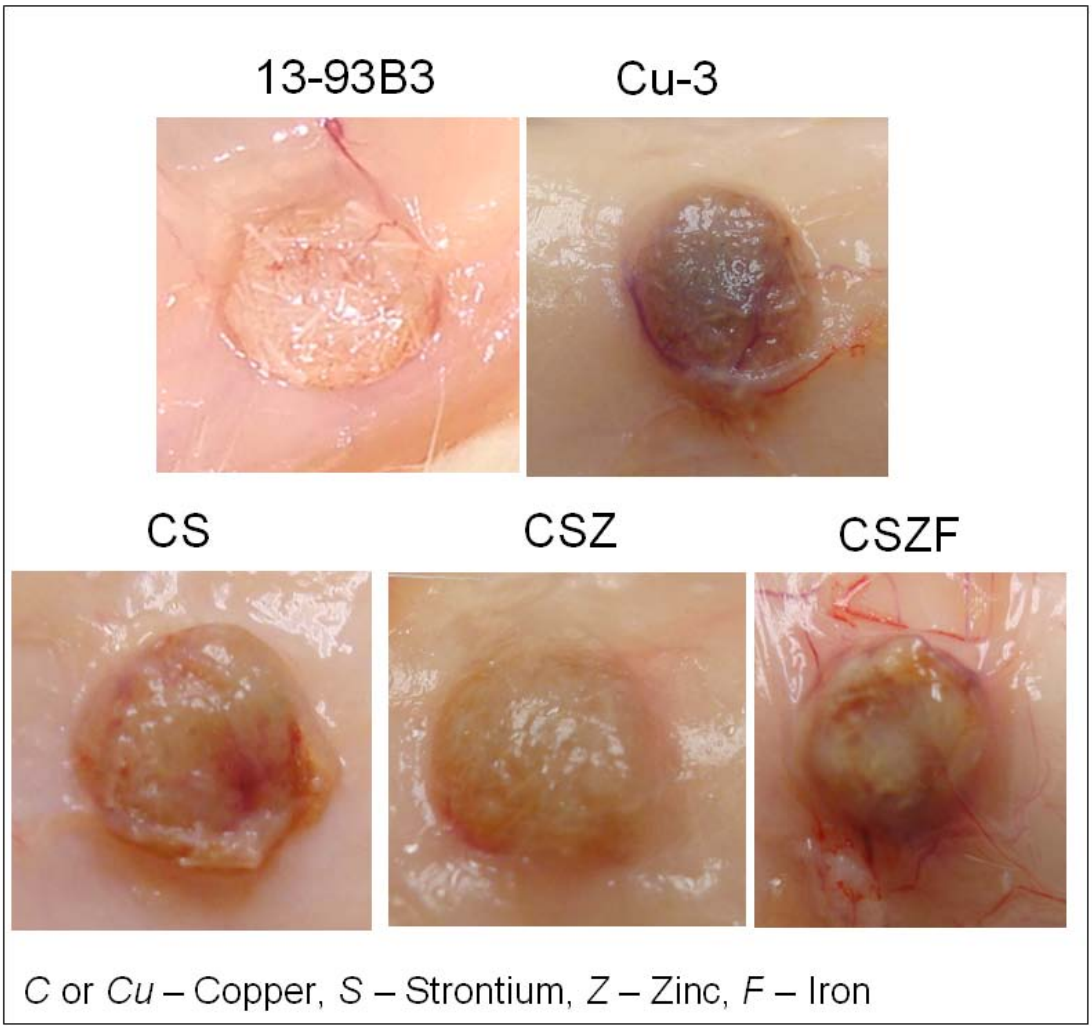

Figure 3 – Bioactive borate glass scaffolds doped with minor elements after implantation in rat subcutaneous tissue. The images show a representative scaffold after six weeks in subcutaneous tissue for the Cu-3, CS, CSZ, and CSZF scaffolds and a 13-93B3 scaffold after four weeks.

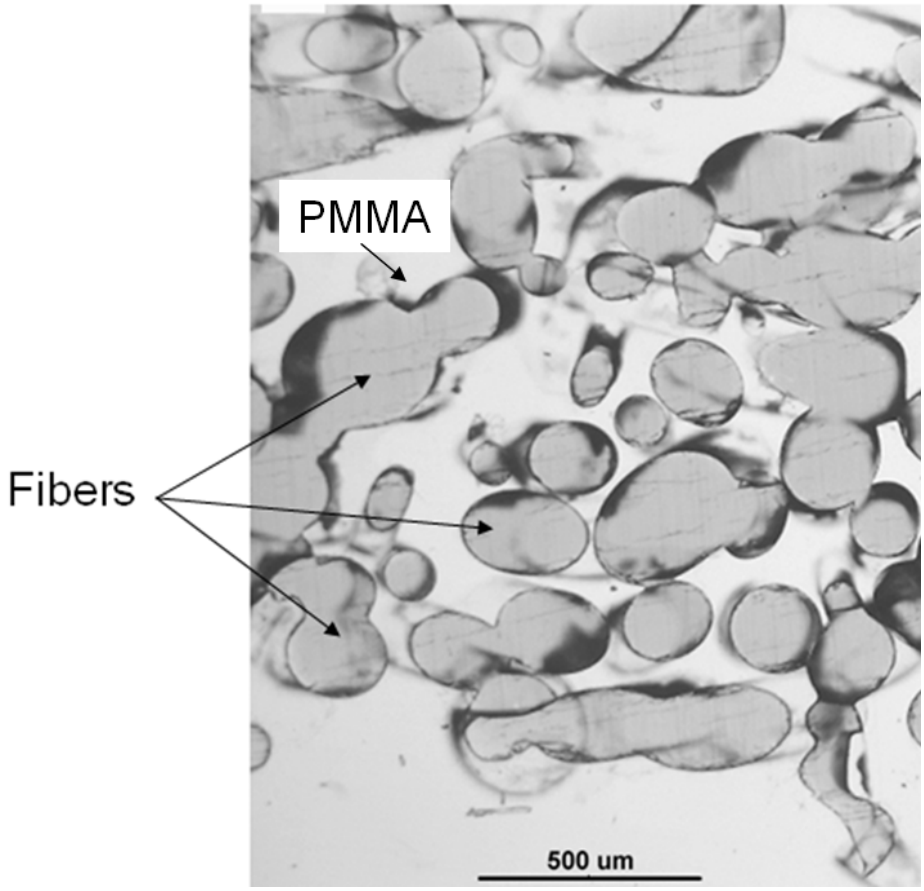

Figure 4 – Optical micrograph of a cross sectioned randomly oriented bioactive glass fiber scaffold. The fibers are gray and look like circular or elliptical depending on the fiber orientation. The scaffold was impregnated with PMMA as indicated to support the fibers during the sectioning and polishing.

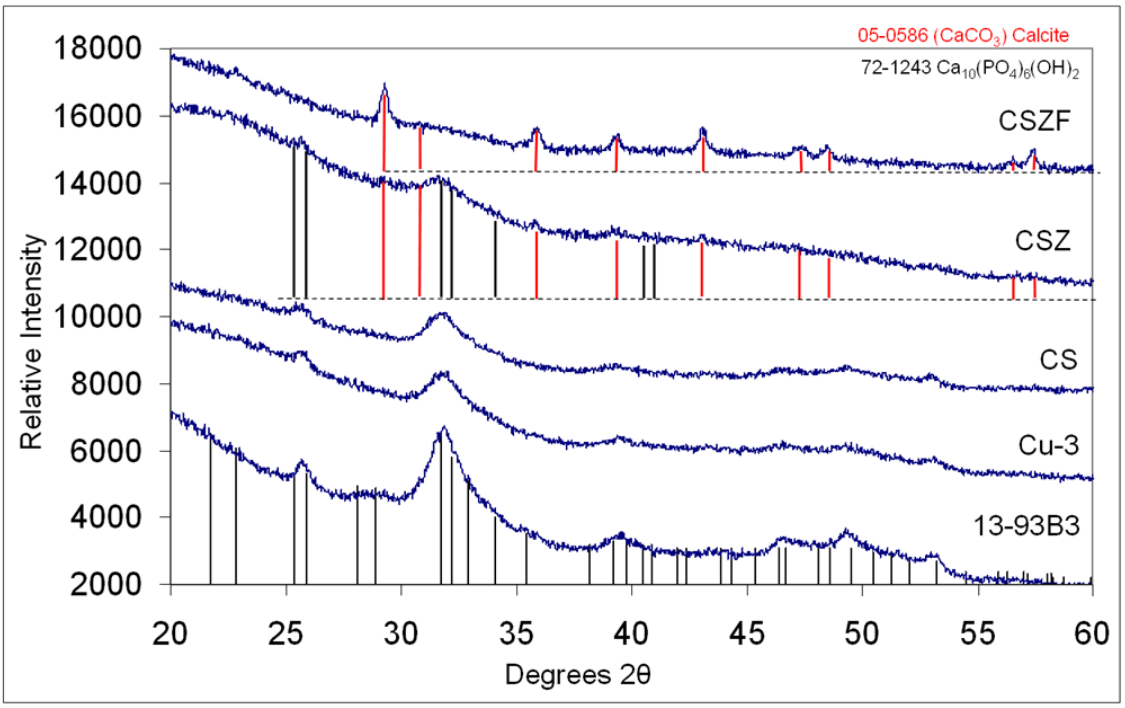

Figure 5 – XRD patterns for randomly oriented borate bioactive glass fiber scaffolds with added minor elements implanted in rat subcutaneous tissue for six weeks (13-93B3 was implanted four weeks). Scaffolds had an original mass of 70mg and were 7mm in diameter and 2mm thick. Cu or C = copper, S = strontium, Z = zinc, F = iron.

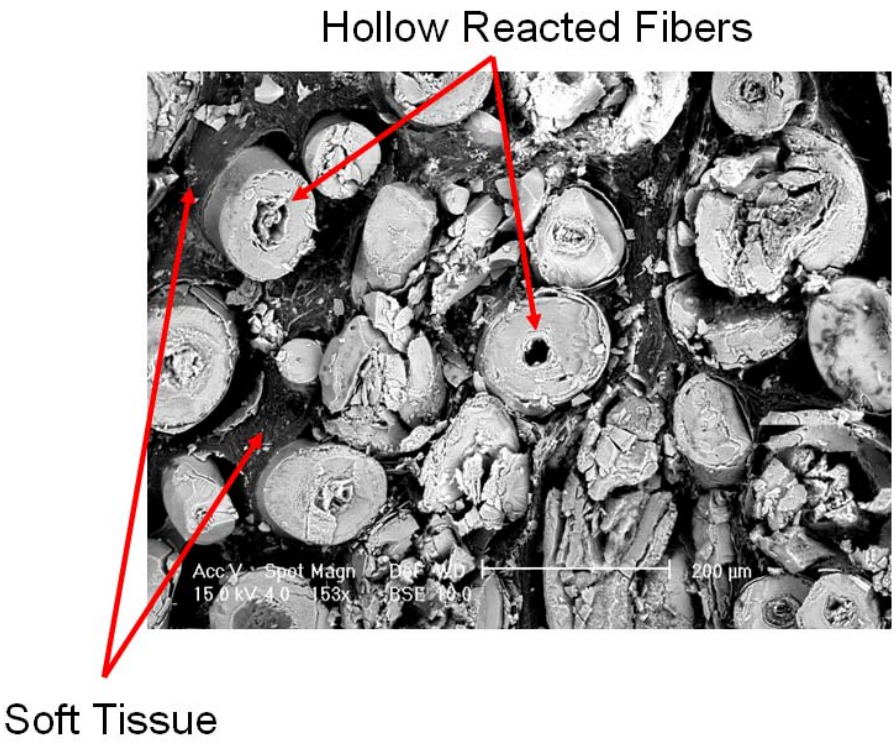

Figure 6 – SEMBSE micrograph of a cross sectioned 13-93B3 scaffold after four weeks in the subcutaneous tissue of a rat. The soft tissue (dark gray) is surrounding reacted fibers are light gray.

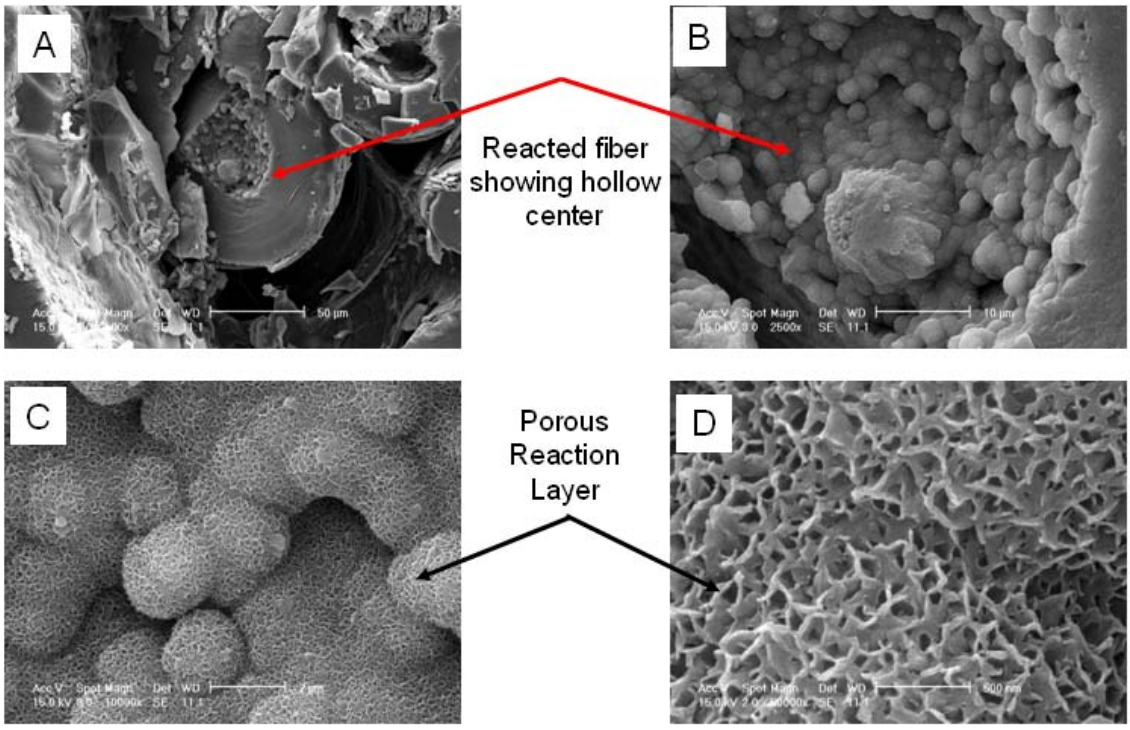

Figure 7 – High magnification SEM micrographs of reacted 13-93B3 fibers after four weeks in the subcutaneous tissue of a rat. Figure 7A of a sectioned fiber showing the hollow center and the wall of the reacted fiber. Figure 7B is a magnified view of the surface of the hollow reacted 13-93B3 fiber in Fig 7A. Figure 7C is a magnified view of the nodules in Fig 7B. Each nodule consists of a porous nanocrystalline structure as shown in Fig 7D. Figure 7D shows the surface of a porous nodule.

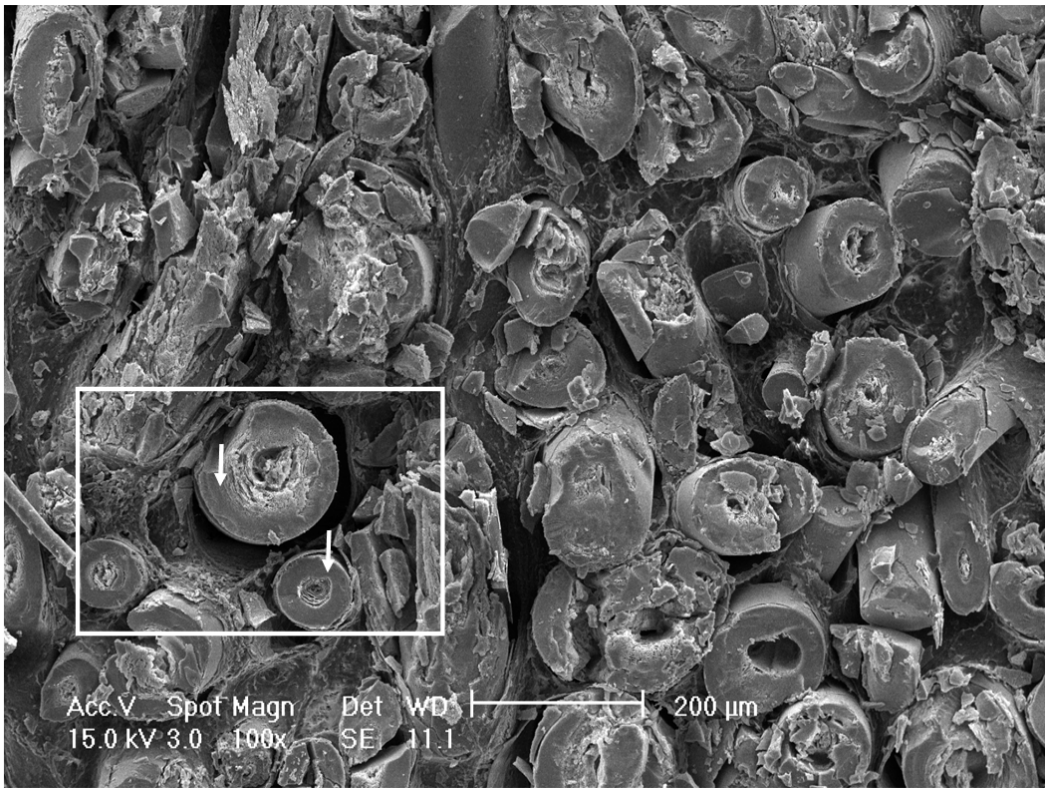

Figure 8 – SEM micrograph of a 13-93B3 scaffold cross section after four weeks *in-vivo*. The cross sections of two reacted fibers (arrows) are further analyzed in Figs 9 to 11.

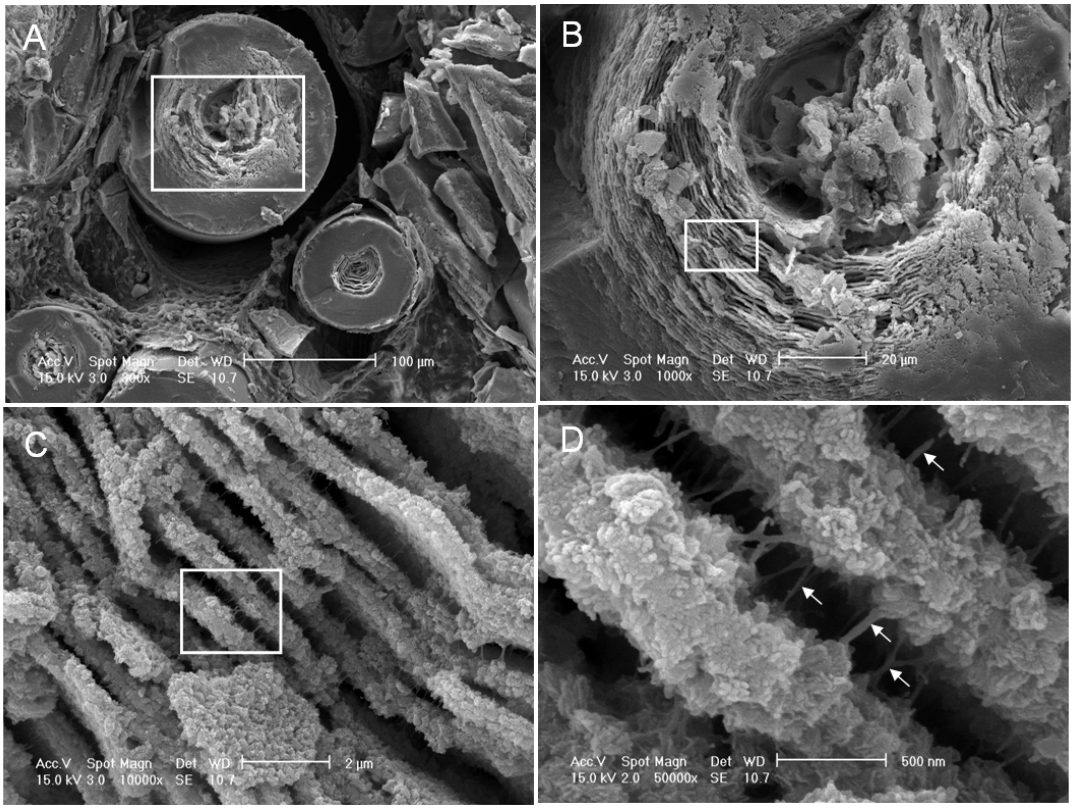

Figure 9 – SEM micrographs of a reacted 13-93B3 fiber in rat subcutaneous tissue for four weeks.

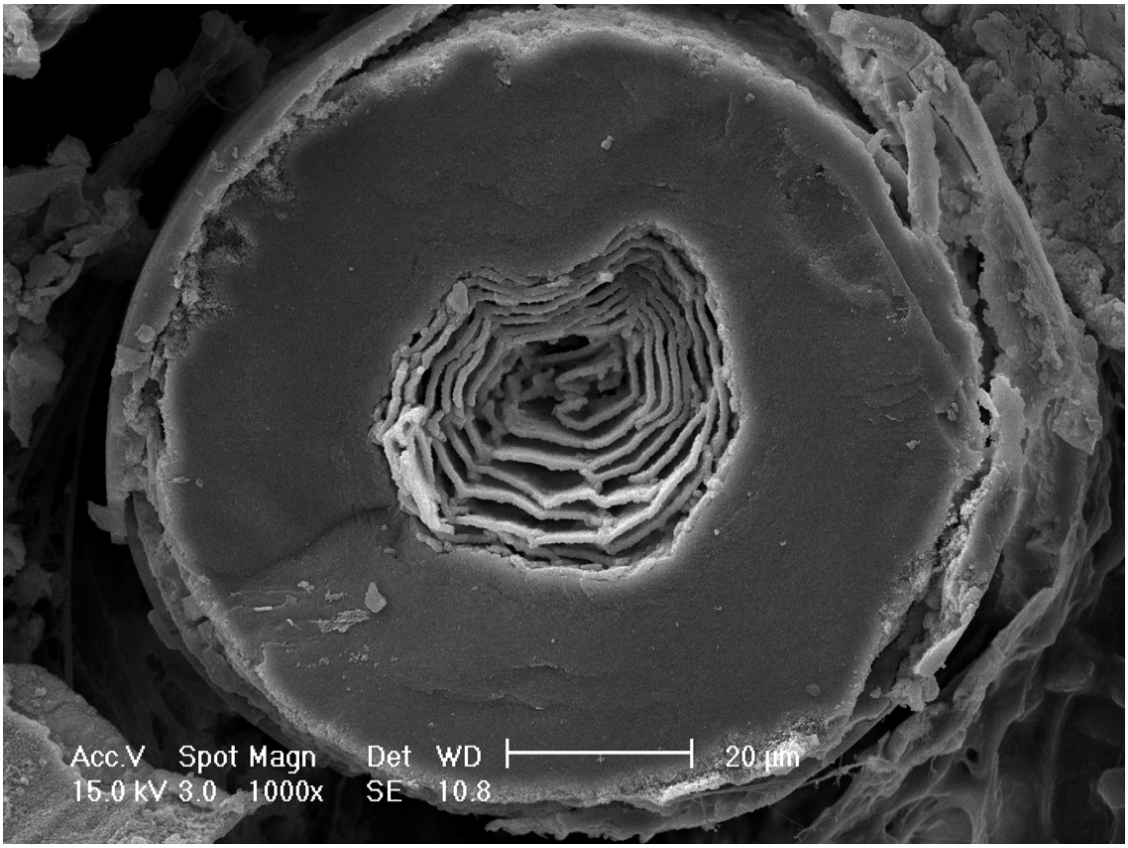

Figure 10 – Appearance of the cross section of the smaller reacted 13-93B3 fiber (four weeks *in-vivo*) in Fig 8.

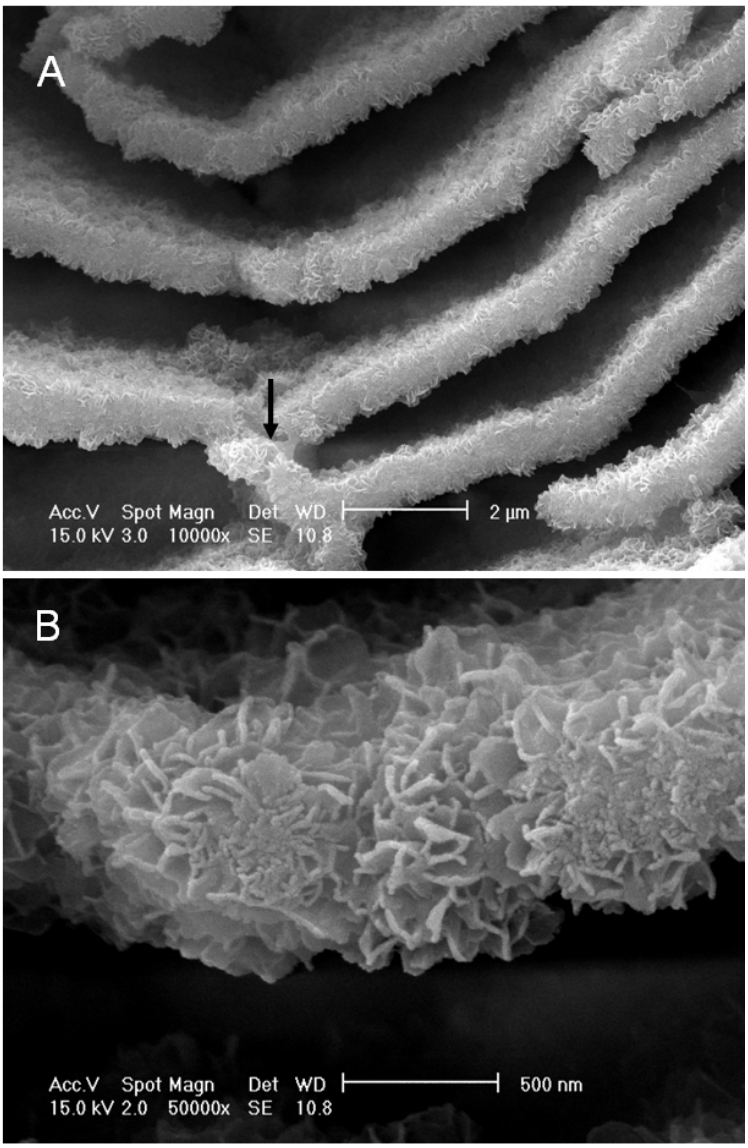

Figure 11 – SEM micrographs of the layered microstructure present at the center of the reacted 13-93B3 fiber in Fig 10. Figure 11A shows several layers, but here a thick strut (arrow) is present connecting the layers. The image in Fig 11B is of a single layer, and it is apparent that the layers are polycrystalline and composed of nanocrystals.

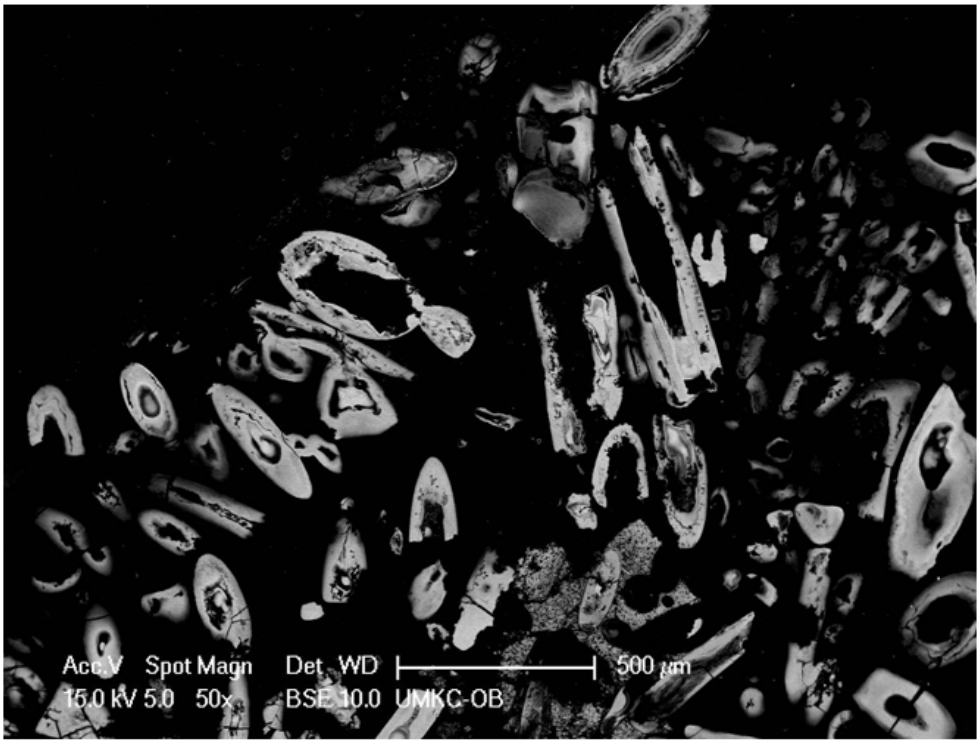

Figure 12 - SEMBSE image of a cross sectioned Cu-3 fiber scaffold that had been implanted in the subcutaneous tissue of a rat for six weeks.

Figure 13 - SEMBSE image of a cross sectioned CS fiber scaffold implanted subcutaneously in a rat for six weeks. A majority of the fibers are excavated (partially hollow) from reaction with body fluids.

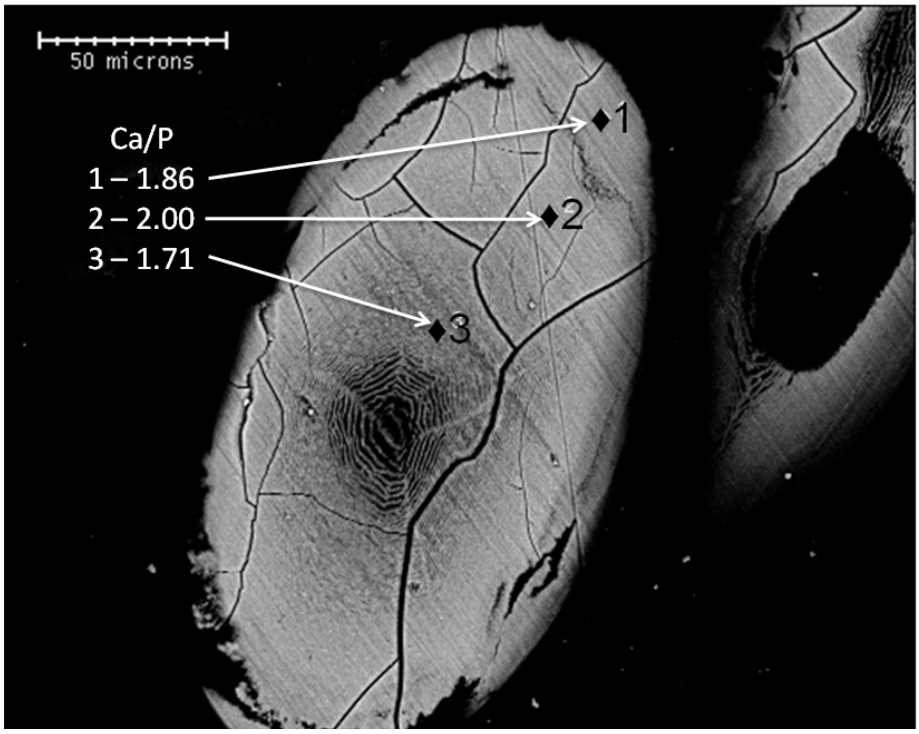

Figure 14 - SEMBSE image of a CS fiber implanted subcutaneously in the back of a rat for six weeks. The Ca/P ratio of the fiber at the three spots is shown in the figure.

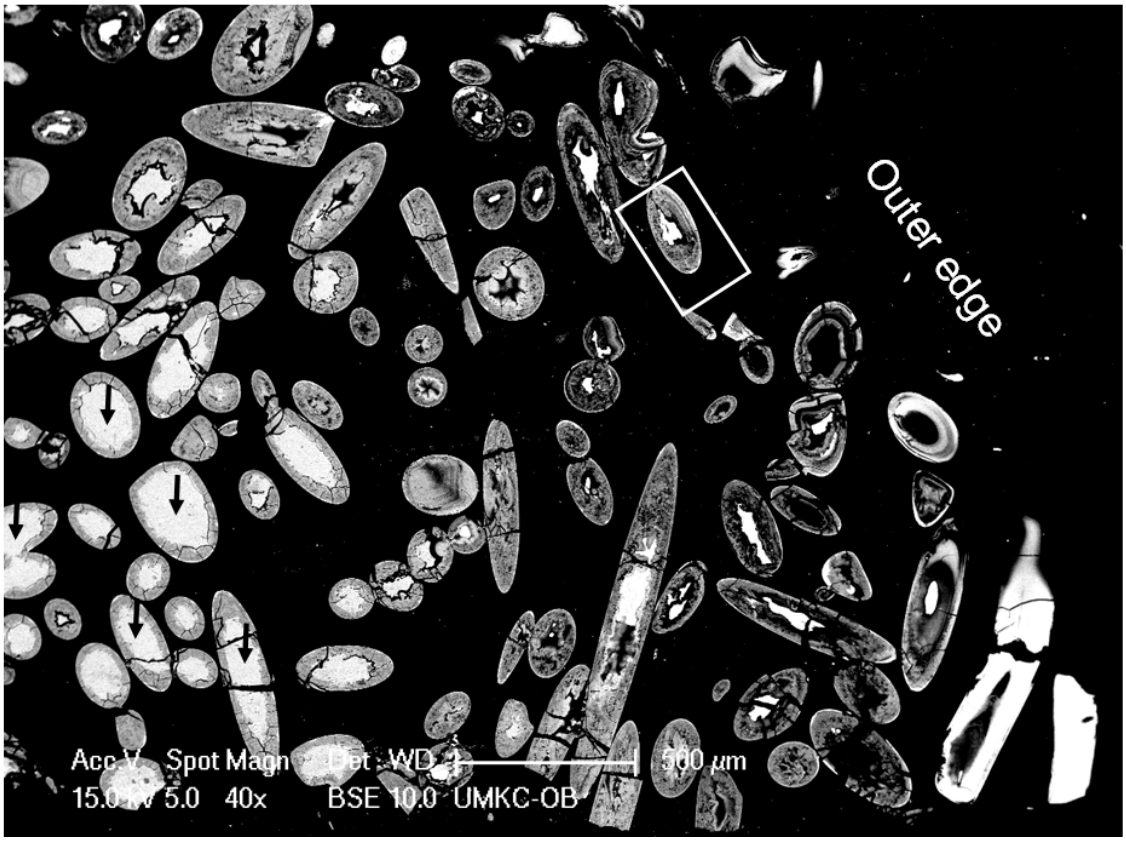

Figure 15 - SEMBSE image of a cross sectioned CSZ fiber scaffold that was implanted subcutaneously in the back of a rat for six weeks.

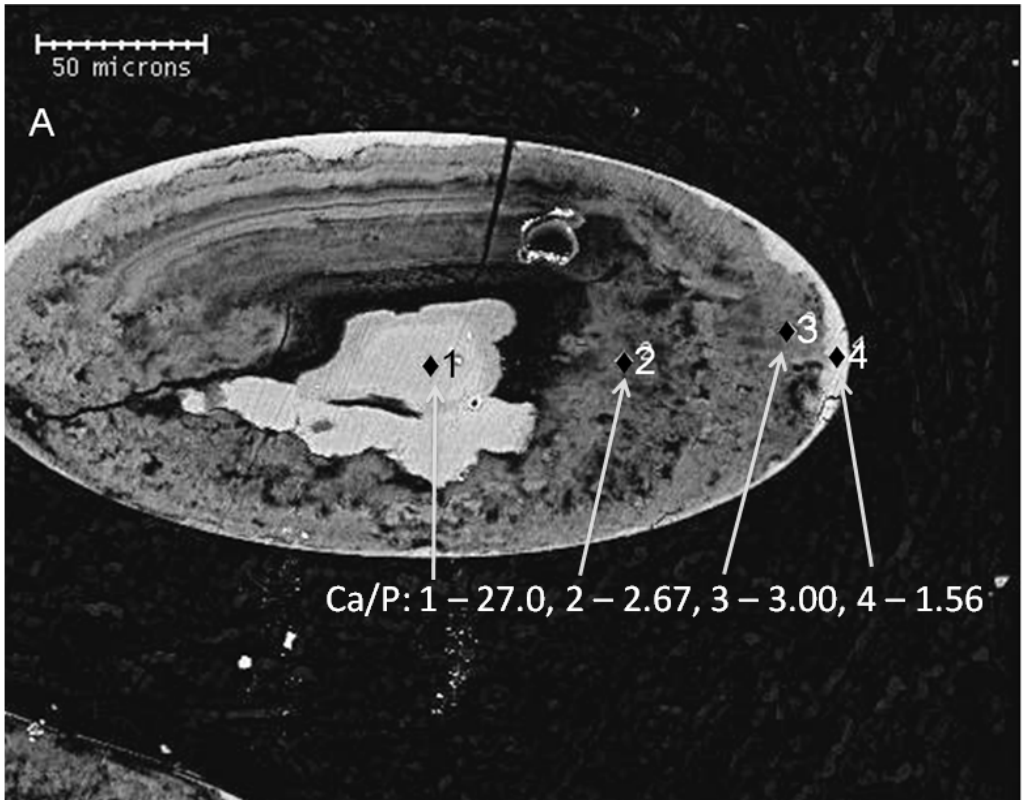

Figure 16 - SEMBSE image of a CSZ fiber implanted subcutaneously in the back of a rat for six weeks.

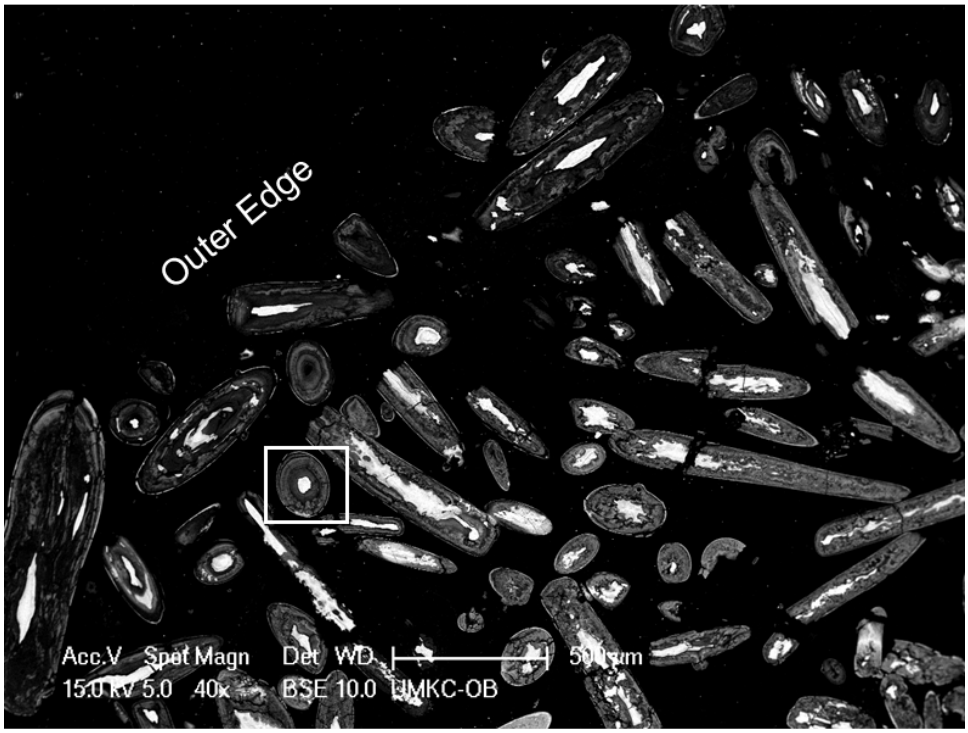

Figure 17 – SEMBSE image of the cross section of a CSZF fiber scaffold that was implanted subcutaneously in a rat for six weeks.

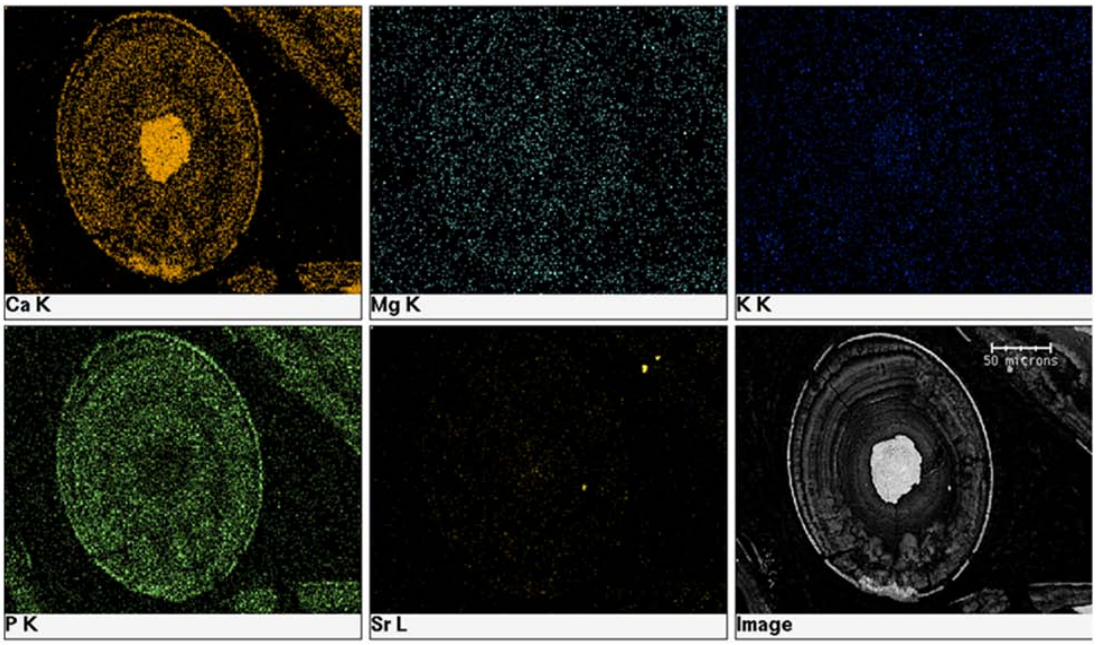

Figure 18 - EDS phase map of CSZF reacted fiber after six weeks in rat subcutaneous tissue. The SEMBSE image at the bottom right of the image is for reference.

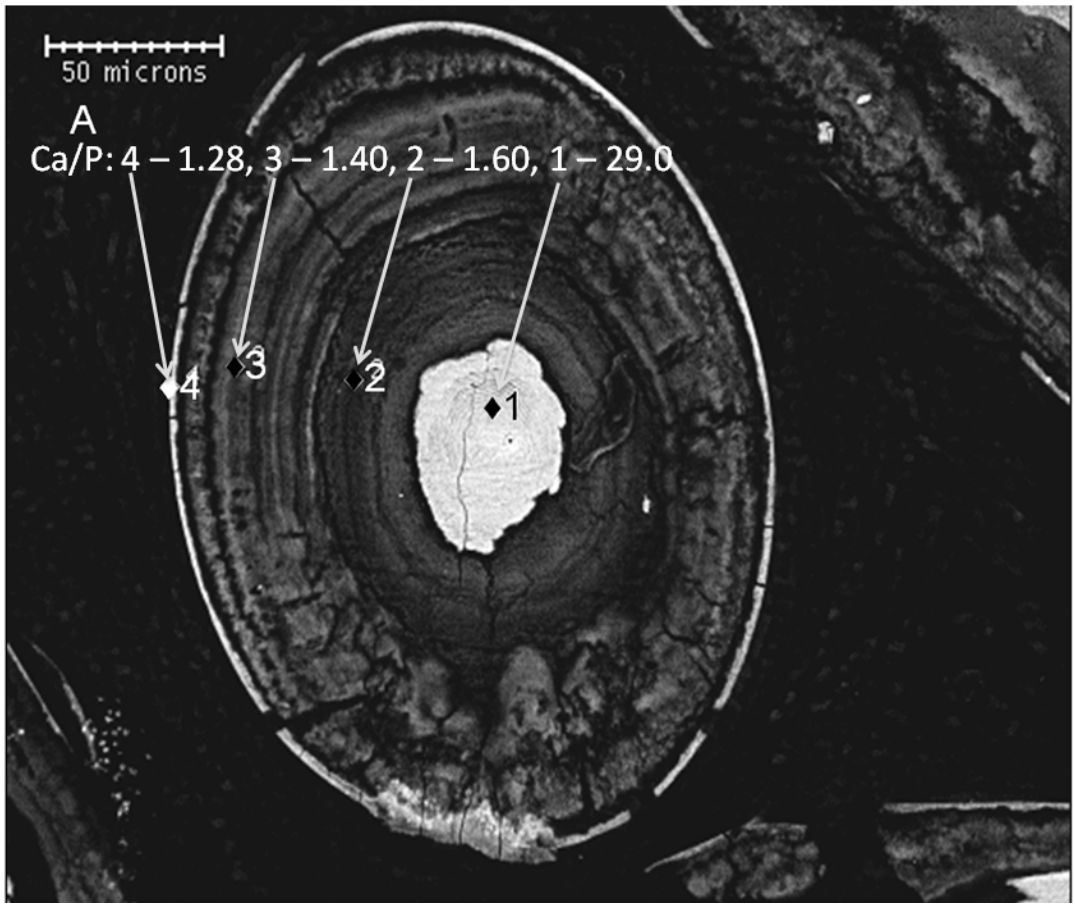

Figure 19 - SEMBSE image of a CSZF fiber implanted subcutaneously in a rat for six weeks.

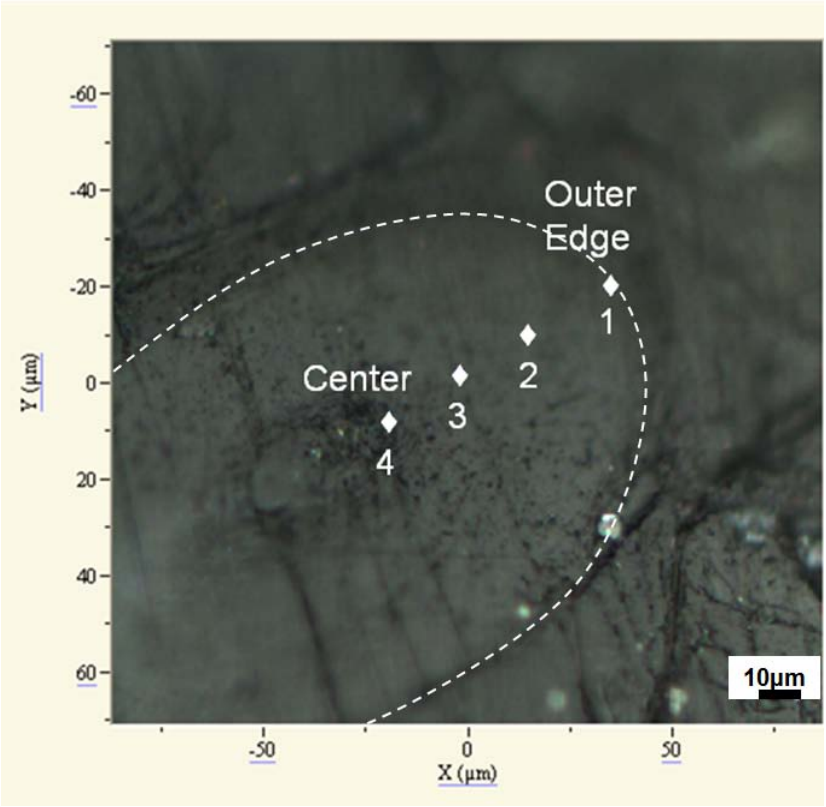

Figure 20 – Optical image of a 13-93B3 fiber reacted in rat subcutaneous tissue for four weeks, mounted in PMMA, and cross sectioned. The outer perimeter of the fiber is denoted by a dashed line, and the center and outer edge of the fiber are labeled as indicated. The four spots inside the fiber were analyzed by micro raman and the spectra are shown in Fig 21.

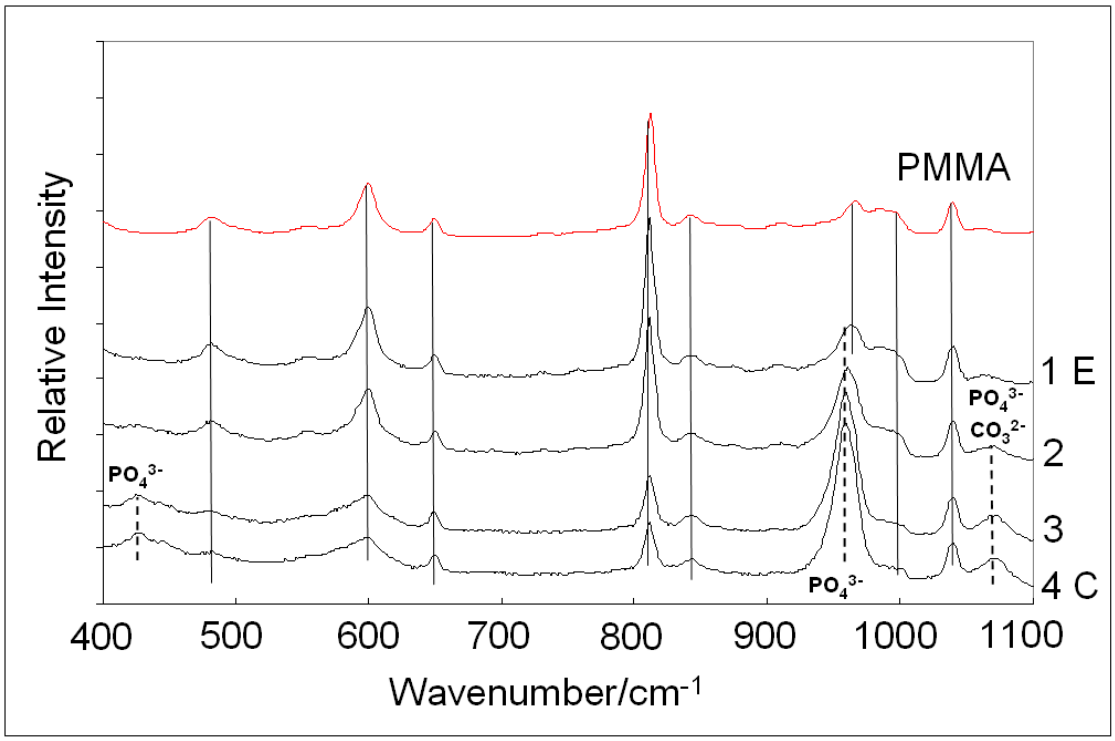

Figure 21 – Micro raman spectra for a 13-93B3 fiber that was implanted in rat subcutaneous tissue for four weeks. The peaks associated with HA are indicated by the dashed lines at (431cm^{-1} (PO_4^{3-} v2), 965cm^{-1} (PO_4^{3-} v1), 1065 to 1070cm^{-1} (CO_3^{2-} v1) and 1076cm^{-1} PO_4^{3-} v3) and the solid lines are for the mounting medium PMMA.

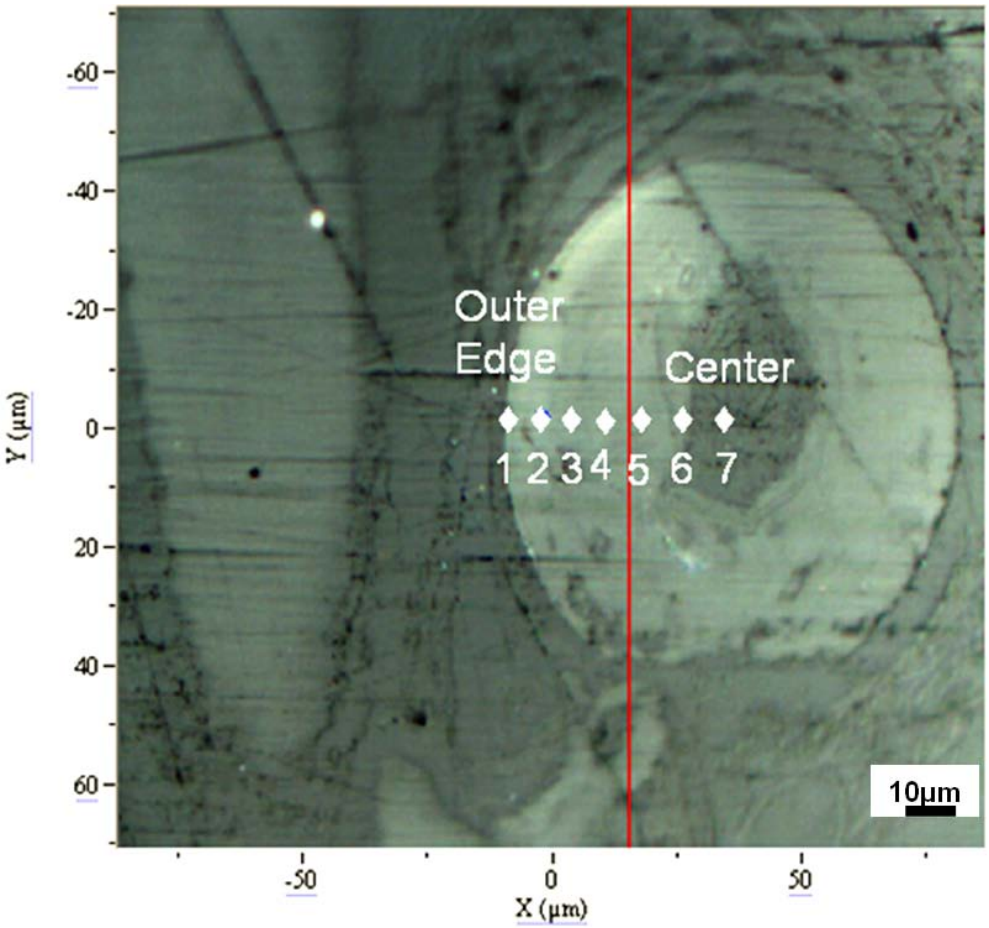

Figure 22 – Micro-raman analysis of a Cu-3 fiber that reacted while in contact with rat subcutaneous tissue for six weeks. The spot size of the laser was 2µm, and is approximated by the size of the indicator diamonds.

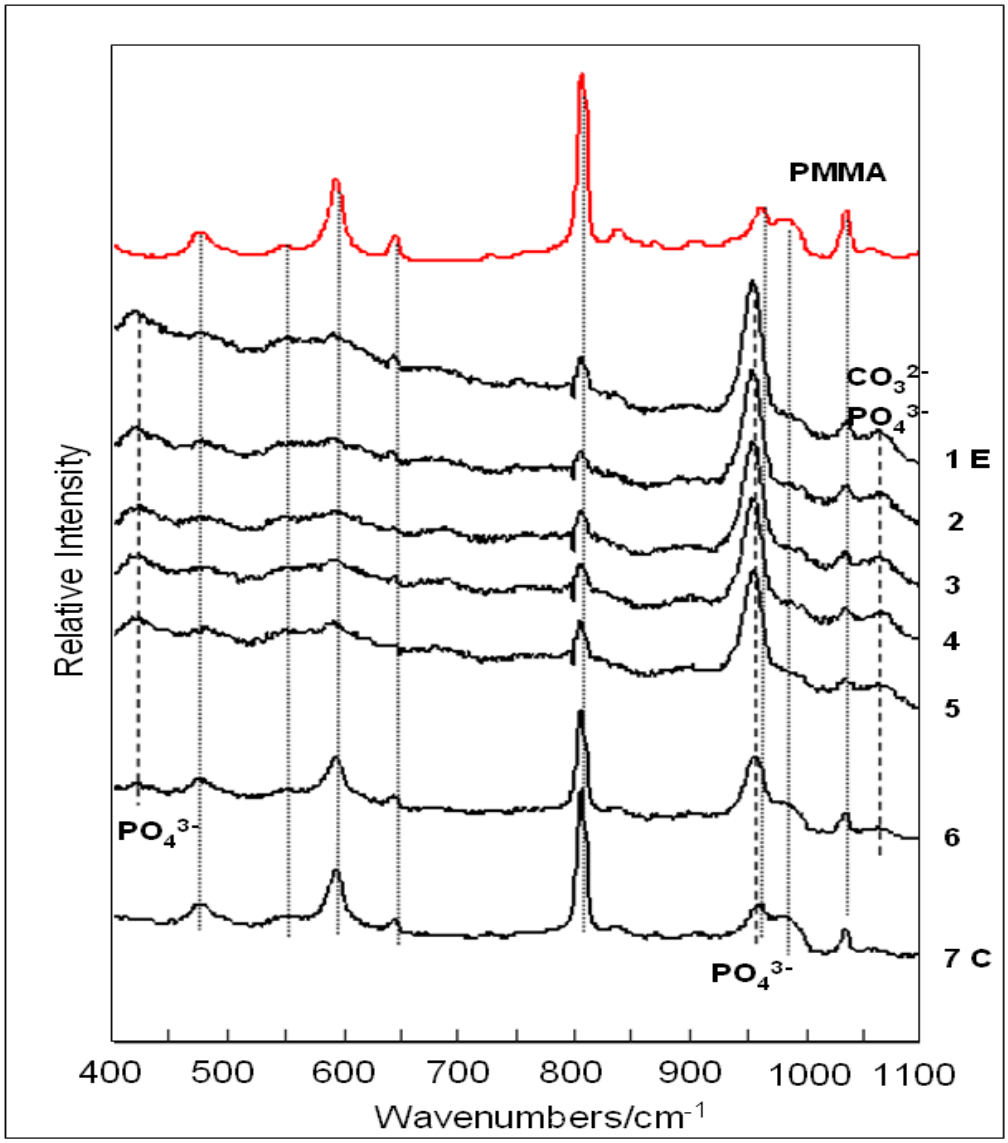

Figure 23 – Micro-raman analysis of a Cu-3 fiber that reacted while in contact with rat subcutaneous tissue for six weeks. The light gray lines represent peaks associated with PMMA, and the pattern for PMMA is at the top of the figure.

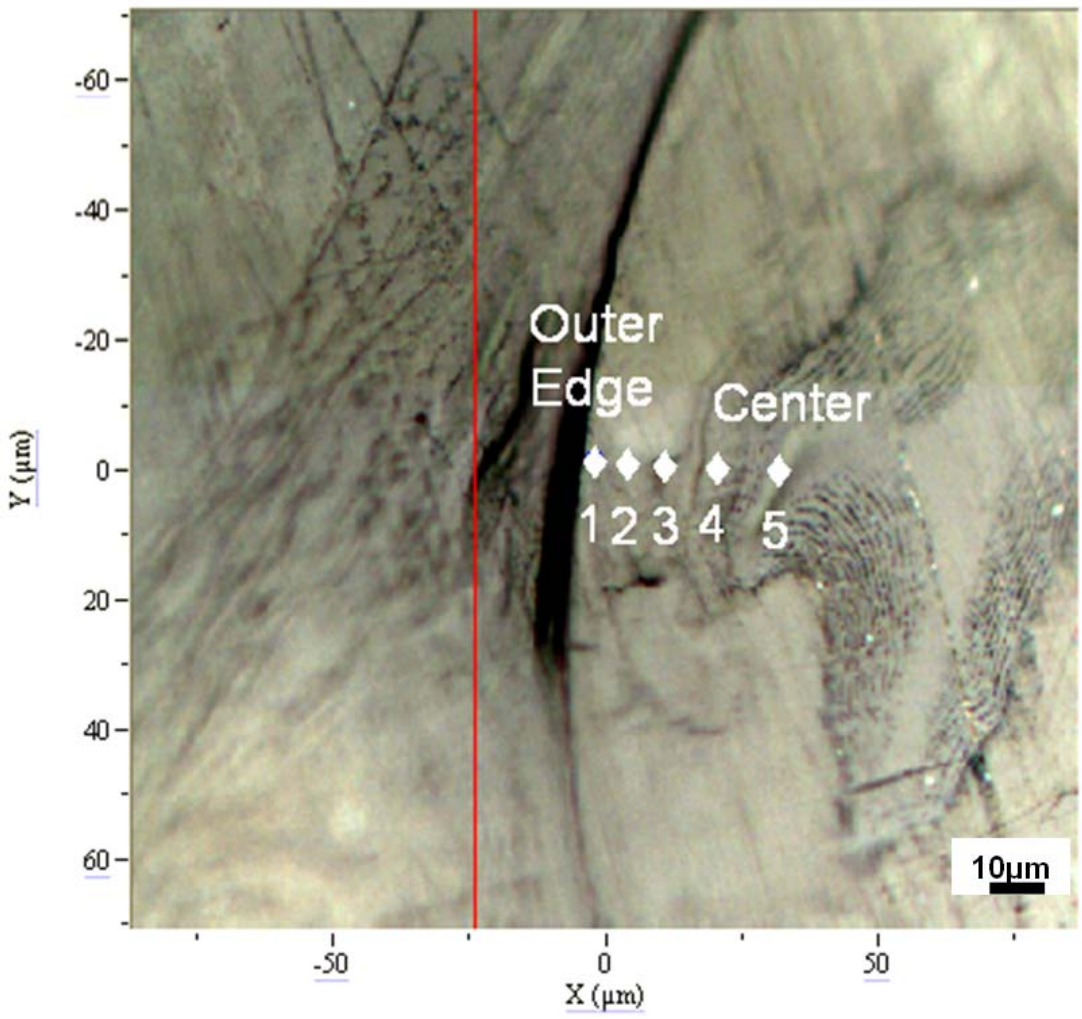

Figure 24 – Micro-raman analysis of a CS fiber that reacted while in contact with rat subcutaneous tissue for six weeks. The fiber was measured at five spots from the outer edge (1) to the center (5) and the spectra are shown in Fig 25. The red line through the image has no meaning and was an artifact of the micro-raman software. The spot size of the laser was 2µm, and is approximated by the size of the indicator diamonds.

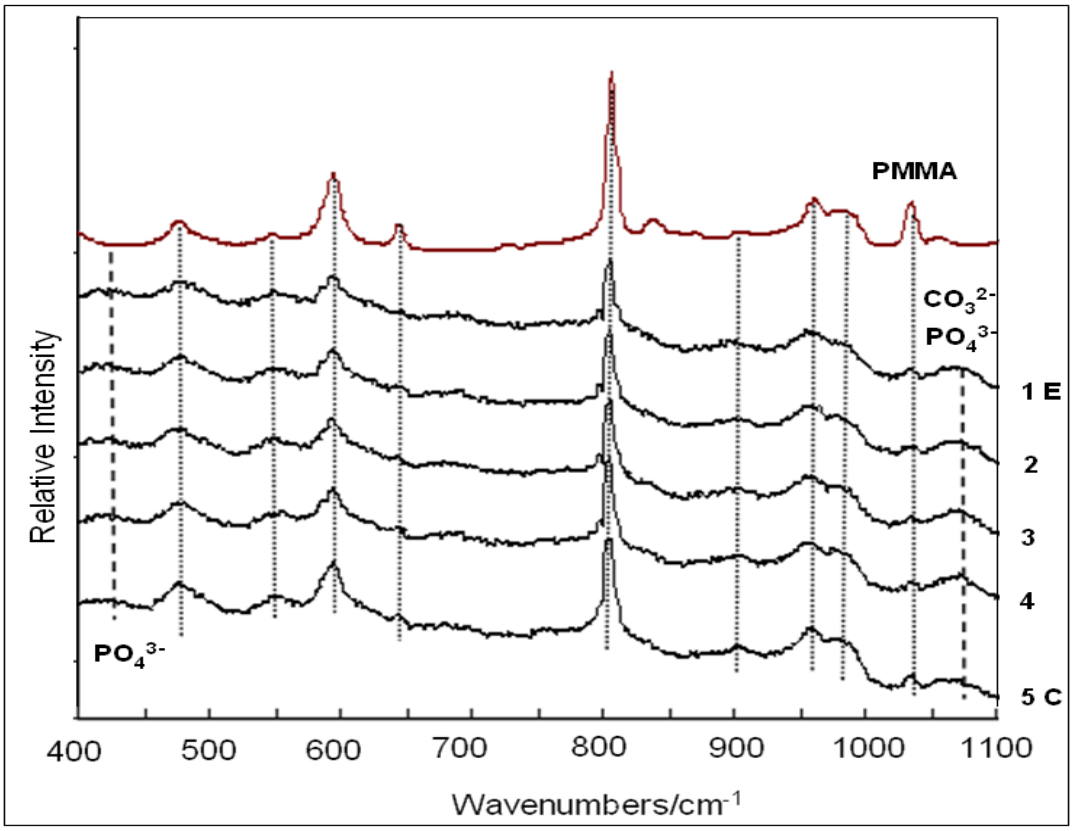

Figure 25 – Micro-raman analysis of a CS fiber that reacted while in contact with rat subcutaneous tissue for six weeks. The light gray lines represent peaks associated with PMMA, and the spectrum for PMMA is shown at the top of the figure.

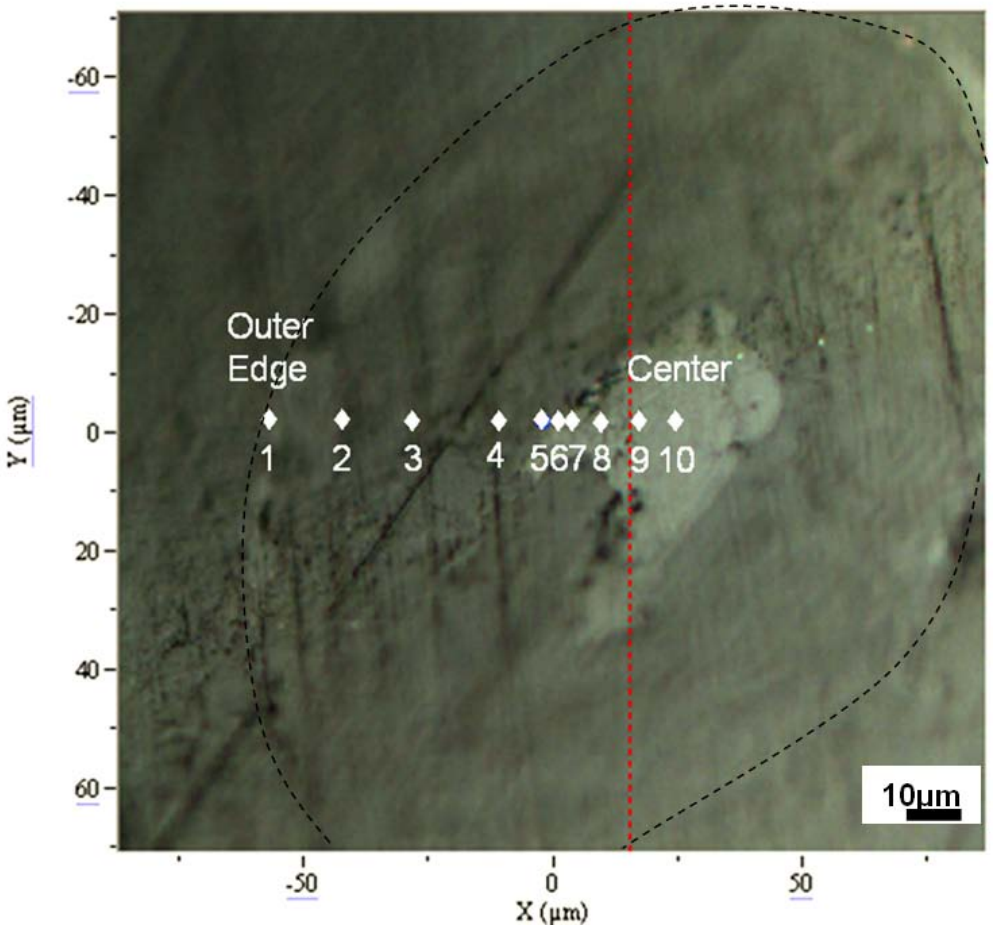

Figure 26 – Micro-raman analysis of a CSZ fiber that reacted while in contact with rat subcutaneous tissue for six weeks. The spot size of the laser was 2µm, and is approximated by the size of the indicator diamonds.

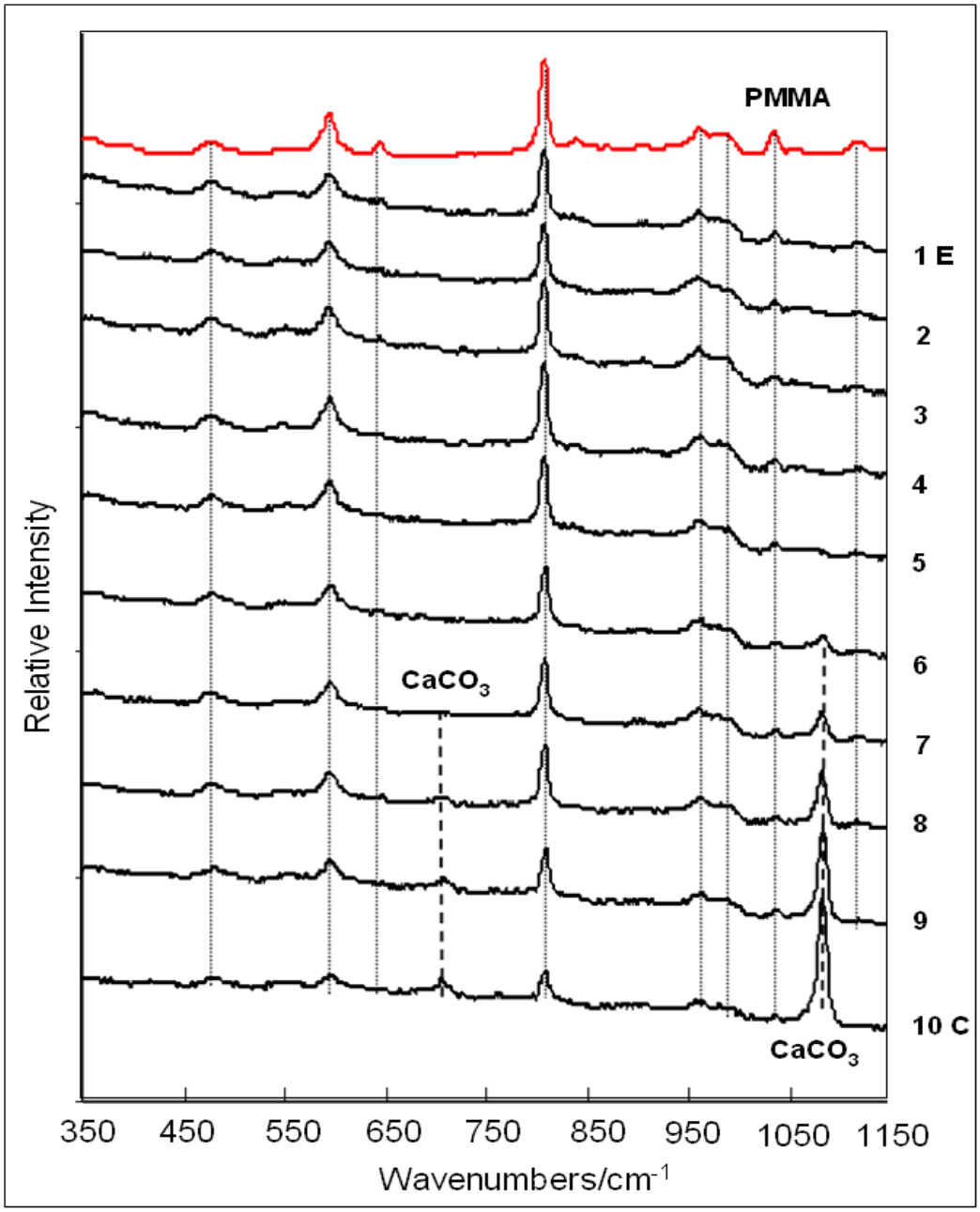

Figure 27 – Micro-raman analysis of a CSZ fiber that reacted while in contact with rat subcutaneous tissue for six weeks. The micro-raman spectra for each of the 10 spots are shown above, outer edge (1 E) to the center (10 C). The peaks associated with calcite, ($CaCO_3$), are indicated with a dashed line at 711/cm^{-1} and 1085/cm^{-1}.

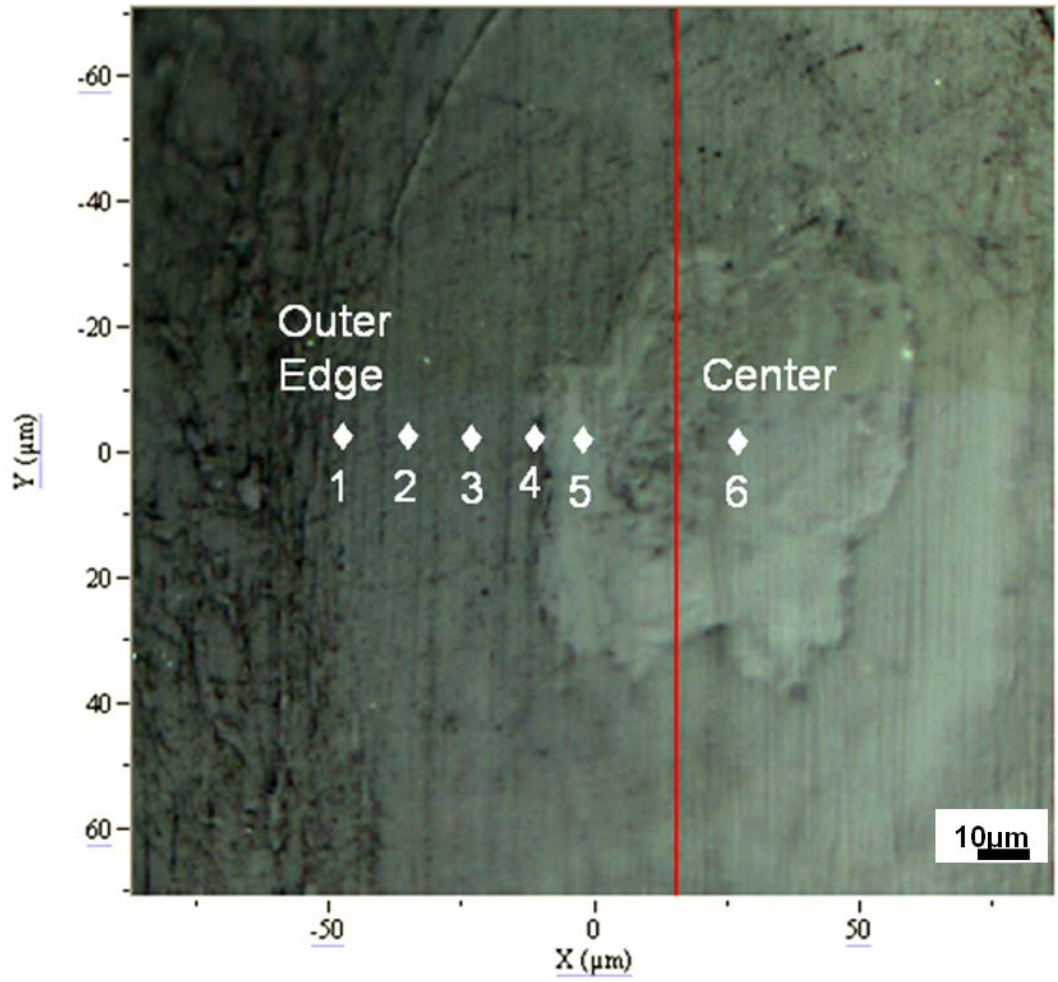

Figure 28 – Micro-raman analysis of a CSZF fiber that reacted while in contact with rat subcutaneous tissue for six weeks. The fiber was measured at six spots from the outer edge (1) to the center (6). The red line through the image has no meaning and was an artifact of the micro-raman software. The spot size of the laser was 2µm, and is approximated by the size of the indicator diamonds.

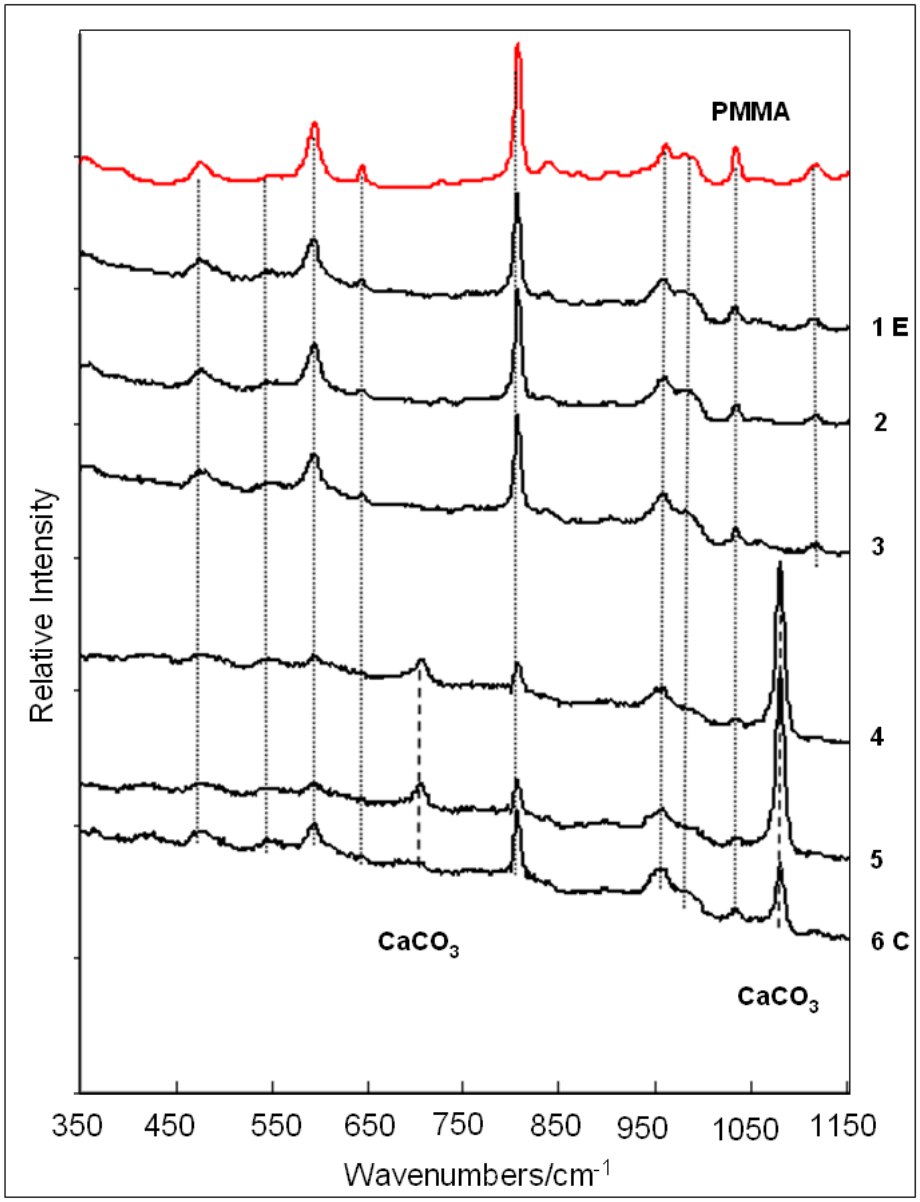

Figure 29 – Micro-raman analysis of a CSZF fiber that reacted while in contact with rat subcutaneous tissue for six weeks. The micro-raman spectra for spots one to six are shown above, outer edge (1 E) to the center (6 C). Calcite had peaks present in spectra four to six which are indicated with a dashed line at 711/cm^{-1} and 1085/cm^{-1}.

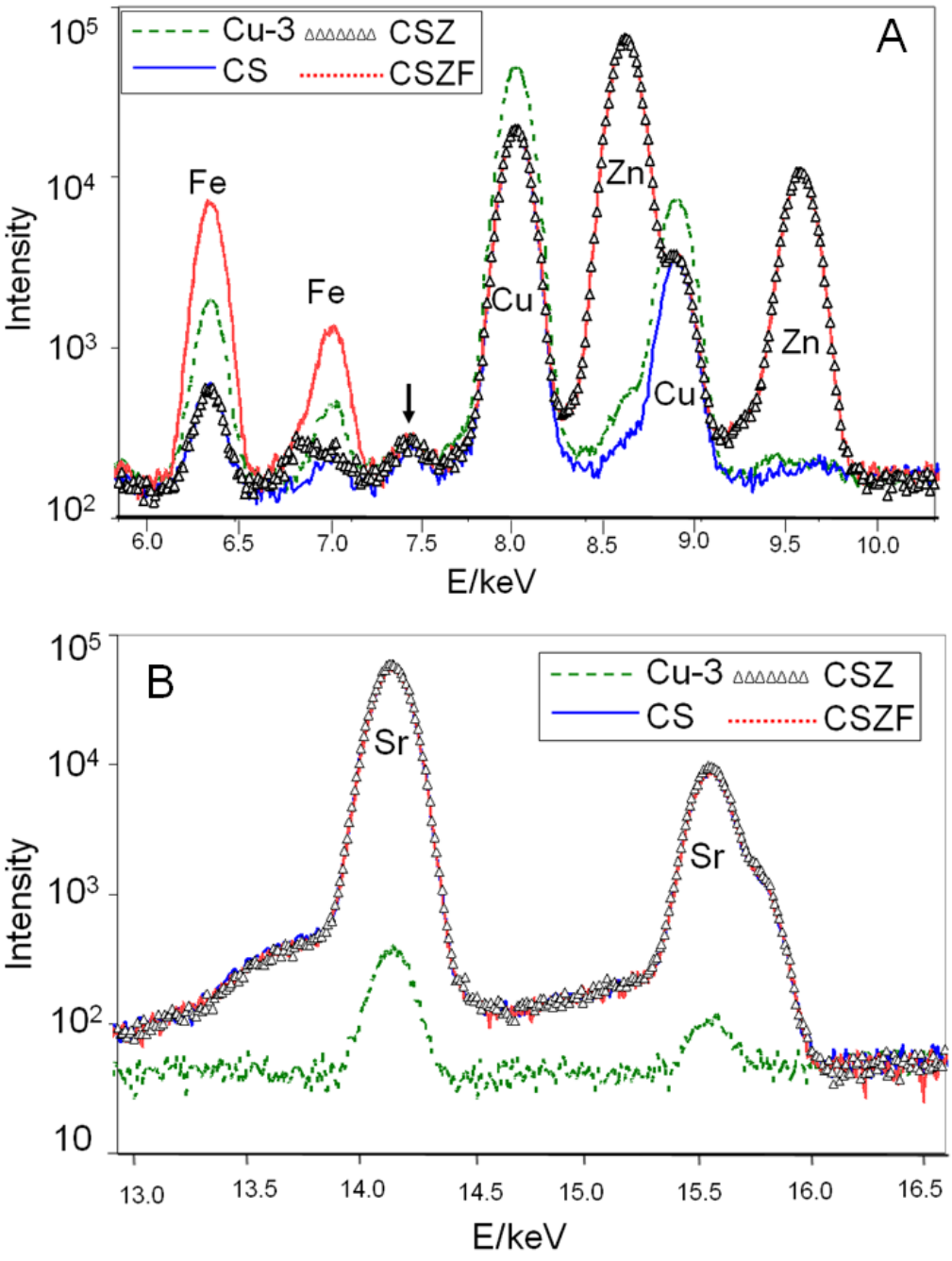

Figure 30 – XRF spectra for the as-made bioactive borate glasses doped with minor elements. Copper (Cu or C), strontium (Sr or S), zinc (Zn or Z), iron (Fe or F). The arrow in Fig 30A is indicating a peak associated with the polymer binder used to mount XRF sample. It is noted that the CS, CSZ, and CSZF patterns for Sr overlap in Fig 30B.

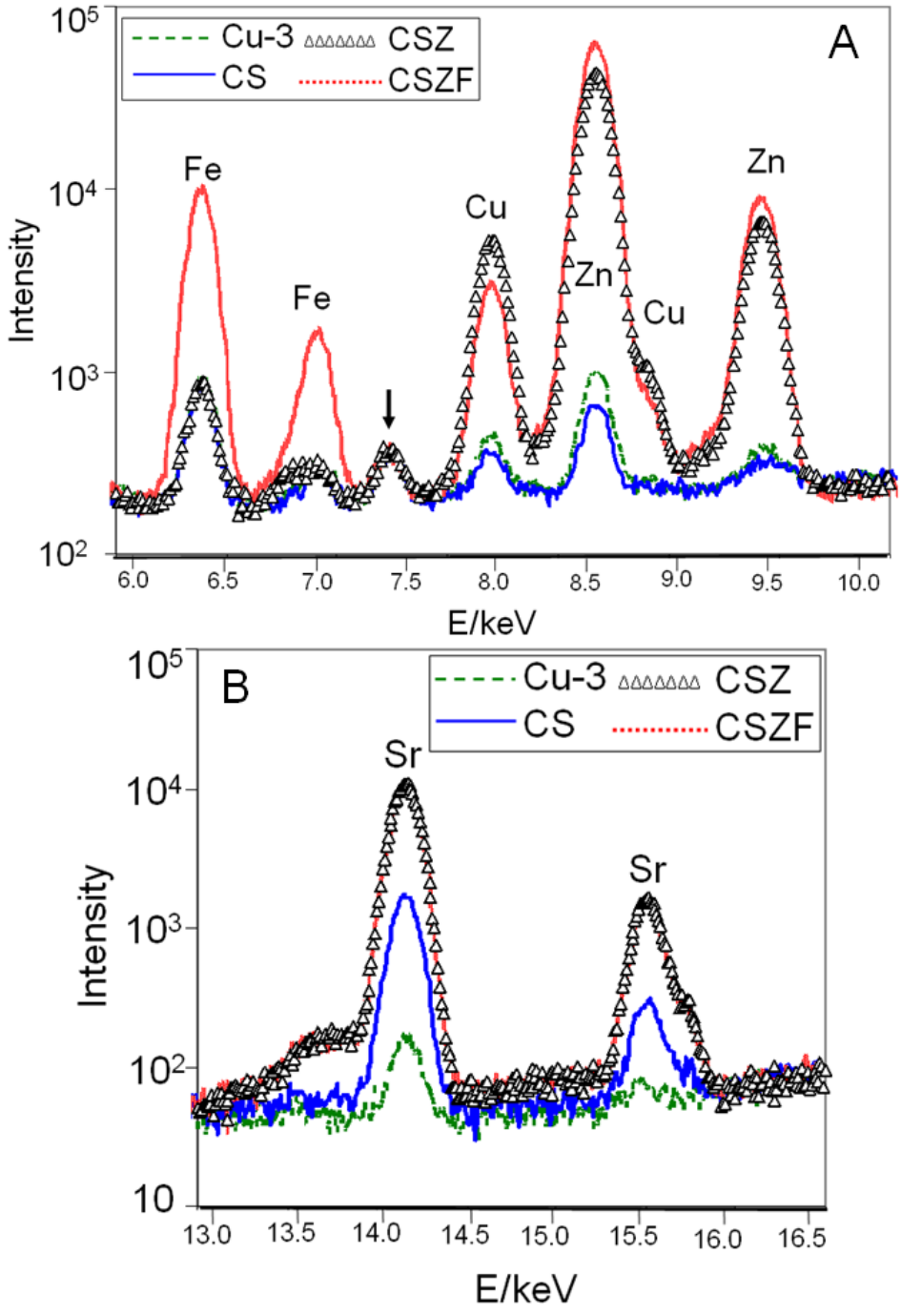

Figure 31 – XRF spectra for each type of bioactive borate glass scaffold doped with minor elements that were implanted in subcutaneous tissue of rats for six weeks. Copper (Cu or C), strontium (Sr or S), zinc (Zn or Z), iron (Fe or F). The arrow in Fig 31A is indicating a peak associated with the polymer binder used to mount XRF sample.

Figure 32- High magnification SEMBSE image of the reacted CSZF fiber (six weeks *in-vivo*).

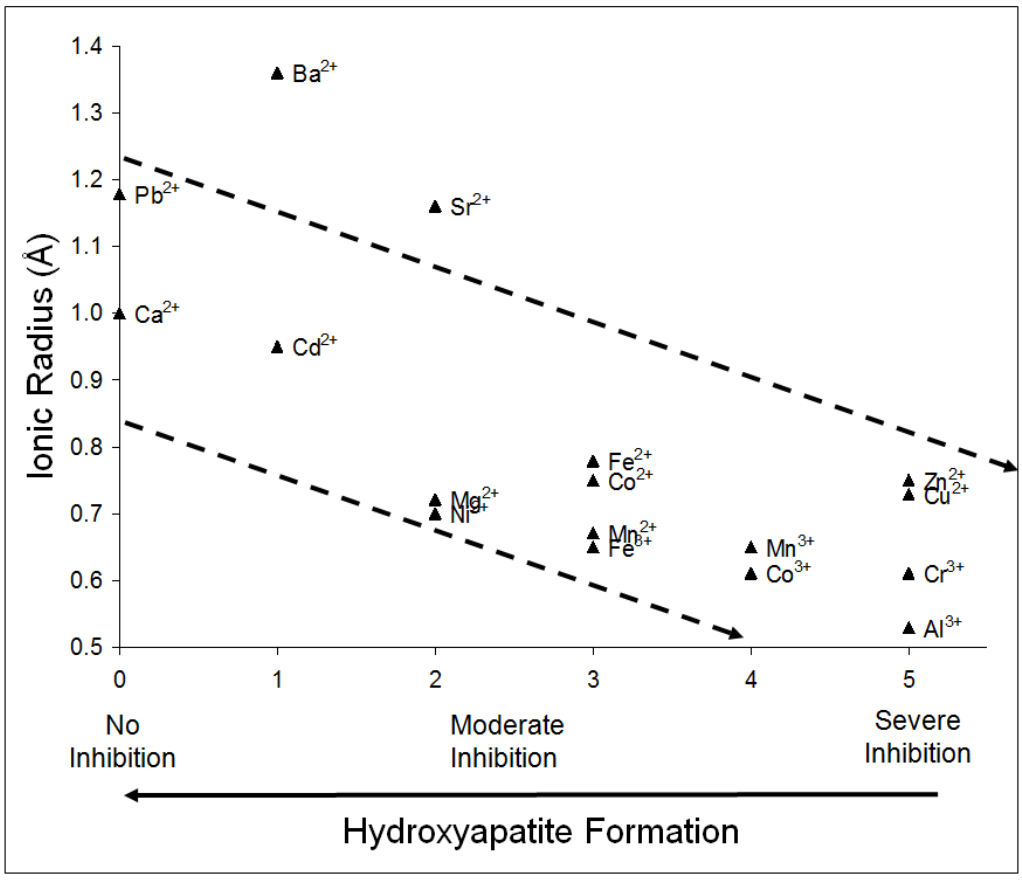

Figure 33 – Schematic relating how hydroxyapatite formation is inhibited by the presence of six coordinated ions in aqueous environments [37-38,50].

6. THE TREATMENT OF WOUNDS WITH BIOACTIVE BORATE GLASS FIBERS

Steven B. Jung[1], Delbert E. Day[1], and Roger F. Brown[2]

[1]Graduate Center for Materials Research, Materials Science and Engineering Department, Missouri University of Science and Technology, Rolla, MO, 65409-1170

[2]Department of Biological Sciences, Missouri University of Science and Technology, Rolla, MO, 65409-1170

6.1 ABSTRACT:

A pad of micron and submicron borate glass fibers was used to treat 15mm full thickness cutaneous wounds of rats and by 15 days the wound area decreased by 85 to 90% of its original size. The dermal, epidermal, and subcutaneous tissues in all four of the 93B3 fiber filled wounds were significantly regenerated by day 22 while only three out of four wounds from the control group (untreated wound) regenerated the subcutaneous tissue. There were no signs of infection present in either the control or 93B3 fiber filled wounds. The wound contraction, the thickness of the granulation tissue and the gap present in the subcutaneous tissue layer after 22 days were all measured and compared via the student t test. There were no statistically significant differences between the control and 93B3 fiber filled wounds. No 93B3 fibers were identifiable in the histological sections at 22 days, but there was evidence of 93B3 microspheres that had reacted with the body fluids and formed hydroxyapatite (HA). Blood vessels were seen adjacent to many of the reacted 93B3 microspheres indicating that the boron released (dissolved) from the microspheres could be promoting an angiogenic effect that is important to wound management and healing.

The advantages of using the 93B3 glass fibers for wound healing are as follows:

- The 93B3 fibers are biocompatible and biodegradable
- The boron released from the glass is potentially angiogenic
- The release of lithium and sodium from alkali borate glasses has been shown to be anti-bacterial
- The 93B3 glass reacts quickly with body fluids releasing calcium that has been linked to regulating healing in skin
- There were no signs of inflammation surrounding any of the reacted 93B3 glass fibers or microspheres

6.2. INTRODUCTION

For decades bioactive glasses have been known to bond with both hard and soft tissue [1]. The majority of the research on bioactive glasses has been directed at the regeneration of bone, but recently, there has been interest in the effects that bioactive glasses may have on soft tissue. The promotion of soft tissue growth such as blood vessels in the presence of bioactive glass has recently sparked interest in using bioactive glass to regenerate soft tissue. Leach et al coated a polymer based, vascular endothelial growth factor releasing scaffold with bioactive glass particles and successfully promoted blood vessels growth *in-vitro* [2].

Soft tissue interactions with bioactive glass have been studied for soft tissue augmentation and for understanding how bioactive glass interactions at the bone to soft tissue interface. Fibers of a 13-93 glass, a silicate based bioactive glass, coated with chitosan were implanted in rabbit soft tissue for up to 24 weeks [3]. The immune response was described as generally mild, and soft tissue was present throughout the bioactive glass implants. Fu et al implanted mesenchymal stem cell seeded 13-93 bioactive glass scaffolds in subcutaneous sites of rats for the purposes of bone growth, however, significant vascular growth adjacent to the outer surfaces of the scaffolds was noted on removal. Histological assessment from rats showed that significant soft tissue filled the

inside of the open pores in the scaffold [4]. Scaffolds composed of randomly oriented fibers and scaffolds with a microstructure similar to trabecular bone composed of 13-93 glass implanted in rat soft tissue were reported to have significant soft tissue growth inside the open pores at six weeks. No significant immune reaction was noted upon removal of the scaffolds, and vascular growth adjacent to the outer surface of the scaffolds was also noted [5].

Calcium, a significant component in most bioactive glasses has been reported to be an important factor in the wound healing of skin [6]. It is suspected that calcium is required for the migration of epidermal cells and also plays an important role in the late stages of healing [6]. The presence of calcium in the immediate vicinity of an open wound could help the body to regulate wound healing processes more effectively, especially in open wounds. Human keratinocytes (main type of cells of the epidermis also known as basal cells) require <0.5mM calcium to proliferate, but fibroblasts (cells that synthesize extracellular matix and collagen) need a concentration >1.4mM. At higher calcium concentrations, keratinocyte proliferation is suppressed, but other biological markers for cell differentiation required for wound healing are promoted [6].

The use of growth factors for treating wounds has not been very successful [7]. The body needs growth factors at certain time intervals to be effective in faster healing, but it is difficult to time the release effectively during treatment. The most effective treatment for wounds has been covering the wound and allowing the body to naturally support the delivery of growth factors or other required nutrients [7].

In an *in-vitro* study, borate glasses were found to have beneficial antibacterial effects [8]. Lithium borate glasses when placed in culture with several harmful bacteria

such as escherichia coli (ecoli), salmonella typhimurium (salmonella), and stapphylococcus aureus (staph), have all been shown to kill the bacteria due to the local increase of pH from the release of alkali (Li) to the immediate surroundings [8]. The ability to reduce or eliminate bacterial growth at the site of an open wound would be advantageous, especially without the need for antibiotics.

Traditionally, bioactive glasses have been silicate based and react relatively slowly with the body fluids over a period of several months [3,9,10]. Bioactive glasses containing boron as the glass former have been shown to react with simulated body fluids up to five times faster than silicate glasses in certain *in-vitro* experiments [11,12]. Fibers (up to 300µm in diameter) of the bioactive borate glass 93B3 have been shown to fully react in four weeks in rat subcutaneous tissue with no noticeable immune reaction. Soft tissue and blood vessels were present inside many of the reacted fibers.

Due to the faster reaction of the borate glass when in contact with body fluids, its biological compatibility, its release of calcium in the immediate wound site, and its potential antibacterial effect, an investigation of a bioactive glass in the form of submicron fibers was undertaken. Borate glass fibers (300nm to 2µm diameter) were made and used as a bandage material to treat full thickness cutaneous wounds. After 22 days, the rate of wound closure was similar between the treated and untreated wounds, but there may be advantages in terms of wound quality (growth and functionality of tissue) of the treated wounds as compared to the untreated wound.

6.3. MATERIALS AND METHODS

6.3.1 Preparation and Sterilization of Bioactive Glass Fibers

The glass fibers used as the wound dressing were made from a borate glass with a nominal composition of 53 B_2O_3, 20 CaO, 12 K_2O, 6 Na_2O, 5MgO, 4 P_2O_5 (wt%) denoted as 93B3. The glass was melted in a platinum crucible for one hour at 1050^oC and stirred every ten minutes prior to casting the melt on a cold copper plate. The 93B3 fibers (shown in Figs 1 and 2) were made by a proprietary process (Mo-Sci Corporation, Rolla, MO). The bioactive 93B3 glass fibers were sterilized by placing ~150mg of fiber in a silica glass vial with an aluminum foil top, heating the vial to 300^oC in an oven (Ney Vulcan 3-130) for four hours, and cooling the oven overnight to room temperature whereupon the sterile fibers were ready for use.

6.3.2 Animals

Four male Sprague Dawley rats supplied by Fisher Scientific (St. Louis MO) were used in the experiment. The rats were approximately four months old, and weighed about 250 grams each. The rats had free access to tap water and food pellets and were caged individually.

6.3.3 Surgical Procedure

Each rat was shaved to remove the hair at the surgical site (Fig 3) and disinfected with iodine and 70% ethanol solution prior to the surgical procedure. Two full thickness cutaneous defects, 15mm in diameter, were made in the skin, one on each side of the spine above the shoulders, see Fig 3. One defect was covered with a dry pad of bioactive 93B3 glass fibers (150mg) while the other defect was used as a control and left empty, see Fig 4.

The wound covered with the glass fibers was staggered, alternatively between the right and left side for successive rats. After the surgery, bandages were placed over the glass fiber pad at the wound sites for four days over the control wounds.

6.3.4 Cutaneous Wound Recovery, Fixation, and Dehydration

After 22 days, the animals were sacrificed by CO_2 inhalation. A section of soft tissue ~20mm by 20mm on an edge surrounding the wound was recovered for histological assessment. The tissue was placed in a 10% formalin solution for four days and then dehydrated by microwave dehydration with a series of ethanol solutions from 80% to 100% [13].

6.3.5 Sample Embedding and Slide Preparation

The dehydrated tissue sections were cut in half, one half stored in ethanol, and the other half placed in a tissue processor (AutoTechnicon Model 2A) for wax embedding. The tissue sample was infiltrated with wax (Paraplast Tissue Embedding Medium, McCormick Scientific LLC) for a minimum of four hours at 45^{o}C before being embedded in a wax block with a paraffin mounting system (Leica EG 1150H). The wax block was placed in a microtome (Leica RM 2235 microtome) and 18um thick sections were cut with TBS Shur/sharp blades, (Triangle Biomedical Sciences, Durham NC). The sections were floated on a warm water bath (Lipshaw Electric Tissue Float, model number 375, Detroit MI) (40^{o}C) to improve the flatness of the sections and then mounted on a glass slide (Fisher Brand Superfrost microscope slides, St. Louis MO). The mounted slides were placed on a slide drier (Fisher Scientific slide warmer, St. Louis MO) overnight to dry the tissue sections.

6.3.6 Wound Healing Assessment

The dimensions of the open wounds was measured periodically and the area of the open wound (unhealed) was calculated as a function of time. An example of the healing progression for a control wound and wound treated with 93B3 glass fiber pad is shown in Fig 5. The wound area as a function of time, the gap in the subcutaneous tissue (distance between the sides of the wound) at 22 days, and the average thickness of the granulation tissue present at 22 days were measured and compared by the student t test to determine statistical differences between the control and wounds treated with the 93B3 glass fiber pad.

6.3.7 Histological Staining – Hematoxylin and Eosin (H&E)

H&E staining of the histological sections was done with a Leica CV Autostainer XL (Phelps Country Regional Medical Center, Rolla MO). Stained slides were viewed with a microscope (Olympus BX50, Olympus Optical Co) at magnifications of 200, and 400x and imaging software (DP Controller, Olympus Optical Co) was used to capture images.

6.3.8 Scanning Electron Microscopy (SEM)

Fibers of the 93B3 glass were imaged with a Hitachi S4700 FESEM (see Fig 2). The fibers attached to an aluminum stub with carbon tape and were coated with ~100Å of gold palladium prior to examination. The accelerating voltage was 10kV and the magnification used varied from 70 to 7000x.

6.4. RESULTS

6.4.1 Histological Assessment of the Wound Sections (H&E)

All four of the H&E stained sections for the control wounds are shown in the composite photos in Fig 6. The dark horizontal line (at the top of the sections) represents the area of the wound where the two sides of the wound joined and were in the process of healing. In Figs 6A, 6C, and 6D granulation tissue is present at the top of the wound (black arrows). The wound in Fig 6B had healed to the point where the granulation tissue had been replaced by dermal and epidermal tissue. The wound sections in Figs 6A and 6B have a band of subcutaneous tissue (bright pink) spanning the bottom of the entire wound area. Figure 6C has subcutaneous tissue present on the right hand side of the wound (black arrow), but there is no subcutaneous tissue present at the wound interface (black line, top of image) or on the entire left side of the section. The gap in the subcutaneous tissue (double ended arrow) in Fig 6C was the longest of any tissue section, control or 93B3 glass fiber treated, at 12.7mm. The section in Fig 6D has a 4mm gap (double ended arrow) located at the interface between the two sides of the wound.

A composite photo of the sections from the wounds filled with the pad of 93B3 fibers is shown in Fig 7. The black horizontal line shows the region were the two sides of the wound came together. Granulation tissue present in Figs 7B, 7C, and 7D, as indicated by the arrows. No granulation tissue was observed in Fig 7A as it had been replaced with dermal and epidermal tissue. A small gap (<2mm) was present in the subcutaneous tissue (double ended arrow) in Figs 7A and 7B, a larger gap (~4mm) was present in Fig 7C and there was no detectable gap in the subcutaneous tissue in Fig 7D.

No evidence was found of the 93B3 fibers in Fig 7, but the small fiber diameter would make them difficult to see at the magnifications used for the histological analysis.

The 93B3 fiber filled wound in Fig 7A, was selected for histological analysis. The entire tissue section and selected magnified areas are shown in Fig 8. The approximate boundary of the original wound is indicated by the horizontal arrow in Fig 8A.

Evidence of the original wound is indicated by the presence of the larger, reacted 93B3 microspheres distributed throughout the subcutaneous tissue, see Figs 8B, 8C, 8D, and 8E. In Fig 8B, the reacted microspheres are at the bottom left of the image, and above them there are hair follicles (vertical arrows) and fat deposits (oval) that are indications that the tissue has not scarred, but in fact returned to its original function. The microspheres in Fig 8B are magnified in Fig 8C, and adjacent to the top of the reacted microsphere is a blood vessel filled with red blood cells (white arrow). In the unhealed portion of the wound in Fig 8A, boxes D and E, more reacted microspheres are present along with blood vessels nearby (see Fig 8D and 8E). The two vertical dashed lines in Fig 8A show the region where the subcutaneous tissue has yet to regenerate, but the dermal and epidermal layers have completely replaced the granulation tissue.

6.4.2 Wound Healing Assessment

The wound area that remained open during the healing process was calculated as a function of time as shown in Fig 9. The average wound area (n=4) for the control was slightly less than that for the wounds treated with the 93B3 fiber pad up to day 11, but, by day 15 the fiber treated wounds and the control wounds were almost the same. After 18 days, the control and 93B3 fiber filled wounds were >99% closed as shown in Fig 9 and

all the wounds were completely closed by day 22. The wound closure data was compared via the student t test, but there was no statistical difference ($p<0.05$) between the control and the wounds treated with the 93B3 fiber pad (see Table 1).

The average gap between the subcutaneous tissue and the thickness of the granulation tissue was also measured to differentiate any differences in healing between the control wounds and the wounds treated with the 93B3 fiber pads. The average gap in the subcutaneous tissue was 4.2±6mm for the control and 1.9±1.6mm for the 93B3 fiber filled wounds. The average thickness of the granulation tissue for the control wounds and 93B3 fiber filled wounds was 1.7±1.2mm and 1.7±1.3mm, respectively, see Fig 10. There was no statistically significant difference between the control wounds and the 93B3 fiber filled wounds for the average gap in subcutaneous tissue or the thickness of the granulation tissue when compared by the student t test (Table 1).

6.5. DISCUSSION AND CONCLUSIONS

The composition of the bioactive 93B3 glass has already been discussed in some detail for why it was chosen for a wound healing application. Borate glasses, specifically lithium borate glasses, have been shown to have antibacterial effects when placed in the presence of escherichia coli, salmonella typhimurium, and stapphylococcus aureus [8]. The high alkalinity of the aqueous environment was determined to be responsible for killing the bacteria. The 93B3 glass fibers, also a high alkali containing borate glass, would be expected to have a similar response on killing bacteria and would do so without the need for antibiotics. The possible antibacterial effect, the release and benefits of calcium to wound healing, the biological compatibility of the glass, and the fast reaction time all were considered important to the performance of the 93B3 glass in wound healing.

The 93B3 glass converts to hydroxyapatite (HA), the same material found in the inorganic component of bone, when in contact with body fluids. Hydroxyapatite is a compatible material with living mammalian tissues, and HA has considerable use as a filler to increase skin thickness [14].

The micron and sub-micron sized fibers shown in Figs 1 and 2 are compressible similar to cotton and are relatively easy to pack into open wounds. The 93B3 fiber did not need to be changed like many traditional wound dressings as it is inorganic and the likelihood of bacteria growing in the dressing was low due to the release of alkali from the glass [8].

The presence of a scab-like material formed from the 93B3 fibers and the wound secretions likely caused the wound to heal at a slower rate as the skin had moved the layer of fibers out of the way to close the wound. In Fig 5A, the wound (right side) is completely covered with a crusty layer composed of 93B3 fibers that reacted with body secretions. The images in Fig 5B and 5C show the layer of fibers (right side) edges curled as the wound contracted. The majority of the 93B3 fibers were removed when the layer of fibers was discarded and the wound was already 85-90% closed (between days 11 and 15). The fact that the fibers stayed in place for ~90% of the wound closure is good since covering the wound is desirable [7].

The granulation tissue that forms at the wound interface is where new capillaries, macrophages, and fibroblasts congregate as soon as four days after the initial damage [7]. The macrophages secrete growth factors necessary for angiogenesis and promote new tissue formation (fibroplasia) while also eliminating bacteria [7]. The fibroblasts build a network of extracellular matrix required for endothelial cell migration, and the vascular

network supports all of the cells by supplying oxygen and the necessary nutrients needed by the cells [7]. As the wound is healed, the granulation tissue is replaced by functional tissue, so the size of the granulation tissue is an indicator of how much tissue still needs to be regenerated. The fact that the average granulation tissue thickness between the control and the treated wound was not statistically significant suggests that the fiber was not inhibiting the re-epithelialization process. No signs of immune reaction or other adverse biological effects attributable to the 93B3 fiber were noticed during the wound healing.

When reviewing the histological control sections, the tissue section of the control wound shown in Fig 6C did not have any subcutaneous tissue present starting at the right hand side of the granulation tissue all the way to the far left of the section. The thinned dermis at the gap in 6C implies poor-quality scar formation and the dashed arrow on the right side of Fig 6C denotes subcutaneous tissue present on the right side of the wound. This was the only section from the control or fiber filled wounds that did not regenerate a subcutaneous tissue layer. Sections of all of the 93B3 fiber filled wounds contained regenerating subcutaneous tissue, therefore, the 93B3 glass fibers may offer an advantage to the wound healing process by bridging the regenerating tissues.

The wounds treated with the pads of 93B3 glass contained blood vessels close to the reacted 93B3 microspheres. Images from Fig 8B, 8C, 8D, and 8E all had vessels in the immediate vicinity of the reacted 93B3 microspheres. The boron release from the reacting fibers may have had a positive effect on the surrounding tissues. *In-vitro* work by Dzondo-Gadet et. al [15] showed that low concentrations of boric acid in solution with

human placental cells promoted the uptake of mRNA and had a stimulatory effect on cell activity similar to a growth factor.

The presence of the 93B3 glass fibers and microspheres may have also acted as a scaffold or guide for the new tissue to use to grow across the wound. After only four days, the 93B3 fibers had reacted with secretions from the wound and formed a crusty layer that looked similar to a scab. The presence of a fiber layer served to keep the wound moist and keep bacteria and other pathogens from entering the wound. The animals were kept in a relatively clean environment and were injected with penicillin to reduce the chances of infection, therefore the benefits of a scab may not have been noticeable.

The data in Table 1 indicate there was no statistically significant difference between the healing time of the wounds covered with the 93B3 glass fiber pads and the control (empty wound). The control and the fiber filled wounds healed at approximately the same rate and were >99% closed by day 18. This outcome was not entirely surprising as the size of the wounds was not of critical size and much of the wound closure was caused by the contraction of the actin fibers in the skin. In humans, this sort of wound closure is only present in young children, whereas, wounds typically close by epithelial cells migration across the wound. Re-epithiliazation of the wound is a better indicator of wound healing than just the rate of contraction [7]. For the treatment of wounds in adult humans, the most important factor is wound coverage [7]. There are several skin substitutes on the market for treating a variety of wound types, but often they are only effective for a short period of the wound healing process by stimulating the production of cytokines which the body uses in healing the wound [7].

The next step with this work would be to alter the glass composition to release specific metal ions that have been shown to promote endothelial cell migration *in-vitro* [16]. These trace elements-- copper, zinc, manganese, iron, and magnesium, have all been identified as essential elements for skin healing at various times in the wound healing process [6]. The evidence for wound healing support is strongest for copper and zinc, and these will be tried first. Another step would be to coat the 93B3 glass fibers with a material such as a growth factor [17] or peptide [18] that promotes wound healing. There are significant practical hurdles in adding degradable proteins to the glass composition. As discussed previously, the bioactive glasses release ions in a controlled manner over a long period of time (days to weeks), which may have benefits in the wound healing process compared to a short burst of growth factor [7]. A non-healing model would also be useful especially in determining any differences between the control and the glass fiber during the endothelial cell migration stage of healing.

Acknowledgements

The authors wish to thank Vernon Modglin for his assistance with the animal surgeries, Penny McCormick of Phelps County Regional Medical Center for her assistance with the histological staining, and Dr. Anna Maglia for use of her histology equipment.

6.6 REFERENCES

1. Hench LL, Paschall HA. Direct chemical Bond of Bioactive Glass-Ceramic Materials to Bone and Muscle. J. Biomed. Mater. Res. 1973;4:25-42.
2. Leach JK, Kaigler D, Wang Z, Krebsbach PH, Mooney DJ. Coating of VEGF-releasing scaffolds with bioactive glass for angiogenesis and bone regeneration. Biomaterials 2006;27:3249-3255.
3. Asikainen AJ, Hagstrom J, Sorsa T, Noponen J, Kellomaki M, Juuti H, Lundqvist C, Hietanen J, Suuronen R. Soft Tissue Reactions to Bioactive Glass 13-93 Combined with Chitosen. J. Biomed. Mater. Res. 2007;83A:530-537.
4. Fu Q. PhD Dissertation. Rolla, MO: Missouri University of Science and Technology; 2009.
5. Rahaman MN, Day DE, Brown RF, Fu Q, Jung SB. Nanostructured Bioactive Glass Scaffolds for Bone Repair. 32nd Int. Conf. Adv. Cer. Comp. 2008.
6. Lansdown ABG. Calcium: a potential central regulator in wound healing in the skin. Wound Repair and Regen. 2002;10:271-285.
7. Singer AJ, Clark RAF. Cutaneous Wound Healing. New Eng. J. Med. 1999;341(10):738-746.
8. Leipply D, Melhus BA, Leonardo MR, Feller SA, Affatigato M. Development of Functional Borate Glass Surfaces to Inhibit Bacterial Growth. Glass Tech. 2006;47A(5):127-132.
9. Hench LL. The story of Bioglass. J. Mater. Sci.: Mater. Med. 2006;17(11):967-978.
10. Hench LL, Wilson J. Surface-Active Biomaterials Science 1984;226:630-636.
11. Jung SB, Day DE. Conversion kinetics of silicate, borosilicate, and borate bioactive glasses to hydroxyapatite. Phy. Chem. Glass. 2009;50(2):85-88.
12. Huang W, Rahaman MN, Day DE, Li Y. Mechanisms for Converting Bioactive Silicate, Borate, and Borosilicate Glasses to Hydroxyapatite in Dilute Phosphate Solution. Phy. Chem. Glass. 2006;47B(6):1-12.
13. Jung SB, Day DE, Brown RF. Comparison of self-bonded three dimensional bioactive glass fiber scaffolds after in-vivo implantation in rats. J. Am. Cer. Soc. 2009, accepted.
14. Berlin A, Cohen JL, Goldberg DJ. Calcium hydroxyapatite for facial rejuvenation. Sem. Cutaneous Med. Surg. 2006;25:132-137.
15. Dzondo-Gadet M, R M-N, Hess K, Nabet P, Belleville F, Dousset B. Action of Boron at the Molecular Level. Bio. Trace Element Res. 2002;85:23-33.
16. McAuslan BR, Reilly W. Endothelial Cell Phagokinesis in Response to Specific Metal Ions. Exp. Cell Res. 1980;130:147-157.
17. Rouwkema J, Rivron NC, Blitterswijk CAv. Vascularization in Tissue Engineering. Trends in Biotech. 2008;26(8):434-441.
18. Stiernberg J, Norfleet AM, Rendin WR, Warner WS, Fritz RR, Carney DH. Accelleration of full-thickness wound healing in normal rats by synthetic thrombin peptide TP508. Wound Repair and Regen. 2000;8:204-215.

TABLES

Table 1. Statistical Significance Between the Control wounds and the 93B3 Filled Wounds For Wound Closure, the Gap in Subcutaneous Tissue at 22 Days, and the Thickness of Granulation Tissue at 22 Days as Determined by the Student t Test

Control	93B3 Fiber	p value	Statistically Significant
4 days	4 days	0.5743	No
7 days	7 days	0.3518	No
11 days	11 days	0.3459	No
15 days	15 days	0.2599	No
18 days	18 days	0.9657	No
Subcutaneous Gap (22 days)	Subcutaneous Gap (22 days)	0.4985	No
Granulation Thickness (22 days)	Granulation Thickness (22 days)	0.9488	No

FIGURES

Figure 1 – Optical photograph of as-formed 93B3 fibers (300nm to 5μm diameter).

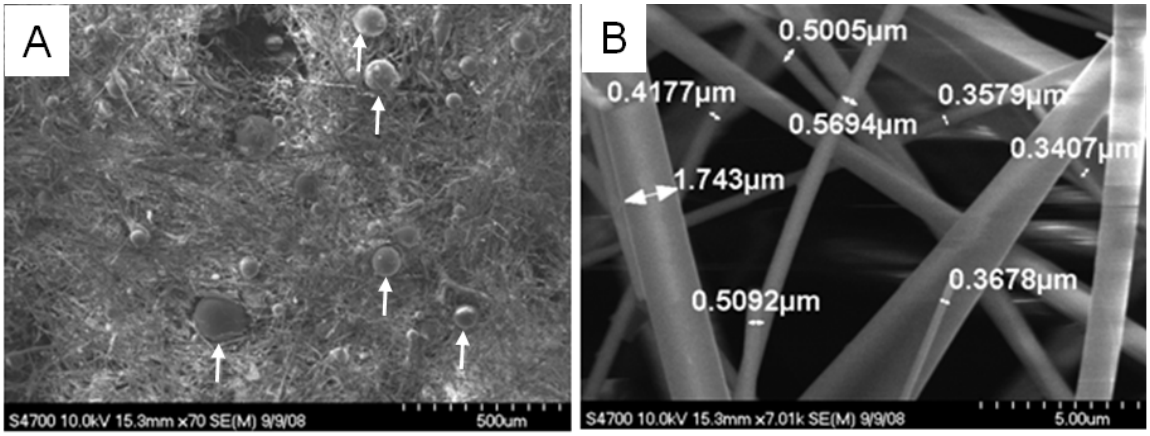

Figure 2 – SEM micrographs of the as-made 93B3 fiber. The image in Fig 2B is a higher magnification of the fibers, which range in diameter from submicron to micron (as labeled).

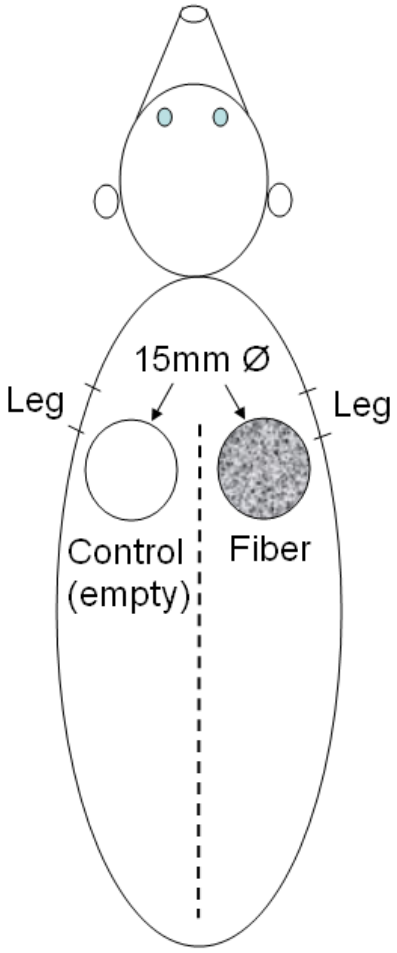

Figure 3 – Schematic of the wound placement on the rats.

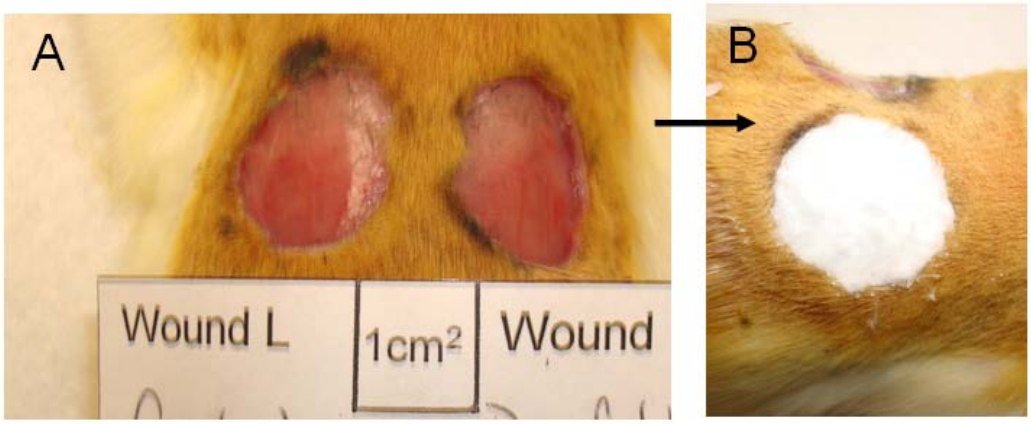

Figure 4 – Photograph of a Sprague Dawley rat showing the full thickness cutaneous defects. Fig 4A shows both freshly formed wounds (15mm diameter) just posterior to the front shoulders. Figure 4B shows the wound after being treated with 93B3 fiber (white material).

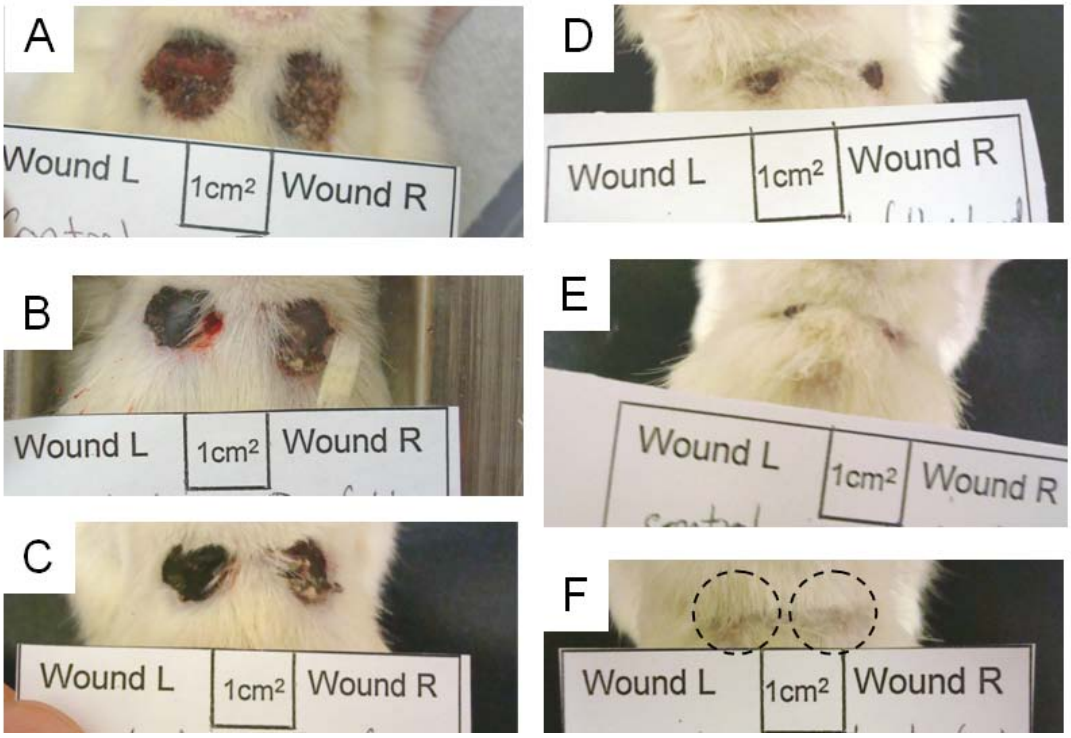

Figure 5 – Progression of wound closure for the full thickness subcutaneous wounds. The times shown are (A) 4 days, (B) 7 days, (C) 11 days, (D) 15 days, (E) 18 days, and (F) 22 days. The control is on the left side and the 93B3 fiber filled wound is on the right. The approximate original wound size is shown by the dashed circles in Fig 5F.

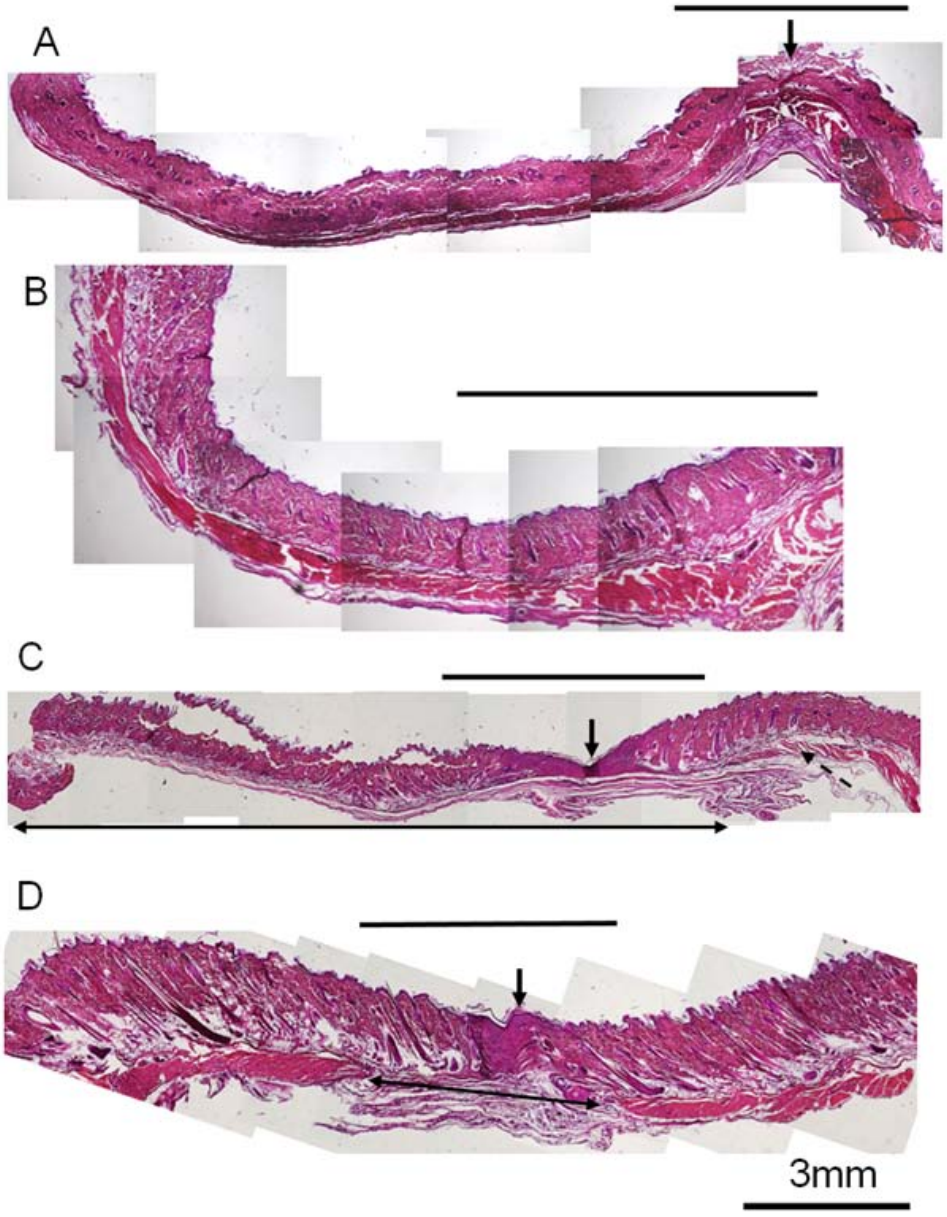

Figure 6 – Histological sections of the full thickness cutaneous control wounds after 22 days (H&E).

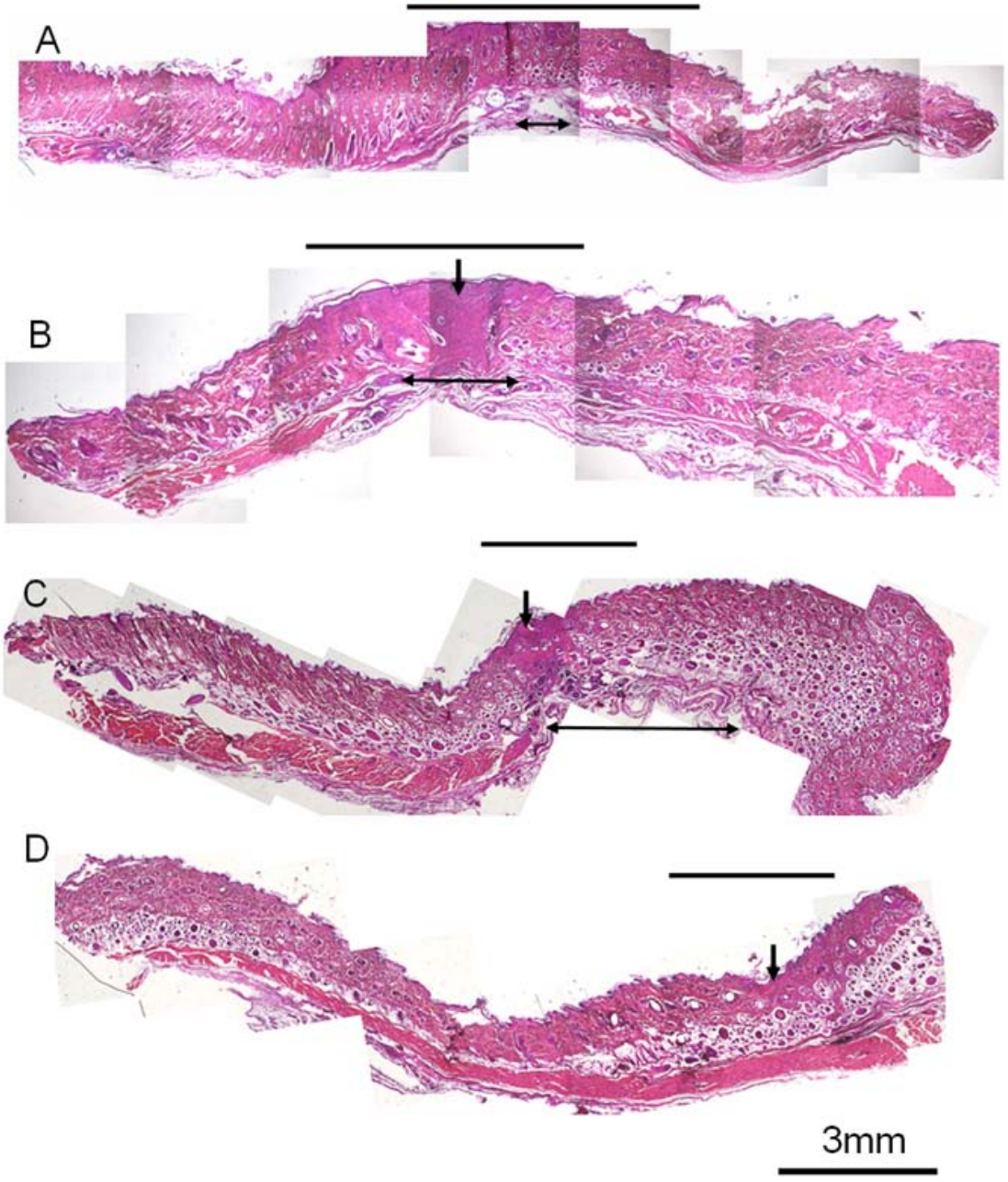

Figure 7 - Histological sections of the full thickness cutaneous 93B3 bioactive glass filled wounds after 22 days (H&E). The black line at the top of each tissue section denotes where there is unhealed tissue. The double ended arrows show the gap in the subcutaneous tissue and the vertical indicate granulation tissue.

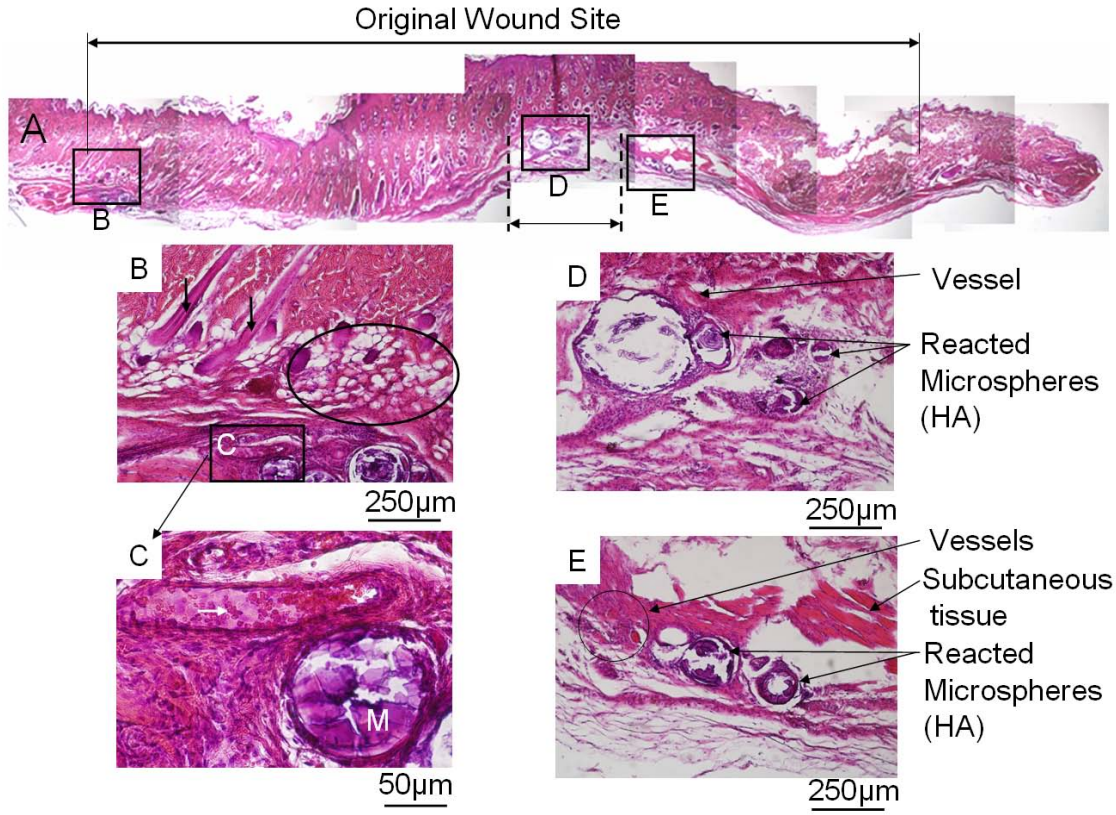

Figure 8 – Histological assessment of a 93B3 filled full thickness cutaneous wound after 22 days.

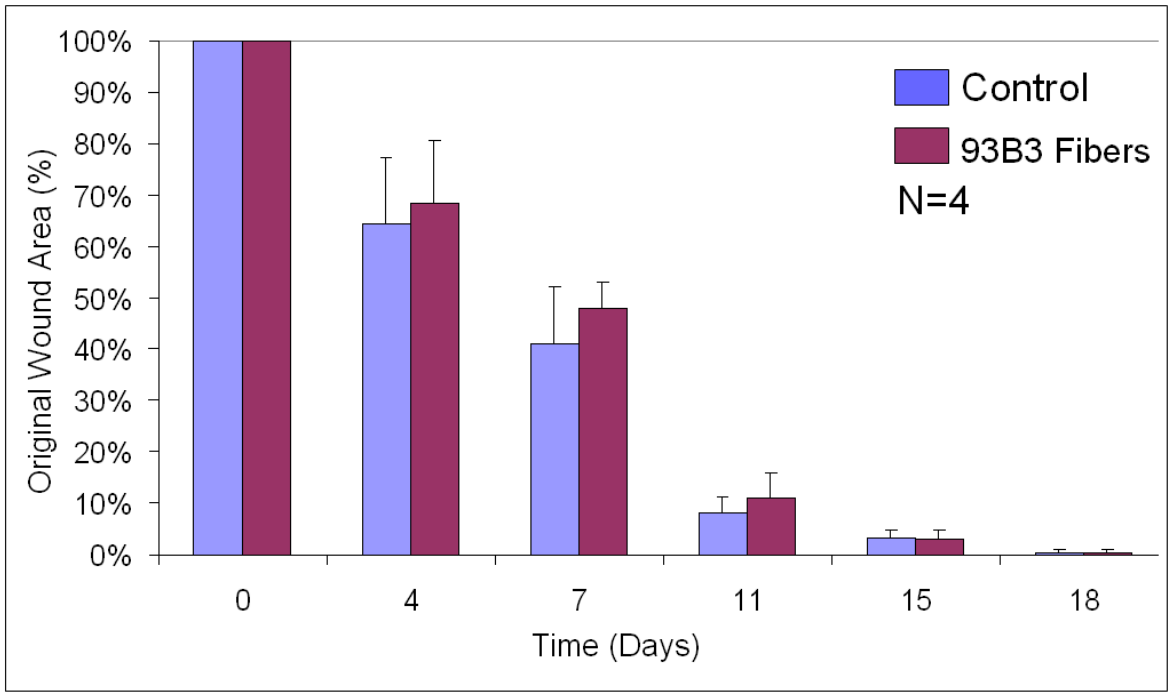

Figure 9 – Comparison of the original wound (%) vs. time for the control (blue) and the wound treated with the 93B3 fiber pad (red).

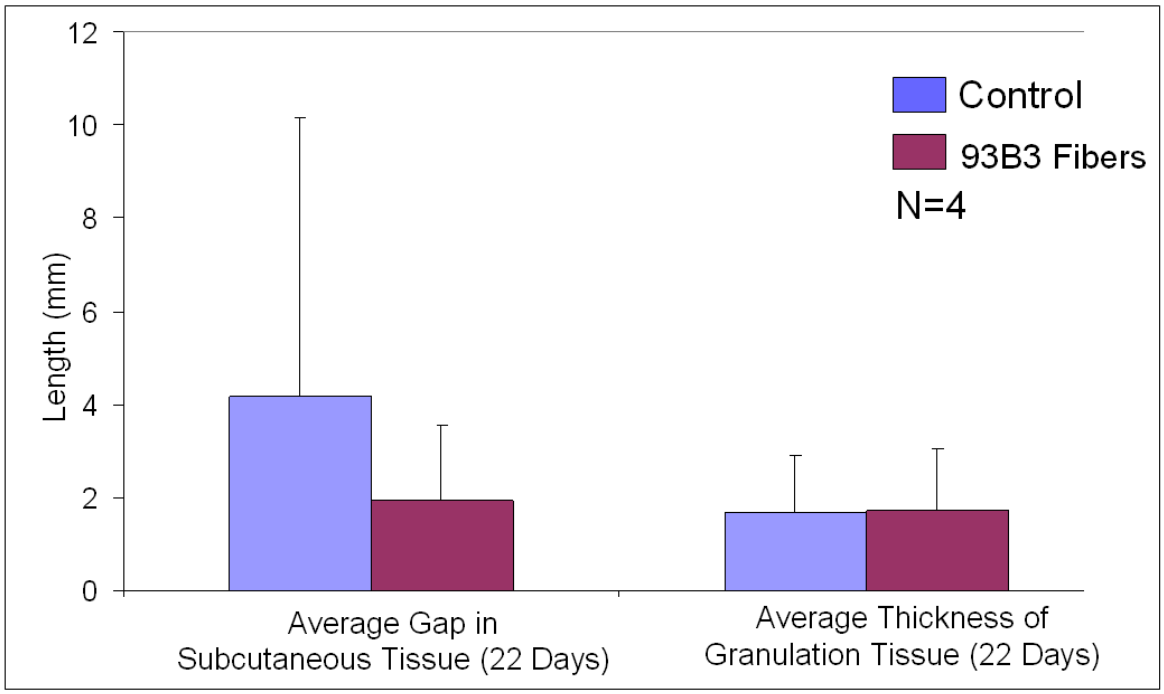

Figure 10 – Average gap in the subcutaneous tissue and average thickness of the granulation tissue present in the 22 day sections. The control is blue and the 93B3 fiber treated (red).

3. CONCLUSIONS

This section combines and summarizes the main conclusions from each of the six manuscripts from the body of the dissertation.

1. Boron released from 13-93B3 scaffolds at an estimated concentration of <126mg/kg/day (sixteen 70mg scaffolds reacting in four weeks) caused no *in-vivo* toxicity in adjacent tissue or systemic organs. The kidney and liver were analyzed from sacrificed rats and no pathological changes beyond incidental were reported. When a 13-93B3 scaffold was placed in a bone site, there was no increase in macrophages or other inflammatory cells, and there was no necrotic tissue in the new bone adjacent the 13-93B3 scaffolds after 12 weeks.
2. Scaffolds composed of 13-93B3 fibers had significantly more bone after 12 weeks in rat calvaria ($p<0.05$) than silicate based 13-93 scaffolds indicating the borate glass was a better bone growth promoter. The reason behind the increased bone regeneration in the borate scaffold is thought to be due to the faster reaction of the scaffold which increased the rate of calcium release. Calcium is known to act as a bone growth stimulator by promoting osteoblast migration and proliferation.
3. Bioactive borate glass was doped with trace elements (copper and zinc) which significantly improved angiogenesis (blood vessel formation) in the soft tissue inside porous, randomly oriented fiber scaffolds. Angiogenesis is important in sustaining tissue growth in scaffolds, and glasses doped with these elements could be an important improvement in increasing the size of tissue engineering scaffolds.

4. For the first time, bioactive glasses containing calcium were made to form non-calcium phosphates when reacted *in-vivo*. The conversion of the glass is thought to be controlled by the size of the atom added as a trace element to the glass. It is speculated that the smaller the ion, the more profound the effect on the inhibition of hydroxyapatite.
5. Cutaneous soft tissue defects were successfully treated with nano fibers of 13-93B3 glass, and the quality of the scar was better than the control (untreated wound). Ions such as calcium are known to increase epithelial cell migration *in-vitro* and are hypothesized to have several physiological roles in wound healing. The reaction of the glass and release of ions such as calcium are assumed to improve wound healing.
6. The hollowing of 13-93B3 fibers when reacted *in-vivo* often had soft tissue and blood vessels present inside. The vessels grew along the length of the fiber, so it is thought that bioactive glass fibers could be used as a method of directing the growth of blood vessels or nerves.

4. FUTURE WORK

1. Continue studies into the potential toxicity of boron in-vivo. The more data the better. Collection of urine and subsequent measure of boron during the reaction of the glass could be a good measure of how the glasses reacted *in-vivo*. Little is known at this point about how boron is released or if it changes as a function of time. Rats are a good model for boron toxicity since they are more sensitive to boron that mice or rabbits.
2. Understanding more about calcium as the major bone promoter from bioactive glass could be important, especially for future use and acceptance of silica free bioactive glasses. *In-vitro* cell culture work on the migration and proliferation of osteoblasts and other tissues in the presence of calcium, or *in-vivo* work with additional silica free glasses with even faster release rates (CaLiB) could be interesting for enhanced bone formation.
3. The angiogenic response of soft tissue with the doped bioactive borate glasses (copper and zinc) could be important in improving bone and soft tissue scaffolds and wound healing treatments. Blood vessel guides and treatment of diabetic or non-healing ulcers could be made partially or wholly from these glasses and significantly improve the treatment options.
4. The conversion of glasses to non-HA materials is a new area of work that has a lot of possibilities. Calcium compounds such as calcite have been reported to be degraded faster than HA by osteoclasts *in-vitro*. It may be possible to control the calcium phosphate phase that forms and make tricalcium phosphate or brushite *in-vivo*. Calcium free glasses replaced with barium or strontium may have benefits

in tissue engineering or other fields of study. In the past, *in-vitro* reaction has simulated the *in-vivo* reaction; so much of this work may be possible *in-vitro*. In addition, other trace elements could be added to the glass, singularly, or in combination to see if phases can be shifted by straining the crystal structure and how solid solutions affect the formation of new materials.

5. The change from a mono layer of HA to a layered structure in borate glasses such as 13-93B3 is still not understood. Borate glasses have been reported to form these layers for almost 15 years, and several reasons for the formation have been suggested, but this phenomenon has never been formally studied. Controlling or at least understanding this microstructural change could be beneficial for making new devices for controlled drug release or other new technologies.
6. Wound healing is potentially a huge new area of study for bioactive glass. The body is compatible with bioactive glass, and the controlled release of ions can be achieved that can improve the rate of healing. The reaction products of bioactive glasses also tend to be antimicrobial, so the glasses may be of use in treating bacterial infections locally in people that are resistant to penicillin.
7. One tissue not studied in the present work was the avascular tissue cartilage. Cartilage survives by diffusion of nutrients and oxygen to blood vessels that exist outside of the tissue. Cartilage is also slow to heal is damaged and healing could be enhanced by the addition of particles of fibers of the angiogenic glasses. A vasculature inside the cartilage scaffold could enhance the rate of diffusion in the scaffold and decrease healing time.

APPENDIX A

POTENTIAL TOXICITY OF BORATE GLASSES IN-VITRO AND IN-VIVO

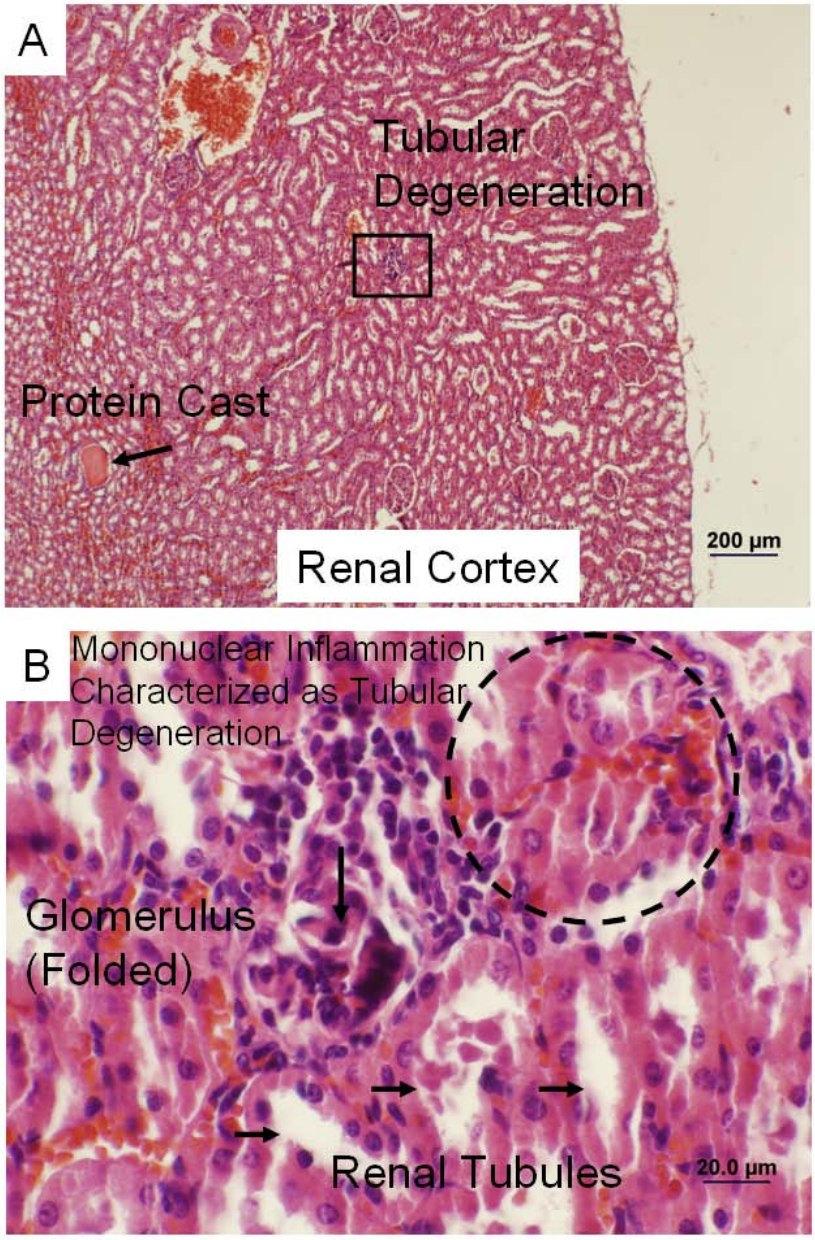

Figure 1 - Photomicrograph of an H&E stained section of the renal cortex from a rat that contains protein casts and tubular degeneration (Fig 1A). Figure 1B is a magnified view of the renal cortex showing a folded glomerulus as indicated by the vertical arrow, renal tubes (horizontal arrows) and mononuclear inflammation characterized as tubular degeneration (dashed circle).

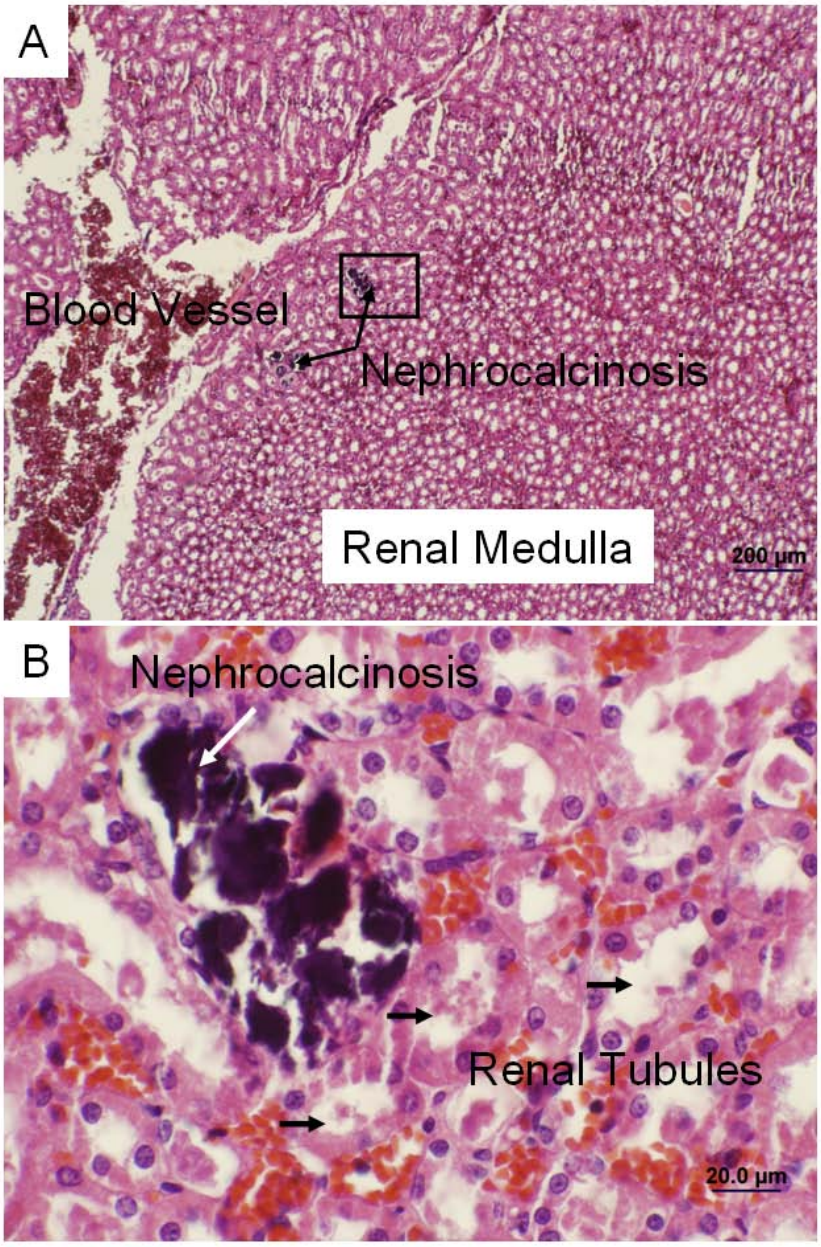

Figure 2 - Photomicrograph of an H&E stained section of the renal medulla from a rat that contains nephrocalcinosis (arrows) and a large blood vessel on the left of the image (Fig 2A). Figure 2B is a magnified view of the renal medulla showing nephrocalcinosis as indicated by the white arrow and renal tubules (horizontal arrows).

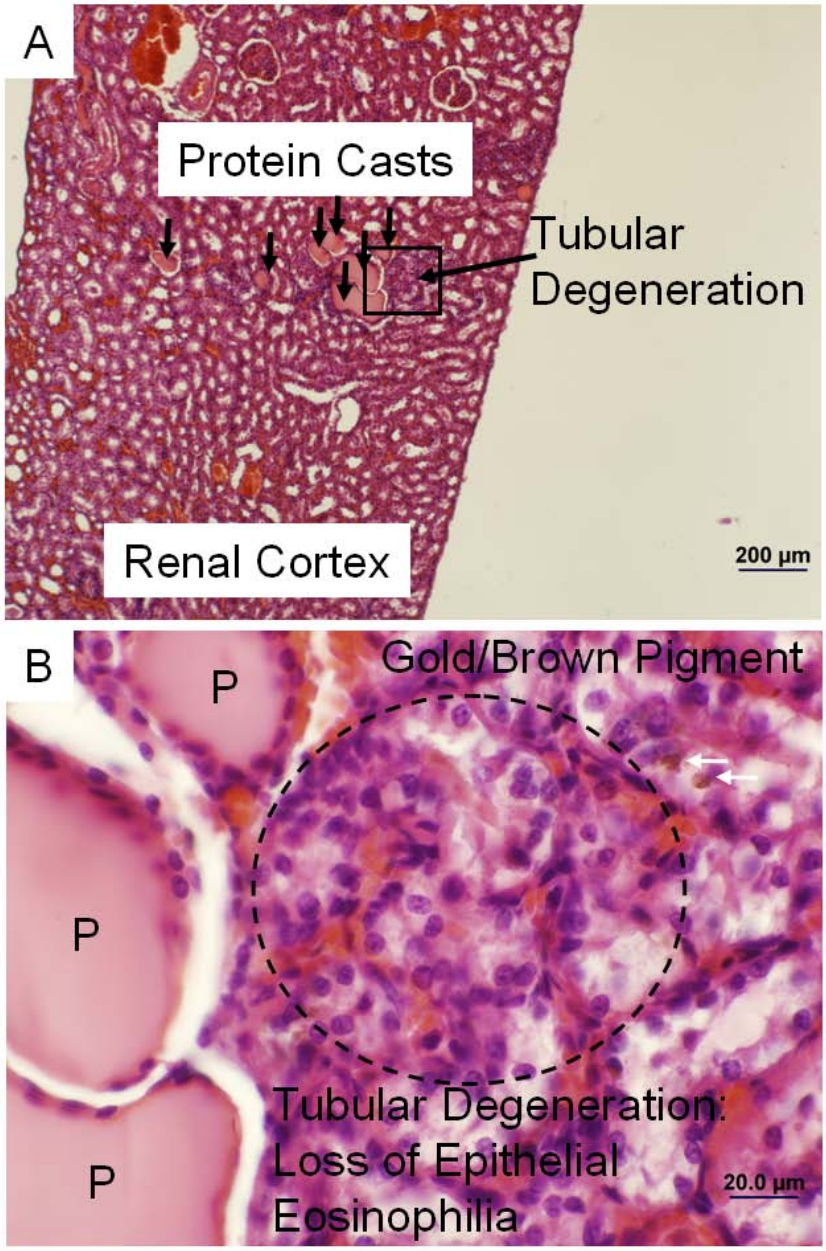

Figure 3 - Photomicrograph of an H&E stained section of the renal cortex from a rat that contains protein casts and tubular degeneration (Fig 3A). Figure 3B is a magnified view of the renal cortex showing three protein casts (P), tubular degeneration due to loss of the epithelial eosinophilia (dashed circle), and gold/brown pigment indicative of infiltrates of mononuclear inflammatory cells.

APPENDIX B

ANGIOGENIC BIOACTIVE BORATE GLASSES

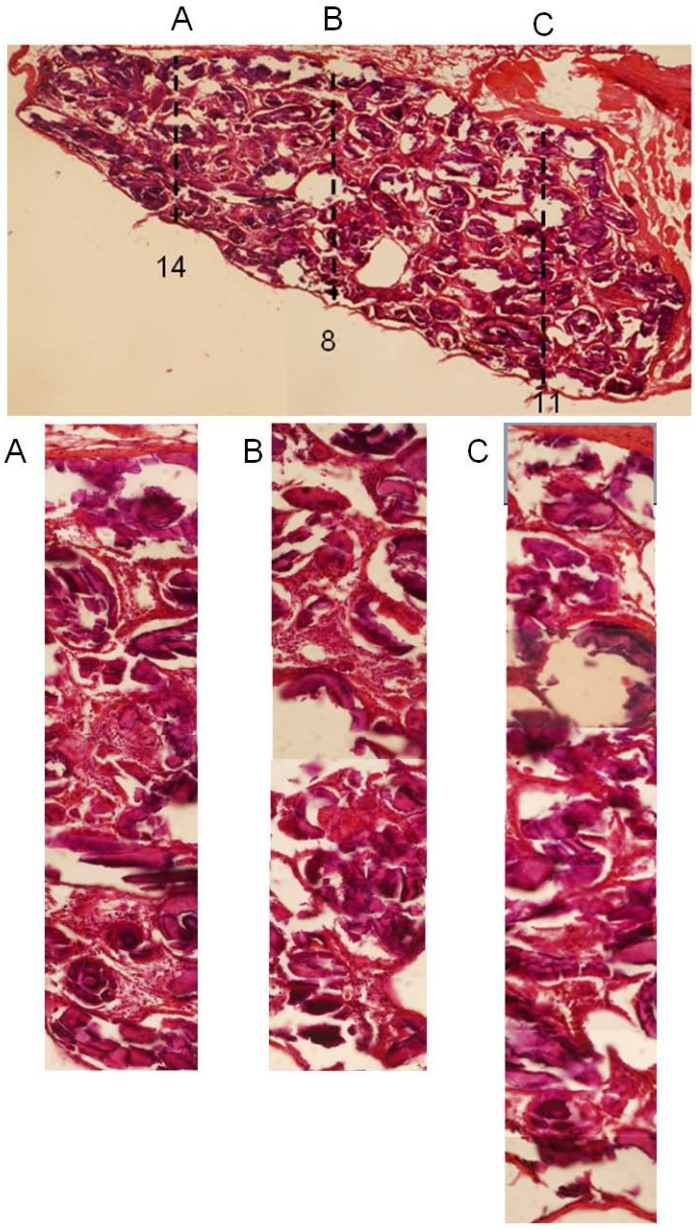

Figure 1 – H&E stained section of a Cu-3 scaffold (1 of 3) used for the blood vessel analysis. The three strips counted in this section are indicated by the dashed lines in the whole section and a magnified view of the strips is shown below. The number of vessels from each strip were 14 (A), 8 (B), and 11(C), respectively. The original scaffold diameter was 7mm.

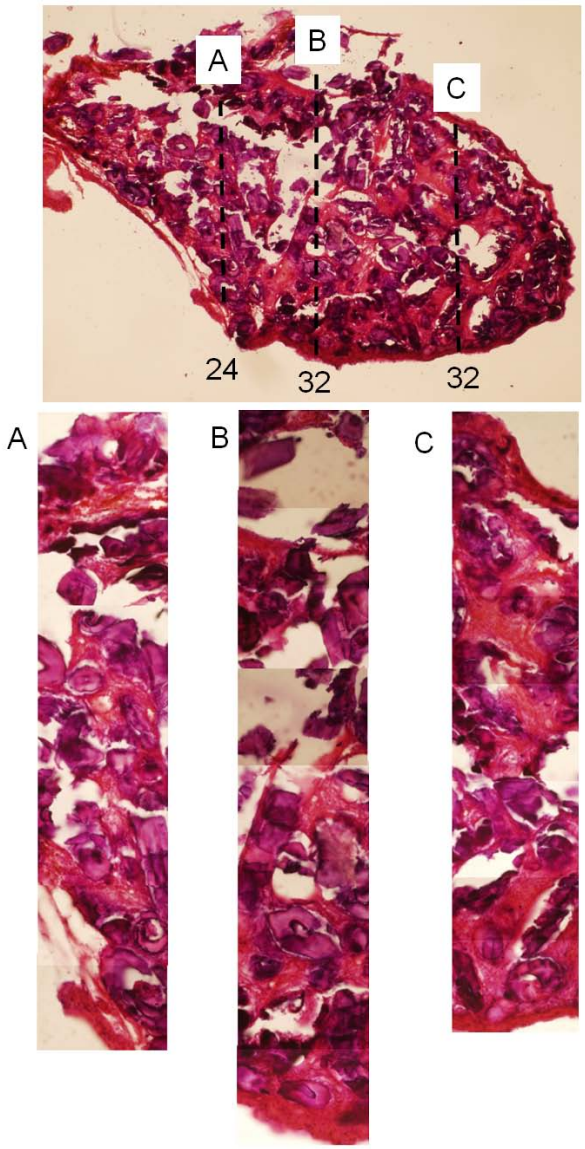

Figure 2 – H&E stained section of a Cu-3 scaffold (2 of 3) used for the blood vessel analysis. The three strips counted in this section are indicated by the dashed lines in the whole section and a magnified view of the strips is shown below. The number of vessels from each strip were 24 (A), 32 (B), and 32(C), respectively. The original scaffold diameter was 7mm.

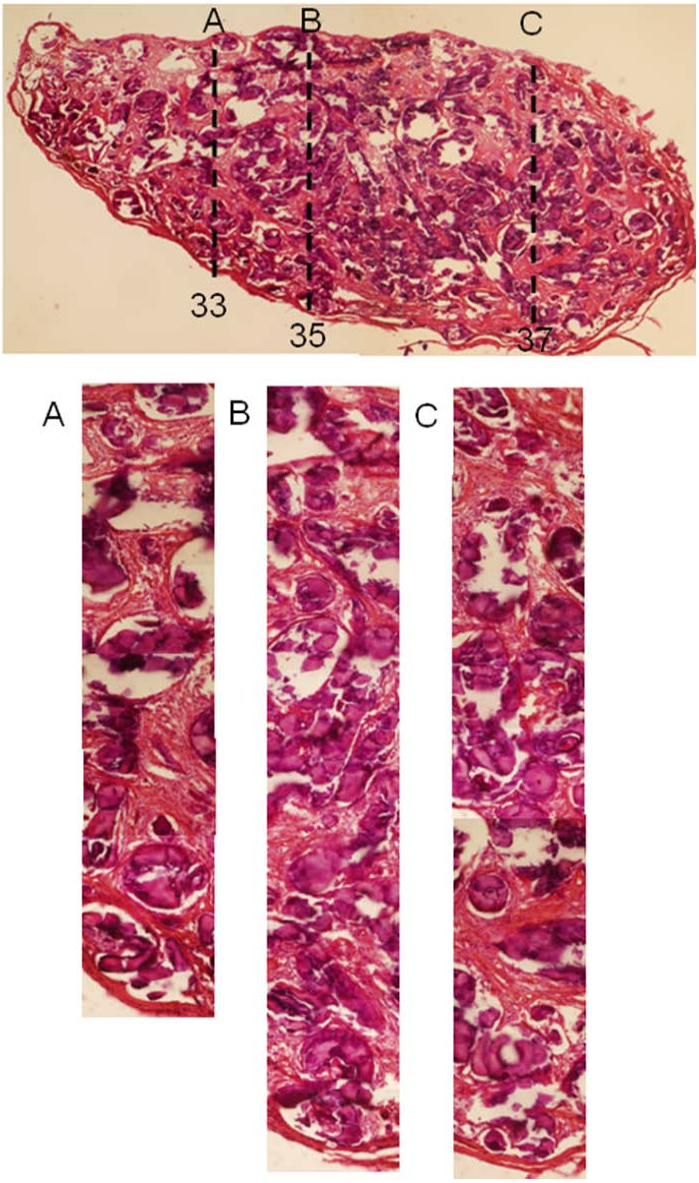

Figure 3 – H&E stained section of a Cu-3 scaffold (3 of 3) used for the blood vessel analysis. The three strips counted in this section are indicated by the dashed lines in the whole section and a magnified view of the strips is shown below. The number of vessels from each strip were 33 (A), 35 (B), and 37(C), respectively. The original scaffold diameter was 7mm.

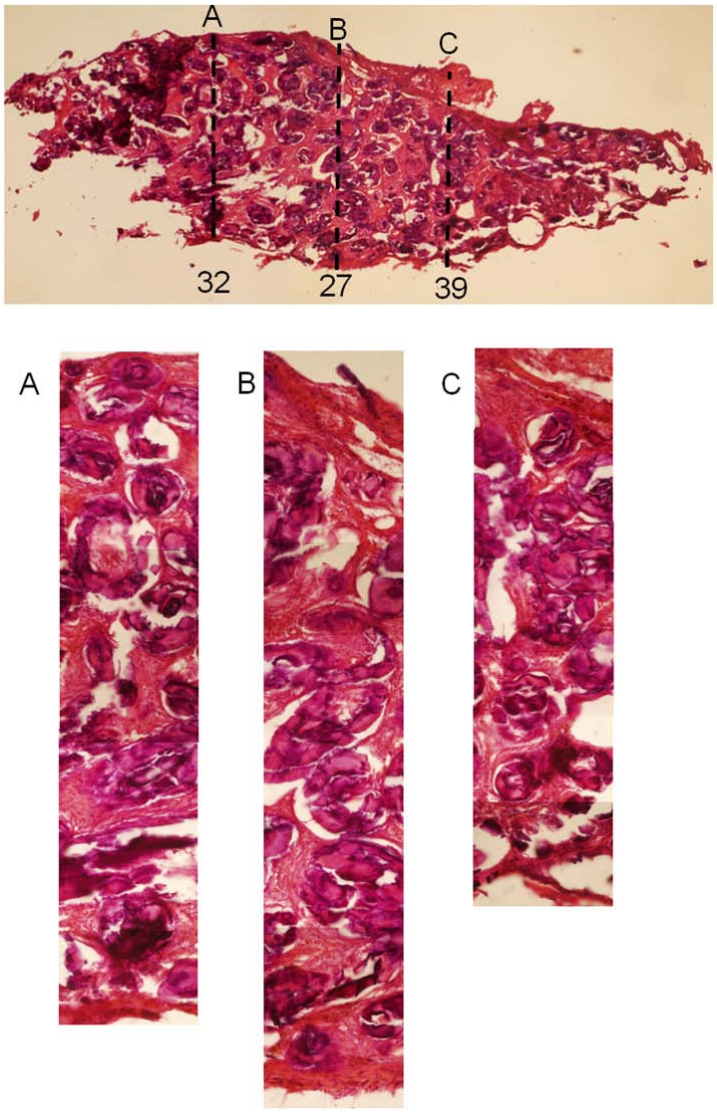

Figure 4 – H&E stained section of a CS scaffold (1 of 3) used for the blood vessel analysis. The three strips counted in this section are indicated by the dashed lines in the whole section and a magnified view of the strips is shown below. The number of vessels from each strip were 32 (A), 27 (B), and 39(C), respectively. The original scaffold diameter was 7mm.

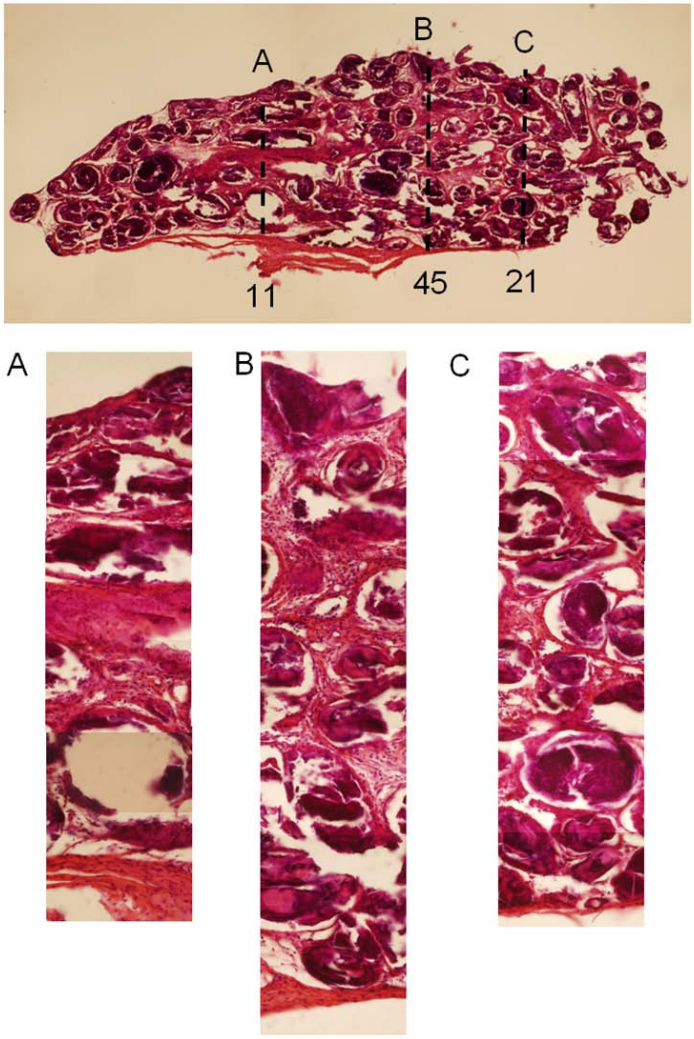

Figure 5 – H&E stained section of a CS scaffold (2 of 3) used for the blood vessel analysis. The three strips counted in this section are indicated by the dashed lines in the whole section and a magnified view of the strips is shown below. The number of vessels from each strip were 11 (A), 45 (B), and 21(C), respectively. The original scaffold diameter was 7mm.

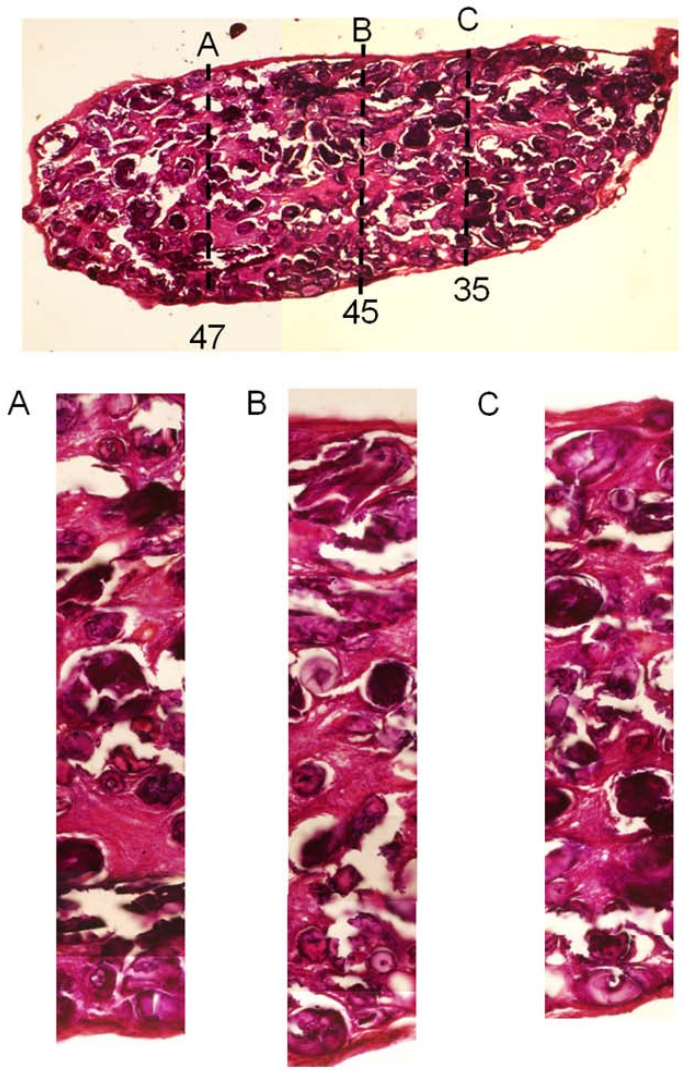

Figure 6 – H&E stained section of a CS scaffold (3 of 3) used for the blood vessel analysis. The three strips counted in this section are indicated by the dashed lines in the whole section and a magnified view of the strips is shown below. The number of vessels from each strip were 47 (A), 45 (B), and 35(C), respectively. The original scaffold diameter was 7mm.

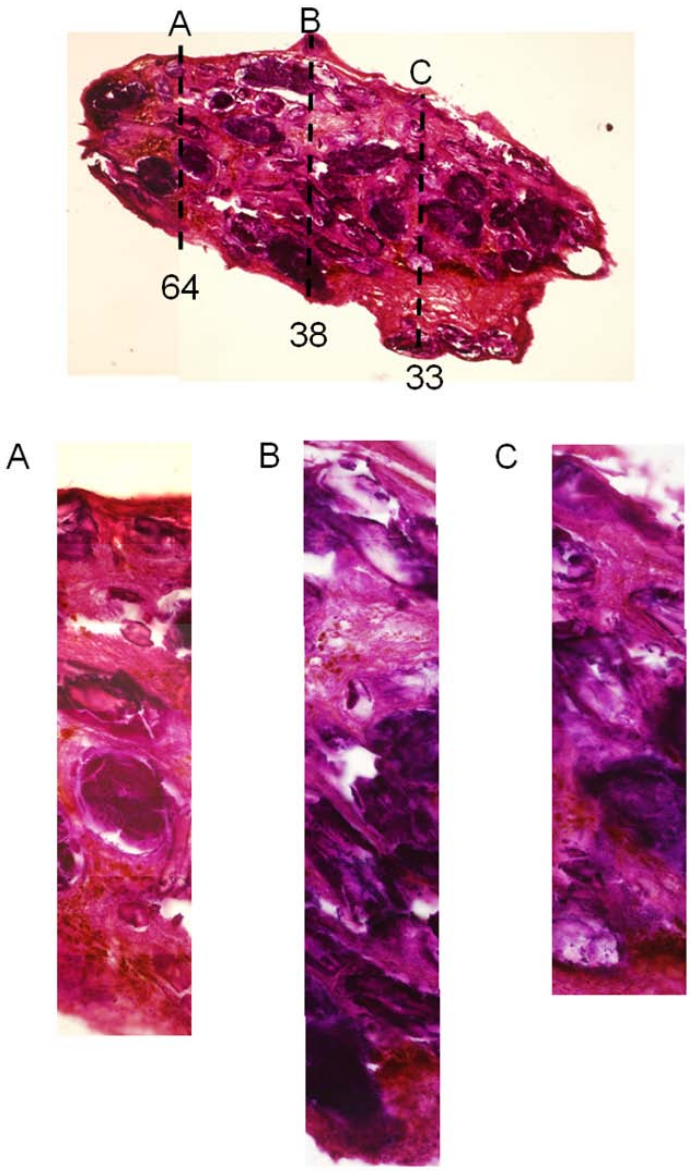

Figure 7 – H&E stained section of a CSZ scaffold (1 of 3) used for the blood vessel analysis. The three strips counted in this section are indicated by the dashed lines in the whole section and a magnified view of the strips is shown below. The number of vessels from each strip were 64 (A), 38 (B), and 33(C), respectively. The original scaffold diameter was 7mm.

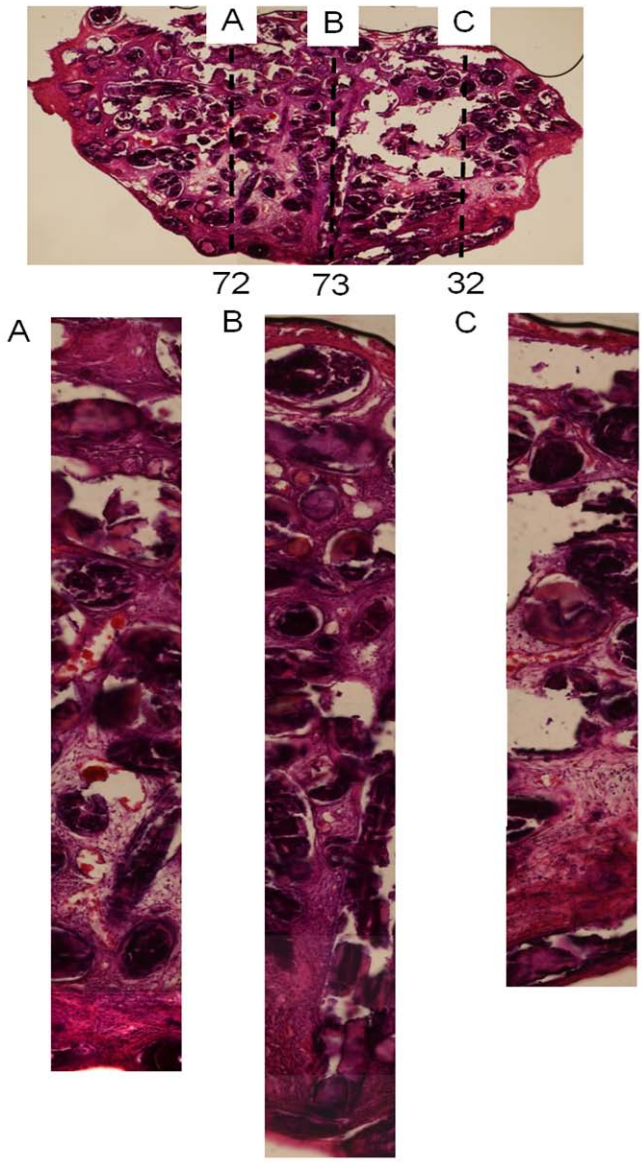

Figure 8 – H&E stained section of a CSZ scaffold (2 of 3) used for the blood vessel analysis. The three strips counted in this section are indicated by the dashed lines in the whole section and a magnified view of the strips is shown below. The number of vessels from each strip were 72 (A), 73 (B), and 32(C), respectively. The original scaffold diameter was 7mm.

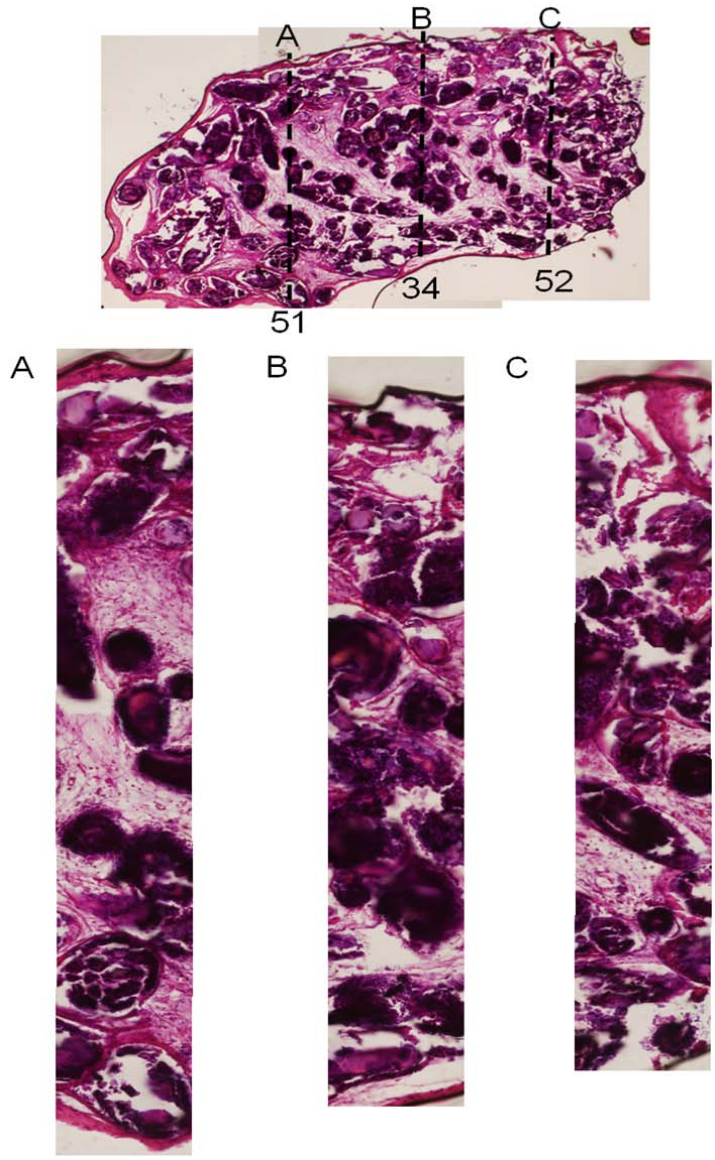

Figure 9 – H&E stained section of a CSZ scaffold (3 of 3) used for the blood vessel analysis. The three strips counted in this section are indicated by the dashed lines in the whole section and a magnified view of the strips is shown below. The number of vessels from each strip were 51 (A), 34(B), and 52(C), respectively. The original scaffold diameter was 7mm.

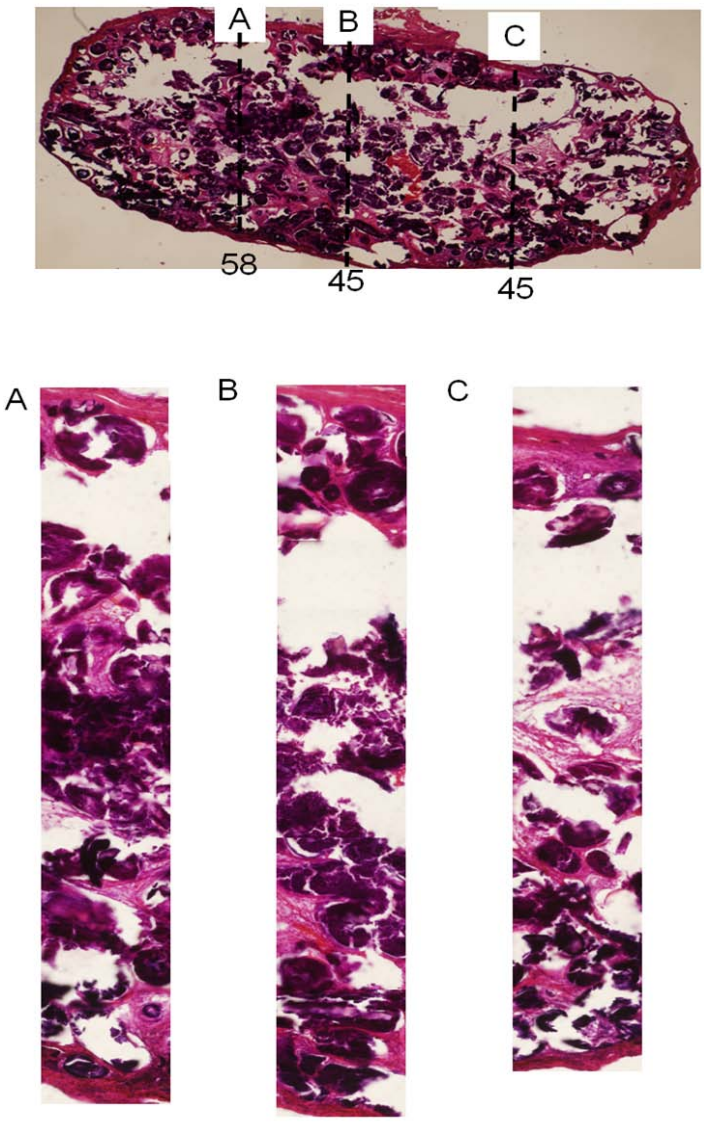

Figure 10– H&E stained section of a CSZF scaffold (1 of 3) used for the blood vessel analysis. The three strips counted in this section are indicated by the dashed lines in the whole section and a magnified view of the strips is shown below. The number of vessels from each strip were 58 (A), 45(B), and 45(C), respectively. The original scaffold diameter was 7mm.

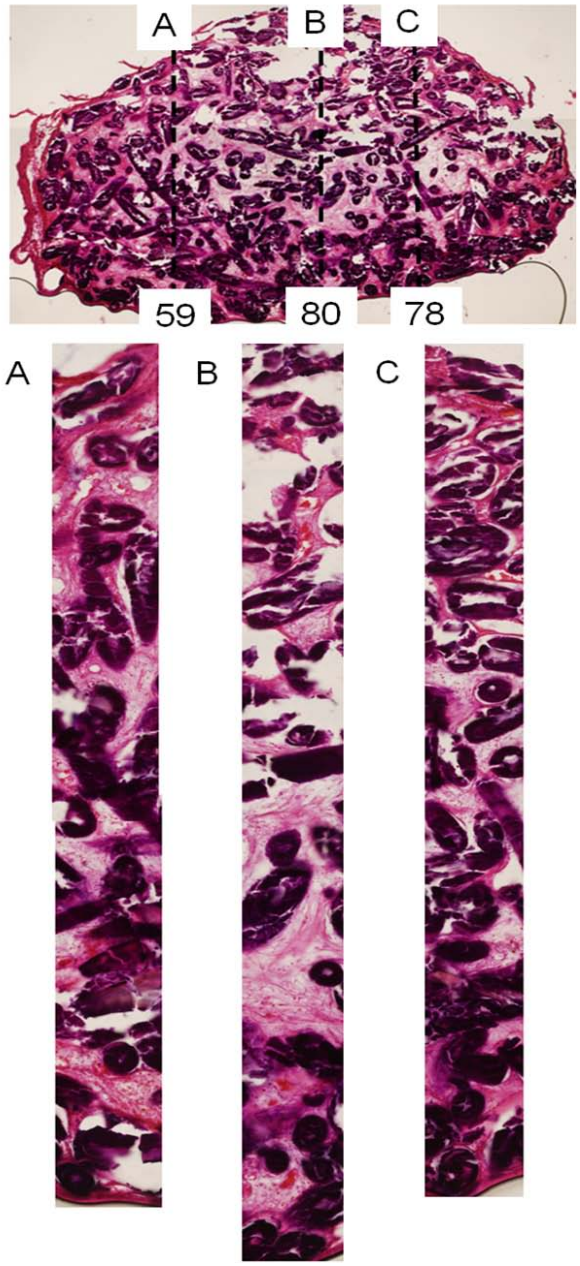

Figure 11– H&E stained section of a CSZF scaffold (2 of 3) used for the blood vessel analysis. The three strips counted in this section are indicated by the dashed lines in the whole section and a magnified view of the strips is shown below. The number of vessels from each strip were 59 (A), 80(B), and 78(C), respectively. The original scaffold diameter was 7mm.

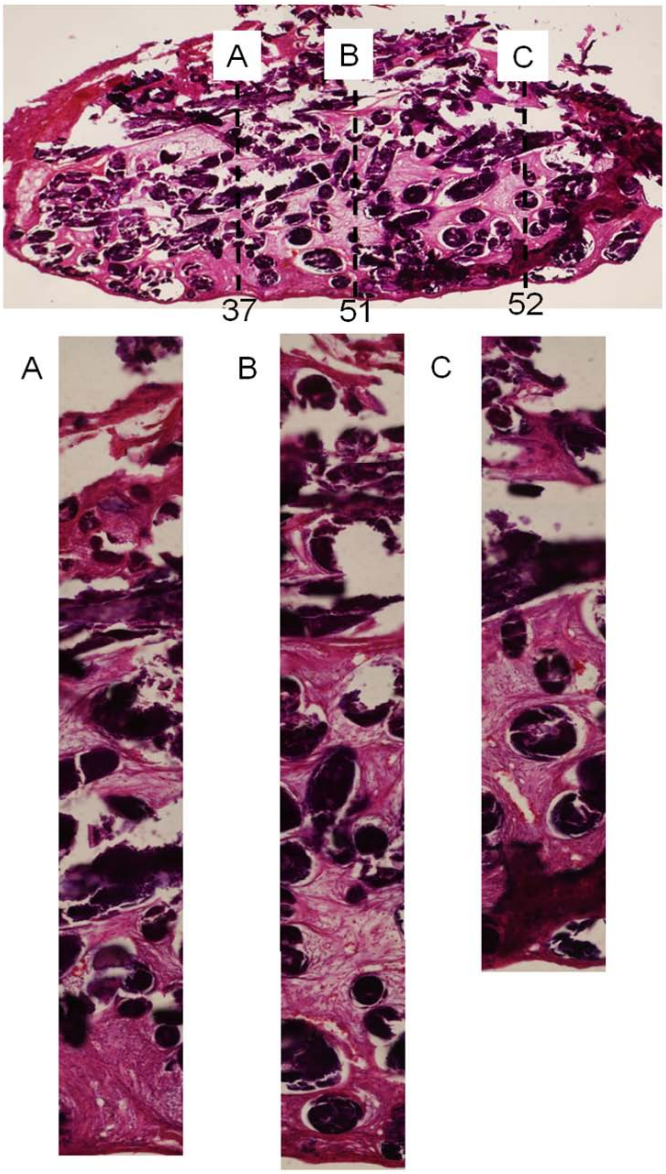

Figure 12– H&E stained section of a CSZF scaffold (3 of 3) used for the blood vessel analysis. The three strips counted in this section are indicated by the dashed lines in the whole section and a magnified view of the strips is shown below. The number of vessels from each strip were 37 (A), 51(B), and 52(C), respectively. The original scaffold diameter was 7mm.

APPENDIX C

BIOACTIVE GLASS SCAFFOLDS FOR SOFT TISSUE REGENERATION

BIOACTIVE GLASS SCAFFOLDS FOR SOFT TISSUE REGENERATION

By

Steven Jung, Missouri University of Science and Technology

ABSTRACT

Melt derived fibers of 13-93 glass have been made into three dimensional random oriented scaffolds for soft tissue regeneration. The scaffolds were implanted in the subcutaneous tissue of rats from two to twenty eight weeks. Significant vascularization and tissue growth was evident after just two weeks in-vivo. The 13-93 glass fibers reacted with the body fluids at a rate of approximately 3μm a week during the duration of the experiment and formed a layer of hydroxyapatite (HA) at the fiber-tissue interface. Collagen, the building block of both hard and soft tissue, was also found coating the reacted glass fibers indicating that the 13-93 glass fibers may be a useful material for soft tissue augmentation and wound dressing.

INTRODUCTION

Bioactive glasses have been known to bond to bone since 1969 [1, 2]. Treatment of middle ear and periodontal defects led to the first investigations into soft tissue bonding of bioactive glass [1, 2]. Wilson showed soft tissue interactions with silicate based bioactive glasses were similar to interactions with bone, first forming a silica gel layer followed by the precipitation of an amorphous calcium phosphate which then crystallized to the crystalline material known as hydroxyapatite (HA) [1, 2]. These first studies indicated that bioactive glasses may one day have use in the treatment of damaged soft tissue.

Like bone, damaged tissues such as skin, muscle, and internal organs need a substrate to which they can attach and grow for effective healing. Scaffolds made of degradable and bioactive materials are preferred as they provide a resorbable substrate beneficial to tissue growth. Polymers alone are not bioactive; however, bioactive glasses or composites of polymers and bioactive glasses show significant promise for treatment of damaged soft tissue. Leu et. al. incorporated 45S5 bioactive glass into a collagen substrate and found that the addition of the glass had a proangiogenic effect[3]. Leach made a polymer scaffold with embedded 45S5 bioactive glass, and used it to release vascular endothelial growth factor (VEGF) and studied the angiogenic effect for use in hard and soft tissue applications [4].

The maximum distance tissue can survive is approximately 100 to 200μm from a blood vessel, so new blood vessel formation is necessary for wounds to heal [5]. Specific to placing artificial materials such as bioactive glass scaffolds in the body, tissues cannot grow into and fill the scaffold until a network of blood vessels have first penetrated the scaffold or at least are promoted to penetrate the scaffold as surrounding tissue infiltrates the scaffold. The importance of vascularization to wound healing is significant and should not be ignored [5]. Vascular endothelial growth factor has been isolated as one of the most important signals for wound healing. Several growth factors natural to the body have been identified as important to wound healing, however, none are as prevalent or have the long-term stimulatory effects for vascular growth as VEGF[6].

The well known bioactive glass, 45S5, is difficult to heat treat to form scaffolds or to pull into continuous fibers, so, other silicate based glasses have been developed with longer working ranges for improved processing [7, 8]. Another bioactive glass known as

13-93 has been used successfully to produce scaffolds with a variety of porosities and microstructures [9-12]. Three dimensional scaffolds composed of 13-93 have been shown to bond to soft tissue, and significant vascularization was observed when these scaffolds were placed in a subcutaneous site [9, 11].

DISCUSSION

The present work describes the use of bioactive glass 13-93 (53 SiO_2, 20 CaO, 12 K_2O, 6Na_2O, 5MgO, 4P_2O_5 in wt%) as a soft tissue scaffold material. The scaffolds used in the present work were 7mm in diameter, 2mm thick, and weighed approximately 70mg. An example of a 13-93 glass fiber scaffold is shown in Figure 1. These scaffolds were studied for soft tissue and vascular growth along with the reaction of the fiber with body fluids. The scaffolds were made by breaking melt derived 13-93 glass fibers into 2 to 3mm lengths, placing the randomly oriented fibers in a ceramic mold, heating the fibers to a temperature sufficient for thermal bonding, followed by cooling the scaffolds to room temperature. The microstructure of a three dimensional glass fiber scaffold is shown in Fig. 2a. During the bonding process, the fibers soften and the edges round. The softened fibers stick together forming the three dimensional scaffold as shown in Fig 2b. The interconnected porosity of the scaffold is approximately 50%, and its compressive strength is approximately 5 MPa.

Soft tissue growth into 13-93 fiber scaffolds has been studied extensively for scaffolds implanted for times between two and twenty eight weeks in subcutaneous sites in laboratory rats. Typically, four implant sites are used on a single animal as shown in Fig 3. The implant site is just under the skin, and the scaffold is implanted by cutting the

skin and sliding the scaffold under the loosely attached tissue. The picture in the lower right hand corner of Fig 3 shows a scaffold being implanted in a subcutaneous site.

After two weeks in-vivo, the scaffold looks like the one shown in Fig 4. The tissue at A is the subcutaneous tissue underneath the skin, B is the scaffold, and C is the skeletal muscle. The scaffold has become infiltrated with soft tissue, and the scaffold is visibly red from blood vessels that had grown into the scaffold. Prior to extraction, the scaffold had become attached to the subcutaneous tissue indicating the tissue and glass were compatible. There was no measurable change in the overall dimensions of the scaffold.

Figure 5a is a H&E stained micrograph of the tissue present inside a 13-93 scaffold after two weeks in-vivo. The glass fibers are labeled with an 'F'. The soft tissue present between the fibers was healthy and vessels containing red blood cells (pink dots) were present throughout the scaffold. The black vertical arrows denote some of the vessels present in the scaffold in Fig 5a. Soft tissue had grown adjacent to the fibers and no negative immune reaction, such as a walling off of the fibers, was observed. This indicates that the 13-93 glass fibers are compatible with soft tissue and that the reaction products of the glass fibers are not producing an inhospitable environment. The reaction products may in fact be promoting growth as silica and other elements present in the glass have been linked to growth factor release and promotion of tissue growth [13, 14].

Figure 5b is a section of the same two week 13-93 scaffold; however, it was stained with PAS stain which stains red blood cells green and soft tissue purple. Tubule lining such as in vessels appears as a purple ring or outline depending on the vessel orientation. Examples of the vessel lining are shown by the black horizontal arrows. The

vascularity is more evident in the PAS stained section than the H&E stained section as denoted by the large number of vessels (vertical black arrows) throughout Fig 5b. The distance between the vessels in the tissue present in Fig 5b range from ~50 to at most ~100µm, which is considered a sufficiently vascularized tissue [5]. Vascular growth into the scaffold is important because the blood supply is the transportation system for supplying nourishment and oxygen and removal of waste and carbon dioxide. Insufficient vascular density can hinder tissue growth and slows the healing of wounds such as with diabetic ulcers and bed sores.

Figure 6 shows the progressive reaction of the 13-93 glass fibers with the body fluids for 4, 9, and 28 weeks in-vivo. After 4 weeks in subcutaneous tissue, the image in Fig 6a, which is a SEMBSE (backscattered image) of a 13-93 fiber, shows a reaction layer at the outer edge of the fibers. At higher magnification, three distinct layers are present. Layer A is pointing to the 4µm layer hydroxyapatite, B is a 5 to 6µm thick silica gel layer, and C is the unreacted glass. The total reaction layer is approximately 10 to 12µm thick.

Figure 6b is a SEMBSE image of a 13-93 fiber after nine weeks in-vivo. The total reaction layer (HA and silica gel) is up to 30µm thick in some areas, and a non-uniform reaction layer is becoming evident. The non-uniform reaction layer has been documented previously both in-vivo[11] and in-vitro[15], but no explanation for this reaction has been suggested to date.

The SEMBSE image in Fig 6c shows the cross section of a fractured 13-93 fiber after 28 weeks in-vivo. The fiber has nearly reacted completely with the physiological fluids; the outer surface at A is a 30µm thick layer of HA. The silica gel layer designated

by B is approximately 6 to 8μm thick, and the unreacted material at the center (C) is composed of SiO_2, CaO, and P_2O_5. None of the Na_2O, K_2O, or MgO from the starting fibers was detected at 28 weeks indicating that they had diffused out of the glass and were removed by body fluids. An interesting observation from these three fibers is that the silica gel layer quickly reached a thickness of approximately 5 to 6μm (within four weeks), and even while the HA layer continuously grew thicker; the gel layer thickness remained constant.

An important observation from the in-vivo experiments using the 13-93 glass fiber scaffolds was the formation of collagen on the reacted fibers and potential uses in tissue engineering. The SEMBSE image in Fig 7a shows strands of collagen coating and spanning the reacted 13-93 fibers in a scaffold that has been in-vivo for 28 weeks. A magnified view in Fig 7b shows the collagen fibrils clearly, and the 64nm periodicity that is unique to collagen molecules [16]. Collagen is the building block of nearly all human tissue, hard and soft, so the interaction and compatibility with bioactive glass for tissue regeneration is important.

Understanding the short and long term benefits of 13-93 bioactive glass scaffolds with soft tissue make these scaffolds candidates for use in treating conditions such as diabetic ulcers, severe burns, or other traumatized soft tissue. A material or scaffold that promotes vascular growth and tissue guiding while promoting the natural healing processes of the body will be an important advancement in the fields of both biomaterials and medical science.

CONCLUSION

Three dimensional scaffolds composed of randomly oriented fibers of the bioactive 13-93 glass are compatible with subcutaneous soft tissue, promote significant vascular and soft tissue growth within just two weeks in-vivo, and react to form HA when in contact with soft tissue. The 13-93 fibers reacted at a rate of about 3μm a week during the 28 week experiment. No immune reactions were detected during the histological examination of the implanted scaffolds, and collagen, the building block of hard and soft tissue, readily forms on the 13-93 fibers when implanted subcutaneously. Therefore, scaffolds or composites composed of 13-93 bioactive glass are good candidates for future soft tissue augmentation applications and wound dressings.

REFERENCES

1. Hench, L.L., *Bioceramics.* Journal of the American Ceramic Society, 1998. **81**: p. 1705-1728.
2. Hench, L.L. and J. Wilson, *Surface-Active Biomaterials* Science 1984. **226**: p. 630-636.
3. Leu, A. and J.K. Leach, *Proangiogenic Potential of Collagen/Bioactive Glass Substrate.* Pharmaceutical Research, 2008. **25**(5): p. 1222-1229.
4. Leach, J.K., et al., *Coating of VEGF-releasing scaffolds with bioactive glass for angiogenesis and bone regeneration.* Biomaterials, 2006. **27**: p. 3249-3255.
5. Rouwkema, J., N.C. Rivron, and C.A.v. Blitterswijk, *Vascularization in Tissue Engineering.* Trends in Biotechnology, 2008. **26**(8): p. 434-441.
6. Sen, C.K., et al., *Copper-induced vascular endothelial growth factor expression and wound healing.* American Journal of Physiology 2002. **282**: p. H1821-H1827.
7. Brink, M., *The Influence of Alkali and Alkaline Earths on the Working Range for Bioactive Glasses.* Journal of Biomedical Materials Research, 1997. **36**: p. 109-117.
8. Brink, M., K. Karlsson, and A. Yli-Urpo, *Bioactive Glasses and Their Use*. 2000: United States.
9. Fu, Q., *Freeze casting of bioactive glass and ceramic scaffolds for bone tissue engineering*, in *Materials Science and Engineering*. 2009, Missouri University of Science and Technology: Rolla. p. 294.
10. Pirhonen, E., L. Moimas, and J. Haapanen, *Porous Bioactive 3-D Glass Fiber Scaffolds for Tissue Engineering Applications Manufactured by Sintering Technique.* Key Engineering Materials, 2003. **240-242**: p. 237-240.

11. Jung, S.B., D.E. Day, and R.F. Brown, *Comparison of self-bonded three dimensional bioactive glass fiber scaffolds after in-vivo implantation in rats.* Journal of the American Ceramic Society, 2009.
12. Rahaman, M.N., et al., *Bioactive Glasses for Nonbearing Applications in Total Joint Replacement.* Seminars in Arthroplasty, 2006. **17**: p. 102-112.
13. Beattie, J. and A. Avenell, *Trace Element Nutrition and Bone Metabolism.* Nutrition Research Reviews, 1992. **5**: p. 167-188.
14. Becker, R.O., J.A. Spadaro, and E.W. Berg, *The Trace Elements of Human Bone.* Journal of Bone and Joint Surgery (American), 1968. **50**: p. 326-334.
15. Pirhonen, E., et al., *Manufacturing, mechanical characterization, and in-vitro performance of bioactive glass 13-93 fibers.* Journal of Biomedical Materials Research, 2006. **77B**(2): p. 227-233.
16. Cormack, D.H., *Ham's Histology*. 8 ed. 1987, Philadelphia PA: J. B. Lippincott Company.

FIGURES

Figure 1 – Image of a 13-93 random fiber scaffold. The scaffold measures 7mm in diameter and 2mm thick and has an open porosity of 50% and a compressive strength of 5MPa.

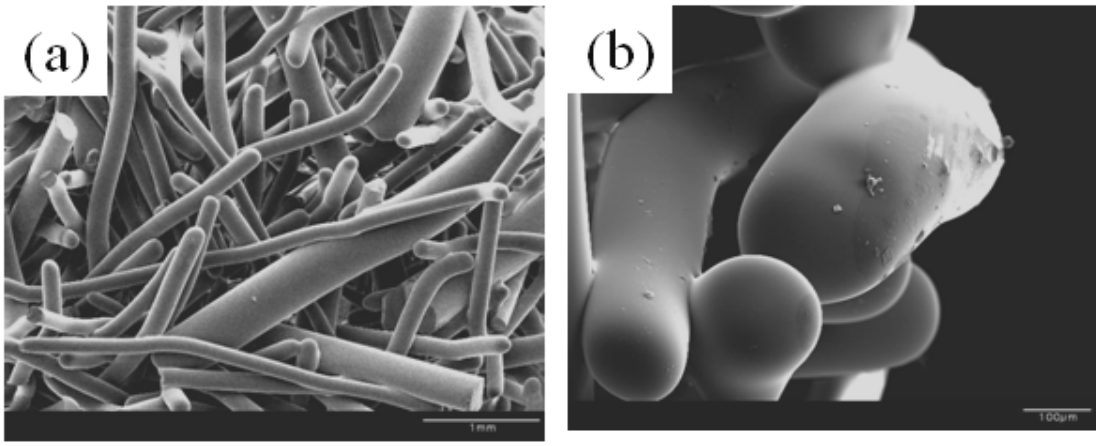

Figure 2 – SEM micrographs of a 13-93 random oriented fiber scaffold. Figure 2a shows the random orientation of the fibers and the rounded end of the fibers due to the heat treatment. Figure 2b is a higher magnification image showing the bonding between the fibers.

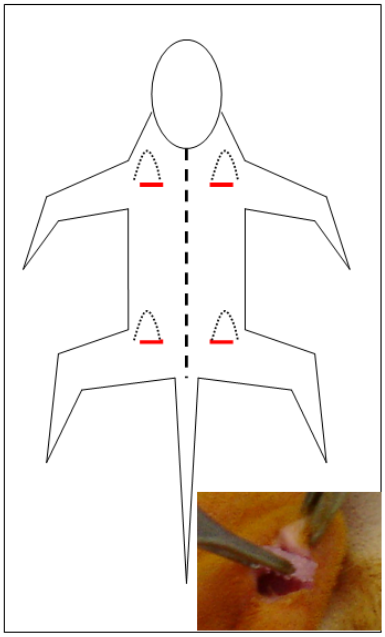

Figure 3 – Schematic showing the scaffold placement in the subcutaneous tissue. Image in lower right hand corner shows a scaffold being implanted under the skin.

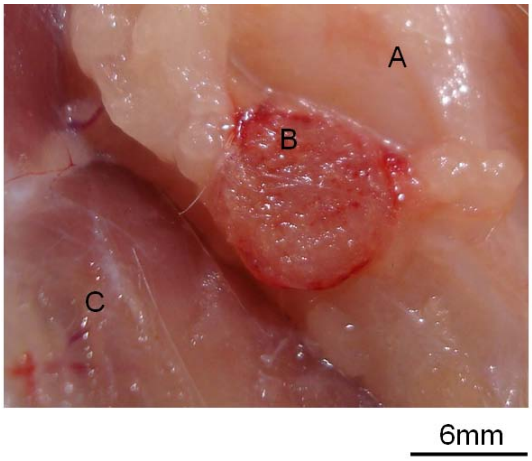

Figure 4 – Image of a 13-93 scaffold after two weeks in-vivo. The tissue under A is the subcutaneous tissue under the skin, B is the scaffold, and C is the skeletal muscle. The scaffold has no changed dimensions from the original, and is now red from soft tissue and vascular growth.

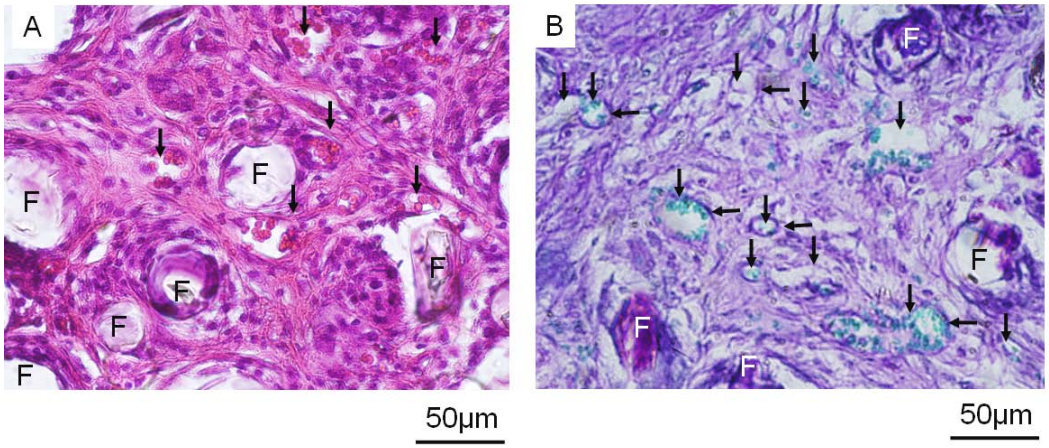

Figure 5 – Histology sections from the 13-93 scaffold implanted two weeks in subcutaneous tissue. Fig 5a is a H&E stained section showing the soft tissue (pink) surrounding the glass fibers (white and labeled with an F). The vertical arrows are pointing out blood vessels with red blood cells inside of them (pink dots). Fig 5b is a PAS stained tissue section, and here the soft tissue is purple and the tubules of the vessels

is a dark purple (horizontal arrow). The red blood cells are green making the vessels more visible (vertical arrows). The glass fibers are labeled with an F.

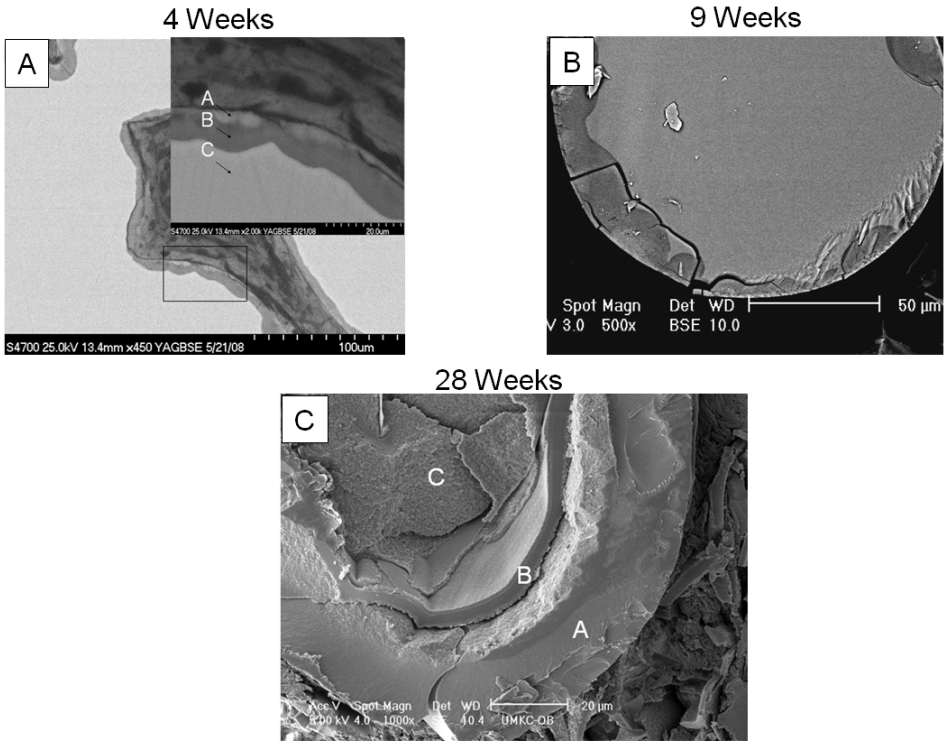

Figure 6 – SEMBSE images of 13-93 glass fibers implanted in a subcutaneous site for four, nine, and twenty eight weeks. Fig 6a shows the reacted edge of the four week implanted fiber where A is the hydroxyapatite layer, B is silica gel, and C is unreacted glass. The total reaction layer is 10 to 12µm thick. Fig 6b is an image of a nine week implanted fiber showing a reaction layer of non-uniform thickness of about 30µm. Fig 6c is an image of a fractured fiber that was implanted for 28 weeks. The total reaction layer is approximately 90µm. The surface layer A is the HA, B is a silica gel layer, and C is residual material consisting of SiO_2, CaO, and P_2O_5.

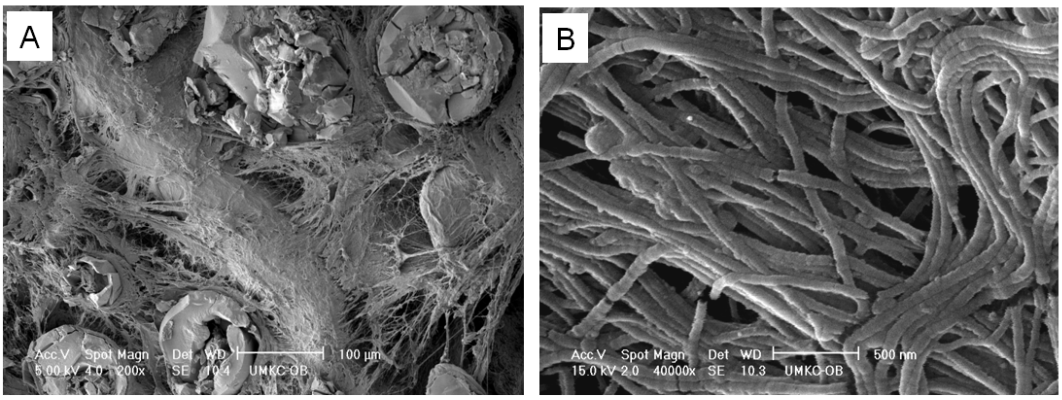

Figure 7 – SEMBSE images of a 13-93 scaffold implanted in subcutaneous tissue for 28 weeks that is coated with collagen fibrils. Fig 7a shows a fractured scaffold surface with collagen strings coating and connecting the glass fibers. Fig 7b is a higher magnification image of the collagen showing the unique 64nm periodicity of the material.

APPENDIX D

COMPARISON OF SELF-BONDED THREE DIMENSIONAL BIOACTIVE GLASS FIBER SCAFFOLDS AFTER IN-VIVO IMPLANTATION IN RATS

COMPARISON OF SELF-BONDED THREE DIMENSIONAL BIOACTIVE GLASS FIBER SCAFFOLDS AFTER IN-VIVO IMPLANTATION IN RATS

by

[1]Steven B. Jung, [1]Delbert E. Day, and [2]Roger F. Brown

[1]Graduate Center for Materials Research, Materials Science and Engineering Department Missouri University of Science and Technology, Rolla, MO, 65409-1170

[2]Department of Biological Sciences Missouri University of Science and Technology, Rolla, MO, 65409-1170

ABSTRACT

Three dimensional assemblies of fibers made from bioactive glass compositions were investigated to determine their usefulness as scaffolds for the repair and regeneration of hard and soft tissues. The microstructure, properties and in-vivo performance were measured for scaffolds (7mm diameter and 2mm thick) made from an interconnected network of discontinuous fibers of bioactive glasses such as 45S5 and 13-93 that were arranged in a random oriented geometry. Scaffolds, made from fibers whose diameter ranged from approximately 100 up to 300 microns, were implanted subcutaneously in laboratory rats for up to four weeks. Scaffolds comprised of randomly oriented fibers seeded with mesenchymal stem cells prior to implantation contained significant new bone-like material after four weeks in-vivo. No bone-like material was observed in un-seeded scaffolds as expected, but these scaffolds were completely penetrated by new soft tissue with noticeable amounts of new vascularization.

Histological staining techniques were used to asses the quality of the infiltrating soft tissue and to identify cells and tissues of interest. Biological staining and scanning electron microscopy back scattered imaging (SEM-BSI) showed new bone tissue had formed throughout the scaffolds seeded with mesenchymal stem cells. Scanning electron microscopy electron dispersive spectroscopy (SEM-EDS) analysis of the cross-section of a 13-93 and 45S5 fiber implanted four weeks was used to measure the compositional change of each fiber type to calcium phosphate, demonstrating the reactivity of both materials *in-vivo*.

INTRODUCTION

Bone density, especially in women, has been documented to decrease with age [1]. Biologically compatible replacement materials of variable strength are needed to deal with this problem [2,3]. Cortical bone is the strongest type of bone, with a compressive strength that ranges from 117 to 167 MPa [2,3]. Cervical vertebrae and lumbar bone, are weaker having a range of compressive strength between 5 to 10 MPa [3], while cancellous bone, a spongy bone material, has a compressive strength of only 0.2 to 4MPa [2,3].

One idea for the regeneration of bone has been to use ceramic materials for bone scaffolds. This option has been widely researched in terms of both materials and processing techniques [1,4-16]. The end result is often a sintered ceramic three-dimensional scaffold with high porosity (70-90%) and relatively low compressive strength (<0.4MPa) [5,7-8]. Ceramics most often studied for bone scaffold use are stoichiometric hydroxyapatite (HA) with the ideal composition of $(Ca_{10}(PO_4)_6(OH)_2)$ [5,7,9,11,15], other crystalline ceramics

such as $CaSiO_3$ or $CaCO_3$ [3,9,10], bioactive glasses like the silicate based 45S5 or 13-93 glasses [1,7,11,13,14,17], and glass-ceramics like bioactive glass-ceramic apatite wollastonite (A/W) [1]. All of these materials have been shown to promote significant cell attachment and tissue growth.

Glassy materials have unique properties that make them attractive for use as biological implants and for three dimensional porous scaffolds. It has been shown that the chemical composition can greatly affect the rate at which a glass either dissolves in liquids similar to those found in the body [18-19] or reacts to form HA. Homogeneous nucleation and crystal growth, such as that of bioactive glass 45S5, makes it possible to engineer glass-ceramic materials with improved mechanical properties such as bending strength, hardness and elastic modulus when properly heat treated [20-24]. Other bioactive glasses, such as the silicate based 13-93, have compositions that are more resistant to crystallization [13,25]. The decreased tendency for crystallization is due to compositional changes that reduce the nucleation and crystal growth rate, which results in a wider working range. This change increases the ability to pull fibers from a melt, which can be self-bonded to form bioactive glass scaffolds of a reasonable mechanical strength with a significant fraction of interconnected porosity [13,14,25].

The scaffolds investigated in the present work consisted of a network of randomly oriented self-bonded glass fibers. Scaffold designations are with respect to the weight fraction of 13-93 glass fibers in each scaffold, so S100 scaffolds were composed of 100 wt% 13-93 glass fibers and S30 was 30 wt% 13-93 and 70 wt% 45S5. The preparation of the scaffolds, porosity, compression strength, and *in vitro* cell growth of MC3T3-E1 pre-osteoblast cells have been previously described for the present scaffolds [26-27].

The main objective of the present research was to compare the *in-vivo* response of the S100 scaffold versus the S30 scaffold by seeding the scaffolds with mesenchymal stem cells prior to subcutaneous implantation. The evaluation of the scaffolds included determining the scaffold's ability to support bone tissue formation and growth from an initial mesenchymal stem cell seeding, a visual examination for breakdown of the bonding between the fibers to assess the structural capabilities *in-vivo*, and a comparison of reactivity between the different glass fiber types in body fluids. These aforementioned criteria should give useful insight into the suitability of a scaffold composed of randomly oriented bioactive glass fibers for the growth and regeneration of bone.

MATERIALS AND EXPERIMENTS

Scaffold Preparation and Physical Properties

Continuous fibers (100 to 300 μm in diameter) of the 45S5 and 13-93 bioactive glass (Table 1) were hand pulled from a melt and broken into 3mm lengths. Fibers for each scaffold were individually weighed for a total of 70mg, so S100 scaffolds contain 70mg 13-93 fiber and S30 contained 49mg 45S5 and 21mg 13-93 fibers. The bioactive glass fibers were placed in a mold consisting of an alumina substrate and a mullite cylindrical tube with a 7mm inside diameter. The molds were then placed inside a box furnace that was pre-heated to 720^{o}C. After 45 minutes of heating, the molds were removed from the furnace and cooled to room temperature. The self bonded scaffolds were removed from the molds and were ready for use [27].

The S100 and S30 scaffolds were previously measured for compression strength and open porosity [26-27]. The S100 scaffold had a compressive strength of 5.3MPa and an average open porosity of approximately 44%, while the S30 scaffold had an average open porosity of 63% and compressive strengths of approximately 0.6MPa.

Table 1. Compositions of Some Bioactive Glasses in mol% and wt% (parentheses denote wt%)

Material	Na_2O	K_2O	MgO	CaO	P_2O_5	SiO_2
13-93 Glass	6 (6)	7.9 (12)	7.7 (5)	22.1 (20)	1.7 (4)	54.6 (53)
45S5 Glass	24.4 (24.5)	0 (0)	0 (0)	26.9 (24.5)	2.6 (6)	46.1 (45)
$Na_4Ca_4Si_6O_{18}$	16.7 (17.5)	0 (0)	0 (0)	33.3 (31.6)	0 (0)	50 (50.9)

Scaffold Sterilization and Seeding with Mesenchymal Stem Cells

All scaffolds were washed twice with ethyl alcohol and heat sterilized at 250^{o}C for 2.5 hours in a small box furnace prior to cell seeding or implantation. Half of the scaffolds were seeded with 150,000 mesenchymal stem cells harvested from Fisher 344 rats (Fisher Scientific, St. Louis, MO). The cells were harvested from the femur of previously sacrificed rats and cultured for 24 hours in glass dishes with Sigma α-MEM 0644 media (Sigma Aldrich, St. Louis, MO): (10% fetal calf serum, 1% penicillin/strep antibiotic, 50mg/ml ascorbic acid, and 10^{-8} molar dexamethasone) at 37^{o}C and in 95% air/5% CO_2 atmosphere.

Animal Experiments

A total of eight male and female Fisher 344, rats ranging in age from eight to ten weeks, were used to assess the biological response of the S100 and S30 scaffolds after being implanted for three and four weeks. The back of each rat was shaved just prior to surgery, sterilized with iodine, and then washed with 70% ethanol to ensure a clean and sterile working area. Each rat was anesthetized with a mixture of isoflourine and medical grade oxygen. The implanted scaffolds are hereafter referred to in by the following designations; scaffold S100 seeded with mesenchymal stem cells is designated S100+, scaffold S100 without mesenchymal stem cells is designated to as S100, scaffold S30 with mesenchymal stem cells is designated S30+ and scaffold S30 without mesenchymal stem cells is designated S30.

One scaffold of each type, S100, S100+, S30, and S30+ was implanted for a total of four scaffolds per animal for a total of 32 scaffolds. Each scaffold was implanted subcutaneously in a pocket that was formed in the back of each rat, one above each shoulder and one above each hind leg, between the skin and the muscle as shown in Fig. 1. The pockets were approximately 15mm wide and 15mm long to ensure that each scaffold was inserted away from the incision site. The incisions were closed with super glue (Krazy® Glue, Elmers Products inc. Columbus, OH). After implantation, 0.1 mL of Penicillin G Procaine was injected into each thigh of the rat to prevent infection. The rats were placed on a heating pad in a cage with fresh air during recovery.

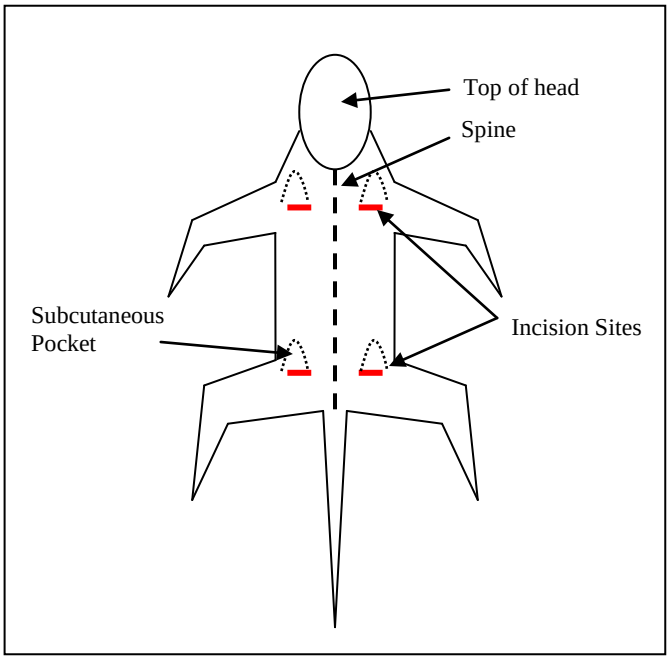

Figure 1. Schematic showing implantation sites for subcutaneous implantation of the S100 and S30 scaffolds in the back of a rat.

Removal of Scaffold from Rats and Scaffold Dehydration

After the allotted three or four week period, the rats were sacrificed in a chamber of CO_2. Each scaffold was surgically removed from the subcutaneous site of each rat and placed in a 10% formalin solution at room temperature (22^{o}C) for 96 hours to fix the tissue. At this point, each scaffold was visually examined as described later.

Each scaffold was dehydrated with a series of seven ethanol solutions ranging from 80 to 100% ethanol using a solution volume ratio of ten times that of the scaffold (~5mL solution/scaffold) [28]. Each scaffold was placed in glass vial and submerged in the ethanol solution. The glass vials were placed in a plastic tray, which was packed in ice to keep the ethanol solution from over heating, microwave irradiated at 80% power at 37^{o}C for two minutes and was continuously submerged in each of the alcohol solutions for a

total of fifteen minutes. After dehydrating, each scaffold was placed in xylene for 24 hours to make any tissue present transparent.

Impregnating Scaffolds with Polymethyl Methacrylate (PMMA)

Each scaffold was infiltrated with a series of three solutions for 48 hours each (0%, 50%, and 100% polymerizing agent perkodox mixed with methyl methacrylate monomer (MMA)) to ensure monomer penetration and controlled polymerization. Just prior to infiltration of the 100% MMA solution, the scaffold was attached to a bed of partially polymerized PMMA. The scaffold was then covered with a layer of MMA and slowly polymerized over a four day period at 4^{o}C.

Scaffold Separation, Sectioning, and Polishing

Each scaffold was sectioned at its center, perpendicular to the 7mm diameter using an Isomet™ slow speed saw (Model 11-1180, Buehler LTD. Evanston, IL) with a LECO® diamond coated blade (LECO® Corporation, St. Joseph, MI) . The cross section of the scaffold was polished with silicon carbide papers ranging from 320 to 1200 grit. The polished surface was attached to a glass slide with superglue and polished to a final thickness of 50 ±10μm.

Scaffold Cross-section Staining

The 50μm section of each scaffold was stained using Sanderson's™ Bone Staining method (Surgipath Canada inc, Winnipeg, Manitoba). The mounted scaffold cross sections were dipped in the preheated stain (50^{o}C) for two minutes, rinsed with

distilled water, and blotted dry with a paper towel. The stained sections were then counter stained with a solution consisting of one gram of acid fuchsin, 99mL of distilled water, and one mL acetic acid for 40 seconds at 22^{o}C to differentiate the soft tissue as blue and bone tissue as red. The cell nuclei of both the soft and bone tissue appear as dark blue dots, cytoplasm (a watery substance that fills cells) is light blue, osteoid seam (a mixture of proteins which is secreted by osteoblast which when mineralized becomes bone) is a purple color, bone matrix material is red, and soft tissue is blue. Each stained section was examined at 10X and 40X magnification using an Olympus MI transmitted light microscope (Olympus Corporation, Japan)**.**

SEM Imaging and EDS Compositional Analysis *In-vivo* Scaffolds

Scanning electron microscopy backscattered imaging SEM-BSI, (Hitachi S-570 SEM) was used to determine the compositional change from the center to the outer edge of reacted fibers of 13-93 and crystallized 45S5 fibers (45S5c) that had been four weeks *in-vivo*. Cross sectioned scaffolds were polished with silicon carbide papers to 1200 grit. The scaffolds were sputter coated with gold palladium and attached to aluminum stubs with carbon tape to eliminate charging. For standard-less EDS, there is no set error, as it depends on the elements analyzed and the accelerating voltage used for generation of the EDS spectra. For this EDS analysis, the data plotted is shown to give a general idea of the reaction and leaching of the fibers.

RESULTS AND DISCUSSION

Scaffolds Prior to Implantation (As-Made)

Figure 2 shows a high and low magnification image of the as-made S100 (Figs 2a and b) and S30 (Figs 2c and d) scaffolds prior to implantation. Figures 2a and Fig. 2c show the random orientation of the fibers in the as-made scaffolds. An example of the bonding developed between the fibers after heat treatment is shown in Figs. 2b and 2d. An important difference in the 13-93 and 45S5 fibers after self-bonding is that the 13-93 fibers remain glassy and smooth, whereas the 45S5 fibers crystallize and a rough surface is formed as shown in Fig. 2d. Previously, 45S5 glass has been reported to crystallize into combeite [7], whose stoichiometric composition is shown in Table 1.

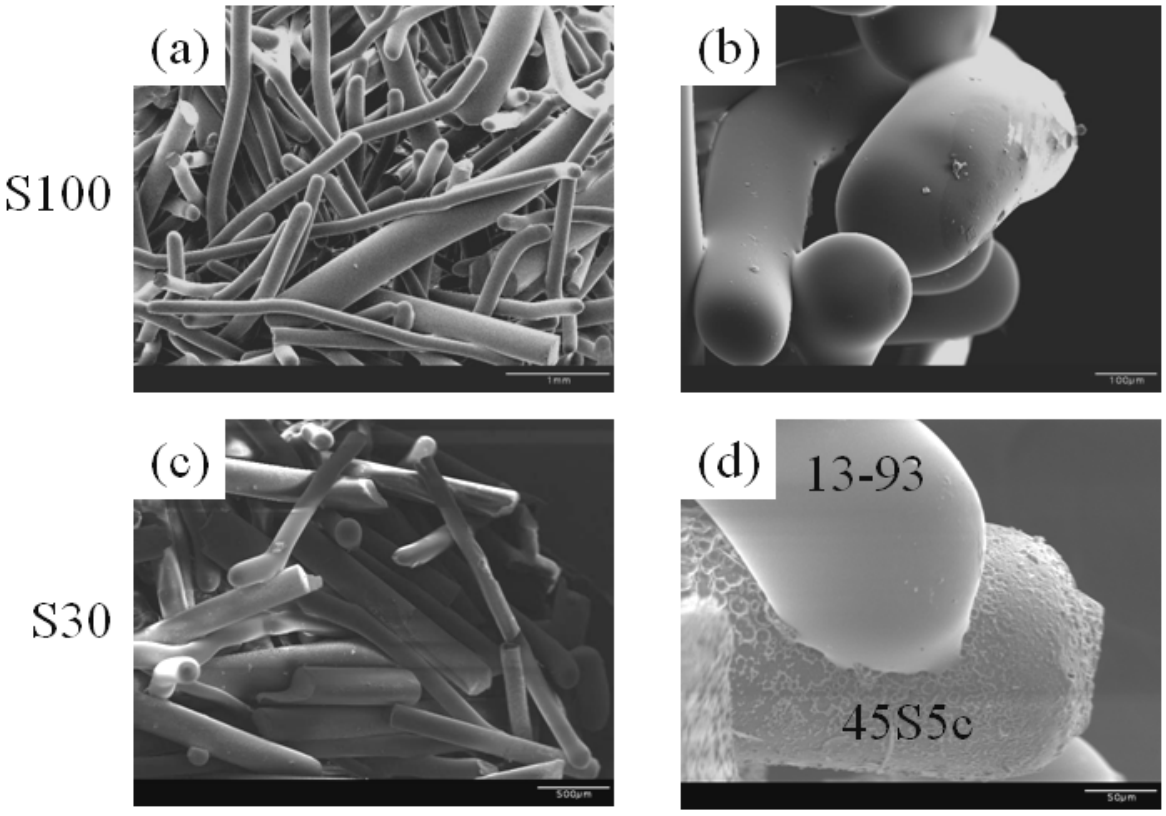

Figure 2. SEM images of the 13-93 fibers in the S100 scaffold (a), and S30 scaffold (c) after 45 minutes at 720^{o}C. The bonding between 13-93 glass fibers in a S100 scaffold is shown in (b) and a 13-93 fiber bonded to 45S5c fiber in S30 scaffold in (d). [26].

Evaluation of Scaffolds Implanted in Rats

Upon removal, the first evaluation was a visual assessment of robustness of the scaffold. Figure 3 shows three scaffolds, (a) an as-made S100 scaffold prior to implantation, (b) a S100+ scaffold after four weeks *in-vivo*, and (c) a S30+ scaffold after four weeks *in-vivo*. The diameter of the two implanted scaffolds was essentially unchanged from the as-made control, and both scaffolds had sufficient strength to remain intact after four weeks *in-vivo*.

Significant soft tissue had infiltrated both scaffolds after four weeks *in-vivo* as is clearly evident from Figs. 3b and 3c. Healthy tissue had grown into the scaffolds, and there was no evidence of infection or inflammation in the surrounding tissue to suggest rejection of the scaffolds. Another interesting observation was that several blood vessels had grown into the S100 and S30 scaffolds; see black circles in Figs. 3b and 3c. The remaining scaffolds, not shown, at three and four weeks, with and without seeded mesenchymal stem cells, all looked similar to those in Fig. 3 in terms of tissue infiltration and the presence of blood vessels.

The reaction products of these two bioactive glasses may be causing an angiogenic effect, which in this case is positive, as the penetrating blood vessels are providing nourishment to the interior of the scaffolds. Previous work completed by others on the angiogenic effect of 45S5 glass found that there may be a link between bioactive glasses and angiogenesis *in-vitro* [29-30]. No one to date has reported on proangiogenic effects for 13-93 glass, *in-vivo* or *in-vitro*, but this work shows compelling evidence that there may be a positive angiogenic effect *in-vivo*.

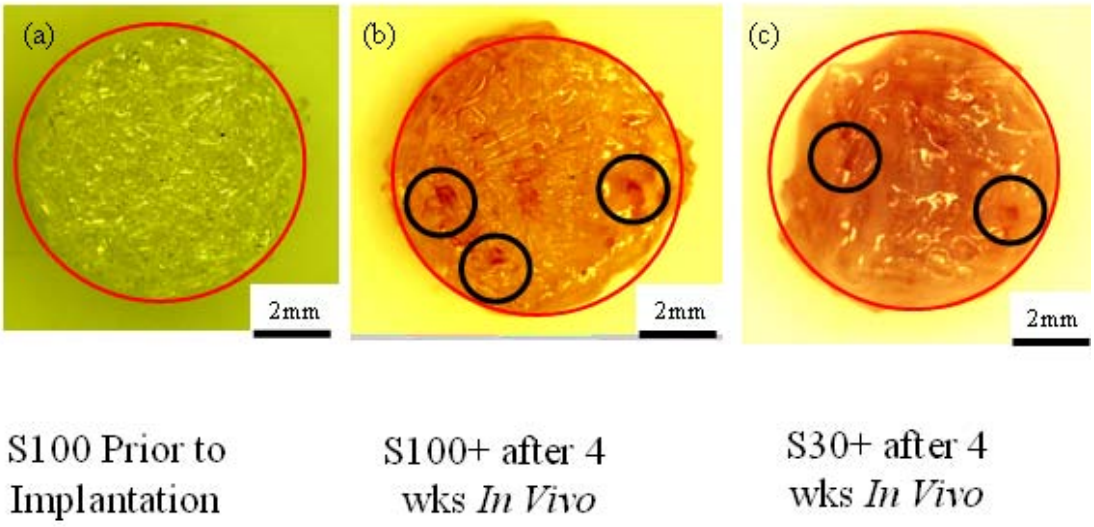

Figure 3. Appearance of glass fiber scaffolds before and after subcutaneous *in vivo* implantation for four weeks. (a) S100 scaffold prior to implantation, (b) S100+ after four weeks *in- vivo*, (c) S30+ after four weeks *in-vivo*. Red circle is 7mm in diameter and denote the starting diameter of the scaffolds.

Evidence of Bone Formation in Implanted Scaffolds

Regions of red tissue in the histology sections were assumed to be bone tissue, therefore, the results of the scaffold cross sections stained for bone tissue identification in both the S100 and S30 scaffolds are as follows. None of the non-cell seeded scaffolds contained any bone tissue as expected since they had no mesenchymal stem cells seeded on them, and were not adjacent to any natural bone tissue. All of the S100 and S30 scaffolds seeded with mesenchymal stem cells and implanted for three and four weeks had red tissue present after being stained and was assumed to be bone tissue.

The 13-93 fibers in the non-seeded S100 scaffolds in Fig. 4 are the white elliptical regions surrounded by a dark line. None of the non-seeded S100 scaffolds contained any detectable bone tissue (red stained region) after three or four weeks *in-vivo*, as is evident in Figs. 4a and 4b. However, soft tissue had penetrated the outer portion of the unseeded

scaffolds and was often present in the center of the scaffold. The presence of this tissue is an indication of the biocompatibility between the soft tissue and the 13-93 fibers.

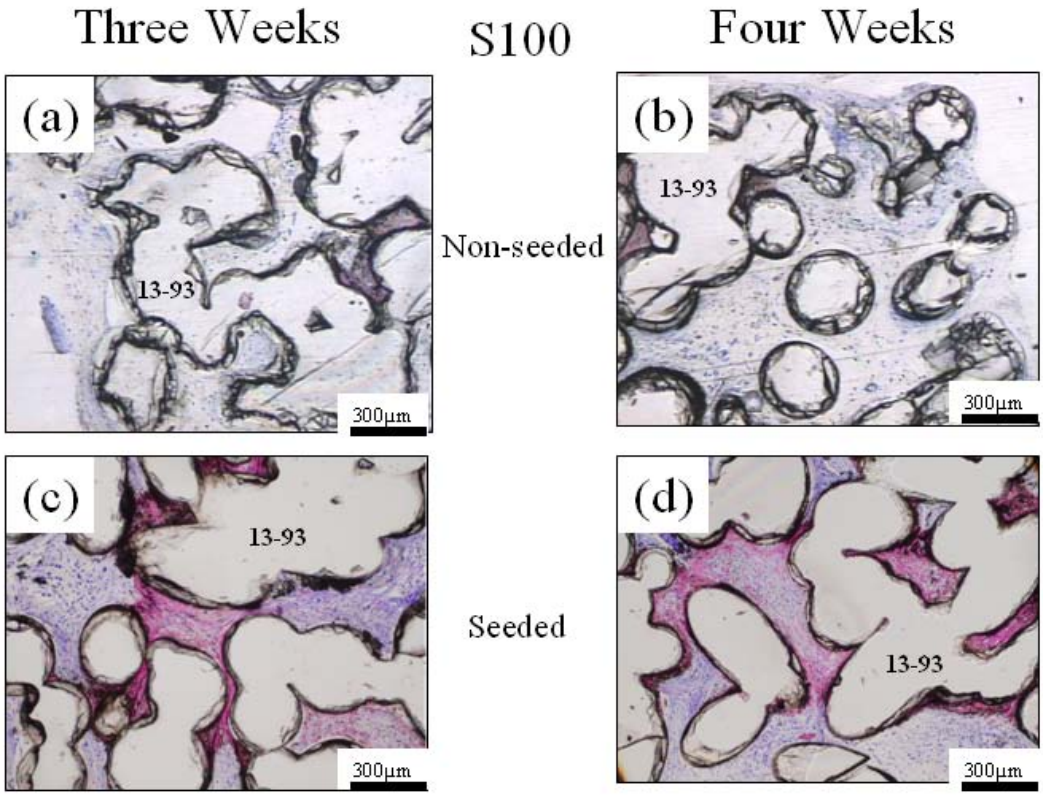

Figure 4. Optical micrograph of randomly selected location in the stained cross section of scaffolds after three or four weeks *in-vivo.* Soft tissue (blue) and bone tissue (red) formation. (a) S100 three weeks, (b) S100 four weeks, (c) S100+ three weeks, (d) S100+ four weeks.

The seeded S100+ scaffolds all contained regions of bone tissue (red regions) after three and four weeks *in-vivo,* as is evident in Figs. 4c and 4d. There is a mix of both soft (blue) and bone (red) tissue present in the three and four week S100+ scaffolds. The amount of bone tissue in the week four scaffold, Fig. 4d, appears to be slightly more than in the three week scaffold, Fig. 4c.

Figure 5 is as enlarged view of Fig. 4d to better show the regions of soft and bone tissue after four weeks *in-vivo*. The blue dots within the blue matrix are nuclei of soft tissue, and the blue dots in the red matrix are nuclei of osteocytes which have incorporated into the bony matrix. In several areas of the scaffold, pockets of bone tissue are attached and growing on the 13-93 fibers. There is a visible reaction layer present on the surface of the 13-93 fibers that formed as the 13-93 fibers reacted with the body fluids of the rat. The reaction layer is the darker gray layer that outlines the 13-93 fibers, and will be described in more detail later.

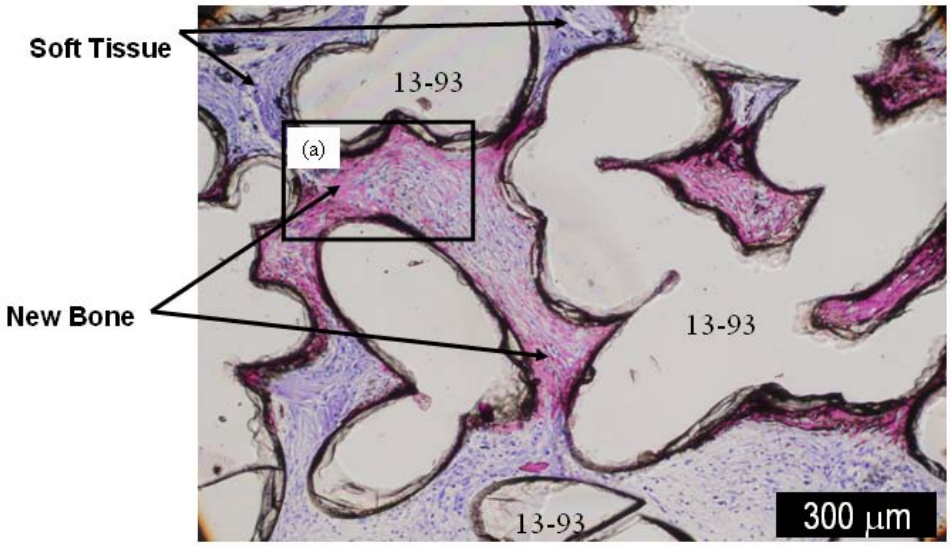

Figure 5. Optical micrograph (100X) of the cross-section of a S100+ scaffold seeded with mesenchymal stem cells after four weeks *in-vivo*. Tissue has been stained where blue denotes soft tissue and red denotes bone (hard) tissue.

The boxed area in Fig. 5 labeled (a) is shown at higher magnification in Fig. 6. The reacted surface layer on the 13-93 fibers varies in thickness between ~10 to 20µm. The dark circles in Fig. 6 encircle osteocytes (blue dots surrounded by a white halo) that are incorporated into the newly formed bone tissue. Only a few examples of the

osteocytes in the bony matrix material are shown in Fig. 6, but osteocytes were seen throughout the new bone as shown in Fig. 5. This is important because it shows that the MSC cells have differentiated to become mature bone and that the S100 scaffold is promoting osteogenesis. The osteoid seam (purple tissue) represents un-mineralized secreted proteins of osteocytes and is the growth front for new bone, as pointed out with arrows at both the far right and lower left of Fig. 6.

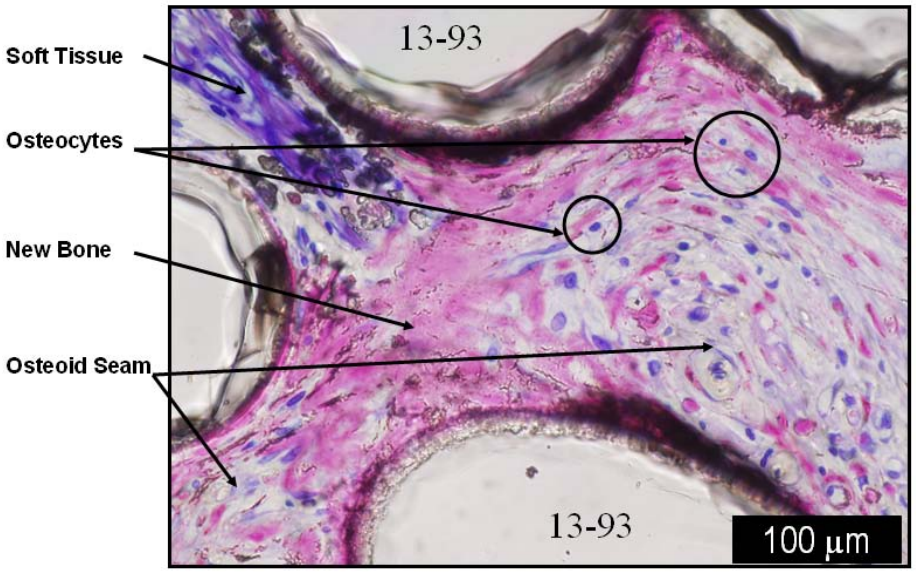

Figure 6. Optical micrograph (400X) of S100+ scaffold cross-section. S100+ scaffold was seeded with mesenchymal stem cells and implanted four weeks subcutaneously in the back of a rat and stained for soft (blue) and bone (red) tissue.

Representative examples of the seeded and non-seeded S30 scaffolds after three of four weeks *in-vivo* are shown in Fig. 7. These cross-sections look significantly different than those for the S100 scaffolds, see Fig. 4. The 45S5c fibers are dark and crystallized as opposed to the glassy white 13-93 fibers. Again, none of the non-seeded scaffolds contained any evidence of bone tissue (red), as is evident from Fig. 7a (S30 three weeks), and Fig. 7b (S30 four weeks). The soft tissue (blue) in Figs. 7a, 7b, and 7c

stained relatively light making it difficult to see, however the cell nuclei stained dark blue. The abundance of nuclei through out the cross-sections indicates significant infiltration of soft tissue. Soft tissue (blue) is visible throughout areas of the scaffold cross-section in Fig. 7d, indicating that it had penetrated and survived within the scaffold environment provided by the mixture of 13-93 and 45S5c fibers.

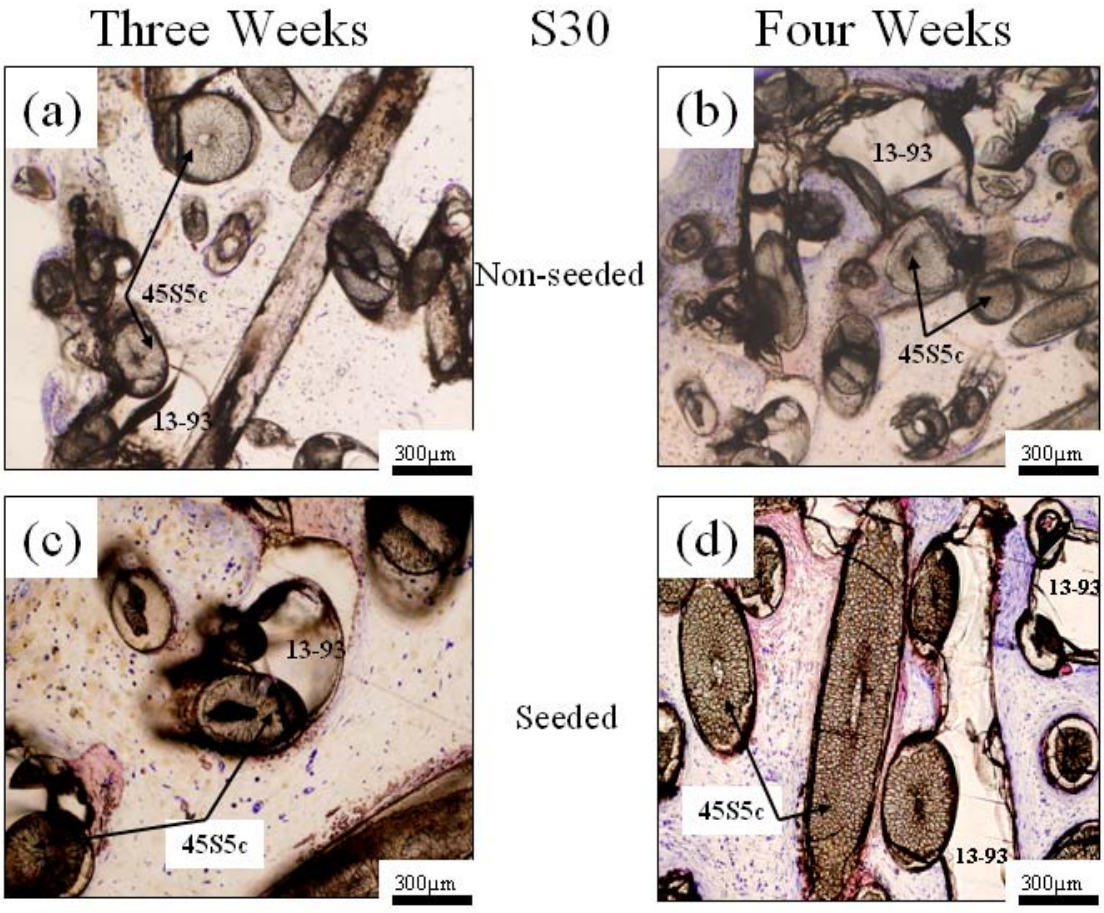

Figure 7. Optical micrograph (100X) of the cross-section of S30 scaffolds after three and four weeks *in-vivo* and stained for soft (blue) and bone (red) tissue formation. (a) S30 three weeks, (b) S30 four weeks, (c) S30+ three weeks, (d) S30+ four weeks.

Figures 7c and 7d are representative sections of the S30+ scaffolds in which bone tissue had formed. There is a mixture of both soft and bone tissue present in these scaffolds, and again the total amount of bone tissue is estimated to be slightly higher after

four weeks *in-vivo*. In Figure 7d, new bone tissue is seen surrounding both the 13-93 and 45S5c fibers. This suggests that both materials are biocompatible and suitable for bone growth. To the author's knowledge, this is the first time that 13-93 and 45S5c fibers have been placed *in-vivo* in the same site, and from this analysis, both fibers appear to interact positively with the living tissue, and there does not appear to be any significant advantage from a biological point of view between the two fibers.

The surface of the 13-93 and 45S5c fibers differs greatly as the 13-93 fibers are smooth, while the surface of the 45S5c fibers are noticeably rougher as shown in Fig. 2d. The cause of the rough surface is unknown, but one possible explanation is that as the 45S5 glass crystallized and the crystals began to grow together, a liquid or viscous phase surrounding the crystals was pushed out causing the rough surface. The microstructure in Fig. 7 shows bone tissue on both the smooth 13-93 and rough 45S5c surfaces, but a determination of which surface is preferred for tissue attachment and growth cannot be made from the present work.

The enlarged view of Fig. 7d shown in Fig. 8, better shows the seeded S30+ scaffold after four weeks *in-vivo*. The high level of crystallization that occurred in the 45S5c fibers when they were heated to form a scaffold is evident from the small irregular grains that are present throughout the fibers in Fig. 8. The 45S5c fibers have visible reaction regions surrounding them, light gray to white in color, that is attributed to their being in contact with the body fluids of the rat. Two examples of the bonding between the 45S5c fibers and a 13-93 fiber are shown on the right hand side of Fig. 8. Both fibers labeled as '13-93' in Fig. 8 are attached to two 45S5c fibers. The attachment appears to be from 13-93 fibers softening and sticking to the 45S5c fibers.

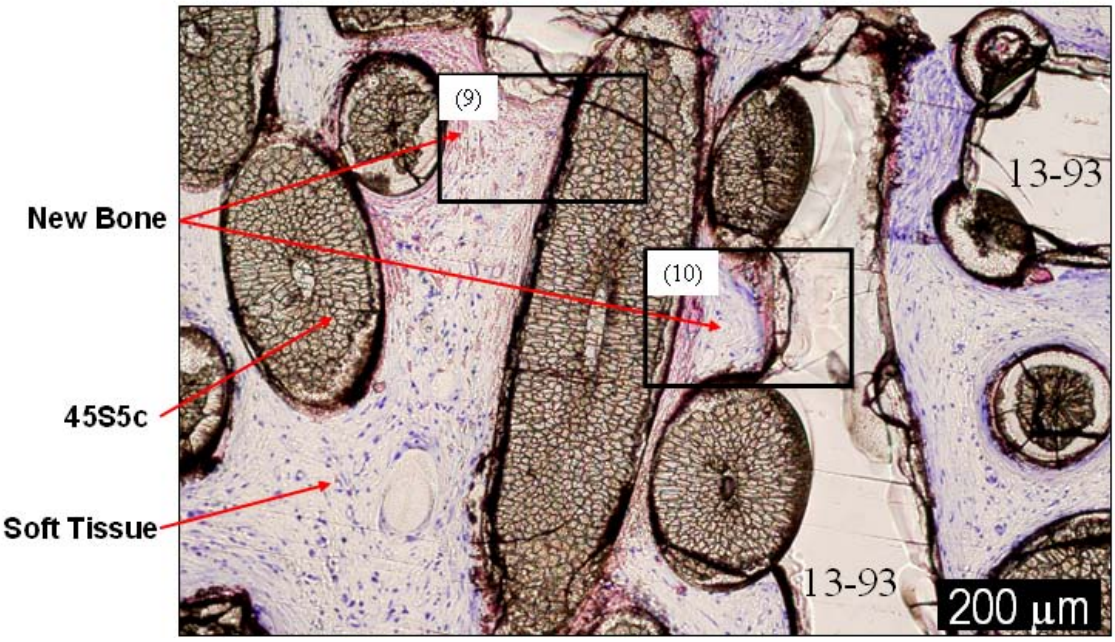

Figure 8. Optical micrograph (100X) of S30+ scaffold cross-section after four weeks *in-vivo*. The S30+ scaffold was seeded with mesenchymal stem cells and implanted four weeks subcutaneously in the back of a rat and stained for soft (blue) and bone (red) tissue. The darker, textured fibers are crystallized 45S5c fibers, where the glassy 13-93 fibers are transparent and featureless.

An expanded view of the region inside the box labeled (9) in Fig. 8 is shown in Fig. 9. A region of new bone tissue is seen between two 45S5 fibers that are bonded to a 13-93 fiber. Osteocytes are visible in the newly formed bone, as observed in the S100+ scaffolds. New bone tissue appears to be attached to both the 13-93 fiber and the 45S5c fiber, with no apparent preference for either fiber. This indicates that both fibers promote new bone growth. Again, as mentioned about the S100 scaffold, the S30 scaffold has osteocytes embedded throughout the new bone indicating that the MSC cells have differentiated and are forming new bone.

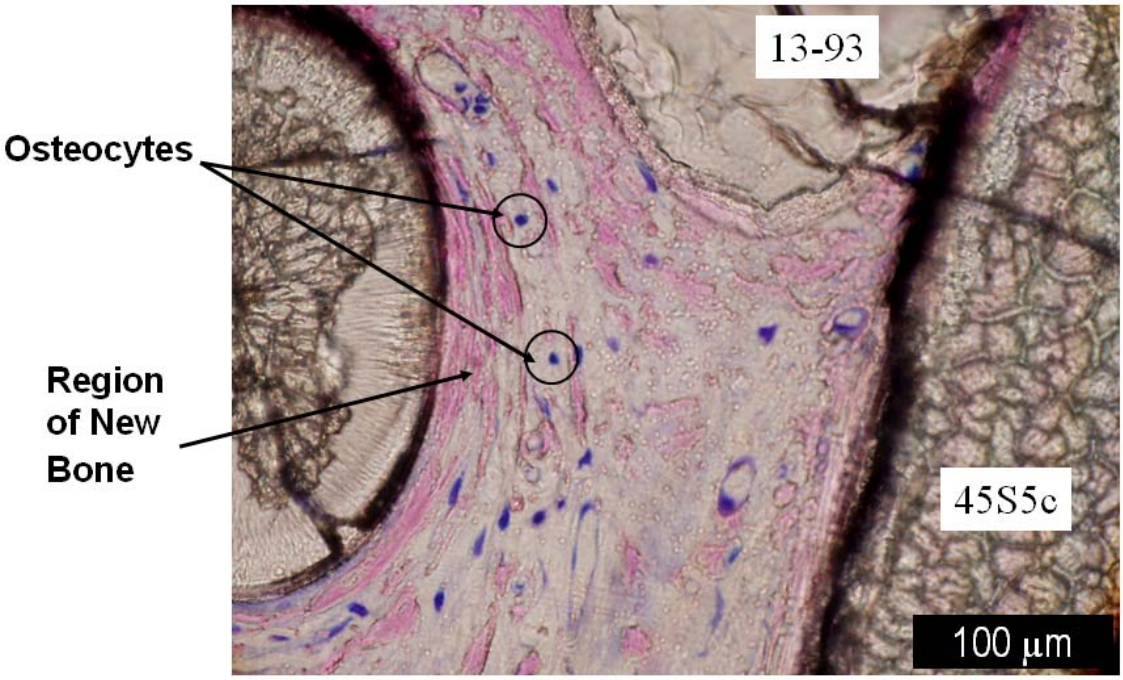

Figure 9. Optical micrograph (400X) of cross-section of the box labeled (9) in Fig. 8. S30+ scaffold was seeded with mesenchymal stem cells and implanted four weeks subcutaneously in the back of a rat and stained for soft (blue) and bone (red) tissue.

The thickness of the reacted region of the 45S5c fiber on the left hand side of Fig. 9 appears to be ~20 to 30µm, which is thicker than the regions seen surrounding the 13-93 fibers. This suggests that the 45S5c fibers react faster than the 13-93 fibers which is consistent with the higher alkali and lower silica content of the 45S5 fibers.

The region, in the box labeled (10), in Fig. 8, is shown as a transmitted light image in Fig. 10a and as a SEM-BSI image in Fig. 10b. Figures 10a and 10b have 45S5c fibers on the left and at the top of the image as denoted by the arrows, and a fiber labeled 13-93 to the right. The X's in Figs. 10a and 10b show regions of the fibers that had reacted *in-vivo.* These regions are rich in both calcium and phosphorus. The Y's correspond to areas of new bone, stained red in Fig. 10a, and the light gray material attached to the edge of the fibers in Fig. 10b. Soft tissue infiltrated with PMMA, labeled

Z, corresponds to the blue tissue in Fig 10a, and the darkest portion of the image in Fig.10b. Figures 10a and 10b look slightly different because the section used for Fig. 10a was stained for histology and the adjacent section of scaffold was prepared for imaging with the SEM. Subsequent polishing removed material from the surface of the scaffold section, which slightly altered the image, but the representative areas of the scaffold are still the same as previously described.

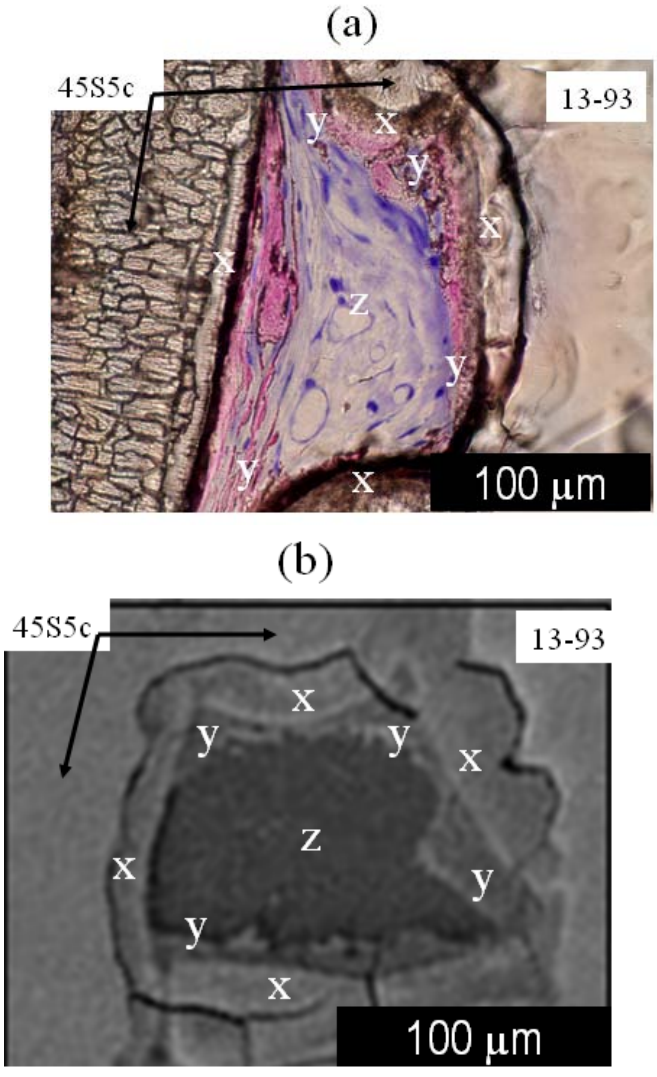

Figure 10. Seeded S30+ scaffold after four weeks *in-vivo.* (a) Optical micrograph (400X) of a portion of the cross-section of a S30+ scaffold. (b) SEM-BSI of same area as shown

as (10a). The X's indicate reacted regions on the fibers, the y's indicate areas of new bone, and the Z's are areas of PMMA infiltrated soft tissue.

The new bone tissue found after three weeks *in-vivo* in the seeded scaffolds in the present work is consistent with prior work[10] completed on porous HA and porous calcium carbonate constructs seeded with marrow cells and subcutaneously implanted in rats for two to six weeks. In the prior work[10], three weeks was the minimum time for new bone to become recognizable in the porous HA and porous calcium carbonate constructs.

Analysis of 13-93 and 45S5c Fiber after Four Weeks *In-vivo*

A 13-93 fiber after four weeks *in-vivo* was imaged with SEM-BSI and also measured for compositional change with SEM-EDS. The dotted line in Fig 11a illustrates the boundary between the adjacent new bone and the calcium rich layer of the 13-93 fiber. The new bone is in direct contact with the outer edge of the 13-93 fiber. Figure 11a is an SEM-BSI image of the cross-section of a 13-93 glass fiber that was part of a S100+ scaffold after four weeks. The calculated oxide weight percent, as measured by SEM-EDS, present at the three positions (A,B, and C) shown in Fig. 11a is shown graphically in Fig. 11b. The change in gray scale across the fiber cross-section in Fig. 11a indicates a change in composition from the unreacted glass; position A, to the outer edge at position C. The unreacted portion of the fiber at position A has a composition close to that of starting 13-93 glass (Table 1). Position B is a silica rich layer containing almost 90 weight percent SiO_2, the rest being CaO and P_2O_5. The CaO and P_2O_5 content increased significantly at the outer edge (position C), indicating a calcium phosphate

layer had formed. The K_2O, MgO, and Na_2O content decreased to near zero at position C as these constituents are soluble in body fluids and leached from the fibers.

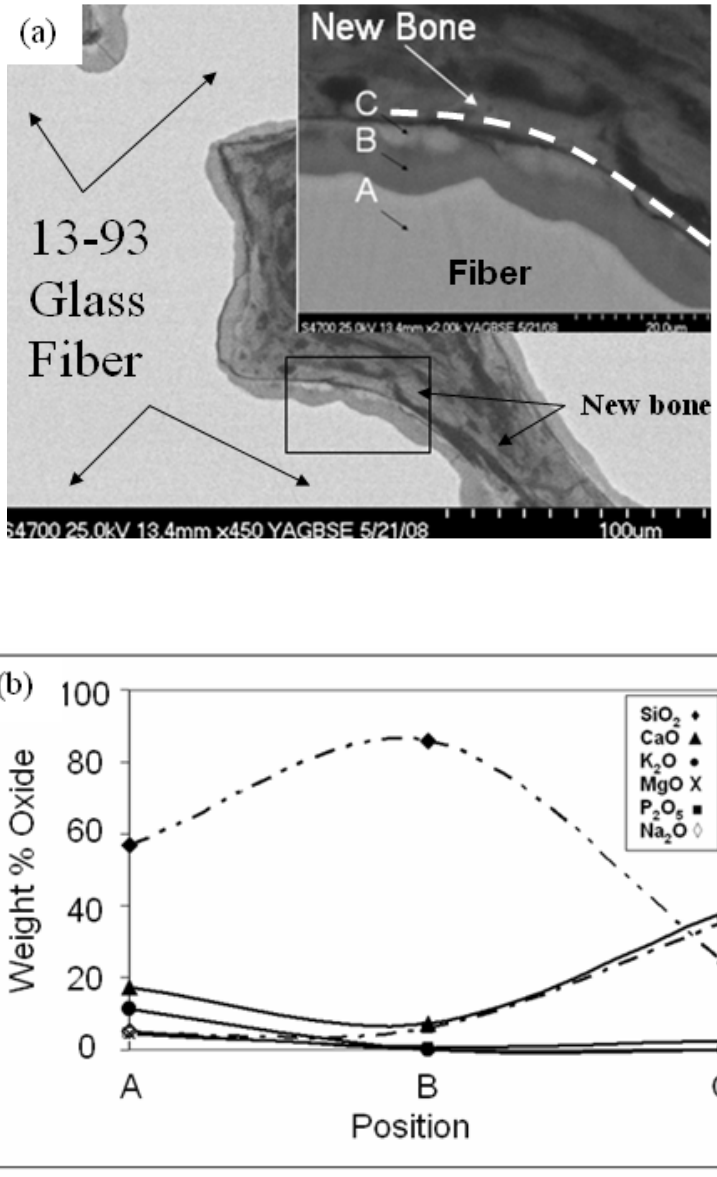

Figure 11. (a) SEM-BSI of a 13-93 glass fiber after four weeks *in-vivo*. (b) Composition (weight % oxide) obtained from SEM-EDS of a reacted 13-93 fiber at the locations A, B, and C. Composition for 13-93 glass given in Table1.

Stoichiometric HA ($Ca_{10}(PO_4)_6(OH)_2$) has a Ca/P molar ratio of 1.67, and the Ca/P ratio at the outer edge of the 13-93 fiber at position C in Fig. 11b was measured

with EDS to be 1.38. This increase in Ca/P ratio at position C indicates that a calcium phosphate material has formed and verifies earlier statements about the formation of a calcium phosphate surface layer on 13-93 fibers due to interactions with body fluids. The formation of a calcium phosphate layer was expected as it has been detected by *in-vitro* testing in SBF [1,11,13, 25, 31] and *in-vivo* in various animal models [1,17].

A 45S5c fiber, after four weeks *in-vivo* and seeded with msc cells, was imaged with SEM-BSI and also measured for compositional change with SEM-EDS. Figure 12a shows an SEM-BSI image and Fig. 12b shows the corresponding plot of composition across a 45S5c fiber after four weeks *in-vivo*. This fiber has undergone significant reaction after four weeks as is apparent by the thick light gray layer that surrounds an easily distinguishable darker core. The variation in composition across the fiber, as determined by EDS, is shown graphically in Fig. 12b. All of the Na_2O has been leached from the 45S5c fiber, even from the core. This leaching of Na_2O has been previously documented for *in-vitro* conversion of 45S5 glass to HA in dilute phosphate solutions [19].

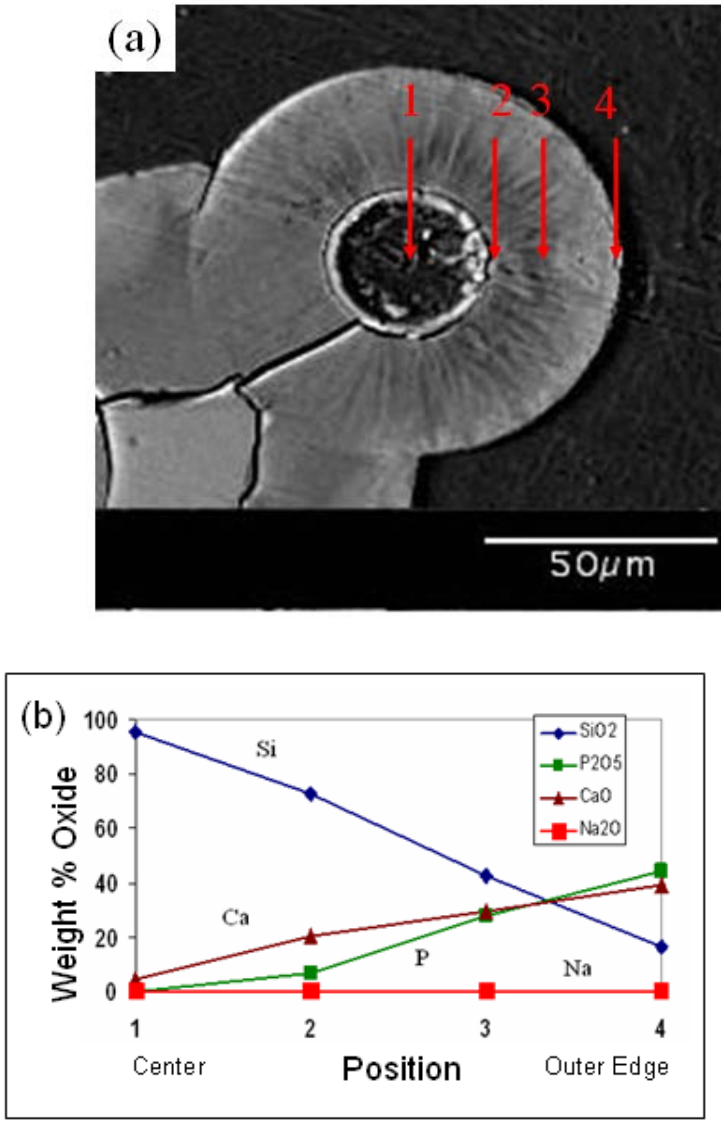

Figure 12. (a) SEMBSI of 45S5c fiber four weeks *in-vivo* (from an S30 scaffold seeded with msc cells). (b) Compositional analysis (weight % oxide) obtained from SEM-EDS of reacted 45S5c fiber as a function of position. Composition of 45S5 glass is shown in Table 1.

The dark core at the center of the fiber in Fig. 12a is greater than 90 weight percent SiO_2. The silica core found in reacted 45S5c fibers in the present work has been similarly described previously with 45S5 glass particles to make calcium phosphate shells *in-vitro* [32] and reacting 45S5 glass fibers with phosphate solutions *in-vitro* [18]. The previous report on calcium phosphate shells[32] stated that all of the SiO_2 was eventually

released from the 45S5 glass spheres, and lead to a hollow shell of calcium phosphate [32]. It is unclear from the present work if the SiO_2 will be totally dissolved from the center of the reacted 45S5c fibers, but it has been shown that it may, given the right physiological conditions [32].

The calcium phosphate rich layer present at position four of the fiber in Fig. 12a, contains only 17 weight percent SiO_2 while the remaining components are CaO and P_2O_5 at ~40 weight percent each. The Ca/P molar ratio is 1.18 and there are high levels of both CaO and P_2O_5 at position three and four relative to other the other oxides which indicates that a relatively thick (25μm) calcium phosphate layer has formed on the outer edge of the fiber in only four weeks. The formation of the calcium phosphate material at the outer edge of the 45S5c fiber does verify earlier statements about a calcium phosphate reaction region, and should be expected as 45S5 has been documented numerous times to form HA both *in-vitro* with SBF [18,19,23,24], and *in-vivo* in animal models [1,17].

CONCLUSIONS

New bone tissue formed in both the S100 and S30 fiber scaffolds seeded with mesenchymal stem cells at both three and four weeks *in-vivo*. Soft and bony tissues were found in the interior of the cell seeded scaffolds after extraction. Cell seeded scaffold cross-sections showed osteocytes were present in the regions of newly formed bony tissue indicating that the MSC cells were differentiating into mature bone. From this analysis, no preference in fiber composition (45S5c or 13-93) was distinguishable for the soft or bone tissue to grow. Therefore, both materials are excellent for tissue engineering applications.

Several blood vessels which penetrated the scaffolds provided nourishment to the tissues inside both the S100 and S30 of scaffolds. Integration of blood vessels into the interior of the scaffolds could be an indicator that the reaction products from 13-93 and 45S5c fibers could be beneficial in terms of triggering angiogenesis (blood vessel formation) *in-vivo*. Proangiogenic glasses and porous self-bonded bioactive glass scaffolds could be beneficial for new soft tissue repair applications.

Compositional SEM-EDS analysis of 13-93 and 45S5c fibers after four weeks *in-vivo* indicated that calcium phosphate rich layers had formed on the surface of the fibers while other glass components had been resorbed in the body fluids of the rats. The reaction layer thickness present on the 45S5c fibers was in the range of 20 to 30μm while the 13-93 reaction layer was only 10 to 20μm.

Neither scaffold type showed signs of mechanical failure or degradation after four weeks *in-vivo*. Based on these observations and the compressive strength measured previously, both S100 and S30 scaffolds are considered sufficiently strong for *in-vivo* use for cancellous bone applications or for soft tissue. Therefore, the present results indicate that self bonded bioactive glass fiber scaffolds constructed of 13-93 and 45S5c with average porosity measurements between 44 and 63% and compressive strengths between 0.6 and 5.3 MPa have the ability to function *in-vivo*, promote bone tissue formation, possibly promote angiogenesis, and be biologically converted to calcium phosphate or resorbed by body fluids.

ACKNOWLEDGEMENTS

Support for this work was provided by a Missouri University of Science and Technology Graduate Research Assistantship. The authors would also like to thank Wesley Glick for assistance with the scaffold implantation.

REFERENCES

1. L. Hench, Bioceramics, *J Am. Ceram. Soc*. **81** (1998) 1705.
2. L. Gibson, M. Ashby, Cellular Solids – Structural properties 2nd edition. (Cambridge Solid State Science Series,1997) p. 429-452.
3. J. Park, R. Lakes, Biomaterials: An Introduction 2nd edition. (Plenum Press, New York, NY, 1992) p. 197.
4. L. Hench, J. Jones. Factors affecting the structure and properties of bioactive foam scaffolds for tissue engineering, *J Biomed Mater Res B: Appl Biomater* **68B** (2004) 36.
5. S. Callcut, J. C. Knowles, Correlation between structure and compressive strength in a reticulate glass-reinforced hydroxyapatite foam, *J Mater Sci: Mater Med*. **13** (2002) 485.
6. H. Kim, J. Knowles, H. Kim, Hydroxyapatite porous scaffold engineered with biological polymer hybrid coating for antibiotic vancomycin release, *J Mater Sci: Mater Med.* **16** (2005) 189.
7. Q. Chen, I. Thompson, A. Boccaccini, 45S5 Bioglass®-derived glass–ceramic scaffolds for bone tissue engineering, *Biomaterials* **27** (2006) 2414.
8. E. Ebaretonbofa, J. Evans, High Porosity Hydroxyapatite Foam Scaffolds for Bone Substitutes, *J. Porous Mater*. **9** (2002) 257.
9. S. Ni, J. Chang, L. Chou, A Novel Bioactive Porous $CaSiO_3$ Scaffold for Bone Tissue Engineering, *J Biomed Mater Res A*; **76A** (2005) 196.
10. H. Ohgushi, M. Okumura, T. Yoshikawa, K. Inoue, N. Senpuku, S. Tamai, Bone Formation Process in porous Calcium Carbonate and Hydroxyapatite, *J. Biomed Mater Res*. **26** (1992) 885.
11. M. Rahaman, R. Brown, S. Bal, D. Day, Bioactive Glasses for Nonbearing Applications in Total Joint Replacement, *Seminars in Arthroplasty*. **17** (2006) 102.
12. R. Martin, M. Chapman, N. Sharkey, S. Zissimos, B. Bay, E. Shor, Bone Ingrowth and Mechanical Properties of Coralline Hydroxyapatite 1 Yr After Implantation, *Biomaterials* **14** (1993) 341.
13. T. Paatola, E. Pirhonen, P. Törmälä, Coating of bioactive glass (13-93) fibers with bioabsorbable polymer, *Bioceramics* **13** (2000) 717.
14. E. Pirhonen, L. Moimas, J. Haapanen, Porous Bioactive 3-D Glass Fiber Scaffolds for Tissue Engineering Applications Manufactured by Sintering Technique, *Key Engineering Mater*. **240-242** (2003) 237.

15. C. P.A.T. Klein, P. Patka, W. den Hollander, Macroporous Calcium Phosphate Bioceramics in Dog Femora: A Histological Study of Interface and Biodegration, *Biomaterials*. **10** (1989) 59.
16. R. Martin, M. Chapman, R. Holmes, D. Sartoris, E. Shors, J. Gordon, D. Heitter, N. Sharkey, A. Zissimos, Effects of Bone Ingrowth on the Strength and Non-Invasive Assessment of a Coralline Hydroxyapatite Material, *Biomaterials*, **10** (1989) 481.
17. M. Vogal, C. Voigt, U. Gross, C. Müller-Mai, In Vivo Comparison of Bioactive Glass Particles in Rabbits *Biomaterials* **22** (2001) 357.
18. A. Yao, D. Wang, W. Huang, Q. Fu, M. Rahaman, D. Day, In Vitro Bioactive Characteristics of Borate-Based Glasses with Controllable Degradation Behavior, *J. Am. Ceram. Soc*. **90** (2007) 303.
19. W. Huang, D. Day, K. Kittiratanapiboon, M. Rahaman, Kinetics and Mechanisms of the Conversion of Silicate (45S5), Borate, and Borosilicate Glasses to Hydroxyapatite in Dilute Phosphate Solution, *J. Mater. Sci: Mater Med*. **17** (2006) 583.
20. L. Hench, D. Clupper, Crystallization kinetics of tape cast bioactive glass 45S5, *J. Non-Crystalline Solids* **318** (2003) 43.
21. E. Soboleva, N. Yuritsyn, V. Ugolkov, Kinetics of Crystal Nucleation of Na_2O-$2CaO$-$3SiO_2$ Based Solid Solutions in Glasses of the Na_2SiO_3-$CaSiO_3$ Pseudobinary Join, *Glass Physics and Chem.* **6** (2004) 481.
22. V. Fokin, O. Potapov, E. Zanotto, F. Spiandorello, V. Ugolkov, B. Pevzner, Mutant Crystals in Na_2O-$2CaO$-$3SiO_2$ Glasses, *J Non-Crystalline Solids* **331** (2003) 240.
23. O. Peitl, E. Zanotto, L. Hench, Highly bioactive P_2O_5–Na_2O–CaO–SiO_2 glass–ceramics, *J Non-Crystalline Solids* **292** (2001) 115.
24. L. Hench, G. La Torre, O. Filho, E. Zanotto, United States Patent #5,981,412. (1999).
25. M. Brink, The Influence of Alkali and Alkaline Earths on the Working Range for Bioactive Glasses, *J. Biomed. Mater. Res*. **36** (1997) 109.
26. S. Jung, Silicate Based Bioactive Glass Fiber Scaffolds for Bone Tissue Regeneration, M.S. Thesis, Missouri University of Science and Technology (2007)
27. R. Brown, D. Day, T. Day, S. Jung, M. Rahaman, Q. Fu, Growth and Differentiation of Osteoblastic Cells on 13-93 Bioactive Glass Fiber Scaffolds, *Acta Biomater*, **4**, 387-96 (2008).
28. O. Laboux, N. Dion, V. Arana-Chavez, L-G Ste-Marie, A. Nanci, Microwave irradiation of ethanol-fixed bone improves preservation, reduces processing time, and allows both light and electron microscopy on the same sample, *J. Histochem. And Cytochem*. **52** (2004) 1267.
29. A. Leu, J. Leach, Proangiogenic Potential of Collagen/Bioactive Glass Substrate. *Pharma Res.*, 2008. **25**(5): p. 1222-1229.
30. J. Leach, Coating of VEGF-releasing scaffolds with bioactive glass for angiogenesis and bone regeneration. *Biomaterials*, 2006. **27**: p. 3249-3255.
31. K. Karlsson, Bioactivity of glass and bioactive glasses for bone repair, *Glass Technol*. **45** (2004) 157.

32. S. Radin, P. Ducheyne, S. Falaize, A. Hammond, *In vitro* transformation of bioactive glass granules into Ca-P shells, *J. Biomed. Mater. Res*. **49** (2000) 264.

APPENDIX E

CONVERSION KINETICS OF SILICATE, BOROSILICATE, AND BORATE BIOACTIVE GLASSES TO HYDROXYAPATITE

CONVERSION KINETICS OF SILICATE, BOROSILICATE, AND BORATE BIOACTIVE GLASSES TO HYDROXYAPATITE

Steven B. Jung*
Missouri University of Science and Technology
Rolla, Missouri, 65409, U.S.A.

Delbert E. Day
Missouri University of Science and Technology
Rolla, Missouri, 65409, U.S.A.

Abstract

Bioactive 45S5 glass has been studied extensively both *in vivo* and *in vitro*, and it is relatively well known that when placed in a phosphate containing solution the glass will react to form the bone-like material hydroxyapatite (HA). In the present work, a kinetic analysis of previously measured weight loss data was done to determine reaction rate constants for four bioactive glasses; one silicate glass, two borosilicate glasses, and one borate glass, via the contracting volume model. The reaction rate increased with increasing B_2O_3 content, with the borate glass reacting nearly five times faster than the silicate 45S5 glass. The three silica containing glasses all deviated from the contracting volume model after approximately 50-70% of the total weight loss; however, when compared to the 3-D diffusion model, the normalized data were in good agreement to 100% of the total weight loss. The deviation from the contracting volume model to the slower 3-D diffusion model indicates a change in conversion model for the silica containing glasses and can likely be attributed to the formation of a silica rich layer of a certain thickness that began controlling the release of ions from the unreacted glass by diffusion.

.

1. Introduction

Bioactive glass 45S5 was first reported to bond to bone by Hench in 1971.[1] Ever since, 45S5 has been used extensively in both research and clinical use for the repair of bone and other living tissues. Silicate based bioactive glasses, such as 45S5, and ceramics have served as important biomedical materials because it has the ability to bond to surrounding hard and soft tissues and enhance bone formation.[2-9]

Borate glasses have only recently been explored for use in biomedical applications. Richard was the first to investigate replacing SiO_2 with B_2O_3 in the 45S5 glass composition.[10] The borate based 45S5 immersed in a K_2HPO_4 solution at body temperature (37^oC) formed a layer of hydroxyapatite (HA), $Ca_{10}(PO_4)_6(OH)_2$, similar to that formed by the silicate based 45S5.[10] The *in vitro* formation of HA from the borate based 45S5 led to further investigation *in vivo*. Particles of the borate based 45S5 glass were placed in a rat tibial defect, and not only promoted bone formation, but did so at a faster rate than the silicate based 45S5 glass.[10]

Possible reaction mechanisms have been described by Huang et. al.[11-12] for the silicate 45S5 glass and the borate analog of 45S5 (all SiO_2 replaced by B_2O_3). The borate glass fully converted to HA by the glass dissolving, the B_2O_3 and Na_2O going into solution, and the CaO reacting with PO_4^{3-} from the phosphate solution. The silicate glass was described to partially convert to HA, while leaving a sodium depleted core surrounded by a silica rich layer.

According to the results of previous studies[10-12], the borate based glass most closely follows a contracting volume type of behavior, where the HA first forms at the outside of the glass particle, and then continually reacts inward toward the center until

completely reacted. The silicate glass forms HA at the outer edge of the particle initially; however it is not clear how the formation of the silica gel layer affects the movement of ions. Therefore, if the silica gel layer becomes the rate controlling mechanism, the weight loss reaction might follow 3-D diffusion kinetic behavior.

The main objective of the following work was to determine if there was a mechanistic difference in the way silicate, borosilicate, and borate bioactive glasses converted to HA. The relative reaction rates of the silicate, borate, and two borosilicate based 45S5 glasses were determined by comparison with the contracting volume model. Finally, the normalized weight loss data was compared to the 3-D diffusion model to see if the conversion reaction changed models during the weight loss experiment.

2. Experimental

2.1 Glass Preparation and Weight Loss for the Silicate, Borate, and Borosilicate Based 45S5 Glasses

The glasses used were based on the bioactive 45S5 glass composition, and the composition of each glass is shown in Table I. The weight loss data used in this analysis and an in-depth experimental procedure was reported by Huang et. al.[11-12]

2.2 Kinetic Evaluation of the Weight Loss Data

In the previous work by Huang[11-12], the weight loss for the glass particles was measured for hundreds of hours beyond a measurable change to make sure the experiment has indeed ended, and is shown in Fig.1. The maximum weight losses for the 0B, 1B, 2B, and 3B were 42%, 35%, 42%, and 57% respectively. The weight loss data reported by Huang et. al[12] were converted to fractional weight change (α) by dividing the measured weight loss values by the maximum weight loss value (Fig.2). The

maximum weight loss was determined by the difference of the mass of the starting glass and that of the end product.

The contracting volume model (CVM) is a geometrical model that is used to theoretically describe the reaction rate of a solid sphere of some material and a reactant (gas or liquid). In this experiment, the CVM was used to model the weight loss from the glass particles suspended and the 0.02M phosphate solution data measured by Huang[11-12]. The values of α vs. time for the four glasses were fitted using the CVM shown as equation (1).[13-14]

Contracting Volume Model $1-(1-\alpha)^{1/3} = kt$ (1)

The 3-D diffusion model, equation (2)[14], is a diffusion model that describes the diffusion of material through some rate controlling medium in three dimensions. The 3-D diffusion model was compared to the normalized weight loss data just as the CVM to see if a change in the glass conversion model could be detected from the weight loss for any of the four glasses.

3-D Diffusion Model $[1-(1-\alpha)^{1/3}]^2 = kt$ (2)

Terms present in equations (1) and (2) are the normalized weight loss (α), which is calculated by dividing the measured weight loss by the total weight loss for the reaction, rate constant (k), and time (t).

3. Results

3.1 Weight Loss of Silicate, Borate, and Borosilicate Based 45S5 Glasses

The weight loss data measured by Huang et. al.[11-12] for the four glasses tested for the first 1800 hours of reaction is shown in Fig. 1. The 0B and 1B glasses reacted at nearly

the same rate for the first 200 hours while the 2B and 3B glasses reacted significantly faster. At the time the experiment was stopped, the 0B, 1B, and 2B glasses had stopped losing weight, however the measured weight losses were less than the theoretical weight losses for the three glasses (Table 1). Theoretical weight loss for these glasses was calculated by assuming the end product would be HA, and all the rest of the components (Na_2O, B_2O_3, and SiO_2) would be in solution. Silica rich cores were found at the center of the 0B, 1B, and 2B glass particles at the end of the experiment, indicating that the silica had not fully dissolved in the phosphate solution.[11] The final (maximum) weight loss of the 3B glass was 57%, which was within 2% of its theoretical limit, and therefore assumed to have gone to completion.

3.2 Isothermal Reaction Kinetics for the Silicate, Borate, and Borosilicate Based 45S5 Glasses

The accumulated weight loss percent data shown in Fig. 1 were converted to α by dividing the measured weight loss by the maximum weight loss for each glass. The solid lines in Fig. 2 show that the normalized weight loss (α) vs. time curves for each glass had similar shapes. The k values used to fit equation (1) to the curves in Fig. 2 are listed in Table 1. The k values ranged from as low of 0.0045 for 0B to as high of 0.0220 for the 3B glass, indicating that the 3B glass reacts approximately five times faster than the 0B glass. The CVM model is a good fit for all four glasses for the first 30 hours of reaction.

After about 50 hours, the normalized weight loss deviated from the CVM model. The reaction rate of the 0B, 1B, and 2B particles decreased from that initially described by the CVM. After 50 hours, the normalized weight loss data is in good agreement with the 3-D diffusion model, indicating a change in reaction model for the three silica containing glasses.

4. Discussion

4.1 Reaction Model of the Glasses with 0.02M Phosphate Solution

The reaction model for the four glasses was determined by plotting α vs. time along with fits of equations (1) and (2) for each glass. A plot with the normalized weight loss data for the four glasses (points) compared to the CVM (solid line) and 3-D diffusion equation (dashed line) is shown in Fig. 3. The first 30 hours of data, for all four glasses, were in good agreement with fits of the CVM, indicating that the HA formation was due to dissolution of the glass in the phosphate solution.

The normalized weight loss data for the 0B, 1B, and 2B glasses deviate from the CVM after about 50 hours. The normalized weight loss after 50 hours fit well fitted by the 3-D diffusion model until the end of the reaction (~600 hours). One explanation for this behavior is that the silica gel layer in the silica containing glasses had reached a thickness such that the movement of ions was controlled by diffusion through the silica gel. The first glass to change from the CVM to the 3-D diffusion model, in terms of normalized weight loss (α), was 0B which contained the most silica, and was followed by the 1B and 2B glasses. It is reasonable to suggest that if the change in model was caused by the formation of a silica gel diffusion layer, then the glass containing the most silica (0B) would form a silica gel diffusion barrier first and so on as seen with the 1B and 2B glasses.

4.2 Effect of B_2O_3 Content on the Reaction Rate Constant

In previous analysis of the 0B, 1B, 2B, and 3B glasses, the general relationship between higher B_2O_3 content and increased reaction rate was identified[11], but no mathematical

relationship was determined that related the B_2O_3 content of the glasses and the rate of conversion to HA. Figure 4 shows the mol% B_2O_3 plotted versus the rate constant k (Table 1) for each of the glasses. There is a measurable change in k between all four glasses, shown by the solid curved line in Fig. 4. This may be a method for accurately determining the effect B_2O_3 is having on the reaction rate constant.

The equation shown in Fig. 4 describes the reaction rate constants of the four glasses in the 0.02M phosphate solution versus the B_2O_3 content. Comparing the phosphate concentration of 0.02M to the ~0.001M phosphate concentration in body fluids[(11)], the equation would seem irrelevant for practical use as 0.02M phosphate solution is not a standard solution concentration. The possible importance of the equation shown in Fig. 4 comes from finding a relationship between B_2O_3 content and the reaction rate constant k. A similar experiment between the 45S5 glasses and a solution such as simulated body fluid (SBF) could be done to develop a similar equation that is more applicable when trying to model a bioactive glass conversion reaction in a real system, such as in the body.

5. Conclusions

The conversion of the 0B, 1B, 2B, and 3B glasses was described using both the contracting volume model and the 3-D diffusion model. The CVM fits the data for the 3B glass over the entire range of α, while the data for the 0B, 1B, and 2B glasses are only fitted well by the CVM for the first 30 hours of reaction. The 0B, 1B, and 2B glasses at long times are better fitted by the 3-D diffusion model, probably due to the formation of a rate controlling silica gel layer in the glass particles. The relative reaction of the 3B glass

was five times faster than the 0B glass, with k values which range from 0.0045 for 0B to 0.0220 for 3B.

The reaction rate constant of 45S5 type bioactive glasses immersed in 0.02M phosphate solution was shown to depend on the B_2O_3 content, and thus warrants additional work to find a similar relationship for a more common solution such as SBF. Simulated body fluid would more accurately model the *in vivo* environment and could be used to tailor glass compositions for desired *in vivo* reaction rates.

Acknowledgements

The authors would like to thank the National Science Foundation (NSF) (grant #0813608) and the International Materials Institute – New Functionalities in Glass (IMI-NFG) (NSF-DMR-0409588) for their support.

References

1. Hench, L. L., Splinter, R. J., Allen, W. C., Greenlee, K., *J. Biomed. Mater. Res*. 1991, **2**, 117.
2. Hench, L. L. Wilson, J., *Handbook of Bioactive Ceramics Vol. 1: Bioactive Glasses and Glass-Ceramics* (CRC Press, Boca Raton, FL, 1990) Vol. 1)
3. Hench, L. L., Hench, J. W., Greenspan, D. C., *J. Aust. Ceram. Soc*., 2004, **40,** 1-42.
4. Hench, L. L., *J. Mater. Sci.: Mater. Med*, 2006, **17**,967-978.
5. Hench, L. L., *Glass Technol*, 2003, **44,** 1-10.
6. Hench, L. L., Paschall, H, A, *J. Biomed. Mater. Res. 5(Part 1)* 1974, 49-64.
7. Clark, A. E., Hench, L. L., *J. Biomed. Mater. Res.*, 1976, **10,** 161-174.
8. Boccaccini, A. R., Chen, Q., Lefebvre, L. Gremillard, L., Chevalier, J., *Faraday discuss*., 2007, **136**, 27-44.
9. Kokubo, T., H. Kushitani, H., Sakka, S., Kitsugi, T., Yamamuro, T., *J. Biomed. Mater. Res.*, 1990, **24**, 721-734.
10. Richard, M. N. C., M.S. Thesis, University of Missouri-Rolla, 2000.
11. Huang, W., Day, D. E., Kittraratanapiboon, K., Rahaman, M. N., *J. Mater. Sci: Mater. Med.*, 2006, **17**, 583-596.
12. Huang, W., Rahaman, M. N., Day, D. E., Li, Y., *Phys. Chem. Glasses: Eur. J. Glass Sci. Technol. B*, 2006, **47**, 1-12.

13. Bamford, C. H., Tipper, C. F. R., *Comprehensive Chemical Kinetics, Vol. 22. Reaction is the Solid State* (Elselvier Scientific Publishing Company, New York 1980).
14. Rahaman, M. N., *Ceramic Processing and Sintering – 2nd edition* (Marcel Dekker Inc. New York, New York, 2003).

Table 1. Nominal Composition of Glasses Used in Weight Loss Experiment[11-12]

Glass	Weight Percent					Theoretical	Actual	
	Na_2O	CaO	B_2O_3	SiO_2	P_2O_5	Weight Loss %	Weight Loss %	k (CVM)
0B	24.5	24.5	0.0	45.0	6.0	56	42	0.0045
1B	24.0	23.9	17.0	29.3	5.8	57	35	0.0065
2B	23.4	23.4	33.1	14.4	5.7	58	42	0.0120
3B	22.9	22.9	48.6	0	5.6	59	57	0.0220

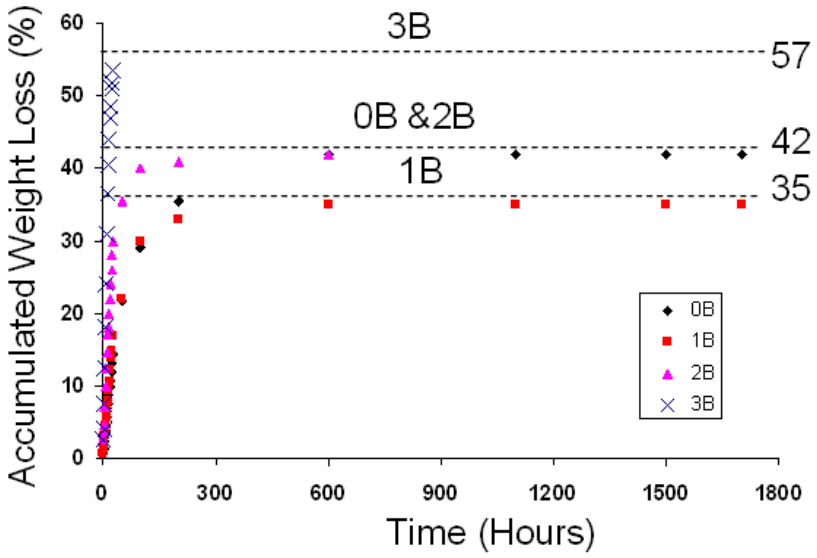

Figure 1. Accumulated weight loss percent[11-12] for the 0B, 1B, 2B, and 3B glasses during the first 1800 hours of reaction in 0.02M K_2HPO_4 solution at 37°C. The dashed horizontal lines denote the maximum weight loss for each glass. The 0B and 2B glasses lost 42%, 1B lost 35%, and 3B lost 57%, respectively.

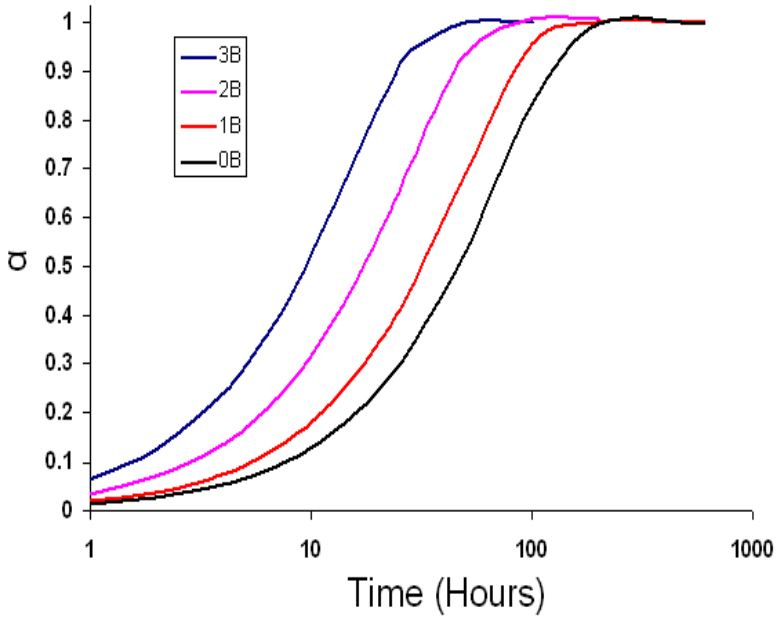

Figure 2. Normalized weight loss (α) vs. time for the 0B, 1B, 2B, and 3B glasses.[12]

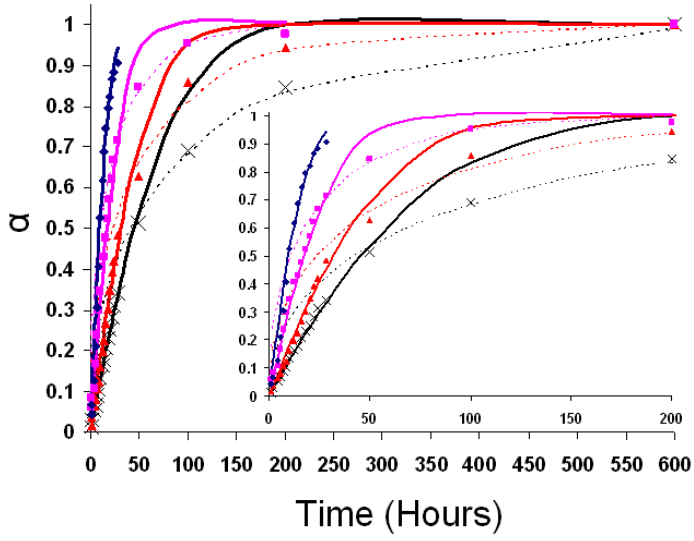

Figure 3. Normalized weight loss (α) vs. time for the 0B (crosses), 1B (triangles), 2B (squares), and 3B (diamonds) glasses compared with the Contracting Volume Model (solid lines) and 3-D Diffusion Model (dashed lines). The CVM is a good fit of the data for the first 30 hours for all four glasses, but after 50 hours, the 3-D Diffusion Model is a better fit for the slower reacting 0B, 1B, and 2B glasses (dashed lines).

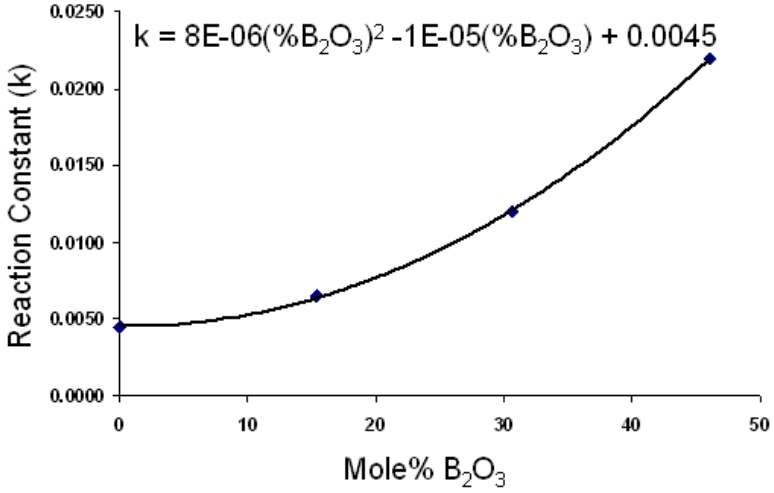

Figure 4. Reaction Constant (k) vs. Mole % B_2O_3 for the 0B, 1B, 2B, and 3B glasses reacted at 37^{o}C in 0.02M K_2HPO_4 solution.

VITA

Steven B. Jung was born May 22nd, 1982 in Belleville IL, USA. Throughout much of grade school and high school, he spent his time on school and swimming. In 2000, Steven started at the University of Missouri-Rolla (now S&T) as an undergraduate. He spent two years on the UMR Swim Team before retiring as an athlete to coop at Kohler Co. (Kohler WI). At Kohler Steven learned that an advanced degree would be important for becoming the person that makes decisions and therefore, in 2005 started his M.S. at S&T under Dr. Delbert Day working on bioactive glass scaffolds for bone tissue engineering. Nearing the end of his M.S., Steven worked a summer at Savannah River National Laboratory (SRNL) on nuclear waste vitrification, and after that experience, it was apparent that a Ph.D. degree was required for running programs and having the role as the 'idea person'. In the spring of 2007, Steven started his Ph.D. at S&T, and continued work on bioactive glass scaffolds, but this time concentrated on borate glasses. Over the next three years, several new inventions were developed, and six U.S. patents were filed. The inventions include: angiogenic bioactive glasses, blood vessel guides composed of bioactive glasses, unidirectional glass fiber scaffolds for cortical bone replacement, glasses that convert to materials other than hydroxyapatite, and bioactive glasses for healing chronic wounds. The work presented here has been the reason behind several prestigious awards including: Selection as a U.S. Delegate for the Meeting of Nobel Laureates (2007), S&T Chancellors Fellowship (2007 to 2010), and an invitation to the U.S.- China Winter School for Glass Technology (2010). After completion of the Ph.D. requirements, Steven will work for MO-Sci Corporation (Rolla, MO) as a Senior Research Scientist developing applications of bioactive glass.